UCID- 21287 Rev. 1

Pollutant Transport Study: Bay Area to North Central Coast Air Basin

Final Report

Joyce E. Penner
Peter S. Connell

Prepared for the California Air Resources Board
under Agreement No. A3-078-32 with the Bay Area
Air Quality Management District

October 1988

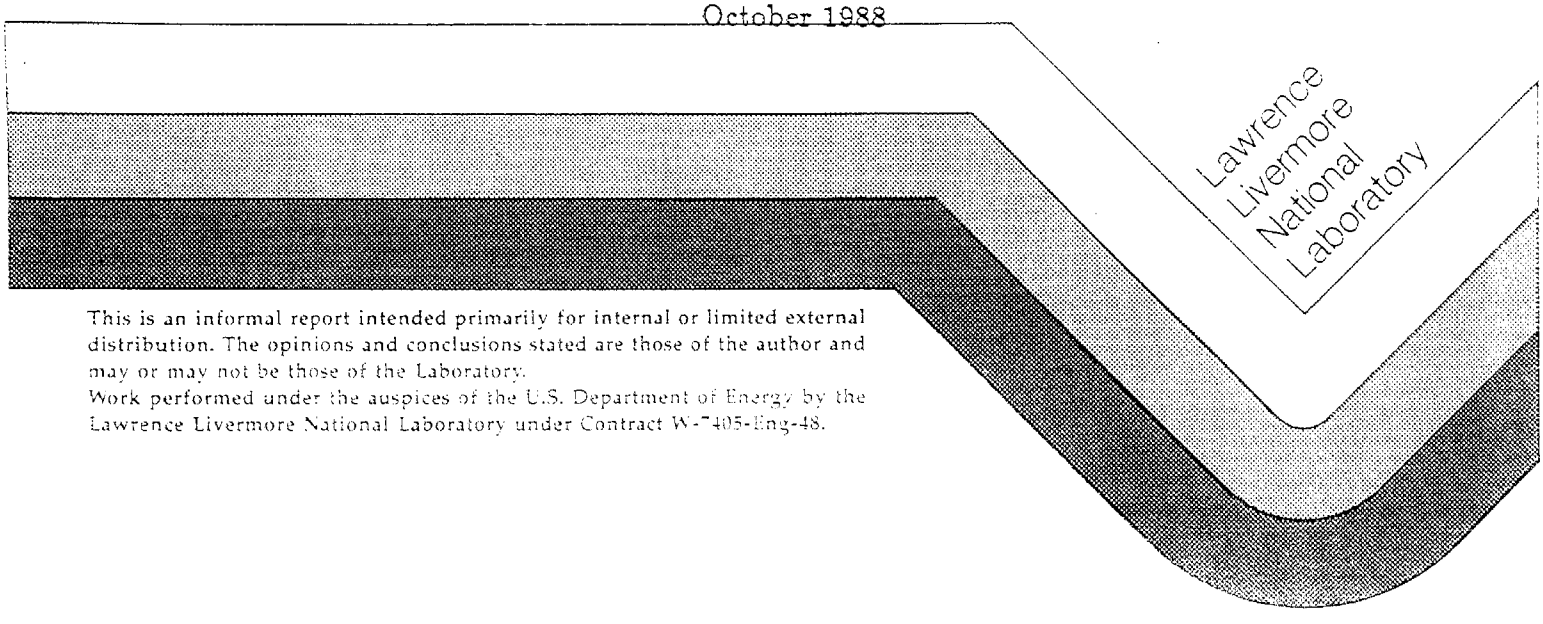

This is an informal report intended primarily for internal or limited external distribution. The opinions and conclusions stated are those of the author and may or may not be those of the Laboratory.
Work performed under the auspices of the U.S. Department of Energy by the Lawrence Livermore National Laboratory under Contract W-7405-Eng-48.

Abstract

A multi-layer photochemical transport model has been developed and applied to study the transport of pollutants from the Bay Area to the North Central Coast air basin. The study has been a joint effort between the Bay Area Air Quality Management District (BAAQMD), the Monterey Bay Unified Air Pollution Control District (MBUAPCD) and the Lawrence Livermore National Laboratory (LLNL). This study was motivated by questions which arose during the 1982 Bay Area Air Quality Plan Update. The primary concern was the impact of hydrocarbon and nitrogen oxide emissions in the Bay Area on downwind areas in the MBUAPCD. In particular, the Bay Area had adopted a hydrocarbon control strategy which did not seek active control of nitrogen oxide emissions. This strategy was based on photochemical modeling with the Livermore Regional Air Quality Model (LIRAQ) which had shown that control of nitrogen oxides would lead to local increases in ozone. The concern was that such a strategy, while helping to decrease ozone locally, would nevertheless increase ozone downwind.

To study this issue required the development of a model capable of treating a several-day smog episode so that transport times sufficient to describe inter-basin transport episodes could be described. This required the development of a multi-level photochemical transport model to self-consistently describe the storage of pollutants overnight above the mixed-layer. In addition, because the model domain size was increased by a factor of eight and the numerical method previously employed in LIRAQ was too expensive of computer time, an operator splitting numerical technique was installed and tested. This also allowed us to install a more accurate advection scheme than that used previously. During the model development, the lumped chemical scheme used in LIRAQ was also updated.

The model was applied to simulate the ozone episode of September 30 and October 1, 1980. For this work, a two basin emissions inventory for 1980 was prepared. In addition, meteorology fields for the two-basin model domain were prepared. In order to do this an updated version of the MATHEW model was developed which allows the user to specify the mixed-layer depth and restricts flow across that layer.

Finally, the effect of Bay Area hydrocarbon and nitrogen oxide emission controls were tested by separately reducing their emissions by 30 percent in the Bay Area. We found that reducing hydrocarbons in the Bay Area had a slight, but beneficial effect on the MBUAPCD. Ozone concentrations were reduced in both air basins. Also, as expected, reducing nitrogen oxide emissions led to increased ozone concentrations in the Bay Area. Surprizingly, however, the effect of NO_x emissions was reversed at MBUAPCD receptor sites. There is a narrow downwind band in which ozone concentrations are decreased by about 1 pphm when NO_x emissions are decreased. However, because the calculated effect is so small, it is also quite uncertain. Both meteorology changes and chemical mechanism changes could alter the result. We therefore recommend that further analysis of both the effect of meteorology and the effect of the chemical mechanism be carried out to better quantify the result and its uncertainty.

Table of Contents

Abstract ii
Acknowledgments v
List of Figures vi
List of Tables xiv
Chapter 1. Introduction and Background 1
Chapter 2. Model Improvements 4
A. Introduction 4
B. Testing of numerical methods 4
C. Timing and accuracy tests for operator splitting with upstream differencing . . 7
D. Installation of a finite element technique 16
E. Upstream differencing with anti-diffusion 19
F. Development of a multi-layer transport kinetics model 20
G. Development of the processor for MATHEW wind fields 22
H. Wind field adjustment with an inversion 23
I. Other model improvements 26
Chapter 3. Development of emissions inventory 36
A. Introduction 36
B. Stationary source emissions 36
C. Motor vehicle emissions in the BAAQMD 36
Link speeds 38
D. Mobile source inventory in the MBUAPCD 38
Spatial distribution 39
Temporal distribution 40
Disaggregation of ARB county emissions 40
E. Emissions from natural vegetation (biogenic) 40
Vegetation file 41
Emission factors 41
Results 41
F. Method for splitting HC into reactivity classes 42
Chapter 4. Meteorology 45
A. Introduction 45
B. Mixed-layer depth 46
C. Wind data 48
D. Atmospheric transmissivity coefficient 50
E. Meteorology of Tuesday, September 30, 1980 50
F. Meteorology of Wednesday, October 1, 1980 52
Chapter 5. Update of Chemical Mechanism 63
A. Introduction 63
B. 1982 chemical mechanism and resulting ozone fields 63
C. Update to 1986 reaction rates 64
D. Smog chamber simulations 65
E. Performance evaluation of the new mechanism 70
F. Appraisal of soundness of mechanism and recommended improvements 72

Chapter 6. Sensitivity Tests of New Model and Performance Evaluation 88
A. Introduction 88
B. Treatment of vertical mixing 88
C. Initial conditions and boundary conditions 90
D. Inclusion of upper layer 91
E. Sensitivity of predicted O_3 to changes in meteorology 92
F. Performance evaluation 93
G. Sensitivity of Monterey Bay Unified Air Pollution Control District to Bay Area emissions 94
H. Discussion of limitations of study 97
Chapter 7. Conclusions and Recommendations 144
A. Appraisal of "state of the model" and future modeling directions 144
B. Data needs 145
References 146
Appendix A. Summary tables of emissions inventory 151
Appendix B. Tabulation of observed and predicted ozone concentrations 186

Acknowledgements

This project has been a joint effort by three agencies: the Lawrence Livermore National Laboratory, the Bay Area Air Quality Management District and the Monterey Bay Unified Air Pollution Control District. Coordination of the project was managed by a steering committee chaired by Lew Robinson and whose members included representatives from each of these three agencies as well as from the California Air Resources Board. In the following report, where specific individuals from the project have had significant written contributions, their names have been added as co-authors of the individual chapters. Members of the steering committee are listed below by agency.

BAAQMD:	L. Robinson
	T. Perardi
	T. Mangot
	M. Kim
	T. Umeda
	D. Duker
	R. DeMandel
MBUAPCD:	D. Quetin
CARB:	C. Bennett
	K. Wagner
LLNL:	J. Penner
	P. Connell

J. Penner and P. Connell wish to thank the other steering committee members whose guidance and discussion throughout the project were both helpful and stimulating. In addition, we acknowledge the advise of both Phil Roth and Gary Whitten. Mike MacCracken's suggestions and comments resulted in a more readable report. Finally, we wish to thank Nancy Badal for her heroic efforts to complete the manuscript typing.

List of Figures

Figure Number	Title	Page
2.1	RMS difference for O_3 plotted as a function of the operator splitting advection time step.	30
2.2	Relative error of O_3 maximum plotted as a function of the operator splitting advection time step.	30
2.3	O_3 field at noon predicted using the Gear method with upstream differencing.	31
2.4	O_3 field at noon predicted using the finite element method with operator splitting and no filter.	31
2.5	O_3 field at noon predicted using the finite element method with operator splitting and the filter recommended by McRae et al. (1982) applied after a combined advection and diffusion step.	32
2.6	O_3 field at noon predicted using the finite element method with operator splitting and the filter recommended by McRae et al. (1982) applied after the advection step.	32
2.7	O_3 concentration predicted at 1500 hours using the Gear solution with upstream differencing.	33
2.8	O_3 concentration predicted at 1500 hours using operator splitting with upstream differencing corrected by anti-diffusion.	33
2.9	Scheme for treating vertical fluxes in the multi-layer model.	34
2.10	Interpolated wind fields from MEDIC.	34
2.11	Adjusted layer-average wind fields assuming $n \cdot u = 0$ along the inversion surface.	35
2.12	Adjusted layer-average wind fields assuming $n \cdot u \neq 0$ along the inversion surface.	35
3.1	Study area for source inventory.	43
3.2	Schematic diagram of procedures used for developing the NCCAB mobile source inventory.	43
3.3	Traffic cycles on Route 17 for 1982, 1983 and 1984.	44
3.4	Traffic cycles on Routes 1, 17 and 101 for 1982, 1983, and 1984.	44
3.5	Traffic cycle data used in the San Francisco Bay Area.	44
4.1	Time variation in growth of the mixed-layer.	55
4.2a	Surface weather map at 0400 PST on September 30, 1980.	55
4.2b	Surface weather map at 0400 PST on October 1, 1980.	55
4.3a	Mixed-layer winds in m s^{-1} for 0900 PST on September 30, 1980.	56
4.3b	Mixed-layer winds in m s^{-1} for 1200 PST on September 30, 1980.	56
4.3c	Mixed-layer winds in m s^{-1} for 1500 PST on September 30, 1980.	56
4.3d	Mixed-layer winds in m s^{-1} m for 1800 PST on September 30, 1980.	56
4.4a	Mixing depths in meters above sea level at 0900 PST.	57
4.4b	Mixing depths in meters above sea level at 1200 PST.	57

List of Figures (cont'd.)

Figure Number	Title	Page
4.4c	Mixing depths in meters above sea level at 1500 PST.	57
4.4d	Mixing depths in meters above sea level at 1800 PST.	57
4.5a	Upper layer winds in m s^{-1} at 0900 PST on September 30, 1980.	58
4.5b	Upper layer winds in m s^{-1} at 1200 PST on September 30, 1980.	58
4.5c	Upper layer winds in m s^{-1} at 1500 PST on September 30, 1980.	58
4.5d	Upper layer winds in m s^{-1} at 1800 PST on September 30, 1980.	58
4.6a	Mixed-layer winds in m s^{-1} for 0900 PST on October 1, 1980.	59
4.6b	Mixed-layer winds in m s^{-1} for 1200 PST on October 1, 1980.	59
4.6c	Mixed-layer winds in m s^{-1} for 1500 PST on October 1, 1980.	60
4.6d	Mixed-layer winds in m s^{-1} for 1800 PST on October 1, 1980.	60
4.7a	Upper layer winds in m s^{-1} at 0900 PST on October 1, 1980.	61
4.7b	Upper layer winds in m s^{-1} at 1200 PST on October 1, 1980.	61
4.7c	Upper layer winds in m s^{-1} at 1500 PST on October 1, 1980.	62
4.7d	Upper layer winds in m s^{-1} at 1800 PST on October 1, 1980.	63
5.1	Surface O_3 mixing ratio for the 1982 mechanism at 1400 hours on September 30, 1980. The units are ppm.	74
5.2	Surface O_3 mixing ratio for the 1982 mechanism at 1500 hours on September 30, 1980. The units are ppm.	74
5.3	Surface O_3 mixing ratio for the 1982 mechanism at 1600 hours on September 30, 1980. The units are ppm.	75
5.4	Surface O_3 mixing ratio for the 1982 mechanism at 1800 hours on September 30, 1980. The units are ppm.	75
5.5	Surface O_3 mixing ratio for the 1982 mechanism with rate constants and photolysis rates updated to 1986 at 1400 hours on September 30, 1980. The units are ppm.	76
5.6	Surface O_3 mixing ratio for the 1982 mechanism with rate constants and photolysis rates updated to 1986 at 1500 hours on September 30, 1980. The units are ppm.	75
5.7	Surface O_3 mixing ratio for the 1982 mechanism with rate constants and photolysis rates updated to 1986 at 1600 hours on September 30, 1980. The units are ppm.	77
5.8	Surface O_3 mixing ratio for the 1982 mechanism with rate constants and photolysis rates updated to 1986 at 1800 hours on September 30, 1980. The units are ppm.	77
5.9	Simulation of the State Air Pollution Research Institute (SAPRI) smog chamber experiment EC245 using the Penner and Walton (1982) mechanism.	78
5.10	Simulation of smog chamber experiment EC245 using the Penner and Walton (1982) mechanism with photolysis and reaction rates updated to 1986.	78

List of Figures (cont'd.)

Figure Number	Title	Page
5.11	Simulation of smog chamber experiment EC245 using a mechanism that treats the chemistry of H_2CO explicitly.	79
5.12	Simulation of smog chamber experiment EC245 using a mechanism that treats the chemistry of both H_2CO and C_2H_4 explicitly.	79
5.13	Simulation of conditions near San Jose using the 1982 mechanism.	80
5.14	Simulation of conditions near San Jose using the 1982 mechanism with rate constants and photolysis rates updated to 1986.	80
5.15	Simulation of conditions near San Jose using the mechanism which treats H_2CO explicitly. All aldehyde emissions are assumed to be H_2CO.	81
5.16	Simulation of conditions near San Jose using the mechanism which treats H_2CO explicitly. Aldehyde emissions are assumed to be 50% H_2CO and 50% higher aldehydes.	81
5.17	Simulation of conditions near San Jose using the mechanism which treats the chemistry of both H_2CO and C_2H_4 explicitly. All aldehyde emissions are assumed to be H_2CO and the alkene emissions are 50% ethene and 50% higher alkenes.	82
5.18	Surface O_3 mixing ratio for the mechanism which treats H_2CO separately at 1400 hours on September 30, 1980.	82
5.19	Surface O_3 mixing ratio for the mechanism which treats H_2CO separately at 1500 hours on September 30, 1980.	83
5.20	Surface O_3 mixing ratio for the mechanism which treats H_2CO separately at 1600 hours on September 30, 1980.	83
5.21	Simulation of smog chamber experiment IC871 from Carter et al. (1986) using the new mechanism.	84
5.22	Simulation of smog chamber experiment IC873 from Carter et al. (1986) using the new mechanism.	84
5.23	Simulation of smog chamber experiment IC871 from Carter et al. (1986) using the condensed mechanism of Lurmann et al. (1987).	85
5.24	Simulation of smog chamber experiment IC871 from Carter et al. (1986) using the condensed mechanism of Lurmann et al. (1987), initialized with the hydrocarbon categories and reactivity weighting scheme of the more highly lumped mechanism developed here.	85
5.25	Simulation of smog chamber experiment IC873 from Carter et al. (1986) using the condensed mechanism of Lurmann et al. (1987).	86
5.26	Simulation of smog chamber experiment IC873 from Carter et al. (1986) using the condensed mechanism of Lurmann et al. (1987), initialized with the hydrocarbon categories and reactivity weighting scheme of the more highly lumped mechanism developed here.	86

List of Figures (cont'd.)

Figure Number	Title	Page
5.27	Simulation of a smog chamber experiment using the new mechanism with initial conditions as in Figure 5.21 except that NO and NO_2 have been reduced by 30 percent.	87
5.28	Simulation of a smog chamber experiment using the mechanism of Lurmann et al. (1987) with initial conditions as in Figure 5.23 except that NO and NO_2 have been reduced by 30 percent.	87
6.1a	Ratio of the surface O_3 concentration at 1 m (dashed line) and at 8 m (solid line) to the layer-average O_3 concentration as a function of the mixed-layer depth for the new formulation. The deposition velocity has been set to 0.66 cm s^{-1} while the four lines correspond to eddy mixing coefficients of 200, 500, 1000 and 2000 cm^2s^{-1}, respectively, increasing left to right.	99
6.1b	Ratio of the surface O_3 concentration at 1 m (dashed line) and 8 m (solid line) to the layer-average O_3 concentration as a function of the surface eddy coefficient, K_z, for the new formulation. The assumed layer depth was 250 m. The three lines correspond to deposition velocities of 0.005, 0.2, and 0.66 cm s^{-1}, respectively, left to right.	100
6.2	Layer-average O_3 concentration predicted when it is assumed that surface concentrations are identically equal to layer-average concentrations. The dashed contour line shows the approximate location of the 0.12 ppm contour.	101
6.3	Layer-average O_3 concentration predicted using the old LIRAQ formulation of surface concentration. The dashed contour line shows the approximate location of the 0.12 ppm contour.	101
6.4a	Predicted NO_x concentration above the mixed-layer at midnight on September 30, 1980.	102
6.4b	Predicted NO_x concentration above the mixed-layer at 0400 hours on October 1, 1980.	102
6.5a	Predicted HC2 concentration above the mixed-layer at midnight on September 30, 1980.	101
6.5b	Predicted HC2 concentration above the mixed-layer at 0400 hours on October 1, 1980.	103
6.6a	Predicted O_3 concentration above the mixed-layer at midnight on September 30, 1980.	104
6.6b	Predicted O_3 concentration above the mixed-layer at 0400 hours on October 1, 1980.	104
6.7	Averaged boundary layer winds for 0900 hours on September 30, 1980 for MET1.	105

List of Figures (cont'd.)

Figure Number	Title	Page
6.8	Averaged boundary layer winds for 1000 hours on September 30, 1980 for MET1.	106
6.9	Averaged boundary layer winds for 1200 hours on September 30, 1980 for MET1.	107
6.10	Averaged boundary layer winds for 1400 hours on September 30, 1980 for MET1.	108
6.11	Averaged boundary layer winds for 1500 hours on September 30, 1980 for MET1.	109
6.12	Averaged boundary layer winds for 1700 hours on September 30, 1980 for MET1.	110
6.13	Averaged boundary layer winds for 0900 hours on September 30, 1980 for MET4.	111
6.14	Averaged boundary layer winds for 1000 hours on September 30, 1980 for MET4.	111
6.15	Averaged boundary layer winds for 1200 hours on September 30, 1980 for MET4.	112
6.16	Averaged boundary layer winds for 1400 hours on September 30, 1980 for MET4.	112
6.17	Averaged boundary layer winds for 1500 hours on September 30, 1980 for MET4.	113
6.18	Averaged boundary layer winds for 1700 hours on September 30, 1980 for MET4.	113
6.19	Boundary layer depth for 1200 hours used in MET1.	114
6.20	Boundary layer depth for 1400 hours used in MET1.	114
6.21	Boundary layer depth for 1200 hours used in MET4.	115
6.22	Boundary layer depth for 1400 hours used in MET4.	115
6.23	Layer-average O_3 concentrations at 1500 hours calculated using MET1.	116
6.24	Layer-average O_3 concentrations at 1600 hours calculated using MET1.	116
6.25	Layer-average O_3 concentrations at 1700 hours calculated using MET1.	117
6.26	Layer-average O_3 concentrations at 1500 hours calculated using MET4. The dashed contour line shows the approximate location of the 0.12 ppm contour.	117
6.27	Layer-average O_3 concentrations at 1600 hours calculated using MET4. The dashed contour line shows the approximate location of the 0.12 ppm contour.	118
6.28	Layer-average O_3 concentrations at 1700 hours calculated using MET4.The dashed contour line shows the approximate location of the 0.12 ppm contour.	118

List of Figures (cont'd.)

Figure Number	Title	Page
6.29	Layer-average O_3 concentrations on the 20 × 20 grid at 1400 hours calculated using MET1.	119
6.30	Layer-average O_3 concentrations on the 20 × 20 grid at 1500 hours calculated using MET1.	119
6.31	Layer-average O_3 concentrations on the 20 × 20 grid at 1600 hours calculated using MET1.	120
6.32	Layer-average O_3 concentrations on the 20 × 20 grid at 1400 hours calculated using MET4.	120
6.33	Layer-average O_3 concentrations on the 20 × 20 grid at 1500 hours calculated using MET4.	121
6.34	Layer-average O_3 concentrations on the 20 × 20 grid at 1600 hours calculated using MET4.	121
6.35	Layer-average NO_x concentrations at 0600 hours calculated using MET1.	122
6.36	Layer-average NO_x concentrations at 0900 hours calculated using MET1.	122
6.37	Layer-average NO_x concentrations at 1200 hours calculated using MET1.	123
6.38	Layer-average NO_x concentrations at 1500 hours calculated using MET1.	123
6.39	Layer-average NO_x concentrations at 1200 hours calculated using MET4.	124
6.40	Layer-average NO_x concentrations at 1500 hours calculated using MET4.	124
6.41	Layer-average HC2 concentrations at 0600 hours calculated using MET4.	125
6.42	Layer-average HC2 concentrations at 0900 hours calculated using MET1.	125
6.43	Layer-average HC2 concentrations at 1200 hours calculated using MET1.	126
6.44	Layer-average HC2 concentrations at 1500 hours calculated using MET1.	126
6.45	Layer-average HC2 concentrations at 1200 hours calculated using MET4.	127
6.46	Layer-average HC2 concentrations at 1500 hours calculated using MET4.	127
6.47	Layer-average O_3 concentration at 1200 hours calculated using MET1. The dashed contour line shows the approximate location of the 0.12 ppm contour.	128

List of Figures (cont'd.)

Figure Number	Title	Page
6.48	Layer-average O_3 concentration at 1500 hours calculated using MET1.	128
6.49	Layer-average O_3 concentration at 1200 hours calculated using MET4. The dashed contour line shows the approximate location of the 0.12 ppm contour.	129
6.50	Layer-average O_3 concentration at 1500 hours calculated using MET4.	129
6.51	Scatter plot of observed and computed O_3 for September 30, 1980 with corrected inventory.	130
6.52	Scatter plot of observed and computed O_3 for October 1, 1980 with corrected inventory.	130
6.53	Observed surface O_3 concentrations at 1600 hours on October 1, 1980.	131
6.54	Computed surface O_3 concentrations at 1600 hours on October 1, 1980. The dashed contour line shows the approximate location of the 0.12 ppm contour.	131
6.55	Layer-average O_3 concentration at 1500 hours for the base case on September 30, 1980. The dashed contour line shows the approximate location of the 0.12 ppm contour.	132
6.56	Layer-average O_3 concentration at 1600 hours for the base case on September 30, 1980. The dashed contour line shows the approximate location of the 0.12 ppm contour.	132
6.57	Layer-average O_3 concentration at 1700 hours for the base case on September 30, 1980. The dashed contour line shows the approximate location of the 0.12 ppm contour.	133
6.58	Layer-average O_3 concentration at 1500 hours for the base case on October 1, 1980. The dashed contour line shows the approximate location of the 0.12 ppm contour.	133
6.59	Layer-average O_3 concentration at 1600 hours for the base case on October 1, 1980. The dashed contour line shows the approximate location of the 0.12 ppm contour.	134
6.60	Layer-average O_3 concentration at 1700 hours for the base case on October 1, 1980. The dashed contour line shows the approximate location of the 0.12 ppm contour.	134
6.61	Layer-average O_3 concentration at 1500 hours for the case with reduced NO_x on September 30, 1980. The dashed contour line shows the approximate location of the 0.12 ppm contour.	135
6.62	Layer-average O_3 concentration at 1600 hours for the case with reduced NO_x on September 30, 1980. The dashed contour line shows the approximate location of the 0.12 ppm contour.	135
6.63	Layer-average O_3 concentration at 1700 hours for the case with reduced NO_x on September 30, 1980. The dashed contour line shows the approximate location of the 0.12 ppm contour.	136

List of Figures (cont'd.)

Figure Number	Title	Page
6.64	Layer-average O_3 concentration at 1500 hours for the case with reduced NO_x on October 1, 1980. The dashed contour line shows the approximate location of the 0.12 ppm contour.	136
6.65	Layer-average O_3 concentration at 1600 hours for the case with reduced NO_x on October 1, 1980. The dashed contour line shows the approximate location of the 0.12 ppm contour.	137
6.66	Layer-average O_3 concentration at 1700 hours for the case with reduced NO_x on October 1, 1980. The dashed contour line shows the approximate location of the 0.12 ppm contour.	137
6.67	Time history for layer-average O_3 at San Jose, Morgan Hill and Gilroy. The solid line is the base case and the long dashed line is the reduced NO_x case.	138
6.68	Time history for layer-average O_3 at Hollister, Watsonville and Aptos (see caption for Figure 6.67).	139
6.69	Time history for layer-average O_3 at Salinas and Carmel (see caption for Figure 6.67).	140
6.70	Time history for layer-average O_3 at two grid points over the ocean with UTM coordinates (545,4130) and 560,4090), respectively. See caption for Figure 6.67.	141
6.71	Time history for surface ozone at San Jose, Morgan Hill and Gilroy for the base case with corrected inventory.	141
6.72	Time history for surface ozone at Hollister, Watsonville and Aptos for the base case with corrected inventory.	142
6.73	Time history for surface ozone at Salinas and Carmel for the base case with corrected inventory.	143

List of Tables

Table Number	Title	Page
2.1	Comparison of CRAY-CPU time usage.	8
2.2	Accuracy statistics for operator splitting technique with $\Delta t = 15$ minutes.	9
2.3	Accuracy statistics for operator splitting technique with $\Delta t = 10$ minutes.	10
2.4	Accuracy statistics for operator splitting technique with $\Delta t = 5$ minutes.	11
2.5	Accuracy statistics for operator splitting technique with $\Delta t = 2$ minutes.	12
2.6	Accuracy statistics for operator splitting with $\Delta t = 10$ minutes and double NO_x.	13
2.7	Accuracy statistics for operator splitting with $\Delta t = 10$ minutes and half NO_x.	14
3.1	Emission inventory summary for 1980 and 1987.	37
3.2	Light-duty vehicle trip end emission factors for 1980.	38
3.3	Percent contribution of vehicle miles traveled (VMT) by vehicle category.	38
3.4	1980 and 1987 total hydrocarbon (HC) and oxides of nitrogen (NO_x) emissions from mobile sources for Monterey, Santa Cruz and San Benito counties.	39
4.1	Observed maximum ozone concentrations in pphm on September 30 and October 1, 1980.	46
5.1	Species treated in Penner and Walton (1982) mechanism.	64
5.2	Updated reaction mechanism using 1986 rates.	66
5.3	Hydrocarbon species represented in Lurmann et al. (1987) mechanism.	69
6.1	Boundary conditions.	91
6.2	Statistics for judging mean concentration.	95
6.3	Statistics for judging concentration trends.	95
6.4	Statistics for judging prediction of concentration maxima.	96
A.1	1980 and 1987 mobile source inventory by 5 km UTM grid square for Monterey, Santa Cruz, and San Benito Counties.	152
A.2	Bay Area Air Quality Management District district emissions by source categories.	158
A.3	Bay Area Air Quality Management District district emissions by source categories.	160
A.4	Bay Area Air Quality Management District county emissions by source categories.	162
A.5	Monterey Bay Unified Air Pollution Control District county emissions by source categories.	180
B.1	Observed and predicted O_3 concentrations.	187

Chapter 1. Introduction and Background

The federal air quality standard for ozone is exceeded only infrequently in the Monterey Bay Unified Air Pollution Control District (MBUAPCD). These pollution episodes have generally been associated with meteorological conditions which could be transporting pollutants from the San Francisco Bay Area to the BAAPCD. Several such events were monitored during September and October 1980 (Dabbert, 1983).

During hearings on the 1982 Bay Area Ozone Plan Update the MBUAPCD expressed concerns that the air pollutants transported from the San Francisco Bay Area could be contributing to exceedances of ozone air quality standards in the Monterey District. A major concern was the fact that the Bay Area Ozone Plan strives to lower ozone concentrations in the Bay Area Air Quality Management District (BAAQMD) by control of hydrocarbons. Nitrogen oxides, the other major contributor to ozone formation, are not specifically singled out for reduction, although some reduction in their emissions may occur as a result of legislated control of automobile exhaust and other measures not specifically initiated by the BAAQMD. This BAAQMD hydrocarbon control strategy was based on models of ozone formation in the Bay Area which indicated that the local formation of ozone is actually inhibited by the presence of nitrogen oxides. As a result of this emissions strategy, it was suggested that the transport of Bay Area nitrogen oxide precursors to Monterey may be large enough to affect attainment of the one-hour State and Federal ozone standards in the Monterey area.

To address the issue of the importance of NO_x precursors to the generation of ozone when long range transport occurs, the Lawrence Livermore National Laboratory (LLNL), the BAAQMD, and the MBUAPCD have cooperated to develop an expanded and updated multi-layer photochemical transport model that is capabable of treating the inter-basin transport of the nitrogen oxide and hydrocarbon precursor pollutants and the photochemical formation and transport of ozone in the San Francisco and Monterey Bay areas. This new model is an extension and improvement of the earlier model used to simulate conditions in the San Francisco Bay Area. The development of an improved air quality model was the responsibility of LLNL and is fully documented in Chapter 2 of this report. To satisfy the goals of this study, a faster, but still accurate, solution technique, was implemented; the model used previously by the BAAQMD (the LIRAQ model) was used as a standard by which to judge speed and accuracy of the new solution technique. The model was also generalized to enable it to treat several layers. This was necessary in order to be able to simulate the storage of pollutants and ozone above the inversion for multi-day simulations. Finally, the model was expanded in horizontal extent. Other minor improvements included an improved calculation of vertical transport coefficients and the addition of spatially dependent deposition velocities. In addition, a processor was prepared which enables winds from the 3-dimensional MATHEW model (rather than from the previous 2-D MASCON model) to be used to provide the layer-average winds required by the new photochemical-transport model.

An emissions inventory for both basins was prepared by the BAAQMD. They were also responsible for assembling the meteorological data input to the MATHEW model and

for evaluating the adequancy of the generated wind fields. A description of the procedures used to develop the emissions inventory appears in Chapter 3, and a description of the meteorology during the two-day episode follows in Chapter 4.

The last major improvement to the model concerns the chemical mechanism. Originally, only the rate coefficients and photolysis rates in the mechanism used in the LIRAQ model (Penner and Walton, 1982) were updated. However, this procedure resulted in significantly lower predicted ozone concentrations. The Penner and Walton mechanism treated four hydrocarbon species. In particular, formaldehyde and all higher aldehydes were treated as a single, lumped species. Because the updated photolysis rates for acetaldehyde are much smaller than those of formaldehyde, it is no longer appropriate to treat both formaldehyde and the higher aldehydes as a single species. A series of smog chamber simulations were carried out to identify an adequate chemical mechanism that would properly simulate ozone formation. These tests, as well as simulation tests with the photochemical model, are described in Chapter 5.

The transport of pollutants from the Bay Area to the Monterey Area has been documented previously (Dabbert, 1983). Nine days were intensively studied, with tracer releases from a variety of locations providing specific evidence of transport. That study provided evidence of two major transport pathways–one down the Santa Clara Valley and one over-the-ocean route from Half Moon Bay. In this work, we have chosen to model one two-day episode from the intensive study period, September 30, 1980 through October 1, 1980. These days were chosen because evidence of both transport routes were available. In particular, on September 30, 1980, tracer releases of SF_6 and F13B1 indicated transport from San Jose to Hollister. In addition, significant ozone concentrations were observed over the Pacific Ocean due west of Moss Landing and Santa Cruz. Above average concentrations were traced following the coast line as far north as Pescadero. On October 1, no tracer releases were made, but the elevated offshore ozone concentrations which had been measured on the previous day were again noted as far north as San Pedro Point.

The model simulations for this meteorological period are presented in Chapter 6. Initial meteorological analysis and photochemical simulations did indeed confirm the presence of two areas of high ozone concentrations–one which follows the coastline southward and one which moves along the Santa Clara Valley. Using this initial meteorology, the predicted model concentrations for ozone in the Monterey area were excellent, except for the Hollister station. This area is one of convergence with some transport from offshore as well as some from the Santa Clara Valley (Unger and Neilson, 1983), and it is not clear whether the ozone peak registered at Hollister was the southernmost leg of the Santa Clara Valley high or was transported ozone from offshore. Further meteorological analysis was made to attempt to improve the Hollister ozone simulation. As discussed in Chapter 6, none of the meteorological simulations provided entirely satisfactory verification results, but due to constraints of time, we chose to evaluate the effect of emissions reductions on ozone using the meteorology that provided the best Hollister results. The adequacy of this analysis procedure is discussed in Chapter 6. A second performance evaluation with a source inventory corrected for an existing error in BAAQMD mobile source NO_x emissions is presented in Appendix B. As shown there, with the correct inventory, model results in the BAAQMD region are improved.

In order to evaluate the effect of the BAAQMD emissions control strategy, two sensitivity simulations were performed. These simulations involved (1) reduction of NO_x emissions by 30 percent and (2) reduction of anthropogenic hydrocarbon emissions by 30 percent. Each of these 30 percent reductions is an idealized assumption of the actual expected emissions control within the BAAQMD over the time period from 1980 to 1987. The separate test of NO_x reduction allows one to evaluate what might happen if the Bay Area were to actively seek to limit nitrogen oxide emissions (assuming control technology were available). The separate simulation for hydrocarbon control differentiates the effects of the current control strategy on Monterey ozone levels. Results from these sensitivity tests are discussed in Chapter 6.

Finally, Chapter 7 discusses our conclusions and recommendations. Interpretation of the results of this study is sensitive to details of the chemical mechanism and our lumped treatment of hydrocarbon chemistry. Some current uncertainties are appraised in Chapter 7 and their possible impact on our results are discussed. Recommendations are made for further study.

Chapter 2. Model Improvements

J. E. Penner
P. S. Connell
P. P. Weidhaas
D. J. Rodriguez
T. Umeda

A. Introduction

The first section of this chapter discusses the numerical procedures we tested in order to develop an acceptably accurate but acceptably fast numerical scheme. The original LIRAQ Gear solution technique is compared first to a method that uses the same transport differencing technique as that used in the LIRAQ model (i.e. upstream differencing), but uses operator splitting to separate the chemistry step from transport in the x- and y-directions. This comparison is used to evaluate a transport time step that gives accurate results in an operator splitting technique. Following this, we tested a finite element technique for transport. This technique is theoretically more accurate (it is fourth order accurate), but can introduce negative concentrations. The negative concentrations must be removed from the concentration fields by some smoothing or borrowing technique. This procedure, of course, is bound to decrease the accuracy of the overall method. The procedure we tested was purported to be highly accurate (McRae et al., 1982). In our simulations, however, we found results that were highly smoothed compared to those from the (theoretically) less accurate upstream differencing method. Therefore, the finite element method combined with the necessary filtering was judged inadequate for our situation. We then tested an upstream differencing method with an anti-diffusion correction. This technique, with operator splitting, was judged acceptable.

The next section discusses the general equations used in the multi-level model and the processing of MATHEW winds for input to the air quality model. The MATHEW model, with the option which accounts for separation of the flow fields above and below a variable-height inversion is described. Finally a few additional model improvements are described. These include the specification of spatially dependent deposition velocities and an improved calculation of the vertical mixing coefficient. Both improvements affect the calculation of vertical profiles within the mixed-layer and these changes are discussed in the last section.

B. Testing of numerical methods

The LIRAQ code developed by MacCracken et al. (1978) solved the pollutant transport and chemistry equation for species concentrations within the mixed-layer. This equation has the form

$$\frac{\partial c_k}{\partial t} = -\frac{c_k}{H}\frac{\partial H}{\partial t} - \frac{1}{\rho H}\frac{\partial}{\partial x}[\rho H u c_k] + \frac{1}{\rho H}\frac{\partial}{\partial x}[\rho K_{xx} H \frac{\partial c_k}{\partial x}]$$

$$- \frac{1}{\rho H}\frac{\partial}{\partial y}[\rho H v c_k] + \frac{1}{\rho H}[\rho K_{yy} H \frac{\partial c_k}{\partial y}] + \frac{S_k}{\rho H}$$
$$+ R_k(\underline{c}) - \frac{\rho w_H}{\rho H} c_{k,H}; k = 1, \ldots, p; \tag{2.1}$$

where $c_{k,H}$ is the concentration above the mixed-layer if w_H <0 or the concentration at the top of the mixed-layer if w_H >0. The term S_k refers to a time-dependent source and $R_k(\underline{c})$ to chemical reaction source and sink terms.

Equation (2.1) may be rewritten as

$$\frac{d\underline{y}}{dt} = F(\underline{y})\underline{y} \tag{2.2}$$

where $F(\underline{y})$ is a $n^2p \times n^2p$ block tridiagonal matrix and $\underline{y}$ is an n^2p vector:

$$\begin{bmatrix} [A_{11}]_{p\times p} & [T_{12}]_{p\times p} & & & \\ [T_{21}] & [A_{22}] & [T_{23}] & & \\ & & & & \\ & & & & \\ & & & & \\ & & & & \\ & & & & \\ & & & [T_{n^2-1,n^2}] & \\ & & [T_{n^2n^2-1}] & [A_{n^2n^2}] & \end{bmatrix} \underline{y} = \begin{bmatrix} c_1(1,1) \\ c_2(1,1) \\ \\ c_p(1,1) \\ c_1(2,1) \\ c_2(2,1) \\ \\ c_p(2,1) \\ \\ c_1(n,n^2) \\ c_2(n,n) \\ \\ c_p(n,n) \end{bmatrix}$$

Each diagonal $p \times p$ matrix $(A_{11}, \ldots, A_{n^2n^2})$ represents the chemical interactions among species as well as the source term and vertical flux terms ($-c/H \times dH/dt + w_H c/H$). Each off-diagonal $p \times p$ matrix $(T_{i,j})$ accounts for transport across a cell boundary. In the LIRAQ model, the transport terms in equation (2.1) were approximated by upstream differencing for the advection terms and centered differences for the diffusion terms. Thus, each single equation (there are n^2p equations) is represented by the difference equation (dropping the species subscript, k):

$$\frac{\partial c}{\partial t} = -\frac{c}{H}\frac{\partial H}{\partial t} - \frac{1}{\rho H \Delta x \Delta y}[\rho \Delta y H_{i+\frac{1}{2},j} u_{i+\frac{1}{2},j} c_{i,j} - \rho \Delta y H_{i-\frac{1}{2},j} u_{i-\frac{1}{2},j} c_{i-1,j}]$$
$$- \frac{1}{\rho H \Delta x \Delta y}[\rho \Delta x H_{i,j+\frac{1}{2}} v_{i,j+\frac{1}{2}} c_{i,j} - \rho \Delta x H_{i,j-\frac{1}{2}} v_{i,j-\frac{1}{2}} c_{i,j-1}]$$
$$+ \frac{1}{\rho \Delta y (\Delta x)^2 H}[\rho \Delta y H_{i+\frac{1}{2},j} K_{i+\frac{1}{2},j}(c_{i+1,j} - c_{i,j})$$

$$- \rho \Delta y H_{i-\frac{1}{2},j} K_{i-\frac{1}{2},j}(c_{i,j} - c_{i-1,j})]$$
$$+ \frac{1}{\rho(\Delta y)^2(\Delta x)H}[\rho \Delta x H_{i,j+\frac{1}{2}} K_{i,j+\frac{1}{2}}(c_{i,j+1} - c_{i,j}) - \rho \Delta y H_{i,j-\frac{1}{2}} K_{i,j-\frac{1}{2}}(c_{i,j} - c_{i,j-1})]$$
$$+ \frac{S}{\rho H_{i,j}} + R - \frac{\rho w_H c_{i,j}}{\rho H} \tag{2.3}$$

In equation (2.3), quantities with no subscript are assumed to be evaluted at the grid location (i,j).

In equation (2.3) we have assumed $u_{i,j} > 0$ and $v_{i,j} > 0$. Otherwise the x- and y-advection terms would have been represented by

$$x - advection: \quad -\frac{1}{\rho H \Delta x \Delta y}[\rho \Delta y H_{i+\frac{1}{2},j} u_{i+\frac{1}{2},j} c_{i+1,j} - \rho \Delta y H_{i-\frac{1}{2},j} u_{i-\frac{1}{2},j} c_{i,j}]$$

$$y - advection: \quad -\frac{1}{\rho H \Delta x \Delta y}[\rho \Delta x H_{i,j+\frac{1}{2}} c_{i,j+1} - \rho \Delta x H_{i,j-\frac{1}{2}} v_{i,j-\frac{1}{2}} c_{i,j}]$$

Equation (2.3) represents an ordinary differential equation amenable to solution by the Gear method (Hindmarsh, 1974). The extra factor of Δy has not been canceled from the x- and y-advection and x- and y-diffusion terms, because the quantities in brackets then correspond to mass fluxes that are developed by the MASCON model (Sherman, 1978).

In order to implement an operator splitting technique, the general scheme is adopted:

$$\begin{aligned} \frac{\partial c^*}{\partial t} &= L_x c^* \\ \frac{\partial c^{**}}{\partial t} &= L_y c^{**} \\ \frac{\partial c_c}{\partial t} &= R(c_c) + \frac{S}{\rho H} - \frac{\rho w_H}{\rho H} c_{c,H} - \frac{c_c}{H}\frac{\partial H}{\partial t} \end{aligned} \tag{2.4}$$

where we have used the definitions:

$$L_x c^* = -\frac{1}{\rho H}\frac{\partial}{\partial x}[\rho H u c^*] + \frac{1}{\rho H}\frac{\partial}{\partial x}[K_{xx} H \frac{\partial c^*}{\partial x}]$$

$$L_y c^{**} = -\frac{1}{\rho H}\frac{\partial}{\partial y}[\rho H v c^{**}] + \frac{1}{\rho H}\frac{\partial}{\partial y}[K_{yy} H \frac{\partial c^{**}}{\partial y}]$$

To solve equation (2.4), the initial conditions for c^* are given by $c(t)$, the initial condition for c^{**} are taken as c^*, etc. The final (chemistry) step in equation (2.4) is solved over the time step of $2\Delta t$, while the other steps are solved over the time step of Δt. After the chemistry step, the reverse sequence, solving first for the effects of L_y and then for the effects of L_x, is employed.

In the implementation of operator splitting employed by McRae et al. (1982), the advection terms were differenced according to a fourth order accurate finite element technique. (The upstream differencing technique employed in LIRAQ is only first-order accurate.) The chemistry step is solved using a predictor-corrector technique which only requires the storage of two previous values of concentration fields. The Gear technique requires up to six previous values if full advantage of its power is to be utilized. Thus the predictor-corrector technique is able to save on computer storage needs and is more amenable to use with an expanded grid model. The primary reason for using a predictor-corrector technique, however, is that the start-up costs in computer time are not as large as those in the Gear technique. For problems run for long time intervals, however, the Gear technique is superior. Because operator splitting requires that the chemistry step be restarted every $2\Delta t$ time step, a technique with low start-up costs is most appropriate.

Our first objective in testing the new numerical method, however, was to design an appropriate test of the operator splitting technique in order to compare it to a solution technique in which the chemical step and transport steps were fully coupled (e.g. as in equation (2.3)). Because the Gear implementation for the solution of equation (2.3) requires a simplified transport scheme (i.e. upstream differencing), we first implemented operator splitting using upstream differencing for the transport steps. This allowed a side-by-side comparison of operator splitting with a fully coupled method. Our tests of numerical accuracy and timing using upstream differencing are described in the next section.

C. Timing and accuracy tests for operator splitting with upstream differencing

As explained above, operator splitting involves solving separate equations with separate time steps for transport in the x- and y- directions as compared to the time steps needed to solve the chemistry terms and terms which describe the transport across the boundary between the mixed-layer and the free troposphere. One expects that the solution of the transport-kinetics equations using the operator-splitting technique will be close to the solution which is found with the fully coupled Gear technique, if the transport time step is adequately small. The purpose of our comparisons in this section is to define what is "adequately small" by direct comparison. The goal and hope is that a large advection time step will prove acceptable and that computer time usage will thereby be decreased.

Table 2.1 shows a comparison of the CRAY CPU times needed to integrate the model with the operator splitting technique using various advection time steps and the CPU time needed for solution of the same problem using the original LIRAQ model with the Gear technique. The Gear technique requires different amounts of CPU time depending on the particular time period being solved. For example, when the meteorology is updated at 1200 hours, the CPU-time per hour of simulation jumps from 25 seconds to 126 seconds. After two hours with the same meteorology fields, the CPU-time per hour of simulation has dropped to only 14 seconds. However, at the next update of meteorology (at 1500 hours), the integration time is increased again, from 14 seconds for the hour before to 97 seconds.

In contrast to the behavior of the Gear method described above, the operator splitting technique uses roughly the same CPU time per hour of integration, independent of history. For the smallest advection time steps, the cost of decreasing the time step is to increase the

Table 2.1

CRAY-CPU-times [sec]

		Operator-Splitting Time Step (min)				
Time	Comments	$\Delta t = 2$	$\Delta t = 5$	$\Delta t = 10$	$\Delta t = 15$	Gear
8:00	start-up	22.5	22.4	22.5	22.3	22.3
9:00	met-upd.†	157.4	65.5	36.9	31.2	124.2
10:00		161.0	68.7	45.5	44.2	139.4
11:00		158.8	66.2	45.3	45.8	15.9
12:00	met-upd.	157.4	65.8	45.3	45.1	24.7
13:00		159.4	68.3	44.9	43.0	126.0
14:00		157.8	65.7	40.3	36.7	17.0
15:00	met-upd.	157.0	65.7	38.9	33.1	14.1
16:00		160.1	67.2	39.2	32.0	96.8
17:00		159.5	67.0	42.0	33.2	26.0
Total (sec)		1,451.1	622.7	400.9	366.8	606.5

†These are times when the meteorology fields were updated so that the following hour required restarting the Gear technique with a small initial time step.

overall time almost linearly. Most of the computer time in the operator splitting technique is spent during the chemistry step, but apparently, at small advection time steps (Δt = 2 minutes and Δt=5 minutes), the time needed to solve the predictor-corrector chemistry step increases linearly with the advection time step. However, as the advection time step is relaxed, to 10 minutes or 15 minutes, the linear gains in time savings found for increasing from $\Delta t = 2$ minutes to $\Delta t = 5$ minutes are no longer realized. Thus, there is only a 10 percent savings in time found for increasing the time step by 50 percent, from 10 minutes to 15 minutes. We note that the overall run time for the Gear method is comparable to that for the operator splitting technique when an advection time step of 5 minutes is used. For a time step of 10 minutes, the operator splitting technique takes roughly two-thirds the CPU time required by the fully coupled Gear technique for a 9 hour simulation.

Although saving computer time was one of the primary reasons for testing the operator splitting technique, we also wanted to assure ourselves that the advection time step eventually used would also provide accurate results. Tables 2.2—2.5 compare the results from the operator splitting method with advection time steps of 15, 10, 5, and 2 minutes, respectively, with those of the Gear method. The tables compare results from the two techniques at 900, 1200, and 1500 hours. These tables summarize, for each species, the root mean square percentage error computed over the entire grid square, the maximum percentage error computed at any particular grid, the percentage error at the grid square with maximum concentration, the absolute error at that grid square, and the concentration in that grid square. The zone at which the maximum concentration was computed is also given.

One expects that as the advection time is decreased, the differences between the two solution methods would decrease. Eventually, if chemistry and transport are solved using

Table 2.2*

comparison of gear vs. operator-splitting; dt = 15 min

statistical summary for all species at 9.000e+00

species	rms pcnt diff	max pcnt diff	rel err at max	abs err at max	max conc	i	j
1	7.926e-01	-3.574e+00	-2.298e+00	-4.500e+10	1.958e+12	5	8
2	1.694e-01	7.994e-01	-2.749e-01	-4.000e+10	1.455e+13	5	8
3	2.694e-01	-1.049e+00	-8.361e-01	-3.000e+10	3.588e+12	5	8
4	1.228e+00	3.973e+00	-1.101e+00	-1.300e+10	1.181e+12	9	19
5	2.818e+00	1.648e+01	-1.699e+00	-6.700e+08	3.943e+10	5	8
6	3.135e+00	1.121e+01	-3.453e+00	-2.330e+09	6.747e+10	9	19
7	7.515e+00	5.591e+01	-6.705e+00	-7.000e+08	1.227e+10	9	19
8	3.147e+00	1.617e+01	-2.438e+00	-1.600e+11	6.564e+12	5	9
9	1.603e+00	-1.001e+01	-2.200e+00	-5.900e+10	2.682e+12	5	8
10	2.608e+00	3.619e+01	-4.568e-01	-1.000e+10	2.189e+12	11	20
11	5.613e-01	3.126e+00	-2.090e+00	-3.400e+12	1.627e+14	5	9
12	1.930e+00	8.027e+00	-2.315e+00	-6.200e+08	2.678e+10	20	13
13	5.271e+00	-2.090e+01	-9.434e-01	-3.300e+07	3.498e+09	9	19
14	4.777e+00	2.585e+01	-7.419e-01	-7.100e+06	9.570e+08	9	19
15	4.849e+00	2.780e+01	-2.469e+00	-7.100e+04	2.876e+06	16	14
16	5.553e+00	1.750e+01	-3.747e+00	-8.000e+05	2.135e+07	11	20
17	8.933e+00	-7.158e+01	1.235e+00	3.300e+06	2.673e+08	14	15
18	4.930e+00	2.629e+01	2.770e+00	7.200e+06	2.599e+08	1	20
19	4.889e+00	2.665e+01	-9.685e-01	-1.200e+07	1.239e+09	9	19
20	2.021e+00	1.103e+01	-3.854e+00	-7.600e+03	1.972e+05	5	8
21	2.638e+00	-1.087e+01	-2.522e+00	-1.860e+05	7.375e+06	19	11
22	2.531e+00	-1.165e+01	-2.009e+00	-1.350e+03	6.719e+04	5	8

statistical summary for all species at 1.200e+01

species	rms pcnt diff	max pcnt diff	rel err at max	abs err at max	max conc	i	j
1	1.444e+00	-5.201e+00	-1.655e+00	-1.310e+10	7.916e+11	5	12
2	5.662e-01	1.696e+00	-1.417e-01	-1.300e+10	9.175e+12	5	11
3	6.440e-01	-2.151e+00	-5.794e-01	-1.200e+10	2.071e+12	5	11
4	8.326e-01	1.920e+00	-5.126e-01	-1.000e+10	1.951e+12	5	12
5	8.110e+00	3.048e+01	-6.497e+00	-5.720e+08	8.804e+09	5	11
6	2.913e+00	5.645e+00	1.601e-01	6.000e+08	3.748e+11	14	15
7	6.983e+00	-2.808e+01	-3.328e-01	-2.600e+08	7.813e+10	9	18
8	8.749e+00	3.183e+01	-7.747e+00	-7.240e+10	9.346e+11	5	11
9	4.896e+00	1.511e+01	-1.834e+00	-7.600e+10	4.089e+12	5	11
10	1.443e+00	-4.901e+00	2.931e-01	1.600e+10	5.459e+12	14	15
11	7.598e-01	1.705e+00	-1.081e+00	-1.300e+12	1.203e+14	5	12
12	2.173e+00	9.993e+00	-3.840e-01	-7.000e+07	1.823e+10	8	12
13	4.843e+00	2.245e+01	2.011e+00	1.870e+08	9.301e+09	14	16
14	6.148e+00	-2.927e+01	-5.085e-01	-6.000e+06	1.180e+09	10	19
15	6.661e+00	-3.285e+01	7.964e-01	4.100e+04	5.148e+06	20	16
16	6.685e+00	3.207e+01	-3.894e+00	-3.390e+06	8.706e+07	14	15
17	1.134e+01	-8.087e+01	1.573e-01	3.000e+06	1.907e+09	5	13
18	6.904e+00	2.919e+01	-2.186e-01	-1.800e+06	8.233e+08	17	15
19	6.373e+00	-2.976e+01	9.844e-01	1.700e+07	1.727e+09	15	15
20	3.639e+00	1.735e+01	-2.019e+00	-8.600e+03	4.260e+05	5	11
21	3.131e+00	-1.598e+01	-1.324e+00	-1.260e+05	9.515e+06	11	2
22	2.920e+00	1.370e+01	-4.739e+00	-2.700e+03	5.698e+04	14	15

statistical summary for all species at 1.500e+01

species	rms pcnt diff	max pcnt diff	rel err at max	abs err at max	max conc	i	j
1	2.378e+00	6.983e+00	2.712e+00	1.280e+10	4.720e+11	9	19
2	4.839e-01	-1.909e+00	-1.020e-01	-7.000e+09	6.866e+12	8	15
3	8.188e-01	-3.017e+00	-8.507e-01	-1.100e+10	1.293e+12	8	15
4	7.888e-01	2.021e+00	3.427e-01	6.000e+09	1.751e+12	7	15
5	9.845e+00	2.283e+01	-3.133e-01	-7.000e+06	2.234e+09	8	8
6	4.001e+00	1.073e+01	4.773e+00	2.540e+10	5.322e+11	10	18
7	8.955e+00	-3.128e+01	1.800e+00	2.200e+09	1.222e+11	8	18
8	1.348e+01	3.208e+01	-2.361e+00	-4.600e+09	1.948e+11	8	8
9	8.833e+00	2.024e+01	-1.270e+01	-2.670e+11	2.103e+12	7	14
10	2.292e+00	-5.916e+00	3.400e+00	2.320e+11	6.823e+12	9	17
11	6.985e-01	-3.016e+00	0.	0.	8.803e+13	7	15
12	3.530e+00	-7.940e+00	5.090e+00	8.500e+08	1.670e+10	10	16
13	6.485e+00	1.969e+01	9.059e+00	1.020e+09	1.126e+10	7	16
14	1.541e+01	-3.259e+01	1.420e+00	1.310e+07	9.223e+08	9	19
15	1.170e+01	-3.768e+01	4.165e+00	1.140e+05	2.737e+06	19	18
16	7.240e+00	2.984e+01	7.763e+00	1.430e+07	1.842e+08	10	17
17	1.402e+01	-7.187e+01	-1.409e+00	-8.400e+07	5.962e+09	8	15
18	9.795e+00	2.695e+01	2.237e+00	1.730e+07	7.734e+08	20	18
19	1.078e+01	-3.374e+01	2.334e+00	3.400e+07	1.457e+09	7	17
20	5.641e+00	2.238e+01	-1.116e+01	-2.090e+04	1.872e+05	7	14
21	4.944e+00	-1.802e+01	2.381e-01	1.400e+04	5.880e+06	2	1
22	3.494e+00	-1.207e+01	2.428e+00	9.500e+02	3.913e+04	7	16

*See footnote on page 15

Table 2.3*

comparison of gear vs. operator-splitting; dt = 10 min

statistical summary for all species at 9.000e+00

species	rms pcnt diff	max pcnt diff	rel err at max	abs err at max	max conc	i	j
1	8.045e-01	-3.574e+00	-2.247e+00	-4.400e+10	1.958e+12	5	8
2	1.421e-01	-5.511e-01	-2.749e-01	-4.000e+10	1.455e+13	5	8
3	2.595e-01	-1.049e+00	-8.361e-01	-3.000e+10	3.588e+12	5	8
4	1.286e+00	3.936e+00	-1.101e+00	-1.300e+10	1.181e+12	9	19
5	2.578e+00	7.567e+00	-2.917e+00	-1.150e+09	3.943e+10	5	8
6	3.239e+00	1.117e+01	-3.483e+00	-2.350e+09	6.747e+10	9	19
7	7.339e+00	5.557e+01	-5.623e+00	-6.900e+08	1.227e+10	9	19
8	2.624e+00	-1.573e+01	-2.986e+00	-1.960e+11	6.564e+12	5	9
9	1.510e+00	-1.042e+01	-1.156e+00	-3.100e+10	2.682e+12	5	8
10	2.255e+00	2.387e+01	-6.396e-01	-1.400e+10	2.189e+12	11	20
11	5.520e-01	3.139e+00	-2.090e+00	-3.400e+12	1.627e+14	5	9
12	2.006e+00	8.054e+00	-2.315e+00	-6.200e+08	2.678e+10	20	13
13	4.563e+00	-1.633e+01	-1.115e+00	-3.900e+07	3.498e+09	9	19
14	4.025e+00	2.595e+01	-7.732e-01	-7.400e+06	9.570e+08	9	19
15	4.130e+00	2.791e+01	-1.599e+00	-4.600e+04	2.876e+06	16	14
16	4.947e+00	-1.528e+01	-3.185e+00	-6.800e+05	2.135e+07	11	20
17	8.310e+00	-7.147e+01	1.496e-01	4.000e+05	2.673e+08	14	15
18	4.190e+00	2.649e+01	-1.193e+00	-3.100e+06	2.599e+08	1	20
19	4.149e+00	2.668e+01	-9.685e-01	-1.200e+07	1.239e+09	9	19
20	1.647e+00	7.605e+00	-2.231e+00	-4.400e+03	1.972e+05	5	8
21	2.410e+00	8.404e+00	-2.807e+00	-2.070e+05	7.375e+06	19	11
22	2.299e+00	8.702e+00	-2.545e+00	-1.710e+03	6.719e+04	5	8

statistical summary for all species at 1.200e+01

species	rms pcnt diff	max pcnt diff	rel err at max	abs err at max	max conc	i	j
1	1.461e+00	5.495e+00	-1.023e+00	-8.100e+09	7.916e+11	5	12
2	3.807e-01	-9.983e-01	-7.629e-02	-7.000e+09	9.175e+12	5	11
3	5.263e-01	-1.523e+00	-3.380e-01	-7.000e+09	2.071e+12	5	11
4	7.405e-01	-1.852e+00	-1.281e+00	-2.500e+10	1.951e+12	5	12
5	7.375e+00	2.283e+01	-6.770e+00	-5.960e+08	8.804e+09	5	11
6	2.861e+00	-6.595e+00	2.401e-01	9.000e+00	3.748e+11	14	15
7	8.167e+00	-3.242e+01	-3.328e-01	-2.600e+08	7.813e+10	9	18
8	8.823e+00	2.668e+01	-7.319e+00	-6.840e+10	9.346e+11	5	11
9	5.825e+00	1.942e+01	-1.834e+00	-7.500e+10	4.089e+12	5	11
10	1.856e+00	-5.191e+00	4.580e-01	2.500e+10	5.459e+12	14	15
11	5.908e-01	-1.382e+00	-1.081e+00	-1.300e+12	1.203e+14	5	12
12	2.116e+00	-5.250e+00	1.810e+00	3.300e+08	1.823e+10	8	12
13	4.625e+00	1.656e+01	5.397e+00	5.020e+08	9.301e+09	14	16
14	7.110e+00	-2.238e+01	-8.475e-02	-1.000e+06	1.180e+09	10	19
15	7.761e+00	-2.419e+01	1.185e+00	6.100e+04	5.148e+06	20	16
16	5.683e+00	2.166e+01	-3.526e+00	-3.070e+06	8.706e+07	14	15
17	1.023e+01	-8.870e+01	2.412e+00	4.600e+07	1.907e+09	5	13
18	6.845e+00	-2.136e+01	4.980e-01	4.100e+06	8.233e+08	17	15
19	7.158e+00	-2.208e+01	1.506e+00	2.600e+07	1.727e+09	15	15
20	3.639e+00	1.398e+01	-1.878e+00	-8.000e+03	4.260e+05	5	11
21	2.948e+00	-1.192e+01	-1.272e+00	-1.210e+05	9.515e+06	11	2
22	2.507e+00	9.217e+00	-4.633e+00	-2.640e+03	5.698e+04	14	15

statistical summary for all species at 1.500e+01

species	rms pcnt diff	max pcnt diff	rel err at max	abs err at max	max conc	i	j
1	3.794e+00	1.227e+01	2.076e+00	9.800e+09	4.720e+11	9	19
2	4.541e-01	1.499e+00	-4.515e-01	-3.100e+10	6.866e+12	8	15
3	1.102e+00	3.192e+00	-1.779e+00	-2.300e+10	1.293e+12	8	15
4	6.457e-01	1.565e+00	4.569e-01	8.000e+09	1.751e+12	7	15
5	1.413e+01	3.779e+01	-1.209e+00	-2.700e+07	2.234e+09	8	8
6	5.641e+00	-1.303e+01	9.827e+00	5.230e+10	5.322e+11	10	18
7	1.500e+01	-4.989e+01	3.437e+00	4.200e+09	1.222e+11	8	18
8	2.046e+01	5.188e+01	-4.312e+00	-8.400e+09	1.948e+11	8	8
9	1.410e+01	3.689e+01	-1.992e+01	-4.190e+11	2.103e+12	7	14
10	3.967e+00	-1.093e+01	8.413e+00	5.740e+11	6.823e+12	9	17
11	6.389e-01	-3.248e+00	-4.544e-02	-4.000e+10	8.803e+13	7	15
12	5.311e+00	-1.243e+01	1.198e+01	2.000e+09	1.670e+10	10	16
13	9.032e+00	-2.137e+01	1.349e+01	1.519e+09	1.126e+10	7	16
14	1.590e+01	-3.777e+01	9.650e-01	8.900e+06	9.223e+08	9	19
15	1.761e+01	-4.141e+01	6.650e+00	1.820e+05	2.737e+06	19	18
16	8.324e+00	2.079e+01	1.602e+01	2.950e+07	1.842e+08	10	17
17	1.484e+01	-7.177e+01	-8.554e-01	-5.100e+07	5.962e+09	8	15
18	1.469e+01	-3.511e+01	2.909e+00	2.250e+07	7.734e+08	20	18
19	1.623e+01	-3.871e+01	5.559e+00	8.100e+07	1.457e+09	7	17
20	8.516e+00	2.063e+01	-1.629e+01	-3.050e+04	1.872e+05	7	14
21	6.961e+00	-1.519e+01	-3.401e-02	-2.000e+03	5.886e+06	2	1
22	4.407e+00	-9.693e+00	4.421e+00	1.730e+03	3.913e+04	7	16

*See footnote on page 15

Table 2.4*

comparison of gear vs. operator-splitting; dt = 5 min

statistical summary for all species at 9.000e+00

species	rms pcnt diff	max pcnt diff	rel err at max	abs err at max	max conc	i	j
1	8.199e-01	-3.695e+00	-2.196e+00	-4.300e+10	1.958e+12	5	8
2	1.347e-01	-5.511e-01	-2.749e-01	-4.000e+10	1.455e+13	5	9
3	2.613e-01	-1.070e+00	-8.082e-01	-2.900e+10	3.588e+12	5	8
4	1.278e+00	4.153e+00	-1.101e+00	-1.300e+10	1.181e+12	9	19
5	1.865e+00	-8.547e+00	-4.768e+00	-1.880e+09	3.943e+10	5	8
6	3.306e+00	1.184e+01	-3.335e+00	-2.250e+09	6.747e+10	9	19
7	8.115e+00	6.213e+01	-5.949e+00	-7.300e+08	1.227e+10	9	19
8	2.268e+00	-1.748e+01	-3.489e+00	-2.290e+11	6.564e+12	5	9
9	1.083e+00	-1.202e+01	1.156e+00	3.100e+10	2.682e+12	5	8
10	1.708e+00	1.166e+01	-8.680e-01	-1.900e+10	2.189e+12	11	20
11	5.475e-01	3.152e+00	-2.090e+00	-3.400e+12	1.627e+14	5	9
12	2.014e+00	8.566e+00	-2.353e+00	-6.300e+08	2.678e+10	20	13
13	4.104e+00	1.445e+01	-1.458e+00	-5.100e+07	3.498e+09	9	19
14	4.050e+00	2.890e+01	-9.822e-01	-9.400e+06	9.570e+08	9	19
15	4.201e+00	3.109e+01	-1.391e+00	-4.000e+04	2.876e+06	16	14
16	3.718e+00	-1.151e+01	-2.717e+00	-5.800e+05	2.135e+07	11	20
17	7.143e+00	-7.136e+01	-1.309e+00	-3.500e+06	2.673e+08	14	15
18	4.214e+00	2.951e+01	-5.310e+00	-1.380e+07	2.599e+08	1	20
19	4.205e+00	2.957e+01	-1.211e+00	-1.500e+07	1.239e+09	9	19
20	9.721e-01	-7.199e+00	6.085e-01	1.200e+03	1.972e+05	5	8
21	2.212e+00	9.093e+00	-2.685e+00	-1.980e+05	7.375e+06	19	11
22	2.008e+00	6.721e+00	-3.721e+00	-2.500e+03	6.719e+04	5	8

statistical summary for all species at 1.200e+01

species	rms pcnt diff	max pcnt diff	rel err at max	abs err at max	max conc	i	j
1	1.140e+00	-5.632e+00	-4.169e-01	-3.300e+09	7.916e+11	5	12
2	2.203e-01	-9.138e-01	-3.270e-02	-3.000e+09	9.175e+12	5	11
3	3.992e-01	-1.691e+00	-2.414e-01	-5.000e+09	2.071e+12	5	11
4	6.082e-01	1.793e+00	-1.640e+00	-3.200e+10	1.951e+12	5	12
5	4.719e+00	1.919e+01	-3.487e+00	-3.070e+08	8.804e+09	5	11
6	2.233e+00	5.176e+00	-1.201e+00	-4.500e+09	3.748e+11	14	15
7	5.119e+00	-1.602e+01	-6.656e-01	-5.200e+08	7.813e+10	9	18
8	4.359e+00	1.597e+01	-2.889e+00	-2.700e+10	9.346e+11	5	11
9	3.767e+00	1.422e+01	-1.296e+00	-5.300e+10	4.089e+12	5	11
10	9.121e-01	-2.061e+00	-1.649e-01	-9.000e+09	6.459e+12	14	15
11	4.623e-01	-1.382e+00	-1.081e+00	-1.300e+12	1.203e+14	5	12
12	1.271e+00	5.202e+00	8.777e-01	1.600e+08	1.823e+10	8	12
13	2.795e+00	1.112e+01	9.354e-01	8.700e+07	9.301e+09	14	16
14	3.285e+00	-1.258e+01	-8.475e-02	-1.000e+06	1.180e+09	10	19
15	3.579e+00	-1.431e+01	1.166e+00	6.000e+04	5.148e+06	20	16
16	3.180e+00	1.327e+01	-3.331e+00	-2.900e+06	8.706e+07	14	15
17	9.353e+00	-8.059e+01	-1.049e-01	-2.000e+06	1.907e+09	5	13
18	3.144e+00	1.238e+01	8.138e-01	6.700e+06	8.233e+08	17	15
19	3.163e+00	-1.297e+01	2.142e+00	3.700e+07	1.727e+09	15	15
20	2.145e+00	8.015e+00	-1.338e+00	-5.700e+03	4.260e+05	5	11
21	1.735e+00	-7.458e+00	-1.135e+00	-1.080e+05	9.515e+06	11	2
22	1.521e+00	6.181e+00	-3.861e+00	-2.200e+03	5.698e+04	14	15

statistical summary for all species at 1.500e+01

species	rms pcnt diff	max pcnt diff	rel err at max	abs err at max	max conc	i	j
1	2.008e+00	-5.787e+00	1.123e+00	5.300e+09	4.720e+11	9	19
2	3.474e-01	-1.297e+00	-2.913e-02	-2.000e+09	6.866e+12	8	15
3	6.953e-01	-1.897e+00	-6.187e-01	-8.000e+09	1.293e+12	8	15
4	4.466e-01	-1.312e+00	1.713e-01	3.000e+09	1.751e+12	7	15
5	8.048e+00	2.918e+01	3.581e-01	8.000e+06	2.234e+09	8	8
6	2.802e+00	-5.838e+00	4.115e+00	2.190e+10	5.322e+11	10	18
7	8.361e+00	-2.887e+01	1.882e+00	2.300e+09	1.222e+11	8	18
8	9.523e+00	2.824e+01	-8.214e-01	-1.600e+09	1.948e+11	8	8
9	7.514e+00	2.303e+01	-8.940e+00	-1.880e+11	2.103e+12	7	14
10	1.687e+00	-4.815e+00	-3.767e+00	2.570e+11	6.823e+12	9	17
11	6.037e-01	-3.326e+00	-1.022e-01	-9.000e+10	8.803e+13	7	15
12	2.664e+00	-6.522e+00	6.287e+00	1.050e+09	1.670e+10	10	16
13	4.558e+00	1.110e+01	7.194e+00	8.100e+08	1.126e+10	7	16
14	8.226e+00	-2.151e+01	4.988e-01	4.600e+06	9.223e+08	9	19
15	9.213e+00	-2.388e+01	5.979e+00	1.390e+05	2.737e+06	19	18
16	4.158e+00	1.264e+01	6.895e+00	1.270e+07	1.842e+08	10	17
17	1.200e+01	-7.165e+01	-2.298e+00	-1.370e+08	5.962e+09	8	15
18	7.428e+00	-1.959e+01	1.332e+00	1.030e+07	7.734e+08	20	18
19	8.287e+00	-2.198e+01	4.187e+00	6.100e+07	1.457e+09	7	17
20	4.330e+00	1.182e+01	-7.372e+00	-1.380e+04	1.872e+05	7	14
21	3.515e+00	-9.197e+00	-1.871e-01	-1.100e+04	5.880e+06	2	1
22	2.445e+00	-6.592e+00	2.632e+00	1.030e+03	3.913e+04	7	16

*See footnote on page 15

Table 2.5*

comparison of gear vs. operator-splitting; dt = 2 min

statistical summary for all species at 9.000e+00

species	rms pcnt diff	max pcnt diff	rel err at max	abs err at max	max conc	i	j
1	8.276e-01	-3.695e+00	-2.247e+00	-4.400e+10	1.958e+12	5	8
2	1.345e-01	-5.511e-01	-2.749e-01	-4.000e+10	1.455e+13	5	8
3	2.652e-01	-1.070e+00	-8.361e-01	-3.000e+10	3.588e+12	5	8
4	1.252e+00	4.153e+00	-1.016e+00	-1.200e+10	1.181e+12	9	19
5	1.616e+00	-8.633e+00	-2.587e+00	-1.020e+09	3.943e+10	5	8
6	3.261e+00	1.189e+01	-3.187e+00	-2.150e+09	6.747e+10	9	19
7	8.138e+00	6.248e+01	-6.438e+00	-7.900e+08	1.227e+10	9	19
8	2.267e+00	-1.750e+01	-2.818e+00	-1.850e+11	6.564e+12	5	9
9	1.033e+00	-1.221e+01	-8.949e-01	-2.400e+10	2.682e+12	5	8
10	1.274e+00	-4.365e+00	-9.137e-01	-2.000e+10	2.189e+12	11	20
11	5.466e-01	3.165e+00	-2.090e+00	-3.400e+12	1.627e+14	5	9
12	1.980e+00	8.593e+00	-2.353e+00	-6.300e+08	2.678e+10	20	13
13	3.833e+00	1.399e+01	-1.144e+00	-4.000e+07	3.498e+09	9	19
14	3.955e+00	2.884e+01	-1.484e+00	-1.420e+07	9.570e+08	9	19
15	4.101e+00	3.109e+01	-1.495e+00	-4.300e+04	2.876e+06	16	14
16	2.825e+00	-9.027e+00	-2.295e+00	-4.900e+05	2.135e+07	11	20
17	6.689e+00	-7.140e+01	-1.609e+00	-4.300e+06	2.673e+08	14	15
18	4.152e+00	2.958e+01	-7.811e+00	-2.030e+07	2.599e+08	1	20
19	4.098e+00	2.947e+01	-1.695e+00	-2.100e+07	1.239e+09	9	19
20	7.878e-01	-7.482e+00	-1.116e+00	-2.200e+03	1.972e+05	5	8
21	2.103e+00	9.182e+00	-2.685e+00	-1.980e+05	7.375e+06	19	11
22	1.853e+00	6.612e+00	-1.697e+00	-1.140e+03	6.719e+04	5	8

statistical summary for all species at 1.200e+01

species	rms pcnt diff	max pcnt diff	rel err at max	abs err at max	max conc	i	j
1	7.775e-01	-5.862e+00	-1.213e+00	-9.600e+09	7.916e+11	5	12
2	1.386e-01	-9.606e-01	-1.417e-01	-1.300e+10	9.175e+12	5	11
3	2.686e-01	-1.755e+00	-5.311e-01	-1.100e+10	2.071e+12	5	11
4	4.028e-01	-1.431e+00	-8.201e-01	-1.600e+10	1.951e+12	5	12
5	1.264e+00	4.587e+00	-2.010e+00	-1.770e+08	8.804e+09	5	11
6	1.573e+00	4.943e+00	-1.494e+00	-5.600e+09	3.748e+11	14	15
7	4.859e+00	1.117e+01	-1.190e+00	-9.300e+08	7.813e+10	9	18
8	1.184e+00	3.439e+00	-2.161e+00	-2.020e+10	9.346e+11	5	11
9	9.680e-01	3.757e+00	-1.418e+00	-5.800e+10	4.089e+12	5	11
10	6.595e-01	1.597e+00	-6.961e-01	-3.800e+10	5.459e+12	14	15
11	4.172e-01	-1.407e+00	-1.081e+00	-1.300e+12	1.203e+14	5	12
12	6.366e-01	1.944e+00	-6.583e-01	-1.200e+08	1.823e+10	8	12
13	1.816e+00	8.177e+00	-1.451e+00	-1.350e+08	9.301e+09	14	16
14	1.878e+00	8.999e+00	-3.390e-01	-4.000e+06	1.180e+09	10	19
15	1.880e+00	-7.478e+00	-5.245e-01	-2.700e+04	5.148e+06	20	16
16	1.855e+00	8.240e+00	-2.297e+00	-2.000e+06	8.706e+07	14	15
17	8.242e+00	-8.049e+01	-2.255e+00	-4.300e+07	1.907e+09	5	13
18	2.038e+00	7.574e+00	-1.227e+00	-1.010e+07	8.233e+08	17	15
19	1.847e+00	7.768e+00	1.737e-01	3.000e+06	1.727e+09	15	15
20	8.187e-01	2.974e+00	-1.408e+00	-6.000e+03	4.260e+05	5	11
21	8.200e-01	-4.653e+00	-1.019e+00	-9.700e+04	9.515e+06	11	2
22	8.018e-01	3.985e+00	-1.299e+00	-7.400e+02	5.698e+04	14	15

statistical summary for all species at 1.500e+01

species	rms pcnt diff	max pcnt diff	rel err at max	abs err at max	max conc	i	j
1	1.587e+00	-5.864e+00	6.356e-02	3.000e+08	4.720e+11	9	19
2	3.374e-01	-1.334e+00	2.476e-01	1.700e+10	6.866e+12	8	15
3	4.747e-01	-1.922e+00	7.734e-02	1.000e+09	1.293e+12	8	15
4	3.517e-01	-1.390e+00	0.	0.	1.751e+12	7	15
5	1.173e+00	5.026e+00	6.714e-01	1.500e+07	2.234e+09	8	8
6	8.379e-01	4.017e+00	-2.443e-01	-1.300e+09	5.322e+11	10	18
7	2.606e+00	9.269e+00	-1.637e-01	-2.000e+08	1.222e+11	8	18
8	2.062e+00	1.227e+01	5.133e-02	1.000e+08	1.948e+11	8	8
9	1.632e+00	8.932e+00	-1.331e+00	-2.800e+10	2.103e+12	7	14
10	3.982e-01	-2.348e+00	-4.397e-02	-3.000e+09	6.823e+12	9	17
11	6.332e-01	-3.384e+00	-7.952e-02	-7.000e+10	8.803e+13	7	15
12	8.792e-01	-5.005e+00	7.784e-01	1.300e+08	1.670e+10	10	16
13	1.609e+00	7.843e+00	3.552e-01	4.000e+07	1.126e+10	7	16
14	2.556e+00	-1.503e+01	1.952e-01	1.800e+06	9.223e+08	9	19
15	2.814e+00	-1.722e+01	7.307e-01	2.000e+04	2.737e+06	19	18
16	1.469e+00	7.586e+00	-2.172e-01	-4.000e+05	1.842e+08	10	17
17	9.365e+00	-7.159e+01	-1.929e+00	-1.150e+08	5.962e+09	8	15
18	2.151e+00	-1.291e+01	-3.103e-01	-2.400e+06	7.734e+08	20	18
19	2.600e+00	-1.578e+01	6.177e-01	9.000e+06	1.457e+09	7	17
20	1.173e+00	7.189e+00	-1.229e+00	-2.300e+03	1.872e+05	7	14
21	1.157e+00	-6.655e+00	-3.571e-01	-2.100e+04	5.880e+06	2	1
22	1.056e+00	-4.921e+00	3.833e-01	1.500e+02	3.913e+04	7	16

*See footnote on page 15

Table 2.6*

comparison of gear vs. operator-splitting; double nox

statistical summary for all species at 9.000e+00

species	rms pcnt diff	max pcnt diff	rel err at max	abs err at max	max conc	i	j
1	1.565e+00	-1.013e+01	-2.115e+00	-4.500e+10	2.128e+12	5	8
2	9.840e-01	-4.274e+00	-2.730e-01	-4.000e+10	1.465e+13	5	8
3	1.127e+00	-5.217e+00	-7.640e-01	-2.800e+10	3.665e+12	5	8
4	1.592e+00	7.312e+00	-3.343e+00	-3.500e+10	1.047e+12	9	19
5	3.593e+00	-2.433e+01	-4.969e+00	-1.700e+09	3.421e+10	5	8
6	3.666e+00	-1.715e+01	-9.879e+00	-3.920e+09	3.968e+10	9	19
7	1.283e+01	7.241e+01	7.430e-01	4.200e+07	5.653e+09	3	20
8	4.929e+00	-2.644e+01	-3.479e+00	-5.000e+11	1.437e+13	5	9
9	4.949e+00	-2.866e+01	2.934e+00	9.300e+10	3.170e+12	8	8
10	3.606e+00	3.870e+01	-1.242e+00	-2.600e+10	2.094e+12	15	14
11	9.826e-01	-4.333e+00	-1.963e+00	-3.200e+12	1.630e+14	5	9
12	2.642e+00	1.644e+01	-2.125e+00	-1.990e+08	9.366e+09	5	8
13	5.737e+00	2.654e+01	-7.436e+00	-2.370e+08	3.187e+09	9	19
14	6.835e+00	4.086e+01	-7.083e+00	-3.380e+07	4.772e+08	1	2
15	7.093e+00	4.257e+01	-7.559e-01	-1.400e+04	1.852e+06	1	20
16	6.555e+00	-2.239e+01	-6.960e+00	-1.280e+06	1.839e+07	15	14
17	9.555e+00	-5.547e+01	-5.419e+00	-7.500e+06	1.384e+08	11	20
18	7.063e+00	4.145e+01	-2.111e+00	-5.000e+06	2.368e+08	1	20
19	6.960e+00	4.169e+01	-6.362e+00	-4.710e+07	7.403e+08	1	2
20	3.104e+00	-1.498e+01	2.710e+00	6.300e+03	2.325e+05	8	8
21	4.023e+00	2.008e+01	-2.169e+00	-1.350e+05	6.225e+06	6	20
22	3.640e+00	-1.990e+01	-1.942e+00	-1.280e+03	6.591e+04	9	19

statistical summary for all species at 1.200e+01

species	rms pcnt diff	max pcnt diff	rel err at max	abs err at max	max conc	i	j
1	2.436e+00	1.317e+01	1.942e+00	2.200e+10	1.133e+12	5	12
2	1.946e+00	-6.105e+00	2.225e-01	2.100e+10	9.440e+12	5	11
3	1.894e+00	-6.118e+00	4.025e-01	9.000e+09	2.236e+12	5	11
4	4.153e+00	-2.183e+01	-6.580e+00	-9.600e+10	1.459e+12	5	12
5	1.141e+01	-4.955e+01	-1.941e+01	-7.810e+09	4.024e+10	5	11
6	1.145e+01	-5.269e+01	9.001e+00	1.920e+10	2.133e+11	11	20
7	2.125e+01	1.161e+02	4.428e+00	2.630e+09	5.939e+10	10	19
8	1.011e+01	-3.801e+01	-6.499e+00	-4.290e+11	6.601e+12	5	11
9	9.993e+00	-5.003e+01	6.054e+00	2.920e+11	4.823e+12	5	12
10	6.866e+00	-2.584e+01	2.648e-01	1.000e+10	3.777e+12	17	16
11	1.975e+00	-4.568e+00	-1.080e+00	-1.300e+12	1.204e+14	5	12
12	6.857e+00	-3.415e+01	-1.171e+01	-1.390e+09	1.187e+10	5	11
13	1.084e+01	-5.162e+01	-1.568e+00	-7.400e+07	4.718e+09	19	19
14	7.336e+00	-3.198e+01	1.013e+00	1.100e+07	1.086e+09	10	19
15	7.684e+00	-3.494e+01	1.359e+00	4.900e+04	3.605e+06	20	16
16	1.416e+01	-5.178e+01	-1.340e+00	-5.600e+05	4.178e+07	17	16
17	1.943e+01	-7.521e+01	2.425e+00	1.540e+07	6.350e+08	14	15
18	8.265e+00	-3.129e+01	-2.405e-01	-1.800e+06	7.484e+08	10	19
19	7.505e+00	-3.264e+01	1.434e+00	2.400e+07	1.674e+09	10	19
20	6.510e+00	-3.195e+01	6.254e+00	3.070e+04	4.909e+05	5	12
21	7.374e+00	-3.524e+01	-2.830e+00	-2.760e+05	9.754e+06	3	17
22	7.830e+00	-3.838e+01	-6.665e-01	-3.100e+02	4.651e+04	2	5

statistical summary for all species at 1.500e+01

species	rms pcnt diff	max pcnt diff	rel err at max	abs err at max	max conc	i	j
1	2.603e+00	-6.727e+00	1.393e+00	1.060e+10	7.610e+11	7	16
2	2.465e+00	-4.453e+00	8.292e-01	6.200e+10	7.477e+12	8	15
3	2.234e+00	-4.253e+00	1.538e+00	2.500e+10	1.625e+12	8	15
4	4.154e+00	-1.108e+01	-3.846e+00	-5.500e+10	1.430e+12	6	15
5	1.063e+01	3.207e+01	-9.024e+00	-1.110e+09	1.230e+10	7	14
6	1.428e+01	-3.995e+01	1.796e+00	5.100e+09	2.839e+11	7	17
7	1.942e+01	-4.643e+01	7.310e+00	7.880e+09	1.078e+11	9	19
8	1.494e+01	3.743e+01	-3.757e+00	-1.010e+11	2.688e+12	7	14
9	9.302e+00	-2.830e+01	1.310e+00	6.500e+10	4.960e+12	7	15
10	7.813e+00	-1.640e+01	2.666e+00	1.120e+11	4.201e+12	20	18
11	2.904e+00	-4.611e+00	9.066e-02	8.000e+10	8.824e+13	7	15
12	5.389e+00	-1.373e+01	3.569e+00	2.490e+08	6.976e+09	7	17
13	1.333e+01	-3.127e+01	5.889e+00	3.010e+08	5.111e+09	7	17
14	1.365e+01	-3.651e+01	2.807e+00	2.510e+07	8.943e+08	9	19
15	1.453e+01	-4.193e+01	3.347e+00	7.300e+04	2.181e+06	2	12
16	1.524e+01	-3.533e+01	5.272e+00	3.800e+06	7.208e+07	7	17
17	1.865e+01	-5.696e+01	1.001e+01	1.520e+08	1.518e+09	8	17
18	1.412e+01	-3.499e+01	3.743e+00	2.380e+07	6.358e+08	9	19
19	1.389e+01	-3.829e+01	2.914e+00	3.800e+07	1.304e+09	9	19
20	5.413e+00	-1.887e+01	2.247e+00	8.600e+03	3.828e+05	7	15
21	6.182e+00	-1.872e+01	-1.518e+00	-8.600e+04	5.665e+06	2	3
22	6.608e+00	-2.221e+01	2.238e+00	6.800e+02	3.038e+04	7	17

*See footnote on page 15

Table 2.7*

comparison of gear vs. operator-splitting: nair nox

statistical summary for all species at 9.000e+00

species	rms pcnt diff	max pcnt diff	rel err at max	abs err at max	max conc	i	j
1	1.918e+00	-8.233e+00	-1.623e+00	-2.700e+10	1.664e+12	5	8
2	1.057e+00	-4.264e+00	-2.091e-01	-3.000e+10	1.435e+13	5	8
3	1.268e+00	-5.531e+00	-5.785e-01	-2.000e+10	3.457e+12	5	8
4	2.183e+00	-5.446e+00	-3.016e+00	-5.200e+10	1.724e+12	5	8
5	4.016e+00	-2.203e+01	-1.159e+00	-3.000e+08	2.588e+10	5	9
6	5.653e+00	-1.598e+01	-6.301e+00	-6.900e+09	1.095e+11	14	15
7	1.104e+01	3.825e+01	-3.650e+00	-8.800e+08	2.411e+10	9	19
8	5.139e+00	-2.402e+01	1.105e+00	2.200e+10	1.991e+12	6	9
9	5.187e+00	-2.980e+01	-2.563e+00	-7.000e+10	2.731e+12	5	8
10	2.564e+00	8.984e+00	-2.186e+00	-6.100e+10	2.790e+12	14	15
11	9.901e-01	-4.333e+00	-1.904e+00	-3.100e+12	1.628e+14	5	9
12	2.573e+00	-1.189e+01	-1.139e+00	-4.900e+08	4.301e+10	5	8
13	5.917e+00	-2.744e+01	-4.406e+00	-2.960e+08	6.718e+09	14	15
14	4.387e+00	1.714e+01	-2.618e-01	-3.000e+06	1.146e+09	9	19
15	4.509e+00	1.754e+01	-1.340e+00	-7.900e+04	5.897e+06	20	13
16	6.023e+00	-2.829e+01	-3.959e+00	-1.440e+06	3.637e+07	14	15
17	1.174e+01	-8.816e+01	-1.400e+01	-5.480e+07	3.913e+08	5	7
18	5.189e+00	1.962e+01	-4.094e+00	-1.660e+07	4.055e+08	20	13
19	4.726e+00	1.765e+01	-2.863e-01	-4.000e+06	1.397e+09	9	19
20	2.410e+00	-1.118e+01	-4.148e+00	-8.500e+03	2.049e+05	5	8
21	3.348e+00	-1.954e+01	-2.031e+00	-1.360e+05	6.695e+06	2	9
22	3.205e+00	-1.968e+01	-2.283e+00	-2.140e+03	9.375e+04	5	8

statistical summary for all species at 1.200e+01

species	rms pcnt diff	max pcnt diff	rel err at max	abs err at max	max conc	i	j
1	2.738e+00	-1.012e+01	3.759e+00	2.120e+10	5.640e+11	10	19
2	2.055e+00	-6.339e+00	-1.167e-01	-1.000e+10	8.572e+12	5	11
3	2.128e+00	-6.636e+00	-5.208e-01	-9.000e+09	1.728e+12	5	11
4	3.089e+00	-1.925e+01	-7.274e-01	-1.700e+10	2.337e+12	5	12
5	1.149e+01	-2.177e+01	-1.005e+00	-2.100e+07	2.089e+09	14	2
6	1.045e+01	-5.116e+01	4.401e-01	3.100e+09	7.044e+11	5	12
7	1.303e+01	-3.640e+01	1.859e+00	2.500e+09	1.345e+11	14	15
8	1.207e+01	-3.516e+01	-5.743e+00	-5.800e+09	1.010e+11	14	2
9	1.144e+01	-4.454e+01	-1.263e+01	-1.550e+11	1.227e+12	5	11
10	4.470e+00	-2.044e+01	-1.075e+00	-8.600e+10	7.999e+12	9	11
11	1.986e+00	-4.567e+00	-9.992e-01	-1.200e+12	1.201e+14	5	12
12	4.855e+00	-2.594e+01	1.294e+00	4.200e+08	3.245e+10	5	11
13	9.447e+00	-4.630e+01	-5.521e-01	-1.400e+08	2.536e+10	5	12
14	6.819e+00	-2.660e+01	4.152e-01	6.000e+06	1.445e+09	14	15
15	7.425e+00	-2.839e+01	3.078e+00	2.370e+05	7.700e+06	8	12
16	9.860e+00	-4.800e+01	8.420e-01	1.700e+06	2.019e+08	5	12
17	1.876e+01	-9.191e+01	-1.101e+01	-5.270e+08	4.785e+09	5	11
18	7.266e+00	-2.249e+01	4.562e-01	4.400e+06	9.644e+08	3	7
19	6.570e+00	-2.654e+01	1.881e+00	4.500e+07	2.392e+09	8	12
20	6.121e+00	-2.228e+01	-9.416e+00	-1.580e+04	1.678e+05	5	11
21	5.946e+00	-2.983e+01	-2.374e+00	-2.310e+05	9.729e+06	10	2
22	6.438e+00	-3.444e+01	-1.839e-01	-1.500e+02	8.157e+04	5	11

statistical summary for all species at 1.500e+01

species	rms pcnt diff	max pcnt diff	rel err at max	abs err at max	max conc	i	j
1	4.367e+00	-1.208e+01	2.894e+00	1.700e+10	5.875e+11	9	19
2	2.810e+00	-4.514e+00	9.127e-01	5.700e+10	6.245e+12	8	15
3	3.131e+00	-4.343e+00	1.537e+00	1.560e+10	1.015e+12	10	16
4	3.317e+00	-9.745e+00	1.314e-01	2.000e+09	1.522e+12	7	15
5	9.906e+00	2.216e+01	1.120e-01	1.100e+06	9.823e+08	5	9
6	9.163e+00	-2.774e+01	-3.085e+00	-2.700e+10	8.753e+11	7	14
7	1.477e+01	-4.044e+01	4.055e+00	1.120e+10	2.762e+11	10	16
8	9.329e+00	2.274e+01	3.109e-01	1.600e+08	5.146e+10	5	9
9	8.410e+00	-2.761e+01	6.418e-01	4.700e+09	7.323e+11	5	9
10	4.438e+00	-1.176e+01	-1.749e+00	-1.610e+11	9.205e+12	7	15
11	2.930e+00	-4.648e+00	1.708e-01	1.500e+11	8.784e+13	7	15
12	3.412e+00	-1.478e+01	8.751e-01	1.100e+08	1.257e+10	12	18
13	8.036e+00	-3.051e+01	-8.704e-01	-9.000e+07	1.034e+10	11	18
14	4.750e+00	-2.904e+01	2.660e+00	3.000e+07	1.128e+09	7	16
15	5.557e+00	-3.108e+01	3.127e+00	1.890e+05	6.045e+06	10	14
16	8.831e+00	-3.142e+01	-4.994e+00	-1.180e+07	2.363e+08	7	14
17	1.854e+01	-8.710e+01	-5.937e+00	-1.140e+08	1.920e+09	11	18
18	4.690e+00	-2.433e+01	2.595e+00	3.200e+07	1.233e+09	10	14
19	4.580e+00	-2.904e+01	2.104e+00	4.100e+07	1.949e+09	7	16
20	4.151e+00	-1.389e+01	-4.703e+00	-3.710e+03	7.888e+04	5	9
21	4.911e+00	-1.867e+01	-1.402e+00	-7.800e+04	5.564e+06	10	2
22	5.079e+00	-2.294e+01	3.013e+00	1.000e+03	3.319e+04	5	9

*See footnote on page 15

The numbered species listed in Tables 2.2–2.7 refer to:

1. HC1
2. HC2
3. HC3
4. HC4
5. HNO_2
6. PAN
7. H_2O_2
8. NO
9. NO_2
10. O_3
11. CO
12. CH_3COCHO
13. HNO_4
14. RO_2
15. 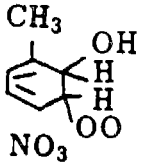

16. NO_3
17. N_2O_5
18. RCO_3
19. HO_2
20. $O(^3P)$
21. HO
22. RO

the same time step, the answers using the two techniques would be very close. As shown in the tables, there is a general convergence between the two solution techniques as the advection time step is decreased but the convergence rate is quite slow. This is illustrated in Figures 2.1 and 2.2. Figure 2.1 shows the root mean square difference between the operator splitting solution for O_3 and the Gear solution as a function of the advection time step used. A similar comparison for the difference in the maximum predicted O_3 between the two techniques is shown in Figure 2.2. As shown there, the differences between the two solution techniques decrease almost linearly as the advection time step is decreased from 10 minutes to 2 minutes. For O_3 the differences using $\Delta t = 15$ minutes are actually smaller than the differences with $\Delta t = 10$ minutes, but there is little reason to believe that that would remain true in all cases. There is little incentive to use a time step short enough to assure good accuracy over the entire grid, i.e. $\Delta t = 2$ minutes, because the cost is then high (see Table 2.1). McRae et al. (1982) recommended the use of a ten minute advection time step, and we have chosen that value for our studies as well.

In order to assure ourselves that a similar degree of accuracy is preserved for altered concentration conditions, we also explored two cases in which NO_x was doubled and halved using $\Delta t = 10$ minutes. Tables 2.6 and 2.7 show a comparison for accuracy for these cases.

Although the differences computed for some of the minor species are rather high, for most of the field, the results seem adequate. In particular, for the species whose concentrations are most important for verification (e.g., HC1, HC2, HC3, HC4, NO_2, NO, O_3, and CO) the errors in the maximum predicted concentration remain below 8.5 percent. Surprisingly, perhaps, operator splitting is at its worst for hydrocarbon to NO_x ratios typical of the Bay Area.

D. Installation of a finite element technique

In order to test timing and accuracy between the Gear solution technique and the operator splitting technique, it was necessary to use the same differencing procedures for the advection terms. This required the use of upstream differencing, because the Gear method was implemented with upstream differencing. However, the flexibility of operator splitting allows any of a broad range of advection differencing methods to be used. Thus it would seem appropriate to implement a scheme that is theoretically more accurate than upstream differencing. Upstream differencing is only accurate to first order. Thus, errors in the solution are expected to be proportional to the first derivative of the concentration. The advection differencing method used by McRae et al. (1982) is a finite element technique that uses linear basis functions. Because all horizontal grid spacings are identical, the finite element technique implemented by McRae et al. (1982) can be interpreted as essentially a finite difference technique. The advantage is that the method based on linear basis functions is fourth-order accurate in space. Thus, one expects the solutions to be significantly more accurate than with upstream differencing.

The essence of the finite element technique is to define all functions as a linear combination of basis functions. That is, to solve the advection equation:

$$\frac{\partial c}{\partial t} + \frac{1}{\rho H}\frac{\partial}{\partial x}(\rho H u c) = 0 \tag{2.5}$$

for each row j of our domain, we define the functions $c(x,t)$ and $\rho H(x,t)u(x,t)$ as a linear combination of the functions ϕ_i:

$$c_i = \sum_{i=i}^{N_k} \alpha_i \phi_i$$

$$\rho H_i u_i = \sum_{i=i}^{N_k} \beta_i \phi_i \tag{2.6}$$

where the basis functions ϕ_i are piecewise linear, and defined such that their value is 1 at x_i and 0 at all other grid points. With these simple functions, the coefficients α_i and β_i in equation (2.6), are easy to evaluate. We simply have $\alpha_i = c_i$ and $\beta_i = \rho H_i u_i$. In the finite-element Galerkin method a dot product between the basis functions and the advection equation is formed and required to vanish. This leads to a series of integrations over various basis functions. The final result is a set of relations between the c_i's and u_i's that must be satisfied in order to solve the advection equation. These relationships are given by the following equations:

$$\begin{aligned}
&\frac{1}{\Delta t}[(c_{i+1}^n - c_{i+1}^{n-1}) + 4(c_i^n - c_i^{n-1}) + (c_{i-1}^n - c_{i-1}^{n-1})] = \\
&\quad \frac{1}{\rho H_i 2\Delta x}[(\rho H_i u_i^{n-1} + 2\rho H_{i+1} u_{i+1}^{n-1})(c_{i+1}^n + c_{i+1}^{n-1}) \\
&\quad + (\rho H_{i+1} u_{i+1}^{n-1} - \rho H_{i-1} u_{i-1}^{n-1})(c_i^n + c_i^{n-1}) \\
&\quad - (\rho H_i u_i^{n-1} + 2\rho H_{i-1} u_{i-1})(c_{i-1}^n + c_{i-1}^{n-1})
\end{aligned} \tag{2.7}$$

Thus, we have formed a set of coupled linear equations that can be expressed in a tridiagonal matrix form ($\mathrm{A}\underline{c} = \underline{b}$) with the elements of the matrix A and vector $\underline{b}$ defined as:

$$\begin{aligned}
a_{i,i-1} &= [1 + \frac{\Delta t}{\rho H_i 2\Delta x}(\rho H_i u_i^{n-1} + 2\rho H_{i-1} u_{i-1}^{n-1})] \\
a_{i,i} &= [4 - \frac{\Delta t}{\rho H_i 2\Delta x}(\rho H_{i+1} u_{i+1}^{n-1} - \rho H_{i-1} u_{i-1}^{n-1})] \\
a_{i,i+1} &= [1 - \frac{\Delta t}{\rho H_i 2\Delta t}(\rho H_i u_i^{n-1} + \rho H_{i+1} u_{i+1}^{n-1})] \\
b_i &= -\frac{\Delta t}{\rho H_i 2\Delta x}[\rho H_i u_i^{n-1} + 2\rho H_{i-1} u_{i-1}^{n-1}] c_{i-1}^{n-1} \\
&\quad + \frac{\Delta t}{\rho H_i 2\Delta x}[\rho H_{i+1} u_{i+1}^{n-1} - \rho H_{i-1} u_{i-1}^{n-1}] c_i^{n-1} \\
&\quad + \frac{\Delta t}{\rho H_i 2\Delta x}(\rho H_i u_i^{n-1} + 2\rho H_{i+1} u_{i+1}^{n-1}) c_{i+1}^{n-1}
\end{aligned} \tag{2.8}$$

This system may be solved using standard techniques in a straightforward manner.

Unfortunately, although the finite element solution technique is theoretically more accurate, it is not positive definite, allowing the development of unphysical, negative concentrations. The accepted solution to this problem is to "filter" the concentration fields in some manner, in order to remove negative concentrations. We implemented the filtering scheme recommended by McRae et al. (1982). This scheme applies the following steps:

1. Set $\chi_\ell = 0$, $\ell = 1$, n_h (for each row of the solution domain).
2. Evaluate $S_e = sign\ (c_e - c_{e-1})$ for $e = j\text{-}4, \ldots, j, \ldots, j+5$. Here, we define

$$\begin{aligned} sign(c) = 1, &\quad \text{if } c/\mid c \mid > 0 \\ -1, &\quad \text{if } c/\mid c \mid < 0. \end{aligned} \tag{2.9}$$

3. Test if $S_j \times S_{j+1} < 0$ (if yes, c_j is an extremum).
4. If yes, test whether $S_{j+1}, \ldots, S_{j+5}$ are of the same sign and if $S_{j-1}, \ldots, S_{j-4}$ are of the same sign. If they are, leave $\chi_l = 0$. If they are not, set $\chi_{j-2}, \ldots, \chi_{j+2} = 1$.
5. Evaluate the kth iteration value of c_j, that is, c_j^k, by:

$$c_j^{k+1} = c_j^k + \frac{0.2}{2}\left[(c_{j+1}^k - c_j^k)(\chi_j + \chi_{j+1}) - (c_j^k - c_{j-1}^k)(\chi_j + \chi_{j-1})\right]^k \tag{2.10}$$

Steps 1 through 5 are repeated for 2 iterations if the local Courant number is less than 0.5 or for 3 iterations if the local Courant number is greater than 0.5.

Our initial implementation of the finite element scheme differed from the McRae et al. (1982) method outlined above because we included the diffusion term in the advection solution, followed by filtering of the resulting field. McRae et al. proposed that the advection step be carried out first, with appropriate boundary conditions, followed by filtering of the dispersive noise with diffusion. Then diffusion is applied to the filtered advected field. Thus the full solution is a three step process. We applied the filter recommended by McRae et al. on the field obtained after both advection and diffusion and found that the solution technique including filtering is more strongly diffusive than upstream differencing. This is illustrated in Figures 2.3–2.6. Figure 2.3 shows the ozone field at noon predicted by the Gear method with upstream differencing. This may be compared to the operator splitting method with no filter applied shown in Figure 2.4. Obviously, there is much more structure shown in the (theoretically) more accurate fields predicted by the finite element method. This unfiltered scheme, however, is not mass preserving, since in order to implement it, we simply set negative concentrations to zero. Figure 2.5 shows the noon ozone field computed using the McRae et al. filter applied after a combined advection and diffusion step. Peak concentrations are significantly reduced over those predicted using upstream differencing. Figure 2.6 shows the ozone field predicted when the McRae et al. filter is applied after the advection step, and then a diffusion step is applied to the filtered field. This solution is even more highly smoothed and appears totally unacceptable.

In view of the above findings, we implemented a third advection scheme, based on upstream differencing with an anti-diffusion step (Smolarkiewicz, 1983). This scheme is

simple to implement and is positive definite, so that negative concentrations are not produced. As we have implemented it, the scheme is second-order accurate, but the theoretical accuracy is easily extended to fourth-order by implementation of additional anti-diffusion steps. The method and our test results are described in the next section.

E. Upstream differencing with anti-diffusion

Smolarkiewicz (1983) describes a simple, low computational cost method of solution for the advection equation which is positive definite. The upstream differencing method used in the Gear solution implementation is desirable because it is positivie definite, but it is accompanied by artificial diffusion which is implicit in the numerical solution. The effects of this numerical diffusion can, however, be minimized by including a specific anti-diffusion step after the initial advection step. The form of the anti-diffusion step is identical to that of the initial advection step, but the advective velocity field is replaced by quantities which depend on the velocity, concentration gradient, and step size. Because these anti-diffusion velocities depend on concentration, the Crank-Nicholson approach would require the inversion of a different transport matrix for each species. For a first test, the anti-diffusion step was carried out using an explicit solution technique. The Courant condition on the time step for the anti-diffusion step is automatically satisfied if the condition is satisfied by the original field. Diffusive transport is then accomplished by a third explicit step on the corrected advective field.

The scheme is as follows:

1. Solve the system as before using upstream differencing but without the diffusion terms. The diffusion terms should be left in the boundary conditions. This results in a purely advected concentration field.

2. Calculate the "anti-diffusion" velocities (or fluxes) for each column (row) and species. The fluxes are given by

$$\tilde{T}_{i+\frac{1}{2}} = \mid T_{i+\frac{1}{2}} \mid (1 - \frac{\Delta t}{\rho H_i \Delta x \Delta y} \mid T_{i+\frac{1}{2}} \mid) \frac{c_{i+1} - c_i}{c_{i+1} + c_i + \epsilon}, \quad \text{where } \epsilon = 10^{-15} \qquad (2.11)$$

   where $T_i = (u/\rho H \Delta y)$. The first term on the right hand side is independent of concentrations and can be evaluated once and saved for use with each species equation.

3. The anti-diffused concentrations are then given by the expression

$$\begin{aligned} c_i' = c_i &- \frac{\Delta t}{2\rho H_i \Delta x \Delta y}((\tilde{T}_{i+\frac{1}{2}} + \mid \tilde{T}_{i+\frac{1}{2}} \mid)c_i + (\tilde{T}_{i+\frac{1}{2}} - \mid \tilde{T}_{i+\frac{1}{2}} \mid)c_{i+1}) \\ &+ \frac{\Delta t}{2\rho H_i \Delta x \Delta y}((\tilde{T}_{i-\frac{1}{2}} + \mid \tilde{T}_{i-\frac{1}{2}} \mid)c_{i-1} + (\tilde{T}_{1-\frac{1}{2}} - \mid \tilde{T}_{i-\frac{1}{2}} \mid)c_i) \end{aligned} \qquad (2.12)$$

   The boundary conditions for this step are simply zero flux conditions, that is, $\tilde{T}_{1/2} = \tilde{T}_{n+\frac{1}{2}} = 0$.

4. Steps 2 and 3 can be optionally repeated to increase the accuracy of the solution although more than one repetition apparently costs more in time than it yields in accuracy.

5. Eddy diffusion now operates on the correctly advected field to produce the final concentrations representing the advancement of one transport step. The explicit equation is

$$c_i^n = c_i^l + \frac{\Delta t}{\rho H_i \Delta x \Delta y}\left(K_{i+\frac{1}{2}}(c_{i+1}^l - c_i^l) - K_{i-\frac{1}{2}}(c_i^l - c_{i-1}^l)\right). \tag{2.13}$$

   Again a zero flux boundary condition is used, since diffusion at the boundaries has been accounted for in the first advection step.

Correcting the upstream differencing solution by an additional "anti-diffusion" step can also be applied in two or three dimensions.

This scheme was implemented in the air quality model. Figures 2.7 and 2.8 compare ozone concentration fields for 1500 hours obtained using the Gear solution with upstream differencing (Fig. 2.7) and using the operator splitting solution with advection treated by upstream differencing corrected by anti-diffusion. The ozone field produced using the Smolarkiewicz (1983) scheme is clearly less diffusive. The peak model concentration increases from less than 9×10^{12} cm^{-3} to more than 10×10^{12} cm^{-3}. Based on these comparisons, we adopted the anti-diffusion scheme for advection transport for use in the three dimensional transport-kinetics model.

F. Development of a multi-layer photochemical transport model

Equation (2.1) may be generalized in order to treat transport and chemical transformation within any arbitrary layer. Thus, the vertically integrated equation for the average concentration of species c in layer i is:

$$\begin{aligned}
&\frac{\partial(h_{i+1}-h_i)\overline{c}}{\partial t} + c(h_i)\frac{\partial h_i}{\partial t} - c(h_{i+1})\frac{\partial h_{i+1}}{\partial t} + \frac{\partial}{\partial x}(h_{i+1}-h_i)\overline{uc} \\
&\quad + \frac{\partial}{\partial y}(h_{i+1}-h_i)\overline{vc} + u(h_i)c(h_i)\frac{\partial h_i}{\partial x} - u(h_{i+1})c(h_{i+1})\frac{\partial h_{i+1}}{\partial x} \\
&\quad + v(h_i)c(h_i)\frac{\partial h_i}{\partial y} - v(h_{i+1})c(h_{i+1})\frac{\partial h_{i+1}}{\partial y} + w(h_{i+1})c(h_{i+1}) - w(h_i)c(h_i) \\
&\quad = \frac{\partial}{\partial x}(h_{i+1}-h_i)K_{xx}\frac{\partial c}{\partial x} + \frac{\partial}{\partial y}(h_{i+1}-h_i)K_{yy}\frac{\partial c}{\partial y} + R(h_{i+1}-h_i) \\
&\quad + K_{xx}(h_i)\frac{\partial c}{\partial x}\Big|_{h_{i+1}}\frac{\partial h_i}{\partial x} - K_{xx}(h_{i+1})\frac{\partial c}{\partial x}\Big|_{h_{i+1}}\frac{\partial h_{i+1}}{\partial x} + K_{yy}(h_i)\frac{\partial c}{\partial y}\Big|_{h_i}\frac{\partial h_i}{\partial y} \\
&\quad - K_{yy}(h_{i+1})\frac{\partial c}{\partial y}\Big|_{h_{i+1}}\frac{\partial h_{i+1}}{\partial y} \\
&\quad + K_{zz}(h_{i+1})\frac{\partial c}{\partial z}\Big|_{h_{i+1}} - K_{zz}(h_i)\frac{\partial c}{\partial z}\Big|_{h_i} + S_i/\rho - v_d c(h_i)
\end{aligned} \tag{2.14}$$

where h_i is the height of the bottom of layer i and h_{i+1} is the height of the top of layer i. In the LIRAQ model, the diffusion coefficients at h_i and h_{i+1} were set to zero and we will continue to assume that the terms that describe transport across levels due to diffusion are small. In addition, the previous mass transport model, MASCON, developed a vertical velocity which explicitly accounted for the rate of change of the mixed-layer depth, so that a separate evaluation of $-c(h_{i+1}) \times \frac{\partial h_{i+1}}{\partial t}$ was not necessary. That is, because of the way $w(h_{i+1})$ was computed by MASCON, it necessarily took account of $\frac{\partial h_{i+1}}{\partial t}$. Because MATHEW is not designed to account for this term, we have added an explicit evaluation of it to the new model. The final difference between our previous implementation of the solution to the general species transport and chemical transformation equation and the present one is the explicit inclusion of the cross-level transport terms:

$$u(h_i)c(h_i)\frac{\partial h_i}{\partial x} - u(h_{i+1})c(h_{i+1})\frac{\partial h_{i+1}}{\partial x} + v(h_i)c(h_i)\frac{\partial h_i}{\partial y} - v(h_{i+1})c(h_{i+1})\frac{\partial h_{i+1}}{\partial y}. \tag{2.15}$$

Previously, these terms were neglected.

In the present application, with two layers separated by the inversion at the top of the mixed-layer, such transport will be negligible (because $u(h_i)$, $u(h_{i+1})$, $v(h_i)$, and $v(h_{i+1})$ are small), but we have allowed for their inclusion in the code, so that the treatment of layers would remain as general as possible. This formulation is consistent with either a Lagrangian-type formulation wherein layer-depth may change throughout the integration period, or with a fixed-grid formulation wherein $h_{i+1} - h_i$ remains constant. Furthermore, the number of layers treated and their depth is completely arbitrary. Although, as described below, due to data limitations we have chosen to implement a two-layer version of the code for application to the San Francisco and Monterey Bay Areas, the model may be easily generalized to treat an arbitrary number of layers. In the applications described below, we chose to utilize mass-consistent wind fields developed by the MATHEW (Sherman, 1978) model to determine the transport of pollutant species. This model creates mass-consistent winds on a fixed Eulerian grid. Because we wished to retain a single equation to describe concentrations within a mixed-layer of varying depth (with time and space), it was necessary to develop a processor which would average the mass fluxes developed by MATHEW over the mixed-layer and second model layer. This processor is described in the next section.

To recapture the previous equation for layer-average concentrations within the mixed-layer, we simply replace $(h_2 - h_1)$ by H_1, (the mixed-layer depth), expand the differential term $\frac{\partial[(h_{i+1}-h_i)c]}{\partial t}$, and collect terms on the right hand side to obtain, for layer 1:

$$\frac{\partial \overline{c}}{\partial t} = -\frac{1}{H}\frac{\partial H_1}{\partial t}(\overline{c} - c(h_2)) + \frac{\partial}{\partial x}(H_1\overline{uc}) + \frac{\partial}{\partial y}(H_1\overline{vc}) + \frac{\partial}{\partial x}H_1K_{xx}\frac{\partial c}{\partial x}$$

$$+\frac{\partial}{\partial y}(H_1 K_{yy}\frac{\partial c}{\partial y})+\frac{u(h_2)}{H}\frac{\partial h_2}{\partial x}c(h_2)$$
$$+\frac{v(h_2)}{H_1}\frac{\partial h_2}{\partial y}c(h_2)-\frac{w(h_2)}{H_1}c(h_2)+R(\overline{c})+\frac{S}{\rho\cdot H_1}-\frac{v_d}{H_1}\cdot c(h_1) \tag{2.16}$$

For layer 2, we have:

$$\frac{\partial \overline{c}}{\partial t}=\frac{1}{H_2}\frac{\partial H_2}{\partial t}(\overline{c}-c(h_2))+\frac{\partial}{\partial x}(H_2\overline{uc})+\frac{\partial}{\partial y}(H_2\overline{vc})+\frac{\partial}{\partial x}H_2K_{xx}\frac{\partial c}{\partial x}$$
$$+\frac{\partial}{\partial y}(H_2K_{yy}\frac{\partial c}{\partial y})-\frac{u(h_2)}{H_2}\frac{h_2}{\partial x}c(h_2)-\frac{v(h_2)}{H_2}\frac{\partial h_2}{\partial y}c(h_2)+\frac{u(h_3)}{H_2}\frac{\partial h_3}{\partial x}\cdot c(h_3)$$
$$+\frac{v(h_3)}{H_2}\frac{\partial h_3}{\partial x}c(h_3)+\frac{w(h_2)}{H_2}c(h_2)-\frac{w(h_3)}{H_2}c(h_3)+R(\overline{c})+\frac{S}{\rho\cdot H_2} \tag{2.17}$$

where now $H_2=h_3-h_2$. The source term for layer 2, i.e. $S/(\rho\cdot H_2)$, of course, only includes sources whose emissions are directly injected above the mixed-layer. These include elevated emissions, when the mixed-layer depth is less than 100 m, or surface emissions, when the inversion is coincident with terrain. Elevated sources are fully injected into the mixed-layer, if its depth is greater than 150 m, and they are fractionally injected into layers 1 and 2, if the mixed-layer is between 100 and 150 m.

G. Development of the processor for MATHEW wind fields

The MATHEW model is designed to run with fixed vertical and horizontal grid resolution. However, as described above, the species transport and chemical interaction model is designed to solve the photochemical transport equation for an arbitrary number of layers with arbitrary depth. The depths of the layers vary with time and space. In order to use the MATHEW wind fields, we developed a processor that would average fluxes from the MATHEW model over the layers that are defined in the photochemical transport model. Such averaging must be accomplished in a manner that preserves the mass-continuity features of the original wind field. Here we present some examples of how the averaging for the species concentration model is accomplished.

The MATHEW model produces a three dimensional wind field that satisfies the mass-continuity equation:

$$\frac{\partial u}{\partial x}+\frac{\partial v}{\partial y}+\frac{\partial w}{\partial z}=0. \tag{2.18}$$

This equation holds at each grid location i, j, k, so that the fluxes entering i, j, k on each face are balanced by the sum of the fluxes out of the zone. If one averages the horizontal fluxes (u and v) over several zones in the vertical, mass continuity will continue to be preserved as long as all fluxes are accounted for.

In our processing of the MATHEW wind fields, we develop an average flux across a given horizontal face by averaging the values of u and v developed by MATHEW between

the levels i, j, k that define the air chemistry model levels. Because the depth of the air chemistry model levels are spatially varying, to be perfectly general one must be careful to include horizontal fluxes across boundaries that actually represent fluxes from one layer to the next. In the photochemical transport model, these fluxes become associated with a "vertical" flux. Thus, the appropriate average flux across face i for zone (i,j,k) would involve averaging the field u over the minimum of $h_{i-1,j,k}$ and $h_{i,j,k}$ to develop an average horizontal flux and accounting for the horizontal flux from min $(h_{i-1,j,k}, h_{i,j,k})$ to max $(h_{i-1,j,k}, h_{i,j,k})$ as a flux between layers.

The schematic shown in Figure 2.9 depicts our scheme.

TX(i,k) is the vertically averaged value of u over the minimum of $\{(H_{i-1,2} - H_{i-1,1}), (H_{i-1,2} - H_{i,1}), (H_{i,2} - H_{i,1}), (H_{i,2} - H_{i-1,1})\}$. TZE$(i-1,2)$ = TZW$(i,1)$ is then the vertically averaged value of u from $h_{i,2}$ to $h_{i-1,2}$. There are analogous fluxes in the y-direction. The fluxes TZE and TZW (for transport in the east/west direction) and TZN and TZS (for transport north and south) are used to compute

$$-\frac{u_i}{h_{i+1}-h_i}\frac{\partial h_i}{\partial x}c(h_i) - \frac{v(h_i)}{h_{i+1}-h_i}\frac{\partial h_i}{\partial y}c(h_i)$$
$$+\frac{u_{i+1}(h_{i+1})}{h_{i+1}-h_i}\frac{\partial h_{i+1}}{\partial x}c(h_{i+1}) + \frac{v_{i+1}}{h_{i+1}-h_i}\frac{\partial h_{i+1}}{\partial y}c(h_{i+1}) \qquad (2.19)$$

in the photochemical transport model while TX (for transport east and west) and TY (for transport north and south) are used to compute:

$$\frac{\partial}{\partial x}(h_{i+1}-h_i)\overline{u\cdot c} + \frac{\partial}{\partial y}(h_{i+1}-h_i)\overline{v\cdot c}. \qquad (2.20)$$

TZ are simply set equal to the MATHEW vertical fluxes across the interface between layers and are used to compute:

$$w(h_{i+1})c(h_{i+1}) - w(h_i)c(h_i). \qquad (2.21)$$

H. Wind field adjustment with an inversion

MATHEW is a three-dimensional, diagnostic wind field model that utilizes a variational analysis technique in adjusting an interpolated set of component velocities for mass consistency at the zonal (Δx by Δy by Δz) level (Sherman, 1978). The purpose of such an adjustment is to find a flow field that satisfies the kinematic boundary conditions on the earth's surface, responds to the temporal and spatial variations of an inversion surface topping the mixed-layer, meets the requirements for the conservation of mass in three dimensions, and fits (to a large extent) the observed winds from a preprocessing code.

The violation of mass conservation by the interpolated wind field is most noticeable along the lower surface of the model domain. Here, a credible representation of terrain

has been created by averaging the surface elevations over areas commensurate with the horizontal grid dimensions and then rounding the result to the nearest grid point level in altitude. Since the model terrain is a fixture in the calculations, care was taken initially to reproduce the important geographic features (such as valleys which might have served as conduits for the transport of airborne pollutants) by raising or lowering a selected number of terrain blocks by appropriate amounts.

Users of the model should always be mindful that MATHEW performs a minimal adjustment. This principle is expressed mathematically in the working equations: variations between U (the adjusted winds) and U^0 (the input winds) are minimized, in an integral least squares sense, subject to the constraint of mass consistency. It can readily be seen that our variational procedure is premised on a critical assumption—that the distribution of winds input the code closely represents the actual flow.

While MATHEW is basically an objective analysis tool, the user can control to a certain extent the outcome of an adjustment by overriding the model-generated values for the Gauss precision moduli (GPM). The GPM are global parameters that define the extent to which MATHEW is allowed to adjust the winds in the horizontal as opposed to the vertical direction. The default method of internally calculating the GPM assumes that mass moves freely in all directions under neutral atmospheric conditions. Since the mass flux is proportional to the area under consideration, we reason that the ratio of the areas of the vertical and horizontal cell faces provides the correct relative values for the GPM. This ratio is adjusted upwards or downwards to account for other stability classes. Because the cell aspect ratio is chosen partly as a function of terrain steepness and complexity, the values of the GPM implicitly include the necessary scale information. If indicated, more suitable GPM can be input to the model at the user's discretion.

Thus far, the description of MATHEW has focused on a version of the model that LLNL uses routinely for air quality assessments. However, for use in applications to the San Francisco and Monterey Bay Areas, we have introduced a material surface to simulate the capping effects of an inversion on the airflow. In effect, we have split the domain over two layers—a mixed (generally, a containment) layer and an upper layer acting as a reservoir both for "clean" air and pollutant mass depending on the temporal stage of the model simulation.

The generation of a regularized representation of an inversion surface is handled by a subsidiary code called INVERBAS. The process of building an inversion begins with the user creating an input file which contains mixing height estimates at arbitrary locations throughout the grid. The code then performs a simple inverse distance squared weighting to interpolate or extrapolate the data to a regular system of points which conforms spatially to MATHEW's horizontal grid. Interpolated values are based on the nearest three "observations," which are found by means of an expanding search radius. Once defined, the mixing height array is smoothed by passing the elements through a 9-point filter. The individual heights are then rounded to the nearest vertical grid level producing the final form for the inversion used by the model.

Winds along the inversion surface are set equal to zero. This condition is maintained throughout the adjustment by applying the boundary conditions $n \cdot U = 0$. With this specification, any mass exchange between the upper and lower layers is prohibited. (There

is an implied exchange over time given the upwards or downwards shift of the inversion from one input period to the next. Movement in this spatially variable surface is used to simulate the daytime growth of the boundary layer and the nighttime formation of a near-surface inversion.)

Sensitivity tests with this newest version of MATHEW have revealed an unexpected response to these conditions. Small slip velocities at the surface in combination with no-flow-through boundary conditions along vertical faces describing the inversion surface lead to a systematic and often severe reduction in the magnitudes of the mixed-layer winds. We have recently added a second option, $n \cdot \neq 0$ along the vertically-oriented panels of the inversion surface, which allows the transport of mass between layers. Importantly, the initial winds in the mixed-layer are reduced by a lesser amount when adjusted for mass consistency. The non-zero velocity components along the inversion surface are assigned through MEDIC, a preprocessing code used to develop the initial wind conditions in all three dimensions.

It is worthwhile mentioning again that the variational techniques in MATHEW are premised on the assumption that a reasonable first-guess field of wind velocities can be supplied by MEDIC. Attention to detail in the preparation of the extrapolated field is therefore critical. Because the number of surface and upper air wind observations is small in comparison to the total number of active nodes in the discretized domain, a spectrum of wind fields can be created, all of which are consistent with the measured data. For this reason, we rely heavily on the interpretive skills of an experienced meteorologist to determine the acceptability of the interpolated wind field. If necessary, MEDIC is rerun with an altered set of parameters to achieve a better representation of the physical state of the atmosphere.

A complete description of the methodology used in the construction of a wind field is beyond the scope of this report. However, users of the models are urged to read the relevant sections of our "User's Guide to the MATHEW/ADPIC Models" (Rodriguez, et. al., 1982). This guide includes a detailed description of the mathematical formalisms relating to MEDIC and MATHEW. Practical advice concerning the selection of input parameters (derived from the cumulative experience of long-term users of the models at LLNL) is also offered. Finally, the global consequences of given selections are discussed.

While the information in the user's guide is substantially correct, it refers only to the one-layer MATHEW and its supporting code MEDIC. Splitting the domain into separate layers, one on top of the other, forced us to re-evaluate our methods of data interpolation and wind field adjustment. As an outgrowth of this process, changes were made to both MEDIC and MATHEW. Previously we assumed that all surface data were collected in the mixed-layer. Consequently, the entire collection was used to define an array of reference velocities at a level near the lower boundary of the model. However, in the two-layer MATHEW, there are no restrictions concerning the emplacement of the inversion; it can either lie above or be coincident with the model terrain. We now disregard the data from towers situated above the inversion when interpolating the reference level velocities. These data are most likely representative of upper level, rather than boundary layer, wind conditions.

We have also changed our method of assigning grid point values in the upper layer. Before, assignments were based on height above ground level. For example, if a point in the upper layer was 500 m above the local terrain, the 500 m above-ground-level wind speeds and wind directions from the available profiles were used to determine a grid point velocity value. Now, however, all interpolations in the upper layer are relative to mean sea level. We believe this latter approach offers a more sensible portrayal of upper level winds. Finally, different GPM can be assigned to the upper and lower layers to reflect the different atmospheric stabilities affecting the parcel transports.

Figures 2.10–2.12 provide an example of how the winds in the mixed-layer are reoriented by a mass adjustment. Figure 2.10 shows the interpolated winds from MEDIC at 10 m above ground level. Figures 2.11 and 2.12 show the adjusted, layer-averaged velocity fields assuming $n \cdot U = 0$ and $n \cdot U \neq 0$ along the inversion surface. Averaging the interpolated, mixed-layer winds in the vertical would not produce a field substantially different from the one shown in Figure 2.10 because of our selection of certain parameters. In this situation, the wind directions were held constant in the vertical until they approached the inversion, at which point, they rapidly sheared to satisfy the conditions along this surface. Our choice of parameters acknowledges the fact that the surface data are more numerous than the upper air data and thus, in all likelihood, they better represent the local flow conditions in the mixed-layer. The influence of terrain is readily apparent in Figures 2.11 and 2.12. Points that lack a velocity vector indicate where in the grid the inversion and terrain heights are equal.

I. Other model improvements

Two other improvements were made to the new model. These included a provision for spatial dependence of deposition velocities and a more realistic method for determining K_z. Both these changes primarily impact the manner in which surface concentrations are related to layer-one average concentrations. This latter aspect of the new model has also been changed and is described in Chapter 6.

In the new model, the deposition velocity for each pollutant was specified in grid-by-grid spatial detail, whereas in the old LIRAQ model deposition velocity was a global parameter for each pollutant. In actuality, only ozone had sufficient observational data to warrant spatially varying its deposition velocity. Ozone deposition velocities were approximated for three general land classes within the Bay Area from data compiled by Sehmel (1980). The following table gives the deposition velocities for ozone over the land classes used in this model.

Ozone Deposition Velocities	
Land Class	Deposition Velocity cm s^{-1}
Water	0.005
Wet-lands	0.2
Land	0.66

The deposition rates for each 5 kilometer grid square were assigned by an area weighted averaging scheme of the above three land classifications.

An improved method for calculating K_z was installed in the MATHEW interfacing program. The original MASCON model used a formula that was valid only for neutral conditions. Thus the vertical eddy coefficient at 1 meter was

$$K_z = 400\overline{\nu}(1+1/7)\left\{\frac{1}{H}\right\}^{1/7} \text{ cm}^2\text{s}^{-1}$$

where $\overline{\nu}$ is the mean layer wind speed. For our mid-day high ozone wind speeds this method yielded K_z values between 400 and 600 $\text{cm}^2\ \text{s}^{-1}$ which is typical of stable and neutral atmospheric conditions. However, the atmosphere at mid-day during these high ozone days is generally considered to be unstable.

The improved method for computing K_z values was adapted from McRae et al. (1982). The method is summarized here.

The solar radiation classification was selected from the following table by using the expression for solar insolation, I,

$$I = (\text{cloud} - \text{factor})\ 1.99\cos(\nu_{zenith})\text{cal cm}^{-2}\text{min}^{-1}$$

where cloud-factor is the solar attenuation due to clouds and ν_{zenith} is the solar zenith angle for the particular simulation time.

Solar Radiation Classes	
Radiation Class	Solar Insolation (cal $\text{cm}^{-2}\text{min}^{-1}$)
Strong	$I > 1.0$
Moderate	$0.5 \leq I \leq 1.0$
Slight	$I \leq 0.5$

Given the wind speed data and the solar radiation class, Pasquill stability classes are assigned by using the following table:

Wind Speed at 10 m (m s^{-1})	Daytime Solar Radiation			Nighttime Cloud Cover	
	Strong	Moderate	Slight	$\geq 4/8$	$\leq 3/8$
<2	A	A–B	B	E	
2–3	A–B	B	C	E	F
3–5	B	B–C	C	D	E
5–6	C	C–D	D	D	D
>6	C	D	D	D	D

The selected Pasquill stability class was used to determine the inverse Monin-Obukhov length $\frac{1}{L} = a + b\log_{10}(z_0)$, where z_0 is the surface roughness and the parameters a and b are given by the following table.

Pasquill Stability Class	Coefficients a	b
A	−.096	.029
A–B	−.067	.029
B	−.037	.029
B–C	−.020	.024
C	−.002	.018
C–D	−.001	.009
D	.0	.0
E	.004	−.018
F	.035	−.036

Spatially varying surface roughness terms were used which represented three different area types.

Area Type	Surface Roughness (m)
Water	10^{-4}
Wet-lands	10^{-1}
Low density residential or tree covered areas	1

For each 5 km grid square an area weighted average among the above three land types was used to compute its actual surface roughness value.

Once the Monin-Obukhov length is determined, the friction velocity, u_*, is computed via

$$u_* = \frac{k v(z_r)}{\int_{z_0}^{z_r} \psi_m \left\{\frac{z}{L}\right\} \frac{dz}{z}}$$

where k is von Karman's constant (0.4), z_r is the wind measurement height (10 meters), $v(z_r)$ is the wind speed at z_r, and ψ_m is a empirically derived function. To prevent very small values of K_z, in our evaluation of u_*, values of $v(z_r)$ less than 1 m s^{-1} are replaced by 1 m s^{-1}. The expressions for $\int_{z_0}^{z_r} \psi_m \left\{\frac{z}{L}\right\} \frac{dz}{z}$ are given in Table 4.3 of McRae et al. (1982) and will not be repeated here.

Finally, the surface layer eddy diffusion coefficient is computed from the Monin-Obukhov similarity theory by:

$$K(z) = \frac{k u_* z}{\psi_p \left\{\frac{z}{L}\right\}}$$

where ψ_p accounts for the buoyancy effect, as did ψ_m above, and is given as follows:

$$\psi_p \left\{ \frac{1}{L} > 0(\text{stable}) \right\} = .74 + 4.7 \frac{z}{L}$$

$$\psi_p \left\{ \frac{1}{L} = 0(\text{neutral}) \right\} = .74$$

$$\psi_p \left\{ \frac{1}{L} < 0(\text{unstable}) \right\} = .74 \left\{ 1 - 9 \frac{z}{L} \right\}^{-1/2}$$

The differences between the old MASCON method and the current method are quite significant. Values of K_z at 1 meter now range from 300 to 2000 $cm^2\ s^{-1}$, values considered appropriate to the stability classes which occur on ozone days. The resulting "surface" ozone simulations show much better agreement with observed values.

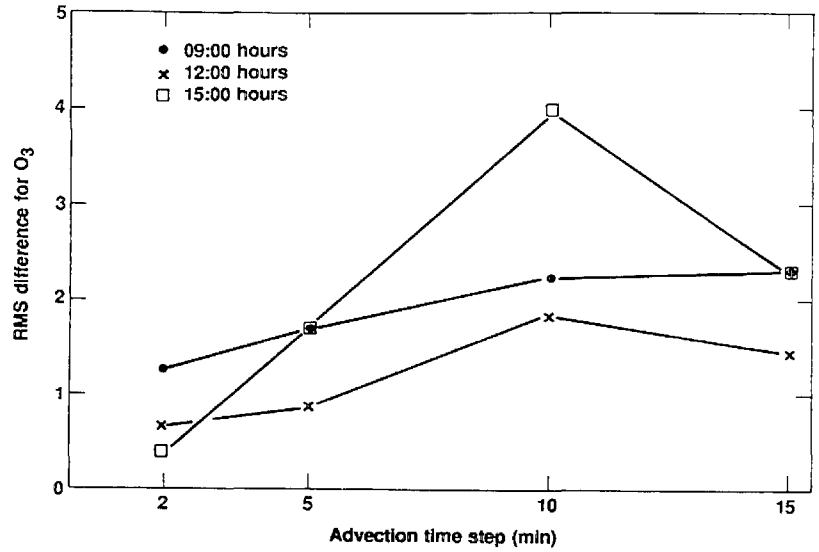

Figure 2.1. RMS difference for O_3 plotted as a function of the operator splitting advection time step.

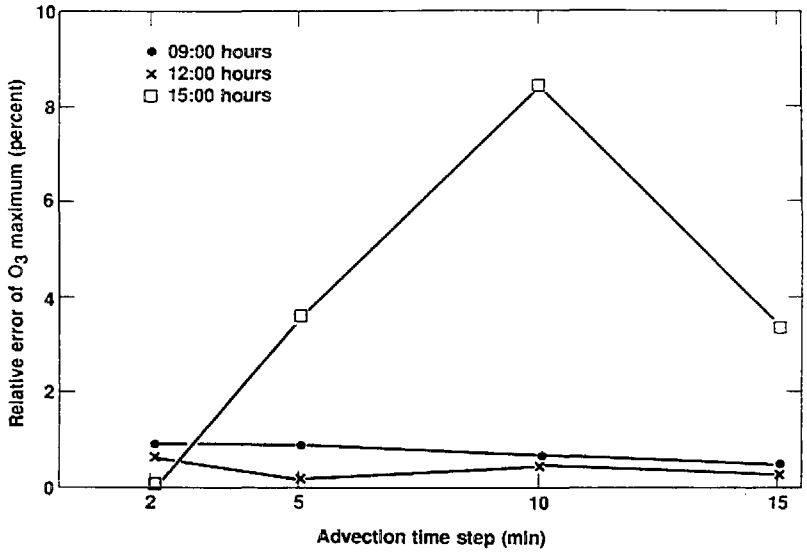

Figure 2.2. Relative error of O_3 maximum plotted as a function of the operator splitting advection time step.

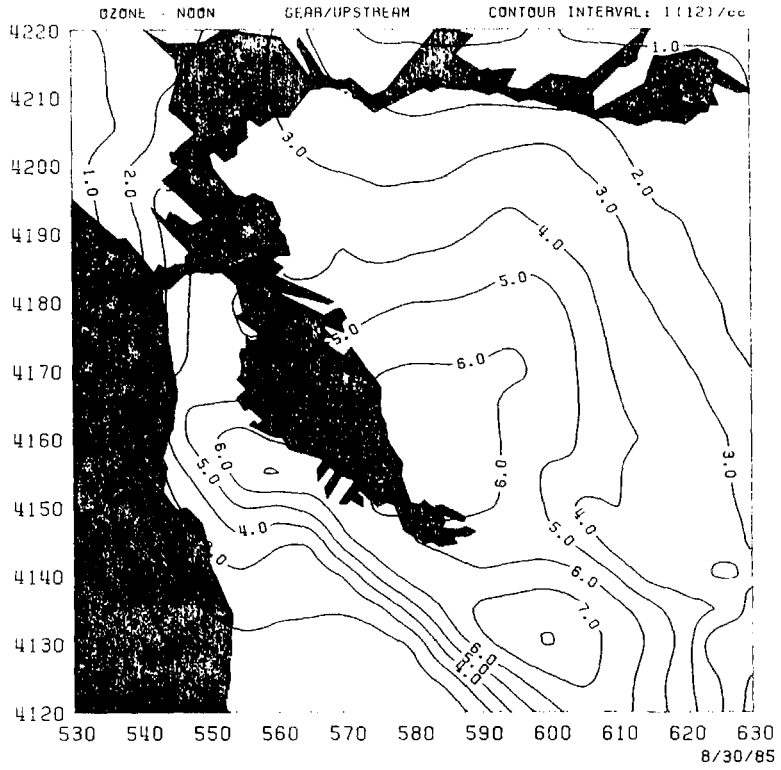

Figure 2.3. O_3 field at noon predicted using the Gear method with upstream differencing.

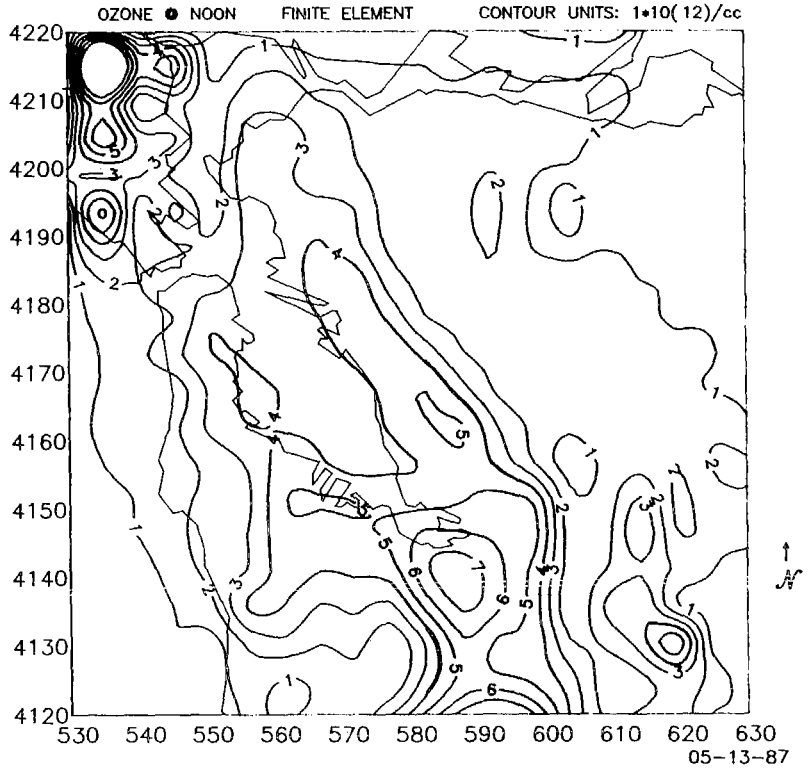

Figure 2.4. O_3 field at noon predicted using the finite element method with operator splitting and no filter.

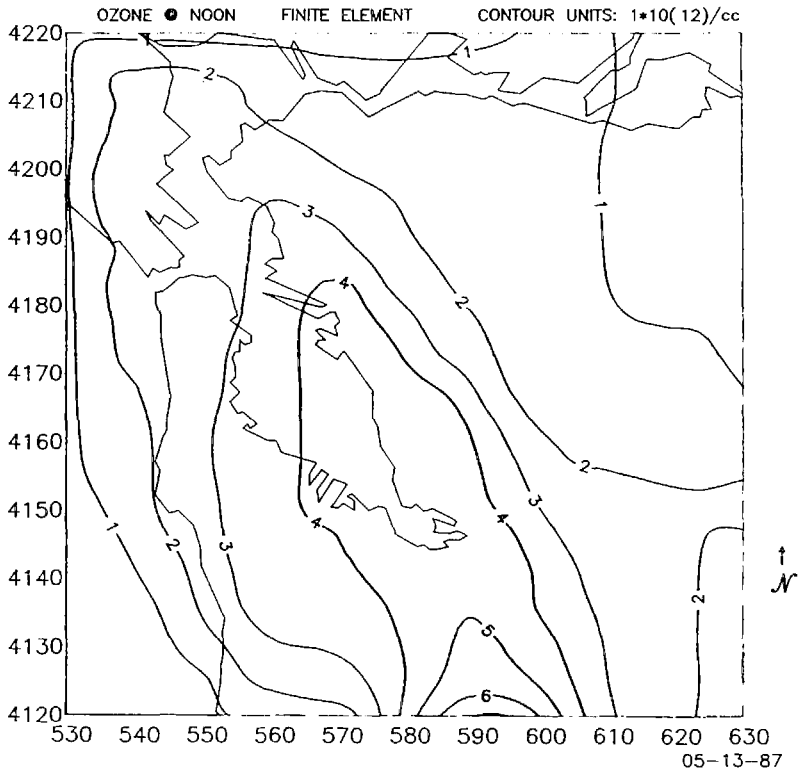

Figure 2.5. O_3 field at noon predicted using the finite element method with operator splitting and the filter recommended by McRae et al. (1982) applied after a combined advection and diffusion step.

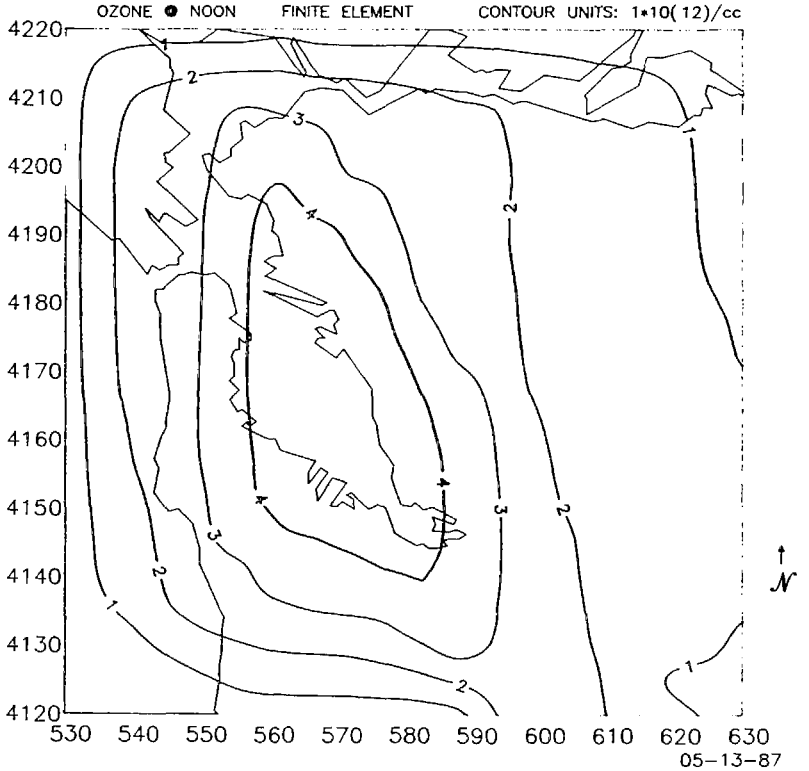

Figure 2.6. O_3 field at noon predicted using the finite element method with operator splitting and the filter recommended by McRae et al. (1982) applied after the advection step.

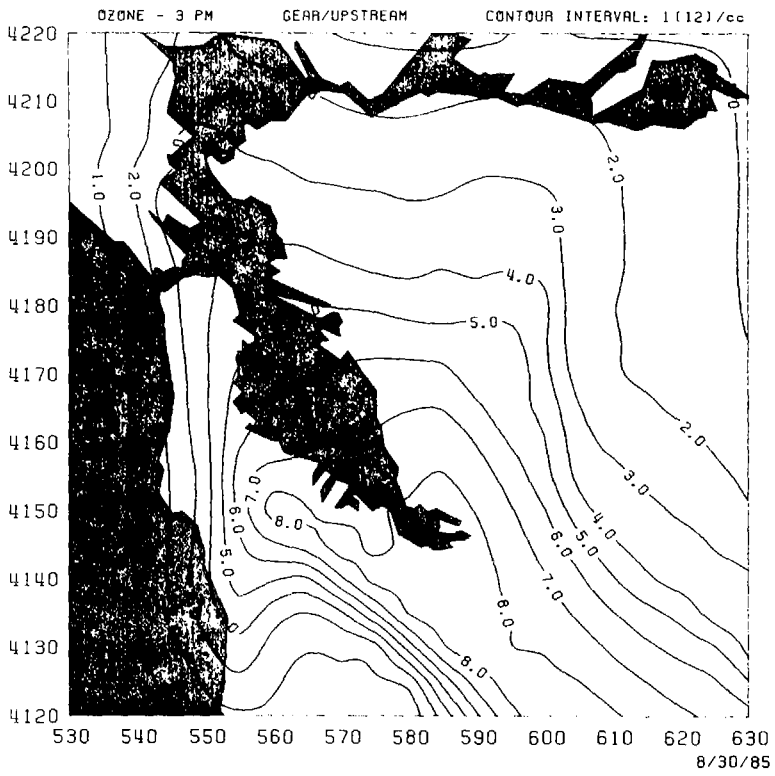

Figure 2.7. O_3 concentration predicted at 1500 hours using the Gear solution with upstream differencing.

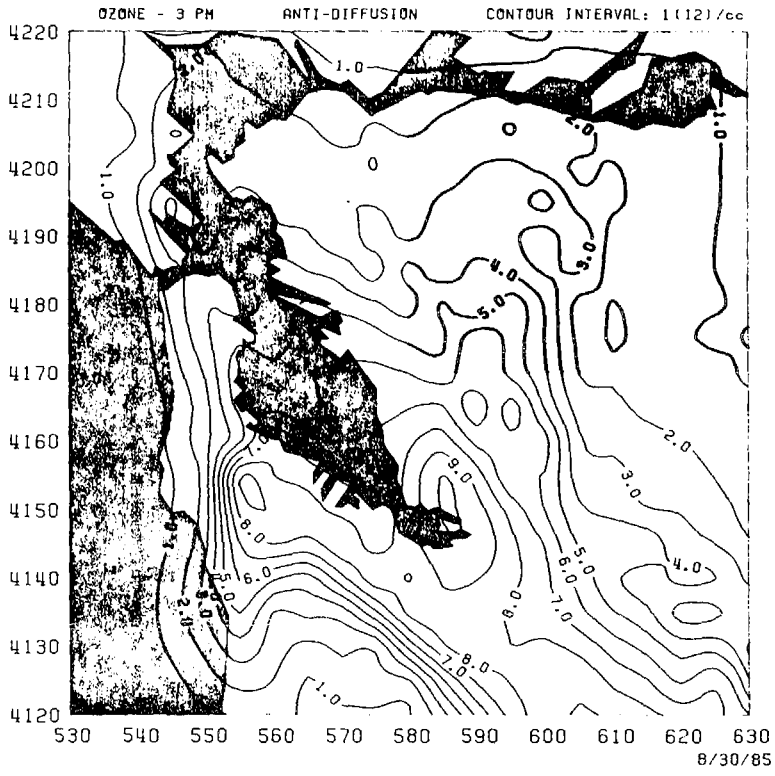

Figure 2.8. O_3 concentration predicted at 1500 hours using operator splitting with upstream differencing corrected by anti-diffusion.

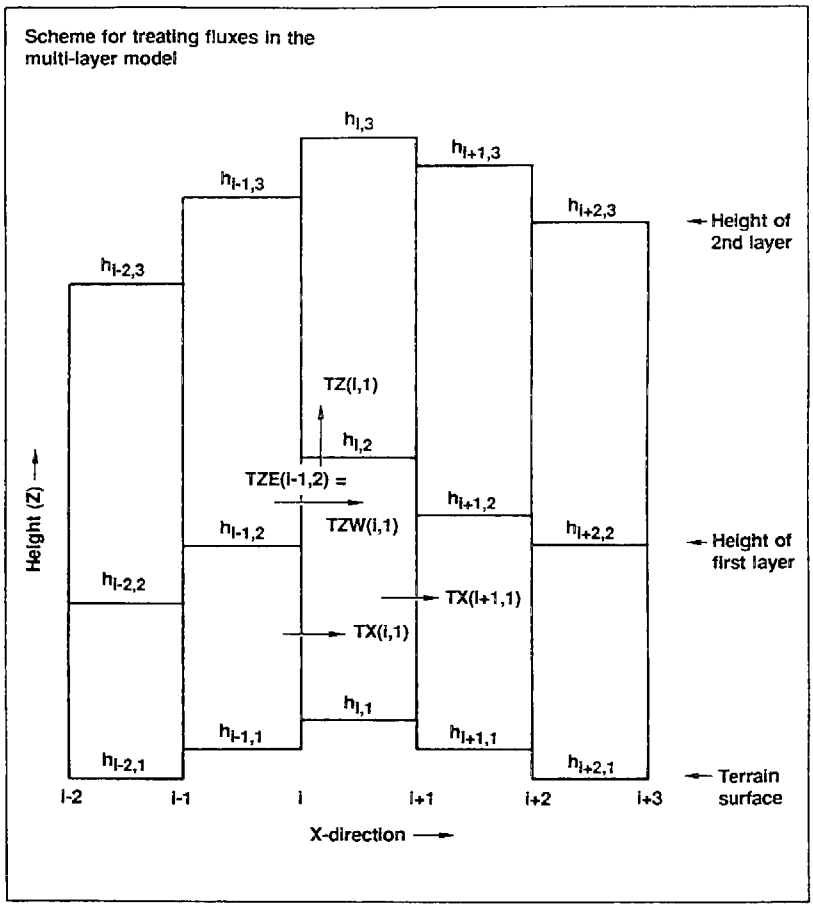

Figure 2.9. Scheme for treating vertical fluxes in the multi-layer model.

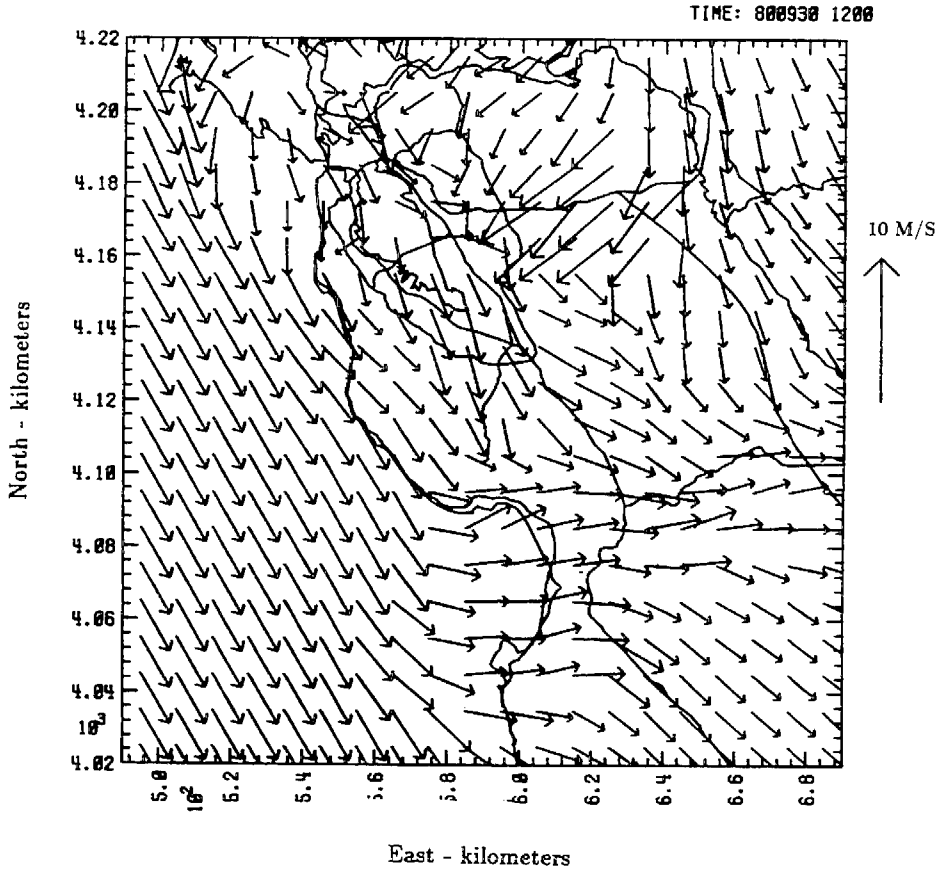

Figure 2.10. Interpolated wind fields from MEDIC.

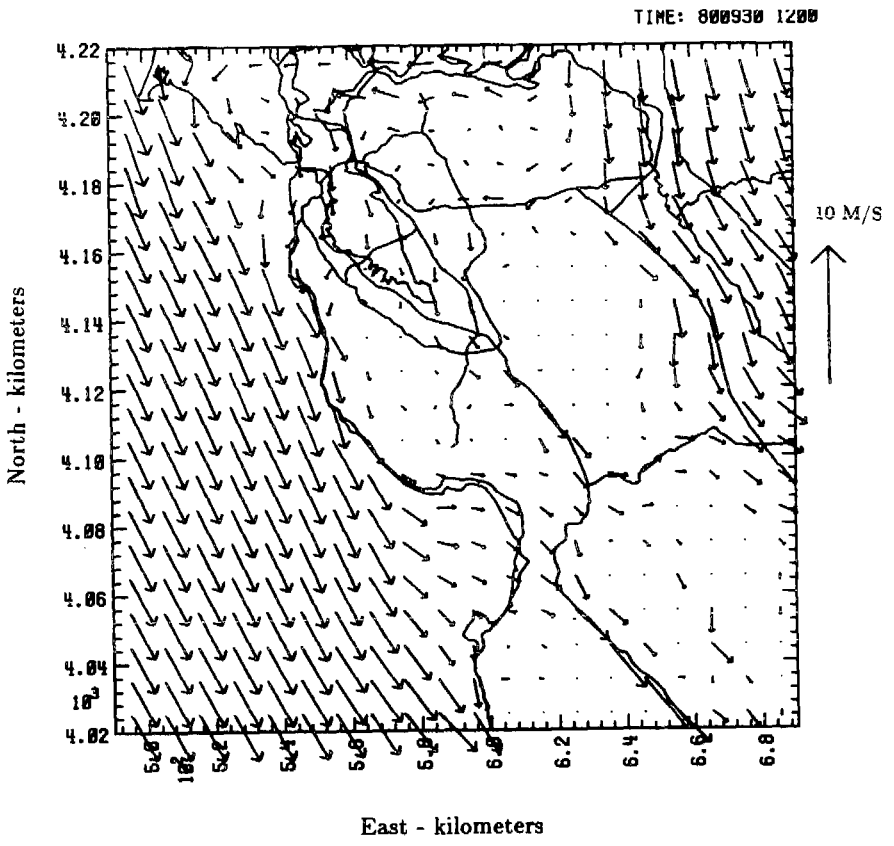

Figure 2.11. Adjusted layer-average wind fields assuming $n \cdot u = 0$ along the inversion surface.

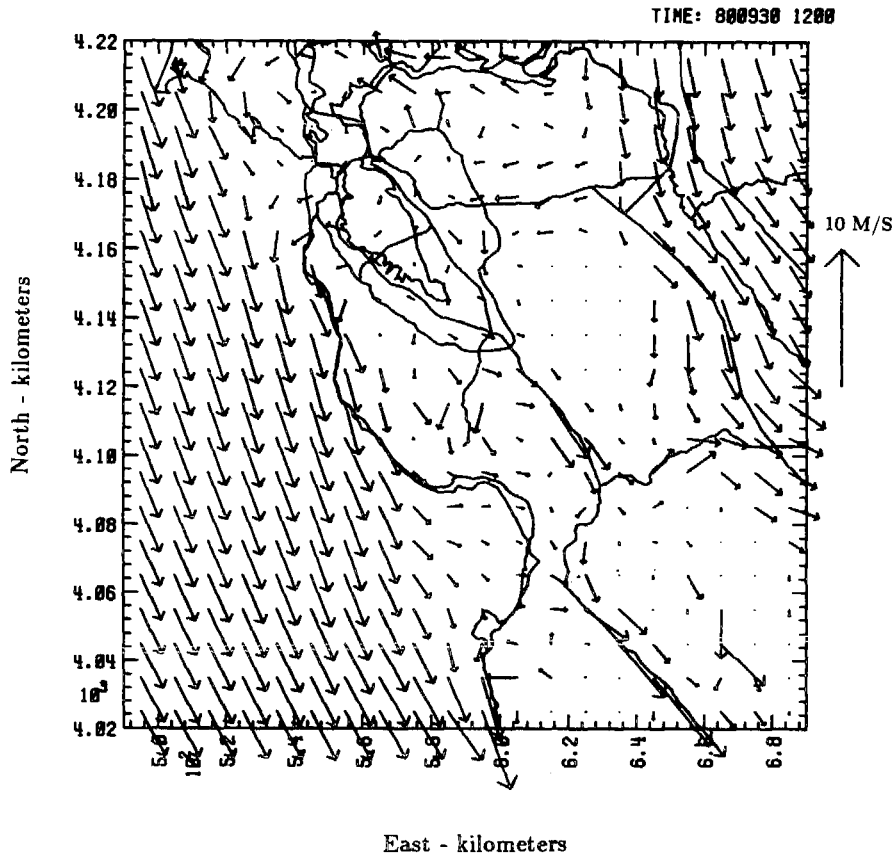

Figure 2.12. Adjusted layer-average wind fields assuming $n \cdot u \neq 0$ along the inversion surface.

Chapter 3. Development of Emissions Inventory

T. Mangot
M. Kim

A. Introduction

This section presents an inventory of emissions of organic compounds and oxides of nitrogen for the Bay Area Air Quality Management District (BAAQMD) and the Monterey Bay Unified Air Pollution Control District (MBUAPCD). The purpose of this emission inventory is to identify the significant sources of pollutants contributing to the ozone problem. Photochemical model runs with this inventory can identify emissions which contribute to high ozone and enable us to conduct sensitivity studies on the effects of controlling the source which contribute these concentrations. In this study, the emissions inventory has been used to simulate ozone formation under the meteorological conditions which occurred on September 30—October 1, 1980. For this simulation, an hourly, region-wide, gridded inventory of nitrogen oxides and various organic species was prepared for a typical weekday in September, 1980.

The BAAQMD compiled the emission inventory with help from the Metropolitan Transportation Commission (MTC), California Air Resources Board (CARB), Association of Bay Area Governments (ABAG), MBUAPCD, and the Association of Monterey Bay Area Governments (AMBAG). The inventories for the BAAQMD and MBUAPCD for 1980 and 1987 are summarized Table 3.1 and tabulated in detail in Appendix A.

B. Stationary source emissions

Emissions from all major facilities having organic or nitrogen oxide emissions greater than 25 tons per year are calculated separately. These are classified as Point Source emissions and are placed in the grids where the facilities are located. All other emitting sources are considered Area Sources. For emission calculations sources of similar type are grouped together into a source category. There are about 150 different source categories identified for this inventory. Detailed documentation of the data and assumptions used to prepare the emission estimates for each source category is contained in the "Source Category Methodology" document prepared by BAAQMD.

Point and area source emissions data for MBUAPCD were obtained from CARB and the data were compiled into BAAQMD inventory format. Procedures were developed for organic compound speciation, hourly emission profiles, and geographical distribution of emissions for each source category. The summary of emissions in the region is contained in Table 3.1 and in Appendix A.

C. Motor vehicle emissions in the BAAQMD

For the San Francisco Bay Area (BAAQMD), the inventory of motor vehicle emissions is divided into two parts:

1. Link emissions—occurring mainly on major streets and highways, these emissions are assumed to be from vehicle engines that are fully warmed up (i.e., hot stabilized).
2. Trip end emissions—these emissions occur at the beginning and end of each trip; consideration is given to the effects of different engine operating characteristics. There are three types of trip end emissions: cold start, hot start and hot soak. The trip end emission factors used for light duty vehicles in 1980 are listed in Table 3.2

Table 3.1. Emission inventory summary for 1980 and 1987

	Summer weekday (Tons per day)	
	Reactive organics (ROG)	Nitrogen oxides (NO_x)
1980		
BAAQMD		
Stationary	366.0	262.0
Motor Vehicle	299.0	285.0
Other*	405.0	—
Total:	1070.0	547.0
MBUAPCD		
Stationary	28.4	75.1
Motor Vehicle	31.0	43.0
Other*	322.0	1.0
Total:	381.0	119.
1987		
BAAQMD		
Stationary	264.0	209.0
Motor Vehicle	175.0	185.0
Other*	396.0	1.0
Total:	835.0	395.0
MBUAPCD		
Stationary	29.0	89.0
Motor Vehicle	18.3	34.0
Other*	303.0	0.4
Total:	350.	123.0

*"Other" includes emissions from vegetation, biodegradation, consumer solvent usage, etc.

The methods and data used to compute link and trip end emissions are quite different, as are their resulting geographic and hourly distributions. Emission factors used are from

Table 3.2. Light-duty vehicle trip end emission factors for 1980

	Grams per trip	
	Organics	Nitrogen oxides
Cold start	10.31	2.41
Hot start (catalyst only)	4.13	.95
Hot soak	8.00	—

Table 3.3. Percent contribution of vehicle miles traveled (VMT) by vehicle category

Vehicle category	
Light-duty auto	81.8 %
Light-duty truck	7.9 %
Medium-duty truck	3.9 %
Heavy-duty gasoline truck	2.5 %
Heavy-duty diesel truck	2.9 %
Motorcycle	1.0 %

EMFAC6D compiled by CARB. The vehicle miles travelled by vehicle category are based on actual Bay Area traffic counts conducted by Caltrans and are given in Table 3.3.

Link speeds

Carbon monoxide and organic emissions decrease with increasing vehicle speed; nitrogen oxide emissions increase with vehicle speed. The method for computing link emission takes this into account by using specified link speeds provided by the MTC travel model, which also produces link trip data. Link speeds can be obtained by a variety of methods; the MTC travel model provides estimates of average link speed and congested link speed.

D. Motor vehicle emissions in the MBUAPCD

Motor vehicle emission data for MBUAPCD counties were provided by CARB. The data were provided as county totals for organics and nitrogen oxides, in tons per day. BAAQMD staff developed procedures for spatial and temporal distributions of these county emission totals into LIRAQ/QSOR format. Spatial disaggregation of the county total emissions into UTM grid squares was based on VMT by roadway facility type. Temporal distribution of the county total emissions was based on actual diurnal traffic cycle data from Caltrans, counties, and cities for the study area.

The 1980 and 1987 mobile source inventories for Monterey, Santa Cruz, and San Benito counties (Figure 3.1) were provided by the California Air Resources Board (CARB, 1983). The data were provided as county totals for particulate matter, HC, NO_x, SO_2 and CO, in tons per day. The mobile source inventory task for the NCCAB is to develop spatial and temporal distributions of these county emission totals provided by the CARB into the LIRAQ/QSOR format. Figure 3.2 illustrates a schematic diagram of procedures used for developing the NCCAB mobile source inventories. Table 3.4 presents 1980 and 1987 mobile source emissions for Monterey, Santa Cruz, and San Benito counties.

Spatial distribution

Manual methods were employed for the spatial distribution of mobile emissions. The approach involved a four-step procedure applied to the study area:

1. Development of the Universal Transverse Mercator (UTM) co-ordinate system for the study area,
2. Collection of transportation network characteristics: link lengths by facility type, average daily traffic (ADT), and average vehicular speed by facility type within UTM grid squares for the study area,
3. Calculation of vehicle miles traveled (VMT) by grid square for three facility types; major highway, minor highway, and local street,
4. Distribution of the county-total HC and CO emissions into UTM grid cells based on VMT by facility type.

Table 3.4. Total hydrocarbon (HC) and oxides of nitrogen (NO_x) emissions from mobile sources for Monterey, Santa Cruz and San Benito counties for 1980 and 1987.

	Emissions (tons/day)			
	HC		NO_x	
County	1980	1987	1980	1987
Monterey	20.39	11.86	23.66	18.17
Santa Cruz	14.24	8.64	17.02	13.72
Santa Benito	1.79	1.05	2.39	1.96
Study area total	36.42	21.55	43.07	33.85

Source: California Air Resources Board (CARB).

United States Geological Survey (USGS) maps with UTM tic marks were used to specify the UTM coordinate system for the study area. These co-ordinates were then drawn onto the USGS map and translated onto the more detailed AAA maps and local planning maps. Information on major highways was provided by the California Department of Transportation (Caltrans, 1984); information on minor highways and local streets was provided by the various counties' public work departments and also by major cities, such as Monterey, Salinas, etc. Based on this information, link length, average daily traffic (ADT) volumes, and then vehicle miles traveled by facility type were compiled for each UTM grid cell in the study area.

Finally, the county total HC and CO emissions were distributed into UTM square based on VMT by facility type. The end results are 5 × 5 km grid mobile emissions for the study area. For 1987 the same procedures were repeated, but with adjustments for projected 1987 VMT and known facility improvements.

Temporal distribution

In order for the multi-layer photochemical transport model to adequately predict hourly ozone and other pollutant concentrations, typical hour-by-hour emissions are needed at the grid cell level. Because the temporal variation of vehicular emissions is a direct function of hourly traffic volumes, hourly variations had to be constructed for average daily traffic in the study area.

Actual diurnal traffic cycle data are available from Caltrans for the NCCAB highway networks. Such data were collected and analyzed in order to evaluate temporal and spatial fluctuations on Routes 1, 17 and 101 for 3 years, 1982 through 1984. The traffic cycles on Route 17 for the three-year period are shown in Figure 3.3. For comparison, the traffic cycles at three stations on Routes 1, 17 and 101 for the 3-year period (1982, 1983 and 1984) are shown in Figure 3.4. The analysis strongly suggested that the traffic cycles are quite consistent regardless of space and time. These data were compared with traffic cycle data used in the San Francisco Bay Area; see Figure 3.5. No critical differences were found. However, the actual traffic cycle data for the study area were used in order to get a better representation of the regional travel configuration.

To calculate hourly traffic volumes, a temporal adjustment curve shown in Figure 5 was applied to the average daily trips.

Disaggregation of ARB county emissions

ARB's 1980 and 1987 mobile source inventories for the three counties were distributed into the UTM grid system by the following 3-step procedure.

1. Based on different emission rates for different average speeds on three transportation facilities, ARB's county control totals for HC and NO_x emissions were distributed into county semi-control totals for three facility types; major highways, minor highways and local street.
2. Each HC and NO_x county semi-control total by facility type was then further distributed into UTM grid cells based on VMT by facility type for each grid cell.
3. Then, emissions from the distribution procedure were summed up for each grid cell to make the final mobile source inventory for the study area.

Appendix A lists the mobile emissions by grid square.

E. Emissions from natural vegetation (biogenic)

In 1980 ABAG initiated a project with partial support from the National Aeronautics and Space Administration (NASA) to prepare an inventory of organic emissions from natural vegetation (biogenic).

The biogenic organic emissions inventory was prepared from two major data bases:

- a map of vegetation distribution in the Bay Area compiled from satellite data gathered by NASA;
- a set of emission factors describing biogenic organic emission rates for all of the land cover (vegetation) classes identified in the region from the NASA data.

Vegetation file

The vegetation file was derived from satellite imagery of California recorded on August 6, 1976. In order to use these data to produce a biogenic organic emissions inventory for the Bay Area, ABAG first had to focus in on the Bay Area portion of that data file, and then identify vegetation classes from the data. Land cover classes in both urban and rural areas were identified and a vegetation file of twenty-three land cover classes was produced. The data file was then converted into a UTM hectare grid and entered into BASIS, ABAG's Bay Area Spatial Information System. Finally, the land cover distribution data were verified by comparison with aerial photography data and by on-site field work analyses of land uses of randomly selected test plots.

Emission factors

Biogenic organic emission factors were expressed as micrograms per meter-squared ground area per hour. They were obtained for each of the twenty-three land cover classes by conducting a Delphi survey of scientists familiar with biogenic organic emissions. The result of this survey was a set of summertime total non-methane organic emission rates representative of day and nighttime conditions. The emission rates also vary with location in the region, because the density of the vegetation population varies with location in the region. Therefore, the Bay Area region was divided into four ecozones.

Because biogenic organic emission rates have been found to be different under day and night conditions, different day and nighttime emission factors were developed from the Delphi results. Finally a set of daytime and nighttime emission factors by ecozones were developed for each of the twenty three land cover classes. All of these data are summarized in Tech. Memo 31 (Hunsaker, 1981), prepared for the 1982 Air Quality Plan.

Results

Total nonmethane biogenic organic emissions in the nine-county Bay Area for a twenty-four hour period of 12 hours of darkness and 12 hours of light were calculated to be 320 tons per day.

The uncertainty in the nine-county biogenic organic emissions inventory has been calculated to be $\pm$ 50 percent. This uncertainty is based on the uncertainties in the area-based emission factors. The vegetation file also contributed to the total uncertainty of the inventory.

The vegetation land cover classification data system used for the Bay Area is not available for the MBUAPCD. Therefore, the calculation method used for the Bay Area could not be applied. The MBUAPCD vegetation emission data were developed using the Bay Area's emission rates and a California vegetation map. The vegetation map used, developed by Dr. A.W. Kuchler, shows various types of land cover by color codes. This color coded classification is different from the vegetation classification used for the Bay Area's emission calculations. An assumption was made that all identically color coded land cover areas on the map had identical emission rates, allowing the MBUAPCD emissions to be estimated by matching the colors of the land cover areas with those of the Bay Area. Total nonmethane biogenic organic emissions in the three MBUAPCD counties for

a twenty-four hour period of 12 hours of darkness and 12 hours of light were calculated to be 250 tons per day.

F. Method for splitting HC into reactivity classes

Source profiles for specific species for each category of emissions were estimated by the Bay Area Air Quality Management District from data summarized by Bucon, Macho, and Taback (1978) for stationary, area, mobile, and airport emissions, and by Hunziger (1981) for biogenic emissions. Specific emission source components are assigned reactivities relative to propene, n-butane, toluene or formaldehyde plus acetaldehyde, depending on the class to which it is assigned. The classification scheme and reactivity weights for most species are given in Duewer, Gelinas, and Reinisch (1975) and Gelinas and Skewes-Cox (1977). Those for the biogenic hydrocarbons are described by Penner (1984).

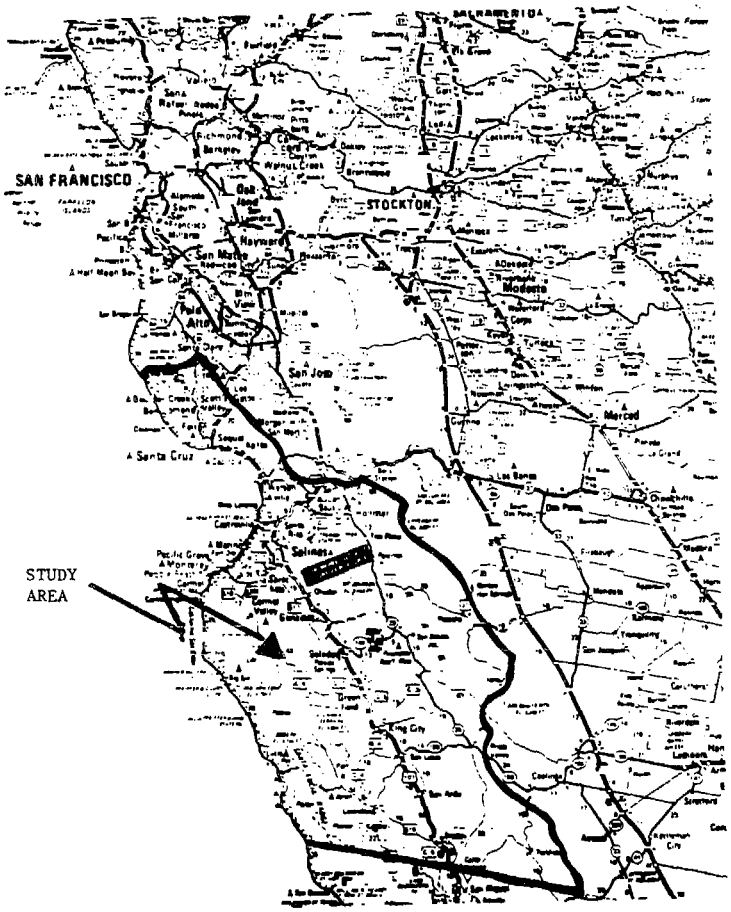

Figure 3.1. Study area for source inventory.

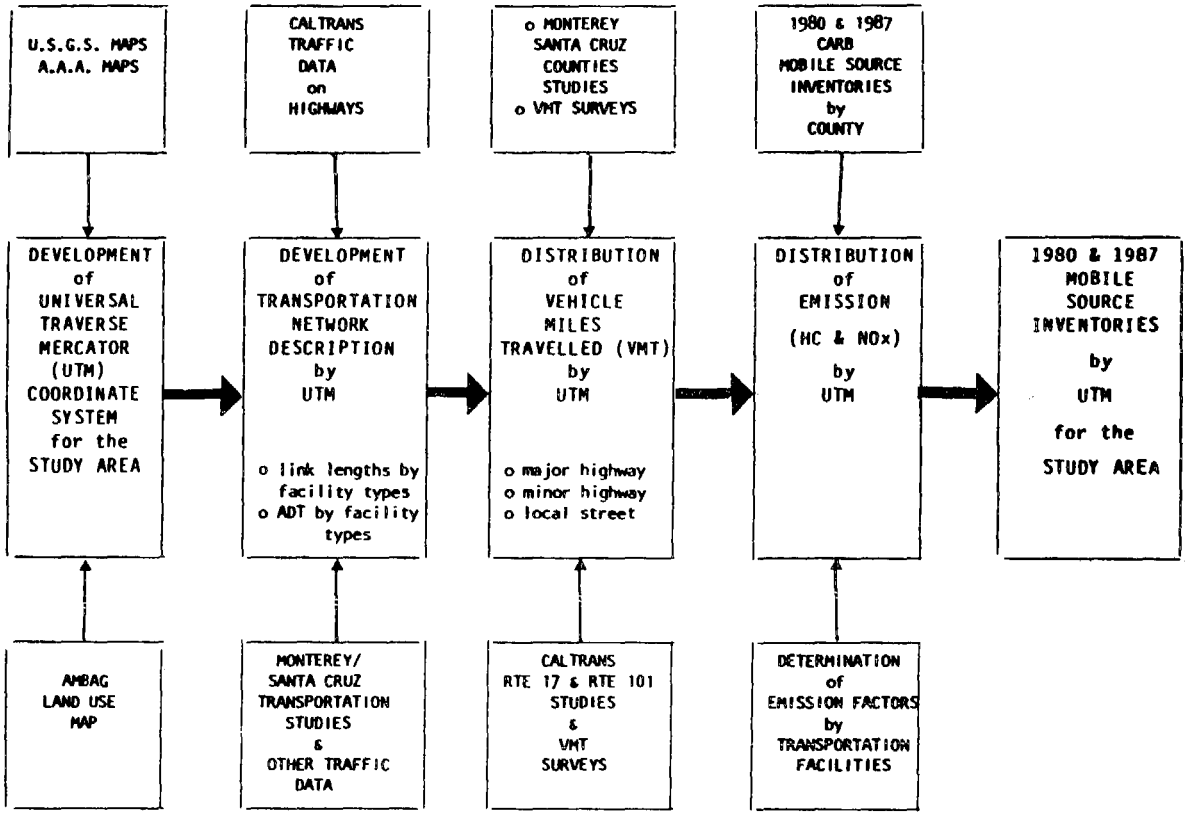

Figure 3.2. Schematic diagram of procedures used for developing the NCCAB mobile source inventory.

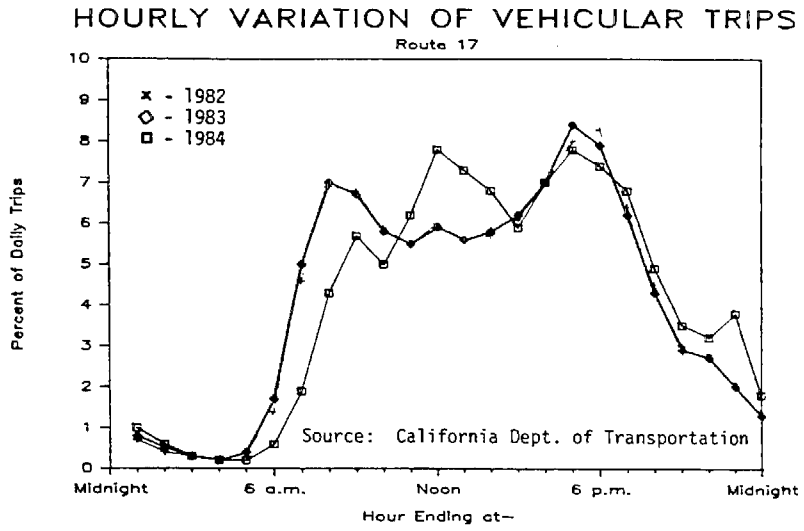

Figure 3.3. Traffic cycles on Route 17 for 1982, 1983 and 1984.

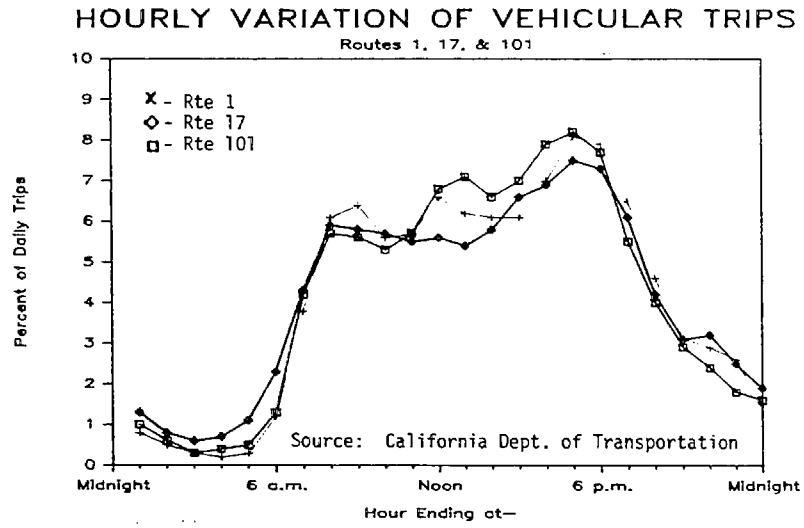

Figure 3.4. Traffic cycles on Routes 1, 17 and 10 for 1982, 1983, and 1984.

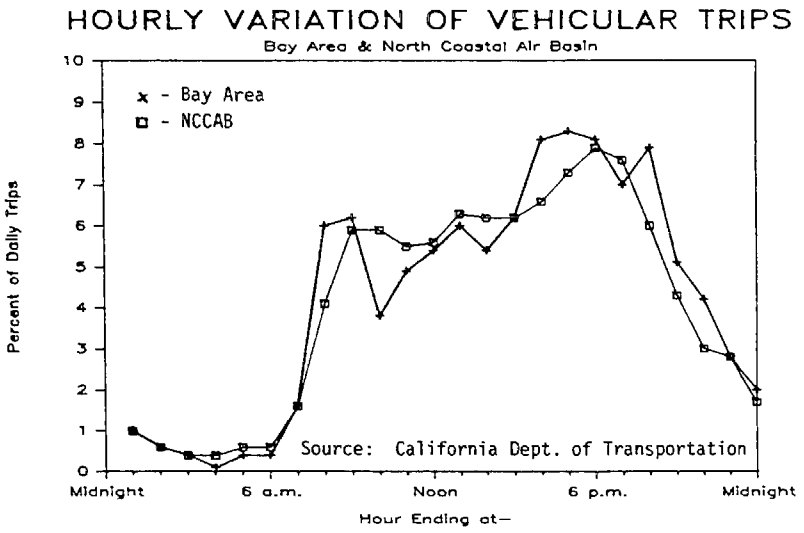

Figure 3.5. Traffic cycle data used in the San Francisco Bay Area.

Chapter 4. Meteorology

D. Duker

A. Introduction

While pollutant emissions do not change significantly from day to day, the air quality does. Over the short period, the variability in the air quality is due, for the most part, to changes in the meteorology. Meteorology describes the mechanisms which transport and diffuse the pollutants within the atmosphere. Thus, meteorology is a key element in air quality modeling. This chapter will describe the meteorolgical data used as input to the multi-layer photochemical transport model for the study of pollutant transport from the Bay Area to the Monterey Bay.

A meteorological period chosen for modeling should be representative of worst case conditions. For ozone modeling, we assume that worst case meteorology occurs during periods of high ozone levels. For the Bay Area, ozone concentrations above 15 pphm are considered high.

Another factor in the choice of the days to be modeled is that our emissions inventory is designed to be representative of weekday emissions. Emissions patterns on weekends are different. Thus, only weekdays with high ozone concentrations were considered.

Finally, because the study is primarily concerned with transport between the Bay Area Air Quality Management District (BAAQMD) and the Monterey Bay Unified Air Pollution Control District (MBUAPCD), the selected period should have a wind pattern that will allow transport between the two air basins.

The period meeting all of the above criteria occurred on September 30 through October 2, 1980. This was a multiday stagnation episode with ozone concentrations reaching 20 pphm in the San Francisco Bay Area and 15 pphm in the Monterey District. Concentrations as high as these levels have not been observed in either District since that time.

Quite fortuitously, the California Air Resources Board had contracted with SRI, International to conduct a field study of the pollutant transport between the BAAQMD and the MBUAPCD during that period. The study included the collection of supplemental air quality and meteorological measurements in the two basins. Later analyses of tracer and airplane flight data collected during the study indicated that during the September 30 to October 1 period, pollutant transport did occur between the BAAQMD and the MBUAPCD.

To allow sufficient time for transport of pollutants between the two air basins, the first two days of this episode were chosen to be modeled. Table 4.1 lists the ozone concentrations observed during those days.

Table 4.1. Observed maximum ozone concentrations in pphm on September 30 and October 1, 1980

Air Basin	September 30	October 1
BAAQMD	19	20
MBUAPCD	14	15

Before the meteorological data can be input into the photochemical transport model, the data must first be processed. The data are first input into the MEDIC program to grid the data. Output from this program is then input into the MATHEW program (Sherman, 1978), which adjusts the gridded winds as needed to insure the wind field is mass consistant.

The multi-layer photochemical transport model requires mean layer wind data and mixed-layer depths for the entire modeling domain. Unfortunately, most of the available wind data are from surface observations; data on the mixed-layer depth are almost non-existent. The rest of this chapter describes the methods employed to generate the needed meteorological data, and displays the fields created by the preprosessor programs.

B. Mixed-layer depth

The mixed-layer depth determines the volume through which pollutants emitted at ground level are easily mixed. During ozone episodes, vertical mixing is usually restricted by an elevated temperature inversion that is between 300 and 600 m deep in the Bay Area. This inversion can be determined by analyzing the vertical temperature profile generated from balloon or aircraft soundings, or by measuring variations in turbulence with an acoustic sounder (the inversion layer being less turbulent than the mixed-layer). During this study period, however, very little additional mixed-layer depth data were collected. There were no acoustic sounder data, but the SRI transport study did take seven aircraft soundings on September 30 and two on October 1. The twice daily Oakland radiosonde temperature profile provided the only other source of information.

These data sources do not provide sufficient information for the photochemical transport model which requires hourly mixed-layer depths. Furthermore, even if mixed-layer depth data were available hourly, interpolation for example of only one or two heights would have resulted in a flat mixed-layer field over the modeling domain. This is normally not realistic because historical data, (e.g., Ahrens and Miller (1969)) have shown a complex mixed-layer depth field. Their report concludes that "a single sounding (such as that made routinely at the Oakland Airport) cannot be representative of the conditions that prevail over the San Francisco Bay Area." Hourly mixing height data from a network of five or six acoustic sounders spread around the Bay Area would be needed to provided the necessary data. Because that level of detail was not available, hourly fields were synthesized by fitting measured data to climatological mixed-layer depth patterns. For example, Williams and DeMandel (1966), Ahrens and Miller (1969), Russell and Uthe (1978), and Russell (1979) found that during the day, the mixed-layer depth field commonly had a trough over the San Pablo-San Francisco Bay, and irregularities that roughly matched the surrounding coastal mountain topography.

The Oakland 0400 PST radiosonde sounding showed a surface-based inversion on both September 30 and October 1, 1980. This apparent lack of a mixed-layer is probably due to the fact that the Oakland radiosonde has a fast ascension rate and cannot detect a shallow well-mixed layer close to the ground. A zero mixed-layer depth is theoretically unrealistic because there is always some mixing due to mechanical turbulence. Mixed-layer depths should be even deeper over urban areas because of the thermal effects of the urban heat islands. Special studies have been made to measure the noctural mixed-layer depth in St. Louis (Godowitch, 1979), New York (Bornstein, 1968), and Bay Area cities (Duckworth and Sandberg, 1954). Using slow ascent balloons and aircraft, investigators have been able to measure nocturnal mixed-layer depths. For example, Schere and Demerjian (1978), using St. Louis high resolution sounding data collected during the RAPS study, estimated the St. Louis minimum mixed-layer depth for their box model to be 150 meters.

No special study data were available for our days to define the early morning depth. However, to insure a reasonable depth for mass tranport and pollutant mixing, urban areas were assigned a minimum depth of 150 meters and rural areas were given a 100 meter minimum mixed-layer depth.

Because we lacked sufficient data to characterize the time rate of change of the mixed-layer depth from sunrise to sunset, we used a rate of change curve similar to that used in the EPA EKMA model (see Figure 4.1) (EPA, 1981). This curve is based on an extensive set of upper air measurements made for the RAPS study in the summer of 1976 in St. Louis, MO. The curve shows that most of the mixed-layer growth has taken place by 1200 LST, with the maximum occurring by 1500 LST.

The use of this curve still requires a knowledge of the mixed-layer depth. Previous studies have shown that summer afternoon mixed-layer depths over the Bay Area are generally low, capped by an elevated subsidence inversion. Ahrens and Miller's (1969) report has numerous aircraft-measured fields showing mixed-layer depths of 50 meters to 600 meters over the Bay Area during the day. Russell and Uthe (1978) show contours of inversion base heights at various times over two days, one of the days having an ozone maximum of 18 pphm. In another study, Russell (1979) reported hourly mixed-layer depths for twenty days in 1979 over the Bay Area. After separating his data into high ozone days and lower ozone days, Russell (1979) developed a pattern showing lower mixed-layer depths on high ozone days. Slade (1968) also discusses how during air pollution episodes, mixed-layer depths are lower than average.

Investigations of the mixed-layer depth in the southeastern U.S. by McCaldin and Sholtes (1970) and Sholtes (1972) suggest a gradual buildup of the mixed-layer depth until late afternoon, followed by a relatively rapid decrease or collapse prior to sunset. Near sunset, the solar incidence angle (angle from the vertical) is larger and each unit of solar flux is spread over a larger area, allowing little heating of the ground. Some convective turbulence is still present, however, from heat radiated by the warm ground.

Russell's (1979) sodar data show the mixed-layer depth around the Bay Area to decrease by sunset, but not as drastically as Sholtes' measurements. Accordingly, the 1800 PST mixed-layer heights were set at a height about midpoint between the maximum at 1500 PST and the nighttime minimum.

By 2100 PST on September 30th, the mixed-layer is expected to be shallow during light wind conditions. SRI aircraft spirals taken at 1900 PST showed surface based inversions at San Jose and Monterey airports.

Detailed information about the behavior of the mixed-layer over the mountainous parts of the Bay Area were not available, so we used a simplified approach. At night, during low wind conditions, the observed surface based inversion acts to decouple the upper level flow from the surface flow. To simulate this, mixed-layer depths were set below topography over the mountainous regions. This will tend to concentrate the precursor pollutants within the respective valleys.

During the daytime, evidence from the BAAQMD tracer study (Sandberg, et al., 1970) indicated that the inversion base height rises with terrain. However, the mixed-layer depth over elevated terrain was found to be shallower than over flat terrain. Accordingly, we set the mixed-layer depth at 200 meters above mountainous terrain in the afternoon, thereby allowing unrestricted flow over the modeling domain.

Mixed-layer depths over the ocean are somewhat simpler to estimate than depths over land because of the smaller diurnal surface temperature variation, and thus reduced variation in convection-induced turbulence. Mechanical turbulence is also usually less important over water because of its smaller surface roughness. Neiburger (1959) reports that the inversion base height during summer months is about 400 meters along the California coast. This agrees well with aircraft measurements by Ahrens and Miller (1969) over the ocean between the Farallon Islands and San Francisco, which showed mixed-layer depths of 200 to 500 meters.

More recent sodar measurements were made off the California coast in July and August 1978 for Project MABLE (Schacher, et al., 1978). One of the sodar sites was located on the Farallon Islands, 25 km west of San Francisco. Other sodar measurements were taken on two research ships sailing along designated routes up to 200 km west of San Francisco. The raw data showed a range of mixed-layer depths from 60 meters to 550 meters. After subdividing the data into high ozone and lower-ozone days, the data suggested that mixed-layer depths over the ocean on high-ozone days were an average of 200 to 300 meters, while lower-ozone days were more likely to have mixed-layer depths of 300 to 400 meters.

C. Wind data

The meteorological preprocessor programs (MEDIC and MATHEW) generate mass fluxes for 30 levels in the vertical, ranging from the surface up to 1500 meters. Before input into the photochemical transport model, however, the levels are averaged to produce two layers of wind fields, the boundary layer and and the upper layer. The boundary layer is considered to be the mixed-layer, and the upper layer extends from the top of the mixed-layer to 500 meters above the maximum height of the mixed-layer for each zone. Both surface and upper air data are needed for each averaging time to create these wind fields.

For this analysis, it was decided to use variable averaging times. During the nighttime, when winds were calm and the mixed-layer depths were not changing, the meteorology was

updated in the model every three hours. During the daytime, the meteorology was updated every one to two hours, depending upon how fast atmospheric changes were occurring.

Surface wind data were available from 80 sites within the San Francisco and Monterey Bay Areas. Not all observing sites had data for every hour of the day, particularly during the evening hours when small airports and coastal reporting sites were closed. Upper air wind data were only available from two sites, the twice daily Oakland radiosonde and the Lawrence Livermore National Laboratory's Site 300 balloon releases at 0700 and 1000 daily.

In data-sparse regions of the modeling area, wind estimates were made (referred to as "synthetic winds"). This generally had to be done in mountainous areas and over the ocean. The synthetic winds were needed because during the gridding process, the model uses winds from the closest sites to determine the grid point value and, if the closest sites are too distant, inappropriate wind vectors can be created. For example, because very few wind measurements are available over the ocean, the MEDIC program would use wind data from land sites and incorrectly estimate wind direction over the ocean.

Because the ocean is flat and has only a small diurnal temperature change, its wind pattern is usually very steady throughout the day. For this modeling period, the few wind observations available from ship reports and the Farallon Islands were sufficiently consistent to allow a fairly confident estimation of wind data over the ocean.

Winds in mountainous regions were more difficult to estimate. Winds in the mountains are known to change with the time of day, and over short distances with the orientation of the slope. Also, the few observations available were usually from mountain tops which may not have been within the mixed-layer. To avoid allowing the mountain winds to affect the wind patterns within the lower lying regions of the modeling domain, the mountain winds had to be reset to values similar to those of nearby lower-elevation sites.

The lack of good wind data is a serious flaw in the entire modeling process. The data sparse oceanic and mountainous areas cover a significant portion of the modeling domain. The passes, which are the most important regions within the modeling domain, have almost no data. It is extremely important to know whether the air is flowing in or out of the passes, but most of the available wind data are from airports. A second problem concerns the temporal representativeness of the wind data. Most measurements are two minute averages taken once an hour. Such data may not adequately represent the hourly averaged winds. Other problems include data sources relying on instruments that may not be well maintained or appropriately sited. Most significant, however, is the lack of upper air wind data.

An unanticipated constraint was introducted by the MATHEW model itself. The MATHEW model requires the wind speed to go to zero at both the ground and the top of the mixed-layer along vertical faces which describe the top of the mixed-layer or the terrain. The result of this constraint is a significant slowing down of the winds within the boundary layer. Although the wind speeds output by MATHEW were therefore somewhat reduced below expectations, we did not alter the input wind data to improve the MATHEW results.

The wind data are entered into MEDIC and MATHEW models to compute mass fluxes (wind speed times mixed-layer depth). The fluxes are used in the photochemical transport model to advect pollutants, and are constant over the selected averaging time.

D. Atmospheric transmissivity coefficient

Photolysis rates in the atmosphere are proportional to the amount of ultraviolet radiation received. Radiation received on a horizontal surface is a function of the cosine of the angle from the vertical (the zenith angle). Thus, radiation received is very dependent upon the day of the year and the time of day. Solar radiation is also affected by reflection and absorption by clouds and aerosols. In the photochemical transport model, a solar radiation parameter, the atmospheric transmissivity coefficient, is used to correct the clear sky photolysis rates to account for clouds and aerosols.

Hourly atmospheric transmissivity coefficients were computed by ratioing measured solar radiation data with the expected clear sky radiation. For this period, the only valid solar radiation data available were from a U.C. Berkeley total radiation pyranometer in San Francisco. The clear sky radiation values were computed using an algorithm developed by Duewer et al. (1980).

Without pyranometer measurements from other sites in the modeling area, a transmissivity coefficient field may still be constructed based on cloud cover. This was not necessary, however, because local airport observations during the two-day period showed that there were no clouds. Consequently, a flat transmissivity coefficient field was used, based on the San Francisco data.

A small correction was made to the measured pyranometer values before calculation of the transmissivity coefficients. The solar radiation measured at ground level has approximately a 6 percent loss due to particulate scattering as the beam passes through the mixed-layer (Luther, 1982). Since we are interested in a layer-average solar radiation value, surface measurements were increased by 3 percent.

E. Meteorology of Tuesday, September 30, 1980

September 30 was the first day of a five day air pollution episode in the San Francisco Bay Area. Eight monitoring stations in the Bay Area reported exceedances of the 1-hour national ambient ozone standard (12 pphm); the maximum observed ozone concentration was 19 pphm. In the Monterey Bay Area, only one monitoring station reported an ozone exceedance; its highest one hour concentration was 14 pphm.

The synoptic weather pattern for the morning of September 30 is shown in Figure 4.2a. The surface weather map shows a high pressure region over the western states. This large scale pattern had higher pressures to the east of California. On a smaller scale, surface pressure data from local airports showed this same gradient pattern with higher pressure to the north and east. This is a typical synoptic pressure pattern during stagnant conditions in the Bay Area.

The prevailing wind pattern on this day produced wind from the northeast. Upper level winds, as measured by the Oakland radiosonde, were light and from the east or the northeast at all levels above 125 meters in the morning, and northeastly at all levels above

600 meters in the afternoon. Surface winds in the San Francisco and Monterey Bay regions were generally dominated by terrain and water-land interface effects. Away from the bay region, surface winds were easterly.

The easterly flow brought warm continental air into the Bay Area, allowing temperatures to rise to the high nineties over large portions of both the San Francisco and Monterey Bay Areas. High temperatures are a prerequesite for ozone formation in these regions. Bay Area statistics show that ozone exceedances are not expected unless temperatures reach at least 85°F (29.5°C).

The morning Oakland temperature sounding had a strong surface-based inversion. In the vertical, the temperature increased 13°C, reaching a maximum temperature of 27°C at 875 meters. Temperature increases greater then 10°C, or maximum temperatures above 20°C are considered significant forecasters of ozone episodes. The inversion appears to have decoupled the upper layer flow from the surface winds. Winds above the inversion were from the east, while Bay Area surface winds were either calm or terrain-following.

A few hours after sunrise, a bay breeze circulation pattern began. Light onshore winds were observed at all surface sites around the San Francisco Bay. Figure 4.3a shows MATHEW output of the wind field at 0900 PST. Such a circulation system has rising air over the land and descending air over the bay. This would depress the mixed-layer depth over the bay, similar to those days studied by Ahrens and Miller (1969) and Russell and Uthe (1978). Airplane spirals taken over Watsonville, Hollister, and San Jose airports between 1000 and 1100 PST showed the mixed-layer depth to be very similar at all three sites; about 150 to 180 meters above sea level. These heights were used for flat terrain portions of the modeling domain. For the rest of the modeling domain, the mixed-layer field was created with a climatological pattern found on high ozone days. The basic pattern had rising mixed-layer depths over the land areas, while over the bay and ocean areas mixed-layer depths were raised more slowly until noon. Figure 4.4a shows the mixed-layer depth height pattern for 0900 PST.

Figures 4.5a and 4.5b show the easterly upper layer wind pattern for 0900 and 1200 PST. The mixed-layer was about 200 meters deep during this period, so the vectors shown are an average of the winds from 200 meters to 1500 meters. Speeds were fairly light for this altitude, about 3 m s^{-1}.

The bay breeze circulation pattern persisted until mid-afternoon in the San Francisco Bay Area. However, in the Monterey Bay Area, a weak onshore pattern began about 1300 PST. At 1430, the San Francisco Airport reported a wind shift from weak northeast winds to strong northwest winds, indicating the beginning of the sea breeze. After this time, the local pressure gradient reverses, and the wind pattern changed to northwesterly, while speeds increased to 6 m s^{-1}. Figures 4.3b and 4.3c show the wind patterns at 1200 and 1500 PST.

Mixed-layer depths in the afternoon stayed fairly shallow. An aircraft sounding over the San Jose Airport at 1340 PST showed the mixed-layer to be about 260 meters deep. Other aircraft soundings over Watsonville, Hollister, and Morgan Hill airports near sunset suggested mixing had gotten no deeper than 400 meters during the day. The 1600 Oakland radiosonde had no indication of a mixed-layer. Consequently, mixed-layer depths were set

to between 300 and 400 meters over flat areas of the modeling domain for the afternoon period. Figures 4.4b and 4.4c show the mixed-layer depth patterns at 1200 and 1500 PST. To allow flow over the mountains, mixed-layer depths were set at approximately 200 meters above terrain in those areas. Because the bay breeze was overwhelmed by the sea breeze in the late afternoon, mixed-layer depths over the bay were made the same as over land areas.

By 1500 PST, the sea breeze can be seen flowing into the Bay Area in Figure 4.3c. Because the surface winds had been offshore earlier in the day, the marine air now entering the Bay Area contained a large mass of polluted air. This infusion of air into the Bay Area pushed air down the Santa Clara valley toward Hollister. In the Monterey Bay Area, the sea breeze had split, with one part of the flow moving southward up the Salinas Valley, while the other part flowed eastward toward Hollister. A convergent zone in the vicinity of Hollister (UTM coordinates 4082,642) occurred when the flow coming down the Santa Clara Valley mets the Monterey sea breeze.

Wind speeds peaked by 1600 PST. The sea breeze did not have the usual cooling effect on the Bay Area. Temperatures in the south bay continued to rise until an hour before sunset. Even San Franciso, which had experienced 7 m s^{-1} winds from the ocean, was still recording 80°F at 1700 PST. This probably indicates that the warm offshore air from the first part of the day was being brought back onshore, and the fact that the sea breeze began fairly late in the day.

By sunset (1800 PST), many stations were again reporting calm winds. Winds in the Carquinez Straits were now from the west, the sea breeze having penetrated into the Central Valley; see Figure 4.3d. In the Monterey Bay Area, the sea breeze had weakened considerably and no longer penetrated to Hollister. Aircraft spirals taken near sunset showed surface-based inversions in the Monterey District and over Morgan Hill in the BAAQMD. Mixed-layer depths were set above minimum levels to reflect wind-induced mechanical mixing and residual thermal turbulence. Mixed-layer depths for this time are shown in Figure 4.4d.

The effects of the weakening of the east to west pressure gradient in the late afternoon, seen in the surface reports, can also be seen in the upper layer winds. The upper level winds loose their easterly component and turn counterclockwise to the NNE at 1500 PST and to the north by 1800 PST (see Figures 4.5c and 4.5d). Wind speeds stayed generally light all day.

Throughout the day, Bay Area airports reported clear skies with no clouds, with some slight obscuration by smoke and haze. Estimating the transmissivity coefficient by ratioing the measured San Francisco pyranometer values with the calculated ideal solar radiation for that hour gave values ranging from 0.88 to 0.92. Because this value was close to one and there was little variation temporally and none spatially, we chose to use a default value of 1.0.

F. Meteorology of Wednesday, October 1, 1980

The second day of the modeling period had slightly higher ozone concentrations than the first. Gilroy and Morgan Hill peaked at 20 pphm while Fremont and Alum Rock

reached 19 pphm. Eight stations within the Bay Area reported ozone concentrations above 12 pphm. In the Monterey Bay, only Watsonville had an excess of the ozone standard, reaching 15 pphm. Hollister, having the highest ozone concentration the previous day, only reached 10 pphm this day. Air temperatures were also higher on this day, reaching 103°F (39.5°C) at sites in both the BAAQMD and the MBUAPCD.

Airports again reported no clouds on this day. Transmissivity coefficients were about the same as the first modeling day, in the range of 0.88 to 0.92. Therefore, we used the same default value of 1.0 as for the first day.

The surface pressure pattern shown in Figure 4.2b shows that the high has intensified over British Columbia. In California, the pressure pattern has stayed about the same as the previous day. Again the atmospheric pressure is higher to the north and east. Local pressure data from airports show that the offshore gradient persisted until 1500 PST.

Winds had become calm at most reporting stations after sunset the previous day, and stayed calm through the night into the morning of the second day. Because many of the airport sensors have a 1 m s^{-1} wind threshold, we changed some airport calm winds to reflect speeds and directions more reflective of downvalley and downslope flow.

Upper level winds were again from the east. The morning Oakland and Lawrence Livermore soundings showed easterly winds to 1500 meters. The afternoon Oakland sounding showed extremely light (0.5 to 1 m s^{-1}) southeasterly winds above the marine mixed-layer. Figures 4.7a-d show the upper level wind flow through the day.

The morning Oakland sounding again had a surface based inversion. The vertical change in temperature was about the same as the previous day, 12.8°C, but the top was 200 meters lower at 685 meters, reaching a maximum temperature of 29.8°C. Thus, the inversion was slightly stronger than the previous day. Mixed-layer depths were left constant overnight. Over urban areas, mixed-layer depths were set at approximately 150 meters above ground level, while over rural areas, mixed-layer depths were set at 50 to 100 meters above ground. To isolate the valleys, mixed-layer depths were set well below terrain in mountainous regions. Because the mixed-layer depth data were generally lacking on this day, we chose to use the same depths for both days.

By mid-morning, the easterly flow had become well organized in the Carquinez Straits, and passed out through the Golden Gate. The 0900 PST wind flow map seen in Figure 4.6a shows this pattern. Within the San Francisco Bay region, a bay breeze circulation had started by this time. Monterey Bay observing stations were still experiencing offshore flow. Along the coast, winds were variable during this period.

At 1200 PST (Figure 4.6b) an over-ocean transport pattern can be seen. Air is moving westward through the Carquinez Straits, south and out through the Golden Gate, then southeastward down the coast, and finally onshore into the Monterey Bay Area. Not all of the air passing through the Carquinez Straits is carried out through the Golden Gate; some of the pollutants are carried southward toward the south bay. This overall pattern continued until after 1500 PST.

By 1500 PST, a weak sea breeze had pushed into the Bay Area and cut off the easterly flow out through the Golden Gate. Ozone levels in the BAAQMD continue to rise in the

south bay as the pollutant cloud was pushed southward. However, in the MBUAPCD, the ozone level peaked at 15 pphm in Watsonville by 1500 PST. After this time, the sea breeze stopped, effectively cutting off the pollutant source. (see Figures 4.6c and 4.6d).

October 1 seemed to demonstrate pollutant transport down the coast from the Golden Gate to the Monterey Bay. However, transport down the Santa Clara Valley to Hollister was weak. Ozone concentrations of 20 pphm were measured in Morgan Hill between 1300 PST and 1500 PST. A short time later, between 1500 PST and 1700 PST, this ozone cloud had moved 15 km south to Gilroy. However, these high ozone levels never reached Hollister, 24 km south of Gilroy. Ozone levels in Hollister peaked at 10 pphm at noon and decreased to 5 and 6 pphm after 1600 PST. Although no wind data were available from Gilroy, Morgan Hill data and Hollister wind data suggest that the ozone air mass was blown to the east of Gilroy, across the Pachecho Pass.

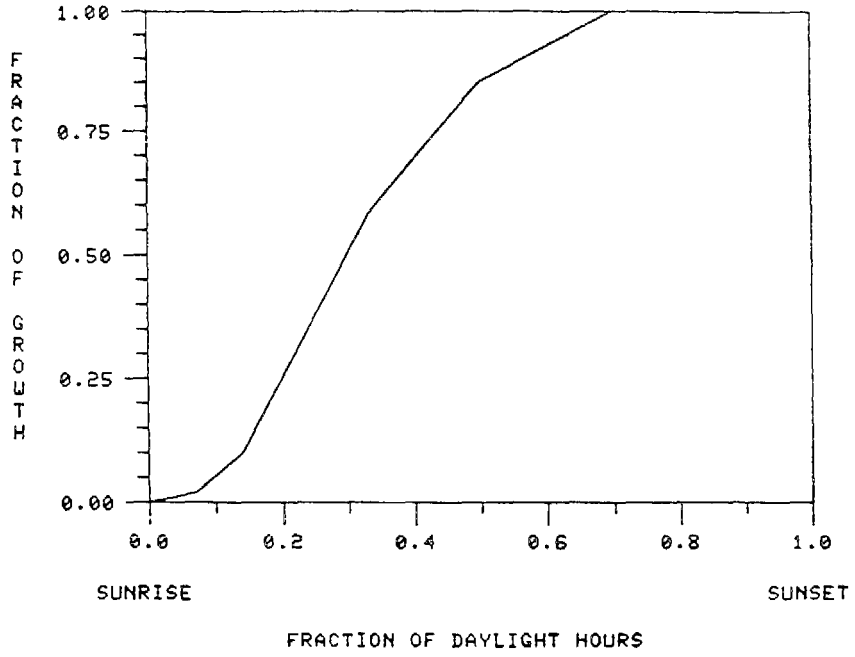

Figure 4.1. Time variation in growth of the mixed layer.

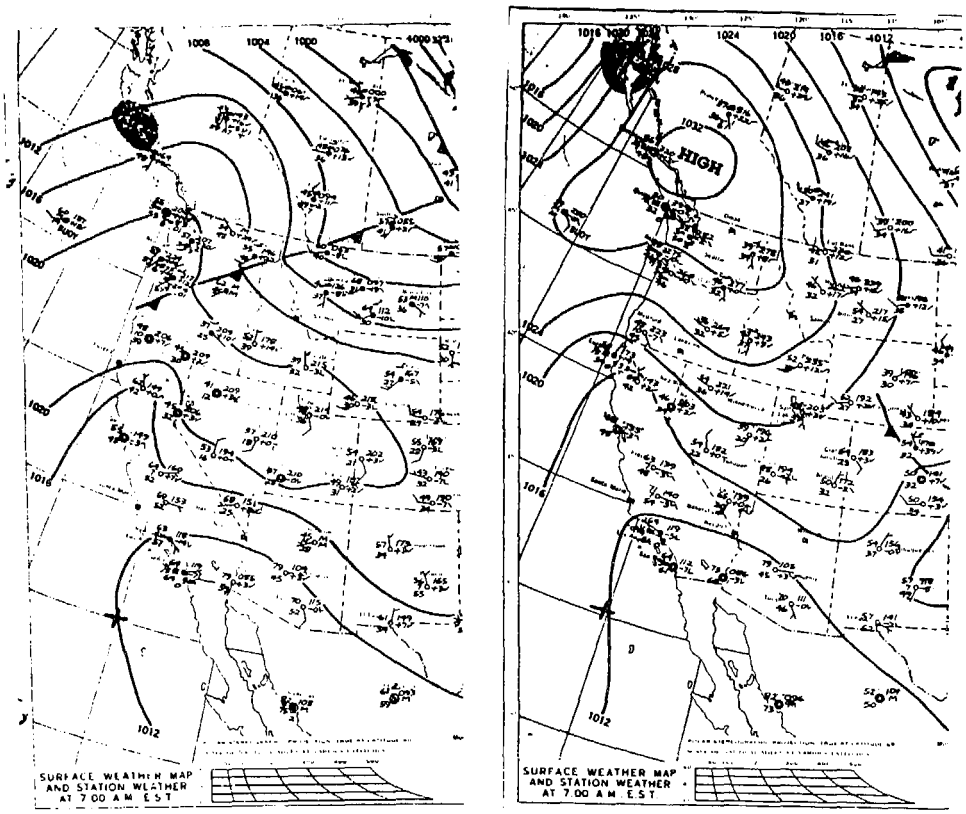

Figure 4.2. (a) Surface weather map at 0400 PST on September 20, 1980. (b) Surface weather map at 0400 PST on October 1, 1980.

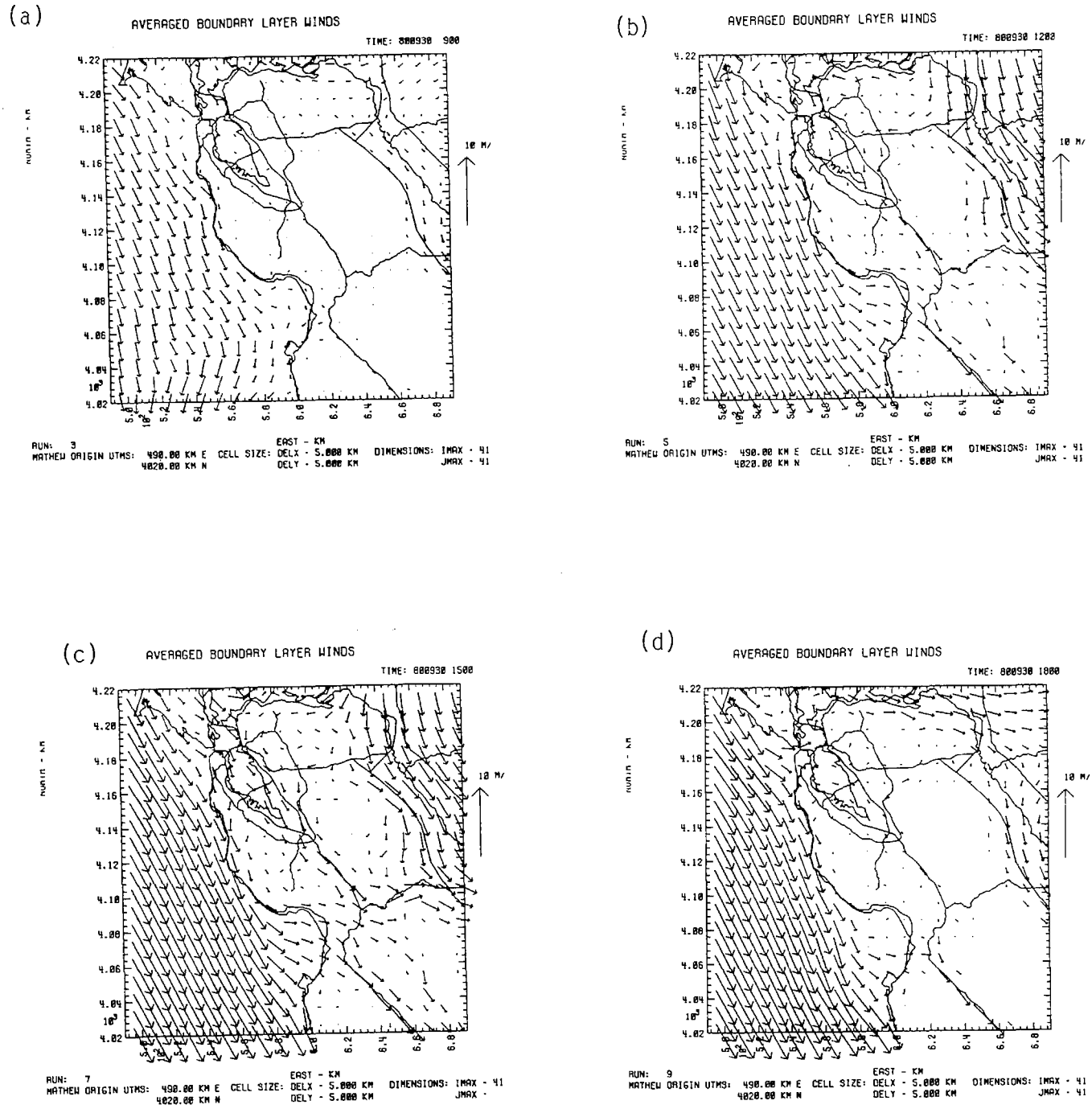

Figure 4.3. (a) Mixed layer winds in m s^{-1} for 0900 PST on September 30, 1980. (b) Mixed layer winds in m s^{-1} for 1200 PST on September 30, 1980. (c) Mixed layer winds in m s^{-1} for 1500 PST on September 30, 1980. (d) Mixed layer winds in m s^{-1} for 1800 PST on September 30, 1980.

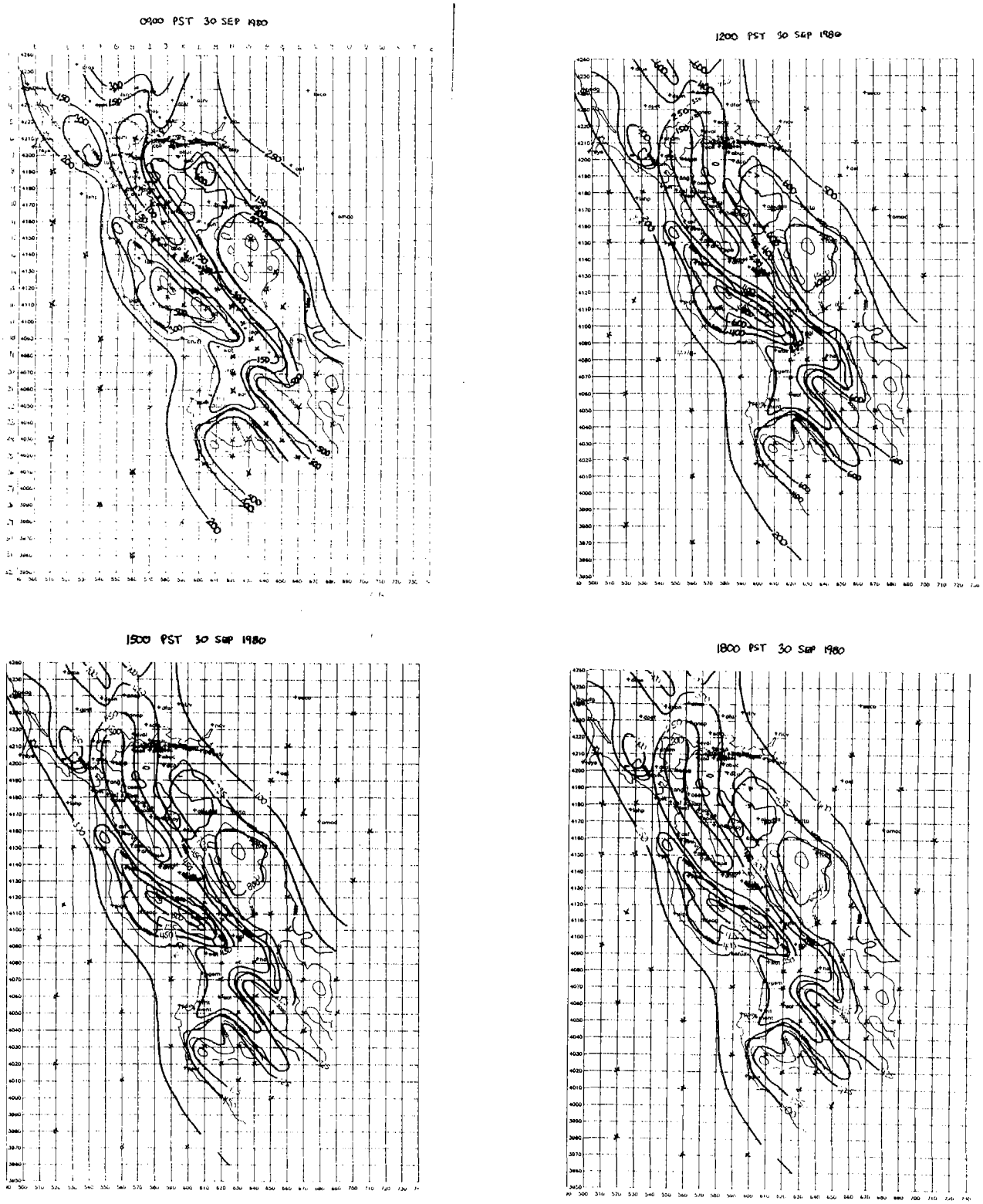

Figure 4.4. (a) Mixing depths in meters above sea level at 0900 PST. (b) Mixing depths in meters above sea level at 1200 PST. (c) Mixing depths in meters above sea level at 1500 PST. (d) Mixing depths in meters above sea level at 1800 PST.

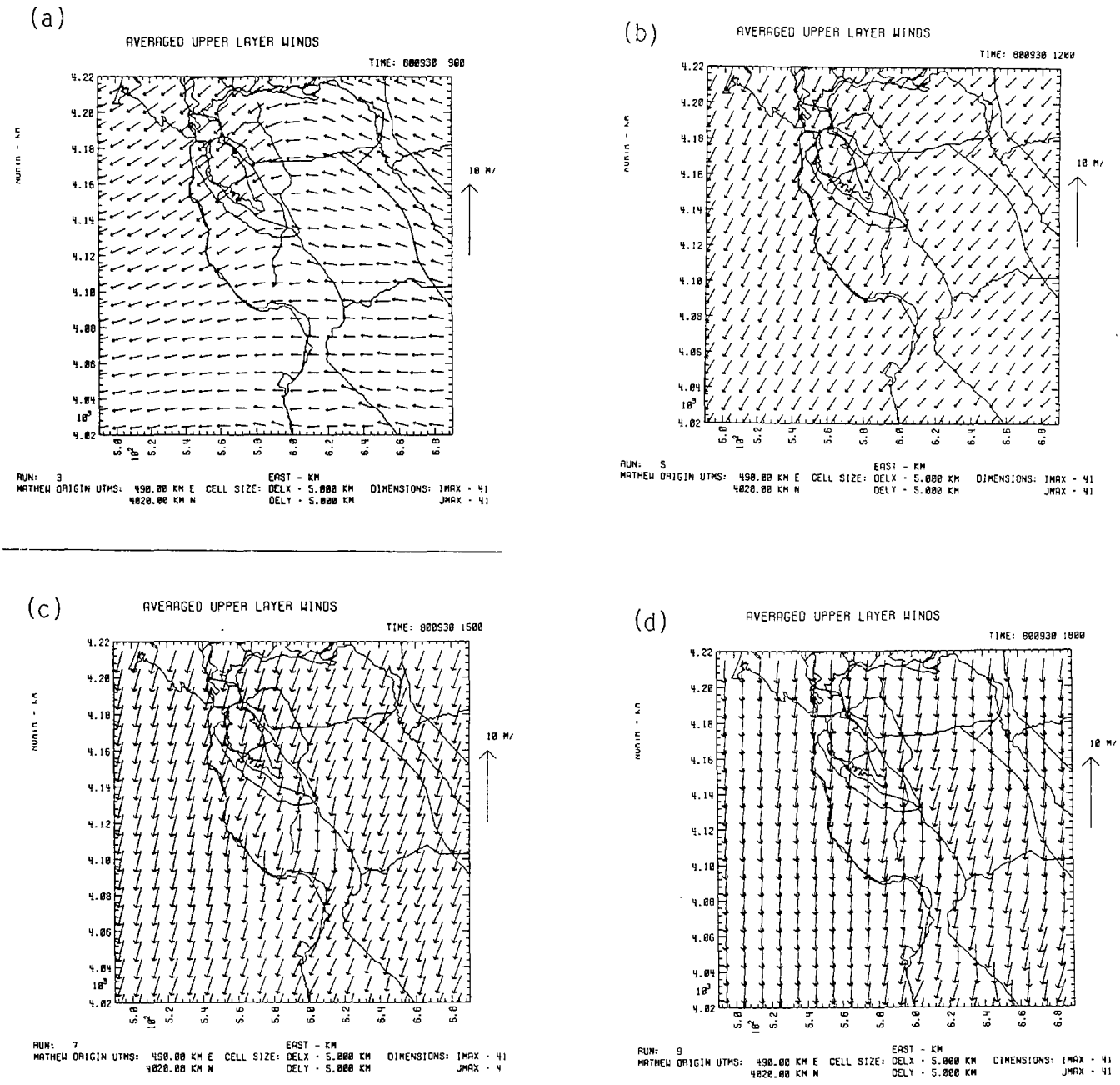

Figure 4.5. (a) Upper layer winds in m s^{-1} at 0900 PST on September 30, 1980. (b) Upper layer winds in m s^{-1} at 1200 PST on September 30, 1980. (c) Upper layer winds in m s^{-1} at 1500 PST on September 30, 1980. (d) Upper layer winds in m s^{-1} at 1800 PST on September 30, 1980.

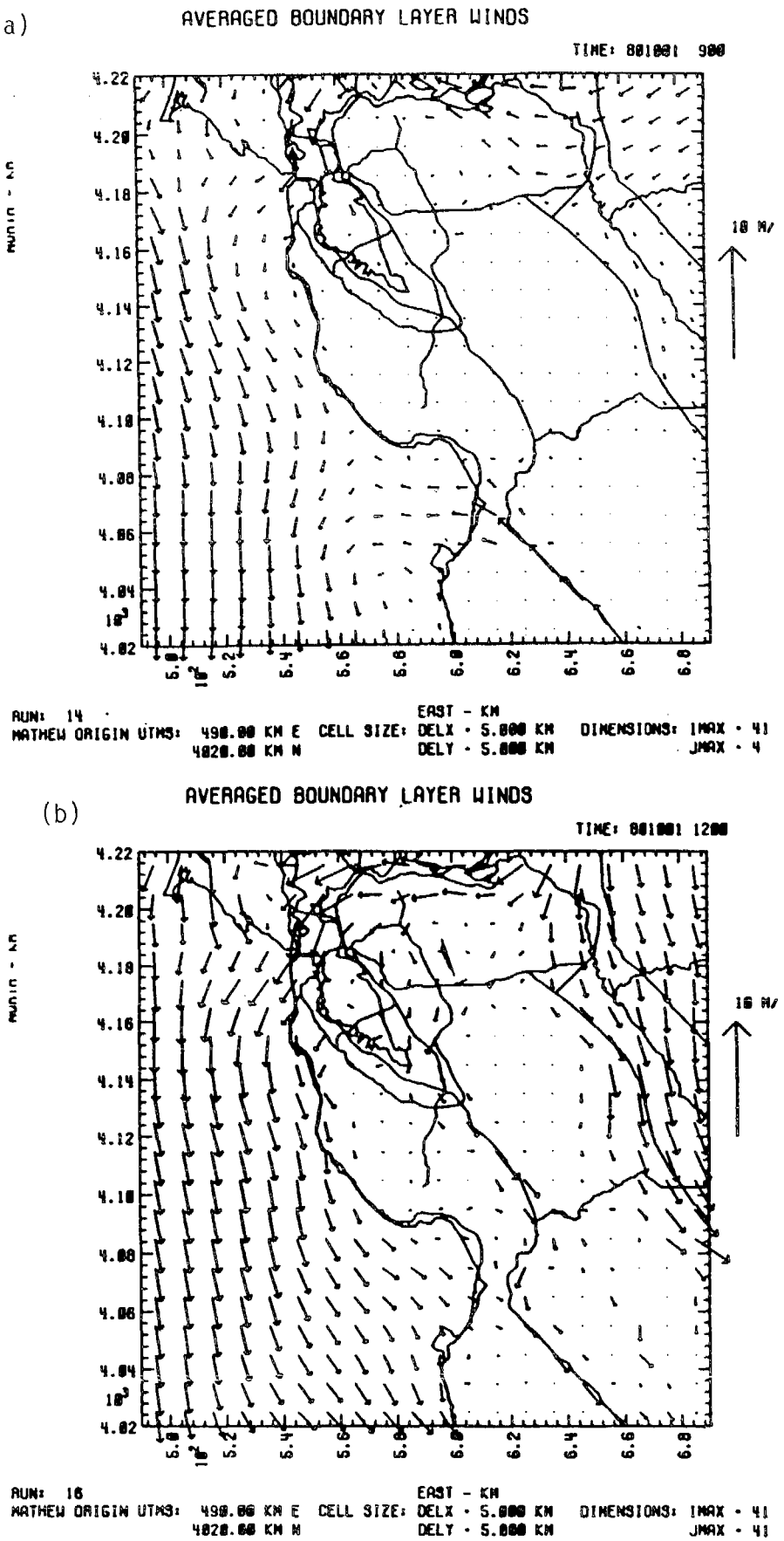

Figure 4.6. (a) Mixed layer winds in m s^{-1} for 0900 PST on October 1, 1980. (b) Mixed layer winds in m s^{-1} for 1200 PST on October 1, 1980.

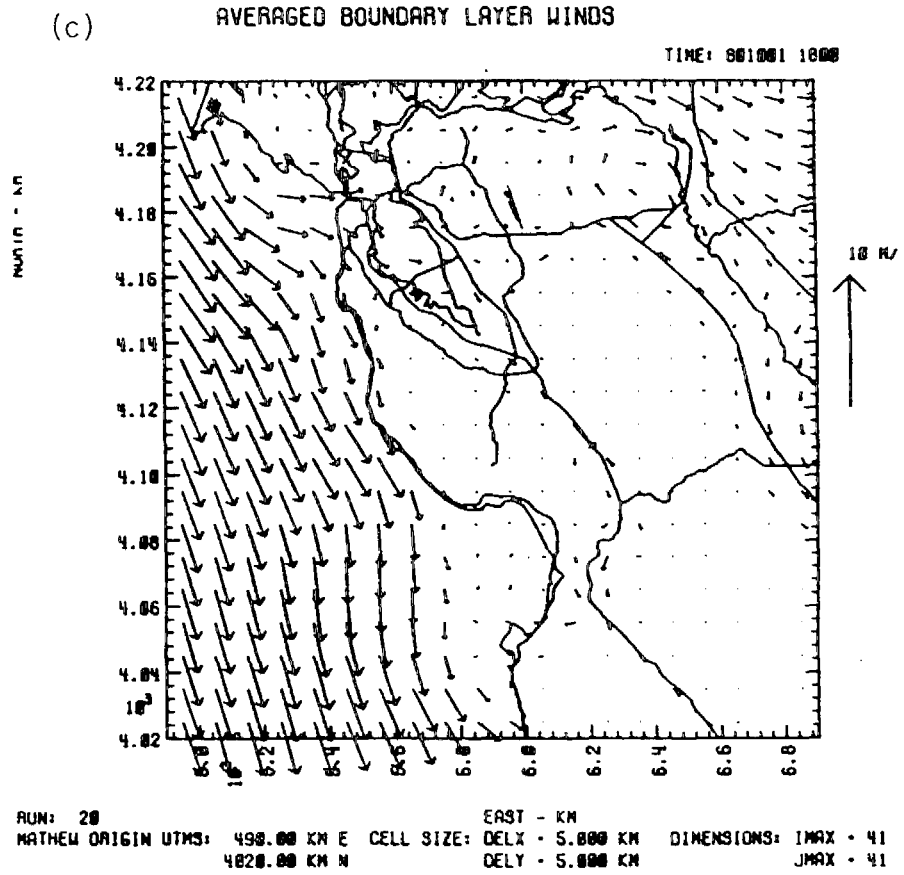

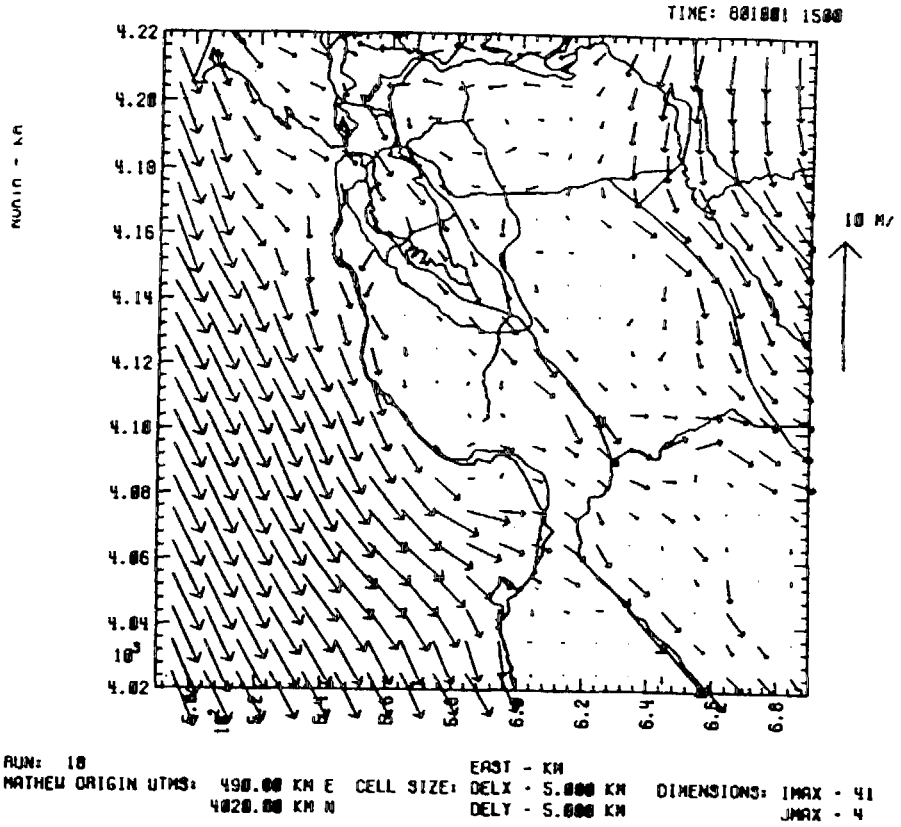

Figure 4.6. (c) Mixed layer winds in m s^{-1} for 1500 PST on October 1, 1980. (d) Mixed layer winds in m s^{-1} for 1800 PST on October 1, 1980.

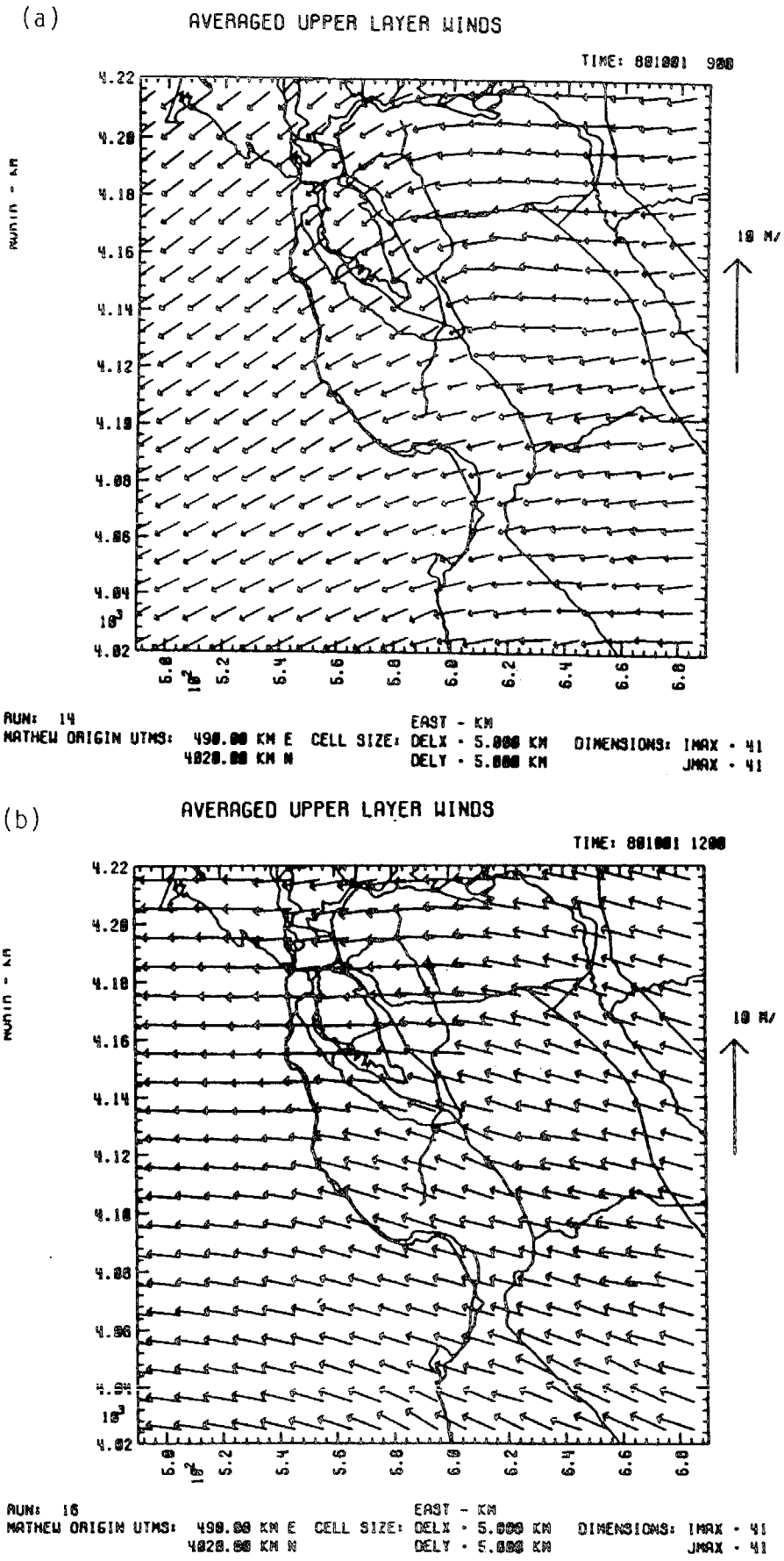

Figure 4.7. (a) Upper layer winds in m s^{-1} at 0900 PST on October 1, 1980. (b) Upper layer winds in m s^{-1} at 1200 PST on October 1, 1980.

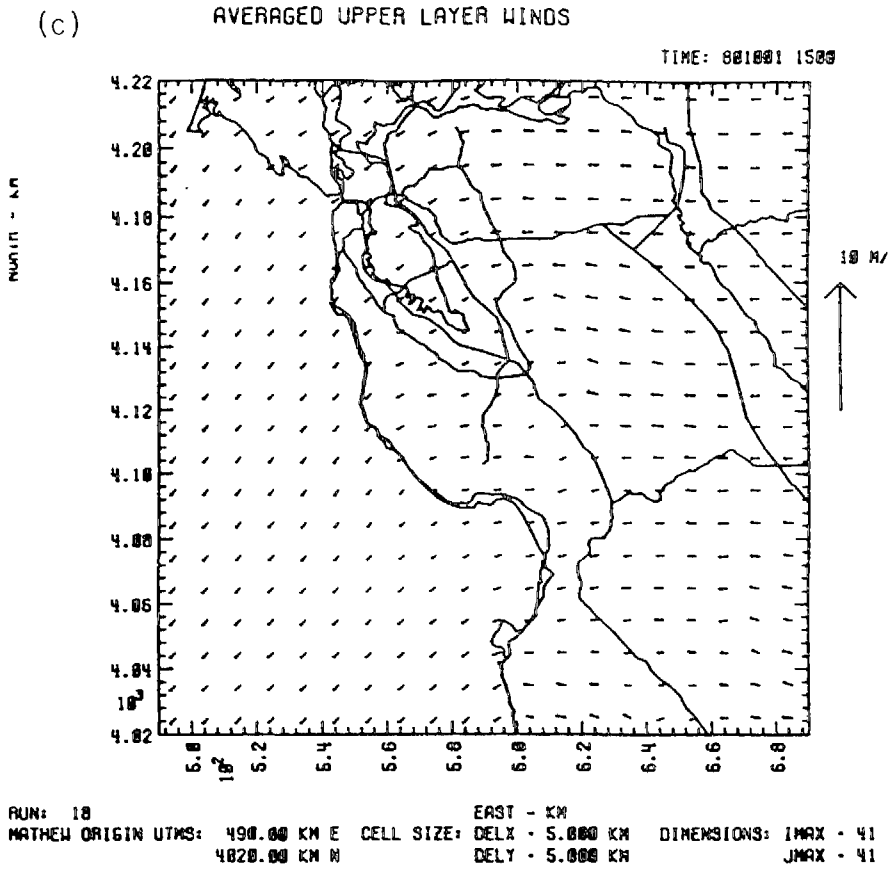

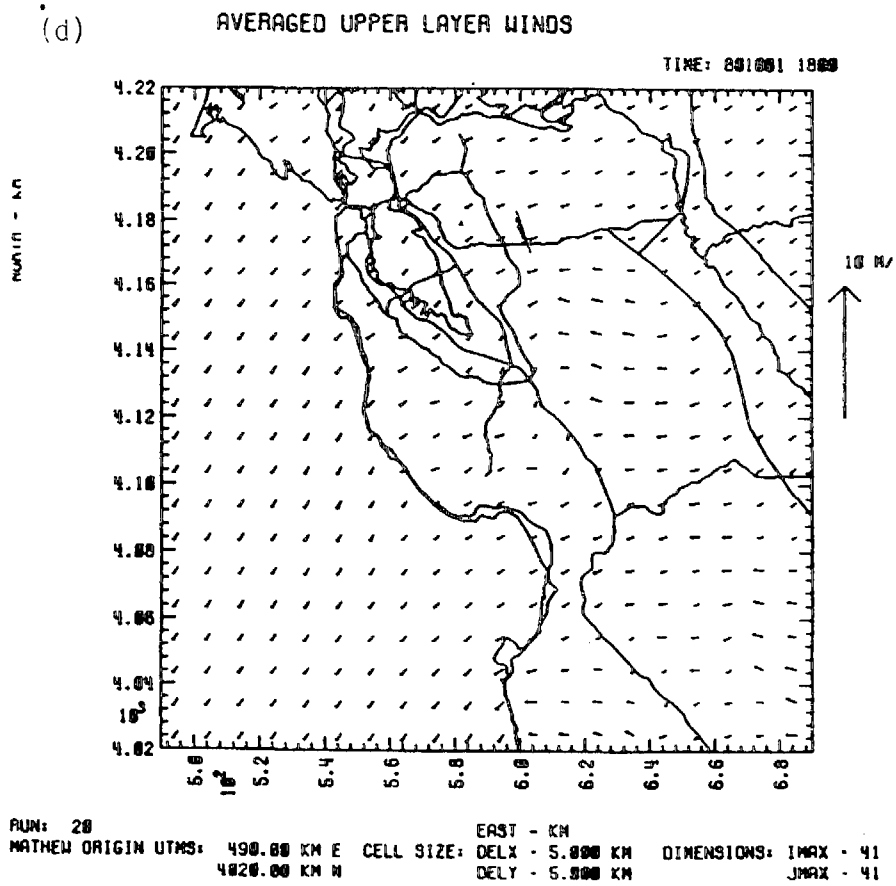

Figure 4.7. (c) Upper layer winds in m s^{-1} at 1500 PST on October 1, 1980. (d) Upper layer winds in m s^{-1} at 1800 PST on October 1, 1980.

Chapter 5. Update of the Chemical Mechanism

J. E. Penner
P. S. Connell

A. Introduction

As part of the development of the new photochemical transport model, we updated the chemical mechanism also. Initially, we simply updated the reaction rate coefficients and photolysis rates needed to specify reaction rates for the mechanism used in the LIRAQ model. As shown below, however, this resulted in a significant decrease in the reactivity of the mechanism. Because initial tests of the model with the original LIRAQ chemical mechanism and reaction rate coefficients showed satisfactory agreement with observed ozone fields, it was clear that the original mechanism with updated reaction and photolysis rate coefficients would not produce enough ozone. We therefore sought to update the mechanism in a way which was compatible with the available emissions inventory and which would maintain a reactivity level close to that of the original mechanism. The following sections compare the performance of the original (1982) mechanism, the original mechanism with reaction rates updated to 1986, and a new mechanism which is similar to the original mechanism except that the chemistry of H_2CO is treated explicitly. The mechanisms are tested in the photochemical transport model and against a limited number of smog chamber simulations. In addition, the performance of the new chemical mechanism is compared to that of a recently developed lumped chemical mechanism that has been tested by comparison with a large number of smog chamber simulations. This latter mechanism could not, at the present time, be implemented in the photochemical transport model because a compatible emissions inventory has not yet been developed. The development of such an inventory would be highly desirable, so that the results reported in Chapter 6 could be re-evaluated using a less condensed mechanism than that developed here.

B. 1982 chemical mechanism and resulting ozone fields

Initial testing of the new multi-layer photochemical transport model used the chemical mechanism developed by Penner and Walton (1982). That mechanism treated the inorganic species listed in Table 5.1 in full detail, but the organic species treatment was "lumped" or "condensed." Thus, any given organic species represented a host of different species. As long as the oxidation pathways and rates for the lumped species were similar, the mechanism provided a reasonable representation of the actual chemical transformation processes. In the 1982 mechanism, all carbonyl species were lumped into the category HC4, and the kinetic rate coefficient for reaction of HC4 with OH was set equal to the average value of the rate coefficient for reaction of formaldehyde (H_2CO) with OH and the rate coefficient for reaction of acetaldehyde (CH_3CHO) with OH. Similarly, the photolysis rates for HC4 were developed by averaging the photolysis rates of formaldehyde and acetaldehyde. By fortuitous cancellation of the effects of an incorrect acetaldehyde photolysis constant, this mechanism gave rather satisfactory simulation characteristics when compared to model calculations with an explicit chemical scheme, at least for hydrocarbon

to NO_x ratios near 2 ppmC/ppm (Leone and Seinfeld, 1985). The mechanism had also previously yielded satisfactory simulation characteristics when applied to the Bay Area and also to St. Louis (Penner et al., 1983). Simulations of the ozone fields in the mixed-layer for the September 30–October 1 episode in the San Francisco/Monterey areas are shown in Figures 5.1–5.4. (The results shown here, however, used preliminary meteorology fields.) The four figures show O_3 at 1400, 1500, 1600, and 1800 hours for September 30, 1980.

Table 5.1. Species treated in the Penner and Walton (1982) mechanism and in the new mechanism*

Inorganic Species	Organic Species	
NO	HCl	alkenes
NO_2	HC2	alkanes
O_3	HC3	aromatics
CO	HC4*	aldehydes
	H_2CO*	formaldehyde
HNO_2	PAN	peroxyacyl nitrate
H_2O_2	RO_2	alkylperoxy radicals
HNO_4	RCO_3	acyperoxyl radicals
NO_3	RO	alkoxy radicals
N_2O_5		oxygenated aromatic radical
HO_2	CH_3COCHO	methyl glyoxal
$O(^3P)$		
HO		

* The new mechanism treats the chemistry of H_2CO explicitly. HC4 is used to represent all higher aldehydes. The chemistry of HC4 is based on that of acetaldehyde. In the Penner and Walton (1982) mechanism HC4 represented formaldehyde and all higher aldehydes.

C. Update to 1986 reaction rates

A few of the reaction rates specified for the 1982 mechanism have been re-measured and re-evaluated since that mechanism was developed and tested. Previously, reaction rate constants and photolysis cross sections had been based primarily on the values recommended in DeMore et al. (1981), WMO (1981), Hudson and Reed (1979), and Atkinson et al. (1980) (see Penner and Walton, 1982). We therefore updated the reaction rates to values consistent with those recommended in DeMore et al. (1985) and Baulch et al. (1984) and those used in the explicit mechanism used by Leone and Seinfeld (1985). The current recommendations for spectral parameters and photolytic reaction products were used in the LLNL 1-D model of the stratosphere and troposphere to derive surface values for first order photodissociation rate constants (Wuebbles, 1981). An ozone overburden of 290 Dobson units was specified in the calculation, consonant with total column ozone climatology from satellite data for September–October at 37°N (J. Ellis, private communication). The 1-D model includes the effects of multiple scattering (Luther et al., 1978) and

photodissociation constants were evaluated for zenith angles between 0 and 90 degrees. The updated reaction mechanism is presented in Table 5.2.

Most rate constants were changed only slightly, but the average photolysis rate for HC4 was decreased significantly. Previously, the actinic cross sections for CH_3CHO were uncertain and the cross section for photolysis of CH_3CHO was simply taken as equal to the cross section for $H_2CO \rightarrow HCO + H$. Measurements by Moortgat et al. (1984) showed that quantum yields for CH_3CHO photolysis were substantially smaller than unity in the wavelength region 290–310 nm which contributes most to CH_3CHO photodissociation at the surface. With the new CH_3CHO actinic cross sections, the average photolysis rate for HC4 decreased substantially. This change, together with a decrease in the methyl glyoxyl photolysis rate, significantly altered the reactivity of the Penner and Walton (1982) mechanism. With only these changes, modeled O_3 fields decreased by almost 50 percent (see Figures 5.5–5.8).

D. Smog chamber simulations

The Penner and Walton (1982) mechanism was compared by Leone and Seinfeld (1985) to five other urban photochemistry mechanisms under initial conditions representative of typical multi-organic smog chamber runs. The number of conversions of NO to NO_2 (exclusive of the reaction of NO with O_3) was shown to be a reasonable measure of the relative reactivity of the various mechanisms for producing ozone. This oxidation occurs most often by the reaction of NO with peroxide radicals, either HO_2 or various organic peroxides.

In comparison to Leone and Seinfeld's explicit mechanism, the Penner and Walton mechanism was more reactive at the higher ratios of initial hydrocarbon to nitrogen oxides (e.g., at ratios of 7 ppmC/ppm and 28 ppmC/ppm). However, Leone and Seinfeld found that at an initial hydrocarbon to NO_x ratio of 1.8 ppmC/ppm, the Penner and Walton mechanism was in substantial agreement with their explicit mechanism. Even though observed 6:00 to 9:00 a.m. hydrocarbon to NO_x ratios in the Bay Area are near 5 ppmC/ppm, we expect the comparison at this lowest ratio is the most similar to how the mechanism would behave in a regional model. This is because in a regional model the effect of continued emissions of NO_x would be to cause the mechanism to behave as it does at lower hydrocarbon to NO_x ratios. Leone and Seinfeld (1985) also investigated the change in reactivity when the photolysis rates for HC4 and methyl glyoxal were updated and found a substantial decrease in reactivity at all hydrocarbon to NO_x ratios.

Thus, based on our previous experience in simulating photochemistry in the Bay Area and St. Louis (Penner, 1984), it was clear that the mechanism would need to be more reactive in order to reproduce the expected ozone concentrations in the Bay Area. Furthermore, because the Penner and Walton (1982) mechanism reproduced the explicit mechanism simulation at the lowest initial hydrocarbon to NO_x ratio quite well, we aimed our efforts at trying to develop a mechanism that would have reactivity similar to the Penner and Walton (1982) mechanism.

Several methods for improving the chemical mechanism in the photochemical transport model were explored. Clearly, because the degradation in simulation quality comes about as a result of lumping chemical species, the best solution would be to eliminate all lumping.

Table 5.2. Updated reaction mechanism using 1986 rates

No.	Reaction	Reaction Rate Coefficients* A	B	C	Notes
Inorganic Reactions :					
R1	$O+O_2+M \rightarrow O_3+M$	3.00−28**	−2.3	0.0	1
R2	$O_3+NO \rightarrow NO_2+O_2$	1.80−12	0.0	1370.0	1
R3	$O+NO \rightarrow NO_2$	1.08−8	−1.5	0.0	1
R4	$O+NO_2 \rightarrow NO+O_2$	9.30−12	0.0	0.0	1
R5	$O+NO_2 \rightarrow NO_3$	1.39−7	−2.00	0.0	1
R6	$O_3+NO_2 \rightarrow NO_3+O_2$	1.20−13	0.0	2450.0	1
R7	$NO_3+NO_2 \rightarrow N_2O_5$	2.20−11	−0.5	0.0	1
R8	$N_2O_5 \rightarrow NO_2+NO_3$	1.45+16	−0.5	11150.0	1
R9	$NO_3+NO \rightarrow NO_2+NO_2$	1.30−11	0.0	−250.0	1
R10	$N_2O_5+H_2O \rightarrow 2HNO_3$	1.3−21	0.0	0.0	2
R11	$HO+NO_2 \rightarrow HNO_3$	5.87−08	−1.5	0.0	1
R12	$HO+NO \rightarrow HNO_2$	4.70−5	−2.6	0.0	1
R13	$HO+CO \xrightarrow{O_2} HO_2+CO_2 \quad O_2$	2.4−13	0.0	0.0	1
R14	$HO_2+NO \rightarrow HO+NO_2$	3.7−12	0.0	−240.0	1
R15	$HNO_2+HO \rightarrow H_2O+NO_2$	6.6−12	0.0	0.0	3
R16	$HO_2+HO_2 \rightarrow H_2O_2+O_2$	2.23−13	0.0	−765.0	1
R17	$HO+HO_2 \rightarrow H_2O+O_2$	1.10−10	0.0	0.0	1
R18	$HO+H_2O_2 \rightarrow HO_2+H_2O$	3.1−12	0.0	187.0	1
R19	$HO+HNO_4 \rightarrow H_2O+NO_2+O_2$	1.30−12	0.0	−380.0	1
R20	$HNO_4 \rightarrow HO_2+NO_2$	4.00+13	0.0	10065.0	1
R21	$HO_2+NO_2 \rightarrow HNO_4$	6.60−6	−2.7	0.0	1
R22	$HO+O_3 \rightarrow HO_2+O_2$	1.6−12	0.0	940.0	1
R23	$HO_2+O_3 \rightarrow HO+O_2+O_2$	1.4−14	0.0	580.0	1
Reactions of H_2CO :					
	$H_2CO+HO \rightarrow CO+HO_2+H_2O$	1.00−11	0.0	0.0	1
	$H_2CO+NO_3 \rightarrow CO+HO_2+HNO_3$	6.00−11	0.0	0.0	1
Reactions of HCl :					
R24	$HCl+HO \rightarrow RO_2+HC4$	2.77−11	0.0	−13.0	4
R25	$HCl+O_3 \rightarrow RO_2+HC4$	6.00−15	0.0	2100.0	5
R26	$HCl+O_3 \rightarrow RO_2+HO_2+H_2CO$	6.00−15	0.0	2100.0	5
R27	$HCl+O \rightarrow RO_2+RCO_3$	1.0−11	0.0	360.0	6
Reactions of HC2 :					
R29	$HC2+HO \rightarrow RO_2+H_2O$	1.68−11	0.0	560.0	4
R30	$HC2+O \rightarrow RO_2+HO$	2.45−11	0.0	2100.0	7

Reactions of HC4 :

R31	$HC4+HO \rightarrow RCO_3+H_2O$	6.71−12	0.0	−260.0	4
R33	$HC4+NO_3 \rightarrow RCO_3+HNO_3$	2.50−15	0.0	0.0	4

Reactions of HC3 :

R34	HC3+HO→ 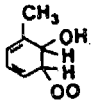 + products	4.30−13	0.0	−810.0	4
R35	$HC3+HO \rightarrow HO_2+$ products	4.30−13	0.0	0.0	7
R36	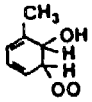 $+NO \rightarrow CH_3COCHO+HO_2+NO_2$	6.80−12	0.0	0.0	7
R37	$CH_3COCHO+HO \rightarrow RCO_3 + H_2O+CO$	1.70−11	0.0	0.0	7

Reactions of organic radicals :

R38	$RCO_3+HO_2 \rightarrow CH_3COCHO$	1.50−12	0.0	0.0	8
R39	$RCO_3+NO \rightarrow RO_2+NO_2$	9.60−12	0.0	0.0	4
R40	$RCO_3+NO_2 \rightarrow PAN$	6.00−12	0.0	0.0	4
R41	$PAN \rightarrow RCO_3+NO_2$	1.12+16	0.0	13330.0	1
R42	$RO_2+NO \rightarrow RO+NO_2$	4.20−12	0.0	−180.0	4
R43	$RO_2+HO_2 \rightarrow H_2O_2+HC4$	7.70−14	0.0	−13000	1
R44	$RO_2+RO_2 \rightarrow RO+RO+O_2$	1.60−13	0.0	−220.0	1
R46	$RO+O_2 \rightarrow HO_2+H_2CO$	2.00−12	0.0	0.0	1,4

Photolysis reactions :†

J1	$NO_2 \rightarrow NO+O$	7.90−3
J2	$O_3 \rightarrow O+O_2$	4.80−4
J3	$O_3 \rightarrow O_2+2HO$	1.96−6
J4	$HNO_2 \rightarrow HO+NO$	1.73−3
J5	$H_2O_2 \rightarrow HO+HO$	7.10−6
J6	$NO_3 \rightarrow NO_2+O$	2.26−1
J7	$NO_3 \rightarrow NO+O_2$	2.84−2
J8	$N_2O_5 \rightarrow NO_2+NO_2+O$	2.31−5
J9	$H_2CO \rightarrow CO+H_2$	1.25−5
J10	$H_2CO \rightarrow CO+HO_2+HO_2$	1.04−5
J11	$HC4 \rightarrow CO+RO_2+HO_2$	2.21−6
J12	$CH_3COCHO \rightarrow HO_2+RCO_3+CO$	1.50−4

* Rate = $A \times T^B \times e^{-C/T}$ in $cm^3\ sec^{-1}$ for 2-body reactions or $cm^6\ sec^{-1}$ for 3-body reactions. Thermal decomposition rates and photolysis rates are in sec^{-1}.

** Notation: $5.58-29 = 5.58 \times 10^{-29}$.

† $\chi = 46\ °$.

Notes :

1. DeMore, W. B., J. J. Margitan, M. J. Molina, R. T. Watson, D. M. Golden, R. F. Hampson, M. J. Kurylo, C. J. Howard, and A. R. Ravishankara (1985) Chemical kinetics and photochemical data for use in stratospheric modeling. Evaluation number 7, JPL publication 85–27.
2. Russell, A. G., G. R. Cass, and J. H. Seinfeld (1986) On some aspects of nighttime atmospheric chemistry, *Environ. Sci. Technol., 20*, 1167–1172, and sources noted herein.
3. Cox, R. A., R. G. Derwent, and P. M. Holt (1976) Relative rate constants for the reactions of OH radicals with H_2, CH_4, CO, NO, and HONO at atmospheric pressure and 296 K. *J. Chem. Soc. Faraday I, 72*, 2031–2043.
4. NCAR (1986) Preliminary evaluation studies with the regional acid deposition model (RADM). NCAR/TN-265 + STR, National Center for Atmospheric Research.

   and

   Stockwell, W. R. (1986) A homogeneous gas phase mechanism for use in a regional acid deposition model. *Atmos. Environ., 20*, 1615–1632.
5. Reference (4). Products were chosen to reflect final products of reaction sequence involving Criegee intermediates not included in the mechanism in this report.
6. Singleton, D. L. and R. J. Cvetanovic (1976) Temperature dependence of the reaction of oxygen atoms with olefins. *J. Atm. Chem. Soc., 98*, 6812–68XX.
7. Leone, J. A. and J. H. Seinfeld (1985) Comparative analysis of chemical reaction mechanisms for photochemical smog. *Atmos. Environ., 19*, 437–464.
8. Reference (4). Product chosen to reflect reactivity and decomposition products of peroxyacetic acid actually formed.

Such a solution is not possible, however, without infinite computer resources. Therefore, some degree of lumping is appropriate.

The chemical mechanisms in common use today lump hydrocarbons to varying degrees. Table 5.3 shows the hydrocarbon species represented in a recently derived mechanism (Lurmann et al., 1987). We note that this mechanism could not be incorporated at this time into a simulation of the Bay Area because no speciated inventory for this mechanism was available. Most mechanisms treat H_2CO and ethene in full detail and separate their representation from that of other aldehydes and alkenes, respectively. Therefore, we explored using separate treatments for H_2CO and ethene in several smog chamber-type simulations.

Figure 5.9 shows the results of a simulation of a multi-hydrocarbon smog chamber experiment (EC245) that was previously used to verify the 1982 mechanism (see Penner and Walton, 1982, and Pitts et al., 1979). The figure shows the O_3, NO, NO_2, and PAN concentrations as a function of time. Figures 5.9–5.12 show the results of the simulation using the 1982 mechanism and 1982 reaction rates, the 1982 mechanism with reaction rates

Table 5.3. Organic species represented in Lurmann et al. (1987) mechanism.*

		Species requiring differentiation in emissions inventory
H_2CO	Formaldehyde	X
ALD2	Acetaldehyde	X
MEK	Methyl/ethyl/ketone	
MGLY	Methyl glyoxal	
PAN	Peroxyacylnitrate	
RO2	Total RO_2 Radicals	
MCO3	CH3CO3 Radical	
ALKN	Alkyl nitrate	
ALKA	> C3 Alkanes	X
ETHE	Ethene	X
ALKE	> C2 Alkenes	X
TOLU	Toluene	X
AROM	Higher aromatics	X
DIAL	Unknown dicarbonyls	
CRES	O-Cresol	
NPHE	Nitrophenols	
RO2R	General RO_2 #1	
BZO	Phenoxy radical	
R2O2	General RO_2 #2	
RO2N	Alkyl nitrate RO_2	
RO2P	Phenol RO_2	
BZN2	Benzaldehyde N-RO_2	

* The total number of species (organic and inorganic) represented in this mechanism is 36.

updated to values appropriate to 1986, a new mechanism with the chemistry of H_2CO treated separately from that of HC4 (higher aldehydes), and a mechanism with H_2CO and ethene treated separately. This last mechanism would require a detailed emissions inventory for ethene in order to implement it in the Bay Area. Such a detailed inventory for the Bay Area and Monterey does not exist at this time.

As shown in the figures, the production rate for O_3 is slowed with the 1982 mechanism when the rates are updated to the values recommended in 1986, although the peak O_3 concentration that is eventually reached is about the same (compare Figures 5.9 and 5.10). Separate treatment for H_2CO causes the ozone peak to increase from about 2.5×10^{12} cm^{-3} (in Figure 5.10) to 3.2×10^{12} cm^{-3} (Figure 5.11) and the peak forms earlier (at about the same time as for the 1982 mechanism with 1982 rates). Separately treating H_2CO and ethene slows the rate of formation of O_3 again, but the peak concentration is about the same as for the simulation with only H_2CO treated separately (see Figure 5.12). These results imply that the degree of lumping can significantly change both the rate of O_3 formation and its peak concentration. The effects of lumping in regional models will be determined by a combination of the the importance of the emissions of any given species

and the degree of error generated in any given simulation by not treating that species separately. For H_2CO, as shown by the simulations for EC245, the degree of error is likely to be significant. For ethene, it may be as well, but since we have no separate emissions inventory for ethene, the degree of error in the regional model cannot be determined.

Smog chamber experiments are often difficult to simulate because vital measurements and chamber characteristics are often lacking. Thus, we also tested the mechanisms described above in a box-model calculation intended to simulate conditions in the full regional model. For this simulation, initial species concentrations were those calculated for an earlier LIRAQ calculation for an area near San Jose (Penner et al., 1983). Emissions were taken equal to the emissions local to the San Jose area, and the layer-depth was allowed to grow throughout the simulation time. Photolysis rates were set to those calculated in the regional model at local noon (see Table 5.2). Previously, this procedure adequately represented the sensitivity of the photochemical transport model to mechanism changes (Penner, 1984).

Figures 5.13–5.17 show the results of this simulation using the mechanisms and reaction rates described above. Because NO_x is continuously injected into the model, the production rate for O_3 is slowed compared to that in the simulation of EC245, and the peak O_3 concentration is not reached until the end of the simulation period. Thus, the peak O_3 concentration reached in the regional model is controlled by both the rate of production of O_3 as well as the potential peak O_3 formation. Comparison of Figures 5.13 and 5.14 confirms the analysis presented above, which showed that the 1982 mechanism with updated reaction rates forms O_3 too slowly. By the end of the regional box-model simulation, the peak concentration is only 1.8×10^{12} cm^{-3}, whereas with the 1982 rates it had been 4.5×10^{12} cm^{-3} (compare with Figures 5.13 and 5.14). Treating H_2CO separately raises the peak O_3 concentration to 3.5×10^{12} cm^{-3} (see Figure 5.15). In this simulation all HC4 emissions have been assumed to be H_2CO, but the result is similar if emissions of HC4 are lumped into the higher aldehyde category (see Figure 5.16). Because we have no emissions data to allow us to also treat ethene separately, the test shown in Figure 5.17 is only indicative of the possible changes with more highly refined chemical mechanisms. This simulation assumed that half of the alkene emissions were ethene and half were higher aldehydes. If this is the correct ratio, the simulated peak O_3 concentrations would decrease significantly. Of course, to the extent that ethene is overemphasized by the assumption that it represents half the initial concentration and emissions of alkenes, the reduction in predicted O_3 concentration is overemphasized.

Tests of the mechanism with updated reaction rates and with H_2CO treated separately were performed in the multi-layer photochemical transport model as well. Figures 5.18–5.20 show the O_3 concentrations generated with the 1986 mechanism with H_2CO treated separately (compare Figures 5.2, 5.3, and 5.4). The peak O_3 concentrations are somewhat smaller with the new mechanism, but, based on previous experience, we expect that an adequate simulation with the new mechanism is possible. The next section describes some added testing of this mechanism.

E. Performance evaluation of the new mechanism

The tests described above in section D are sufficient to allow us to expect that the performance evaluation of the new model with the new mechanism should be similar to

previous evaluations of LIRAQ which used the Penner and Walton (1982) mechanism. However, the soundness of the new mechanism as far as its ability to predict how regional O_3 concentrations would respond to emissions inventory changes has not yet been demonstrated. Previously, the 1982 mechanism was evaluated by its ability to reproduce the measured O_3 concentration in a series of hydrocarbon-NO_x smog chamber simulations. The simulation of EC245, presented previously, was one of nine multi-hydrocarbon simulations used to test the previous mechanism. In addition, separate simulations of propene, n-butane, and toluene were performed to test the representations of these species by HC1, HC2, and HC3, respectively. The chamber simulations were based on known chamber characteristics and data gathered as of 1982.

Since that time, a great deal of information and smog chamber characterization work has been performed. At least for the SAPRI chamber experiment, chamber wall sources and losses for a variety of radical species are thought to be better understood than they were previously (Carter et al., 1982). Thus it seems appropriate to test the new mechanism for its ability to reproduce some of the newer smog chamber data. Current resources did not allow a large characterization set to be made. However, we have tested the new mechanism's ability to simulate a multi-hydrocarbon/NO_x chamber experiment, wherein both the hydrocarbon mix is thought to be representative of typical urban conditions, and the hydrocarbon to NO_x ratio is typical of values measured in the Bay Area (Carter et al., 1986). We also separately tested the response of the mechanism to reductions in hydrocarbons as determined in a separate smog chamber experiment. To the extent that the lumped mechanism adequately reproduces the response of the chamber O_3 to these reductions, we expect that its predictions for the Bay Area and Monterey will be adequate. One caveat, however, concerns the role of chamber wall reactions. If these are important in determining the response of the chamber (and also of the mechanism used to simulate the chamber), then the response is not representative of the atmospheric response expected for such a change. Thus, the smog chamber validation may not be adequate. Furthermore, since source and reaction rates for radical species in the chamber are determined by examining reactions in a "clean" chamber and then extrapolated to more polluted environments, they may change when experiments under more highly polluted conditions are run. In that case, the characterization by Carter et al. (1986) could be wrong or incomplete.

Figures 5.21 and 5.22 show a simulation of smog chamber experiments IC871 and IC873 from Carter et al. (1986), respectively. In these simulations the photolysis rate for NO_2 was that measured in the chamber, while those of the other species were assumed to have the same ratio to the NO_2 photolysis rate as was calculated for an overhead sun in the photochemical transport model. The simulation of IC871 was chosen to test the ability of the new mechanism to predict ozone formation at hydrocarbon to NO_x concentrations similar to those observed in the Bay Area. The simulation of IC873 was chosen to test the ability of the mechanism to predict the ozone response when hydrocarbon concentrations are decreased. Comparing Figure 5.23 with Figure 5.21 shows that the new mechanism produces ozone somewhat faster than the observations show, but the relative decrease obtained when hydrocarbons are reduced is reasonably well described. Thus, the mechanism used here predicts a decrease in peak O_3 of about 48 percent when hydrocarbons are reduced, while the observations show a decrease of about 57 percent.

Figure 5.23 shows a simulation of the smog chamber experiment IC871 with the ERT/SAPRI condensed mechanism (Lurmann et al., 1987). As shown there, the ERT/SAPRI mechanism (which represents a less condensed mechanism) is somewhat less reactive than the mechanism developed here. The peak in O_3 is not yet reached by the end of the simulation and the highest value is only 8×10^{12} cm^{-3} (compared to 13×10^{12} cm^{-3} for the more highly lumped mechanism). Much of the difference in reactivity between these two mechanisms can be explained by the different treatment of primary hydrocarbon emissions. To show this, we ran a simulation of IC871 in which all hydrocarbons were emitted into the hydrocarbon classes ALKE (to correspond to HC1), ALKA (to correspond to HC2), and TOLU (to correspond to HC3), and the reactivity weighting scheme was the same as that used in the more highly lumped mechanism developed here. This simulation is shown in Figure 5.24. The peak ozone concentration reached in this simulation is about 10×10^{12} cm^{-3}, which corresponds quite well with the peak reached in the simulation shown in Figure 5.21. Much of the remaining differences are due to the further lumping of derivative organic species in the more highly lumped mechanism (compare Tables 5.1 and 5.3).

Figure 5.25 shows a simulation of the smog chamber experiment IC871 with the ERT/SAPRI condensed mechanism. At this lowered hydrocarbon to NO_x ratio, the ERT/SAPRI mechanism predicts only half as much O_3 as the more highly lumped mechanism. In this case, lumping the primary emissions into the ERT/SAPRI categories ALKA, ALKE, and TOLU does little to increase the simulated O_3 concentration (see Figure 5.26). Apparently, at this ratio, the lumping of derivative organic species can significantly enhance the rate of radical formation and, thus, the peak O_3 concentration.

F. Appraisal of soundness of mechanism and recommended improvements

The current mechanism can adequately simulate the expected response of ozone to reductions in hydrocarbons in the SAPRI smog chamber at HC/NO_x ratios near those expected in the Bay Area, but appears to be over-reactive at the lowest hydrocarbon to NO_x ratio tested (i.e., at 3.6 ppmC/ppm). The mechanism developed here is also more reactive than the ERT/SAPRI mechanism. Because the ERT/SAPRI mechanism was developed from a full, explicit mechanism that tested well against the smog chamber data, by this comparison, the current mechanism is too reactive and overpredicts O_3 at the lowest hydrocarbon to NO_x ratios. This conclusion is contrary to the conclusion reached by Leone and Seinfeld (1985) for low hydrocarbon to NO_x ratios (i.e., at ratios of 1.8 ppmC/ppm), whose comparison of their explicit mechanism to the mechanism of Penner and Walton (1982) was used to guide the present development. They found that the mechanism performed best at the lowest hydrocarbon to NO_x ratios. Apparently, significant differences still remain in explicit mechanism development and in mechanism condensation techniques and, thus, it is not possible to quantify how reliable the present mechanism is. According to the analysis of Leone and Seinfeld (1985), the present mechanism does quite well. But in comparison to the ERT/SAPRI mechanism, the present mechanism is too reactive. As pointed out by Leone and Seinfeld (1985), these differences will probably remain as long as smog chamber characterization remains incomplete.

The slower O_3 formation rate predicted with the ERT/SAPRI mechanism could have significant implications for both ozone development and control strategies in the San

Francisco-Monterey Bay areas. While both mechanisms correctly predict a decrease in O_3 when hydrocarbons are reduced, the relative decrease is larger for the ERT/SAPRI mechanism. The chamber simulations were extended to a situation in which NO_x was reduced as well. For these simulations, the more highly condensed mechanism results in a similar peak O_3 concentration, but it occurs much sooner, while the ERT/SAPRI mechanism gives an increase of 12.5 percent (compare Figures 5.27 and 5.28). Thus, the quantitative response of these two mechanisms to NO_x controls would also differ.

As discussed in Chapter 6, simulations with the multi-layer photochemical transport model indicate that decreasing NO_x in the San Francisco Bay Area would result in ozone increases close to the source region, but small ozone decreases in outlying regions. In the outlying regions, ozone is decreased primarily because the transformation of NO to NO_2, and thus the photooxidant development, is more rapid with lowered NO_x, leaving less potential for further ozone formation at downwind locations. Because the ERT/SAPRI mechanism forms ozone less rapidly and converts NO to NO_2 less rapidly, the inner area of ozone increase with decreased NO_x emissions could be more extensive, but it could also extend the downwind area of ozone decrease to further outlying regions. Whether such a change would then be experienced at any of the MBUAPCD stations depends on the effect of local MBUAPCD emissions on the chemistry development. To test such a possibility would require a full regional simulation with an emissions inventory appropriate to the less condensed mechanism. In our view, such a study should be initiated to more properly quantify the effect of San Francisco Bay Area emissions on the MBUAPCD.

In addition to the mechanism differences noted above, there are differences between the ERT/SAPRI mechanism and other mechanisms (G. Whitten, private communication (1987), Leone and Seinfeld (1985)). The lack of agreement between mechanisms is the result of real uncertainties in mechanism development due to the lack of data on primary reaction kinetics and products as well as real uncertainties in smog chamber characterization. There is also a lack of agreement as to the best condensation technique. As long as these uncertainties exist, it will not be possible to eliminate the quantitative differences in control strategy predictions. A measure of the degree of uncertainty can be obtained by using several of these mechanisms to evaluate any given control strategy (while keeping the other model characteristics constant). Such an uncertainty analysis would be highly desirable in the present case.

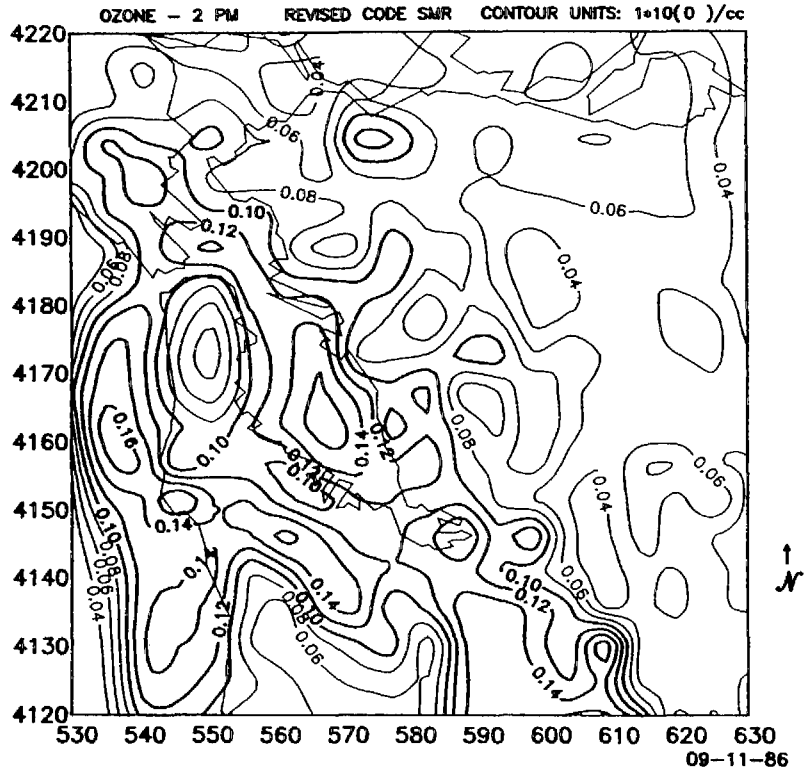

Figure 5.1. Surface O_3 mixing ratio for the 1982 mechanism at 1400 hours on September 30, 1980. The units are ppm.

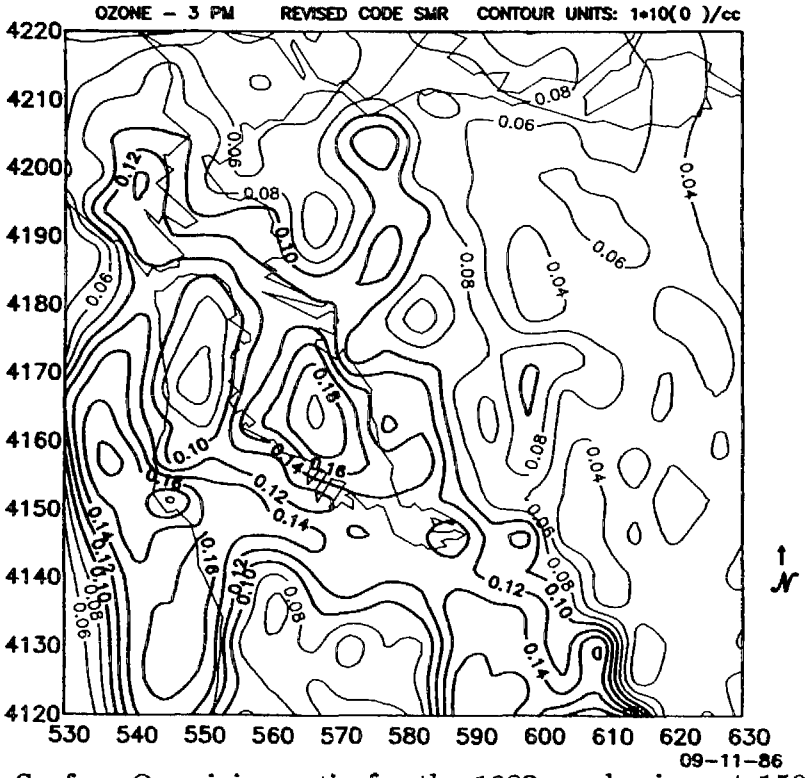

Figure 5.2. Surface O_3 mixing ratio for the 1982 mechanism at 1500 hours on September 30, 1980. The units are ppm.

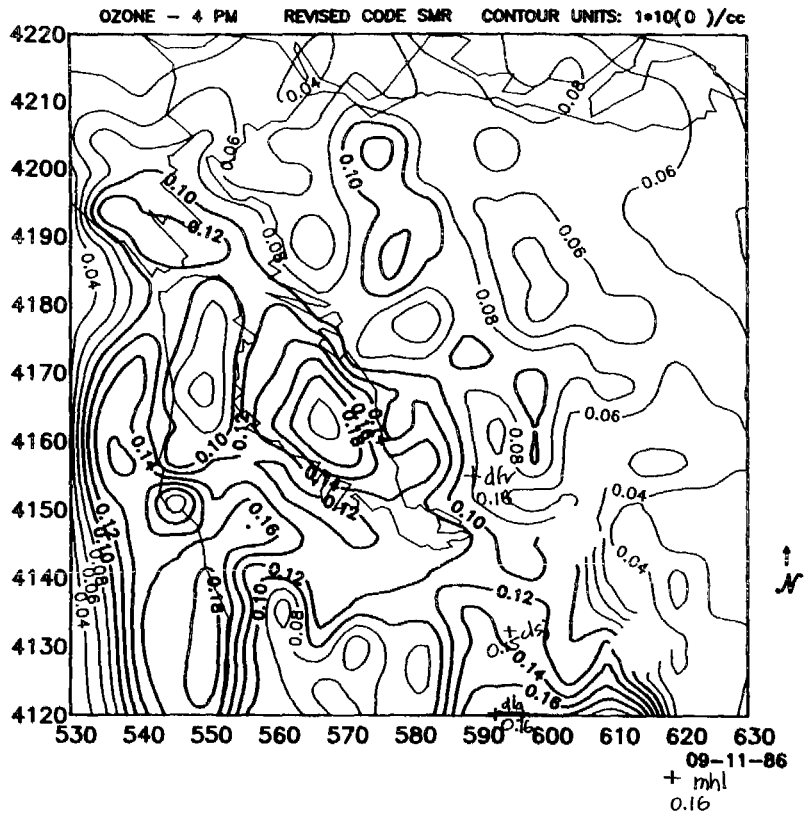

Figure 5.3. Surface O_3 mixing ratio for the 1982 mechanism at 1600 hours on September 30, 1980. The units are ppm.

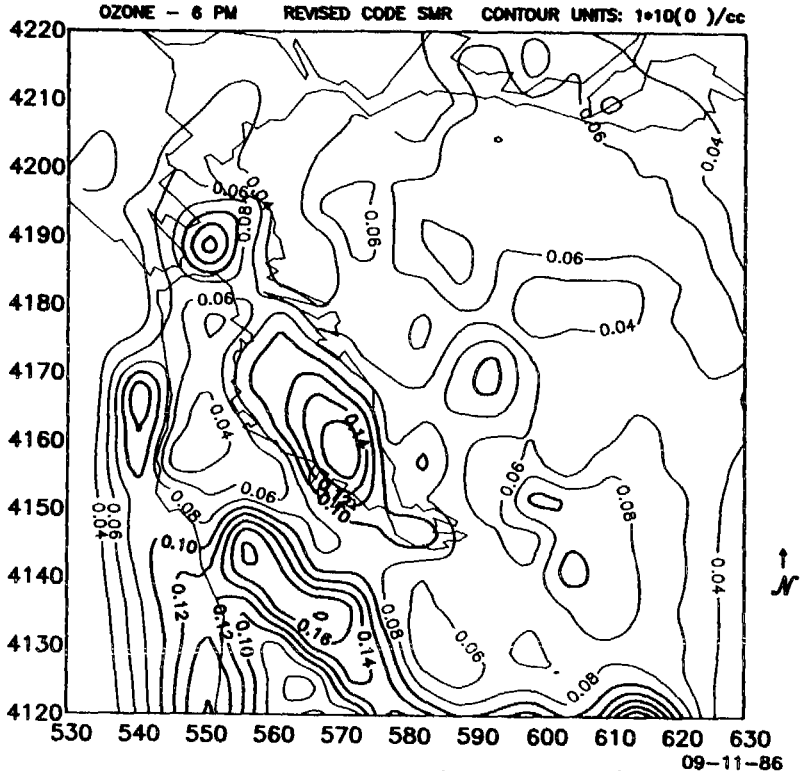

Figure 5.4. Surface O_3 mixing ratio for the 1982 mechanism at 1800 hours on September 30, 1980. The units are ppm.

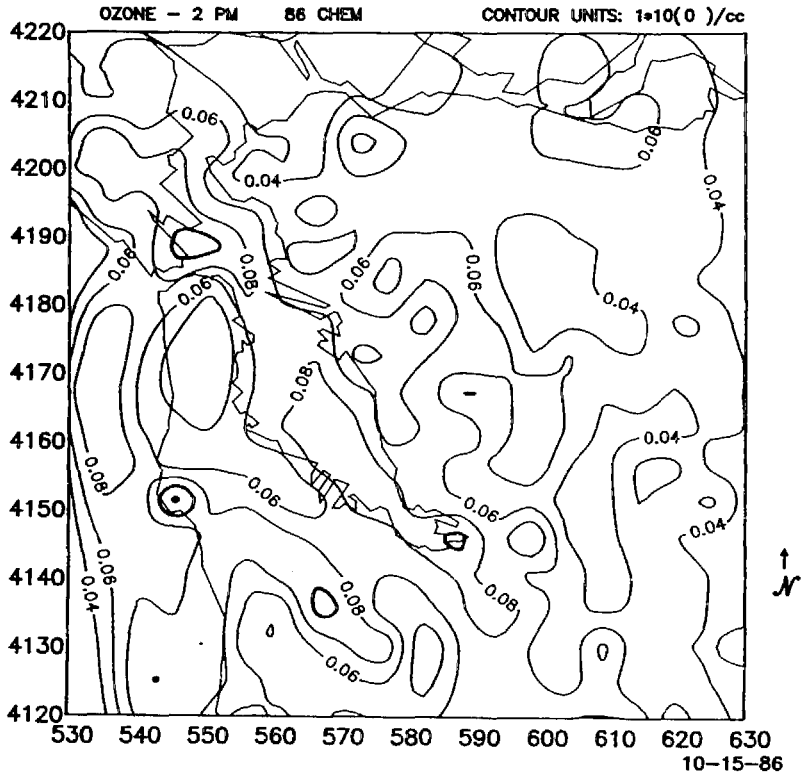

Figure 5.5. Surface O_3 mixing ratio for the 1982 mechanism with rate constants and photolysis rates updated to 1986 at 1400 hours on September 30, 1980. The units are ppm.

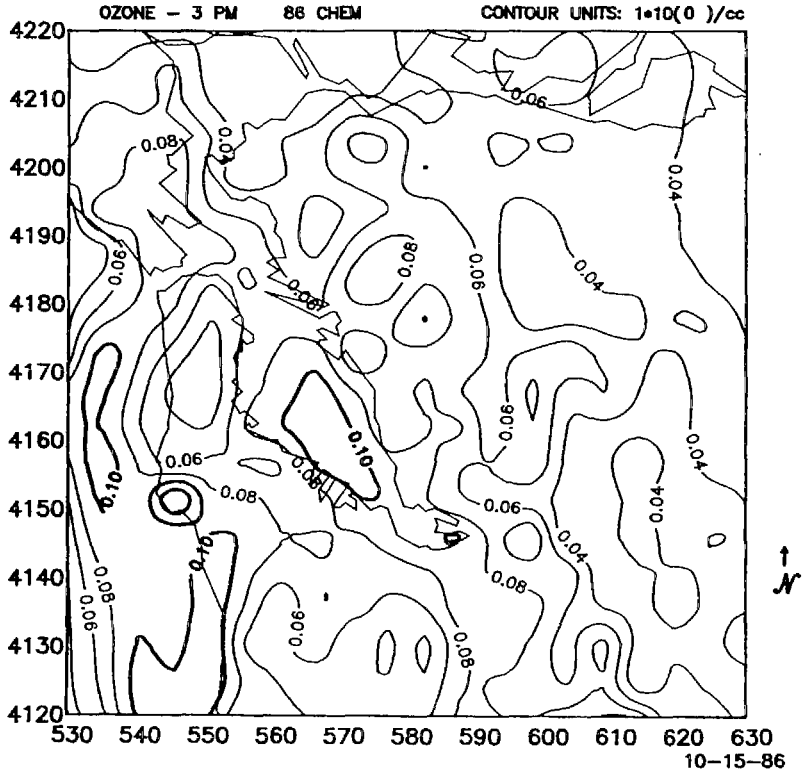

Figure 5.6. Surface O_3 mixing ratio for the 1982 mechanism with rate constants and photolysis rates updated to 1986 at 1500 hours on September 30, 1980. The units are ppm.

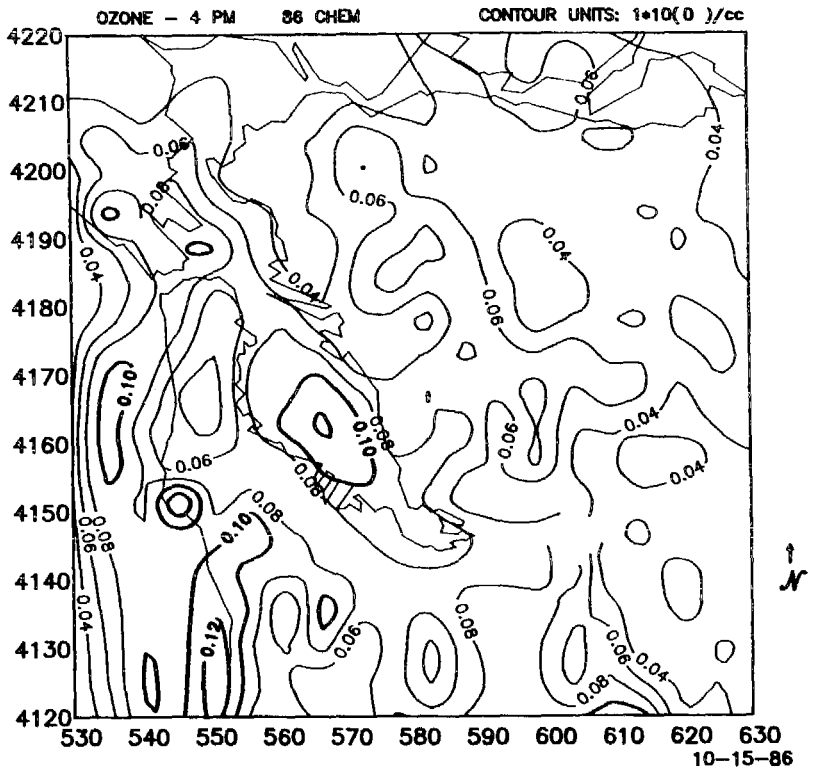

Figure 5.7. Surface O_3 mixing ratio for the 1982 mechanism with rate constants and photolysis rates updated to 1986 at 1600 hours on September 30, 1980. The units are ppm.

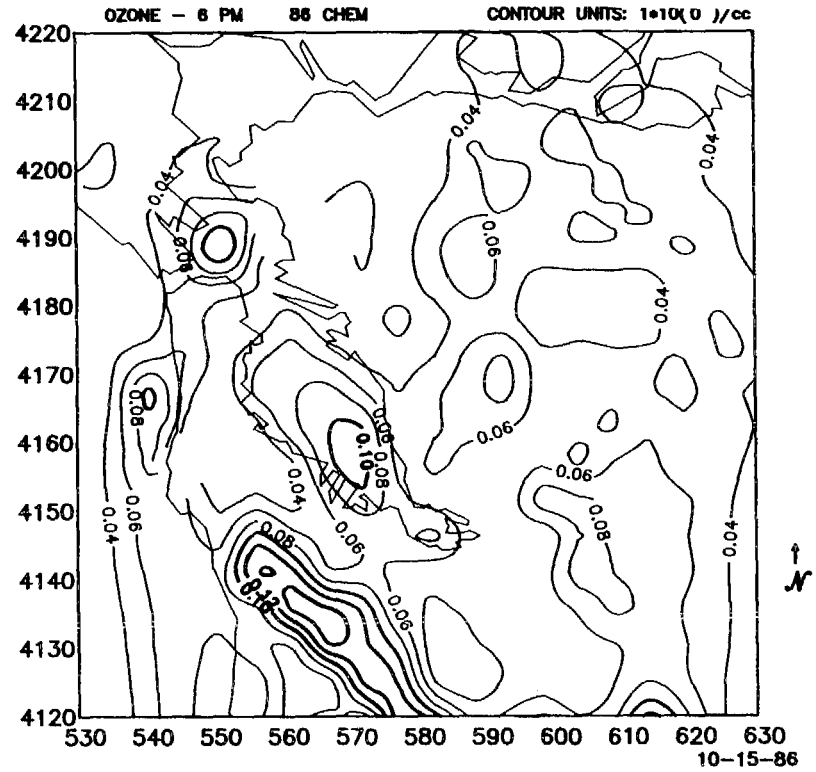

Figure 5.8. Surface O_3 mixing ratio for the 1982 mechanism with rate constants and photolysis rates updated to 1986 at 1800 hours on September 30, 1980. The units are ppm.

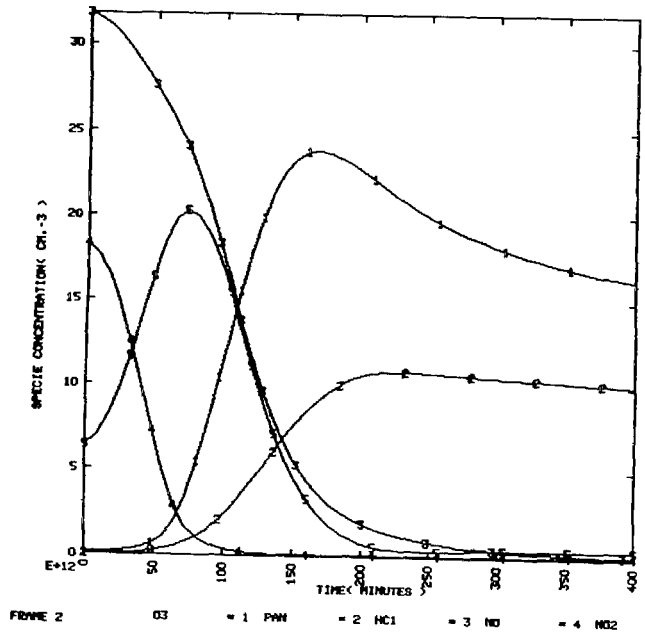

Figure 5.9. Simulation of the State Air Pollution Research Institute (SAPRI) smog chamber experiment EC245 using the Penner and Walton (1982) mechanism.

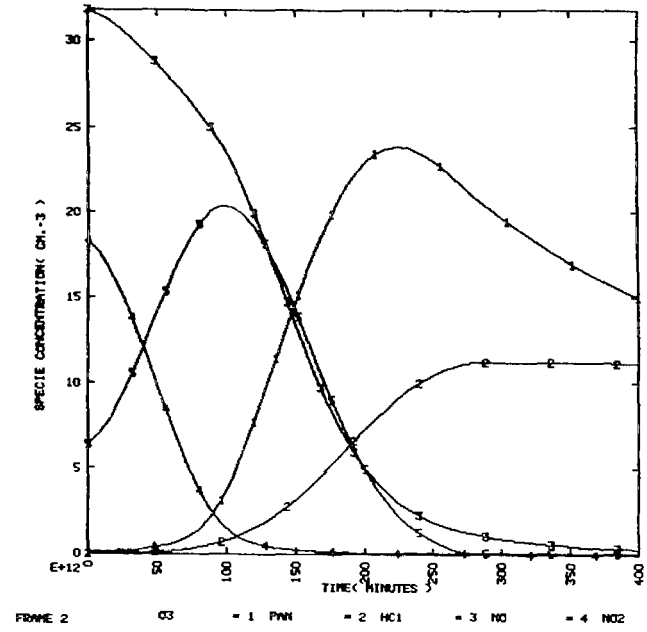

Figure 5.10. Simulation of smog chamber experiment EC245 using the Penner and Walton (1982) mechanism with photolysis and reaction rates updated to 1986.

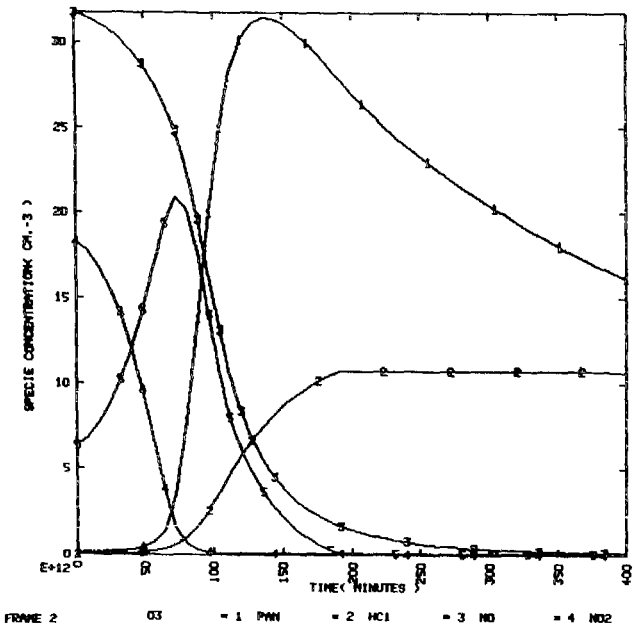

Figure 5.11. Simulation of smog chamber experiment EC245 using a mechanism that treats the chemistry of H_2CO explicitly.

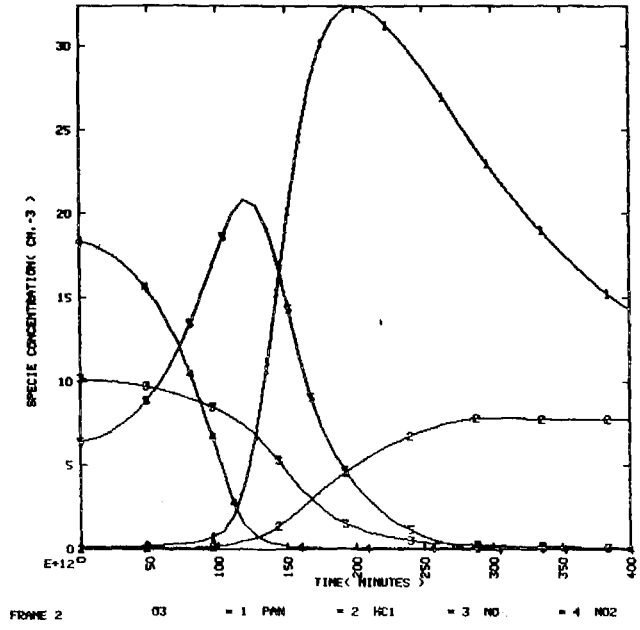

Figure 5.12. Simulation of smog chamber experiment EC245 using a mechanism that treats the chemistry of both H_2CO and C_2H_4 explicitly.

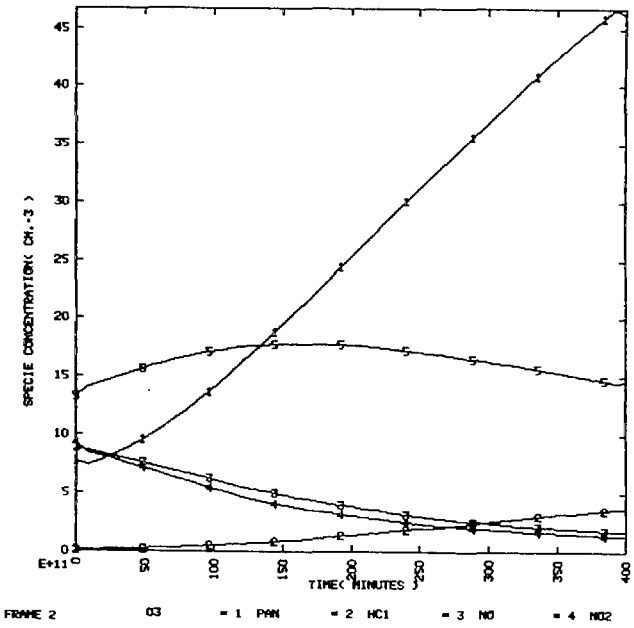

Figure 5.13. Simulation of conditions near San Jose using the 1982 mechanism.

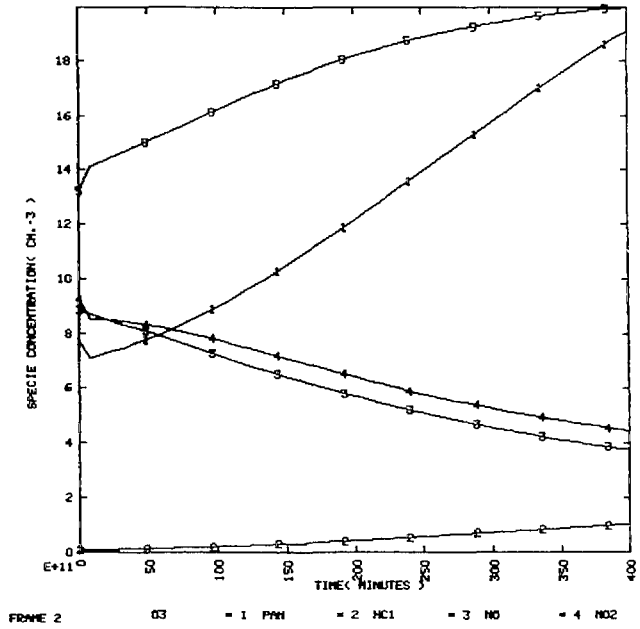

Figure 5.14. Simulation of conditions near San Jose using the 1982 mechanism with rate constants and photolysis rates updated to 1986.

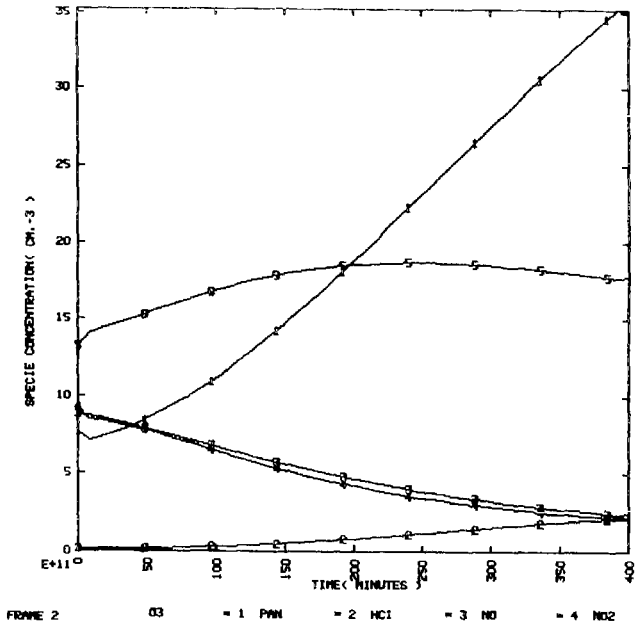

Figure 5.15. Simulation of conditions near San Jose using the mechanism which treats H_2CO explicitly. All aldehyde emissions are assumed to be H_2CO.

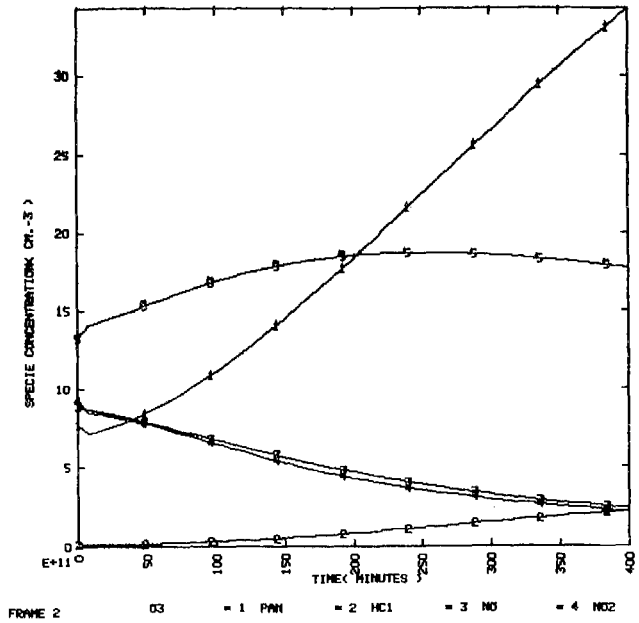

Figure 5.16. Simulation of conditions near San Jose using the mechanism which treats H_2CO explicitly. Aldehyde emissions are assumed to be 50% H_2CO and 50% higher aldehydes.

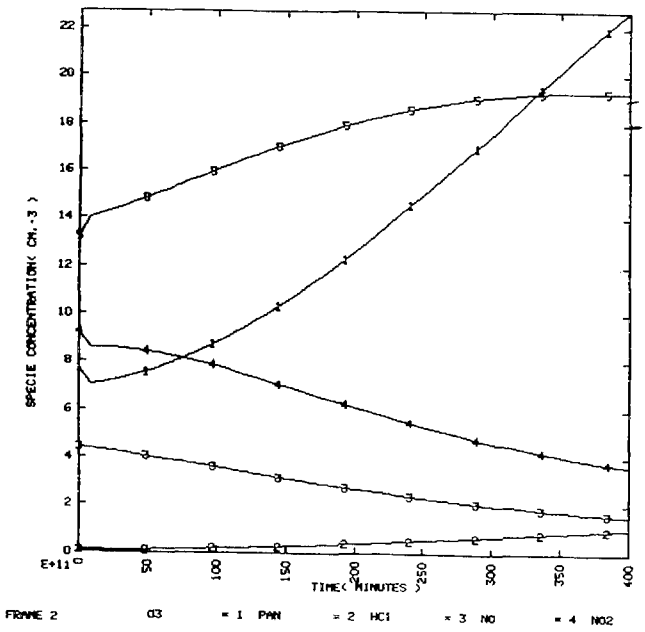

Figure 5.17. Simulation of conditions near San Jose using the mechanism which treats both H_2CO and C_2H_4 explicitly. All aldehyde emissions are assumed to be H_2CO and the alkene emissions are 50% ethene and 50% higher alkenes.

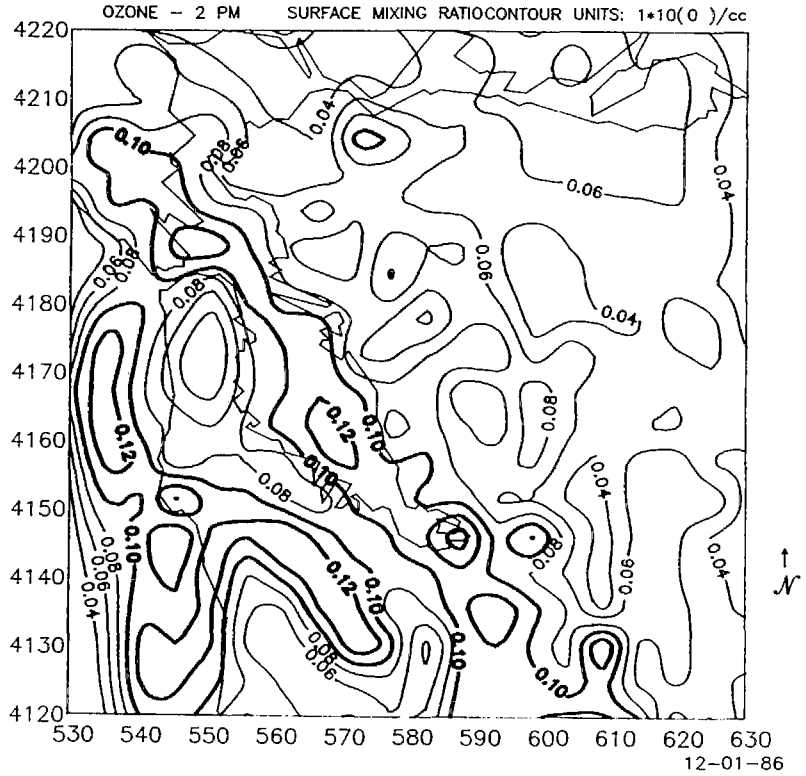

Figure 5.18. Surface O_3 mixing ratio for the mechanism which treats H_2CO separately at 1400 hours on September 30, 1980.

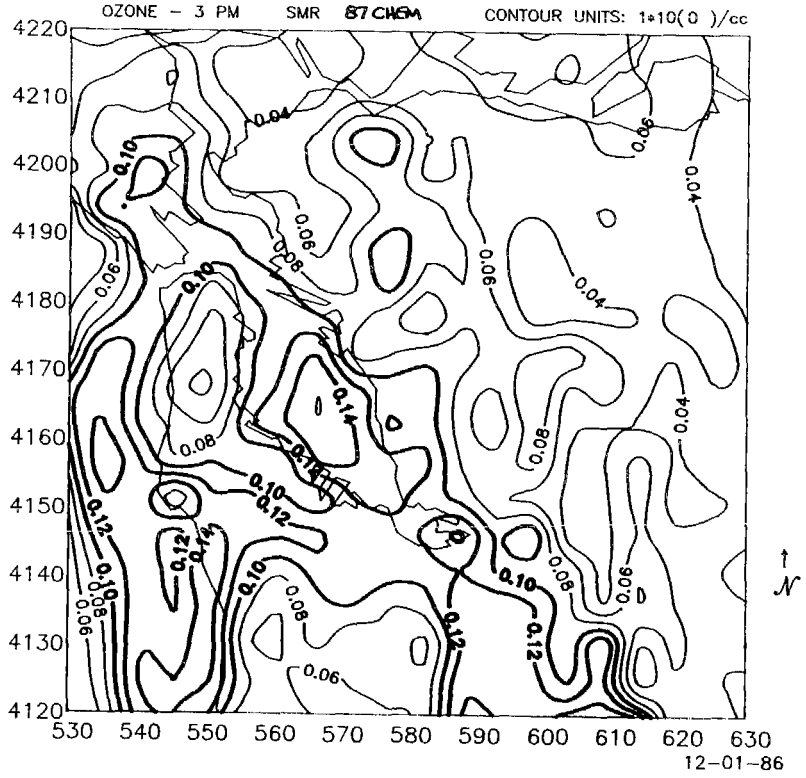

Figure 5.19. Surface O_3 mixing ratio for the mechanism which treats H_2CO separately at 1500 hours on September 30, 1980.

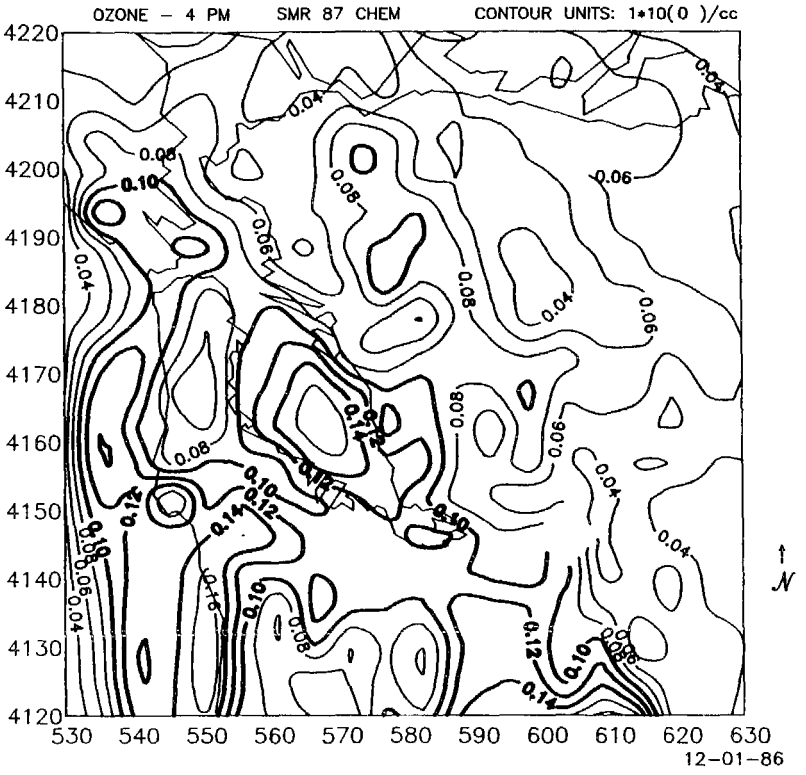

Figure 5.20. Surface O_3 mixing ratio for the mechanism which treats H_2CO separately at 1600 hours on September 30, 1980.

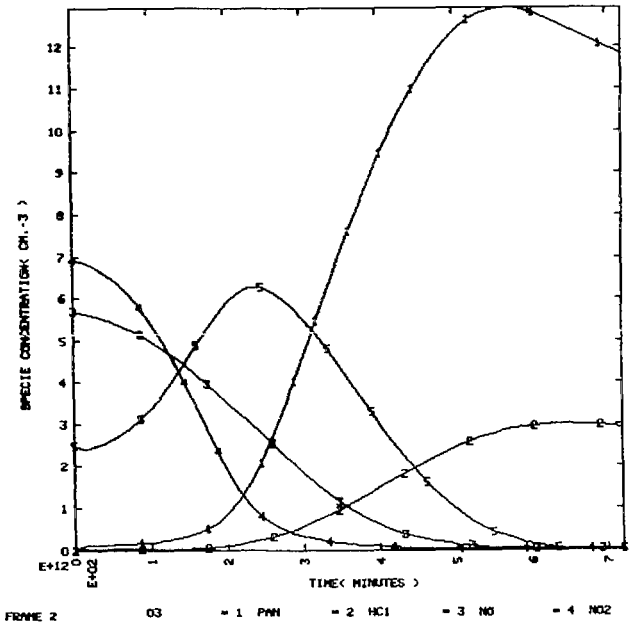

Figure 5.21. Simulation of smog chamber experiment IC871 from Carter et al. (1986) using the new mechanism.

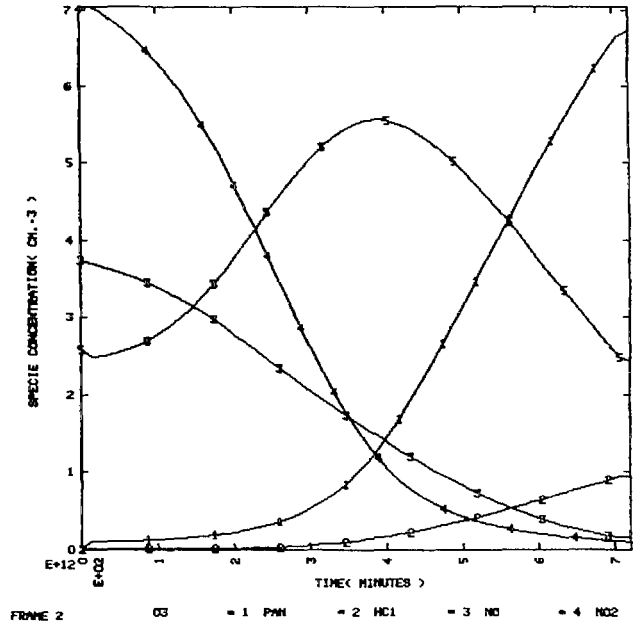

Figure 5.22. Simulation of smog chamber experiment IC873 from Carter et al. (1986) using the new mechanism.

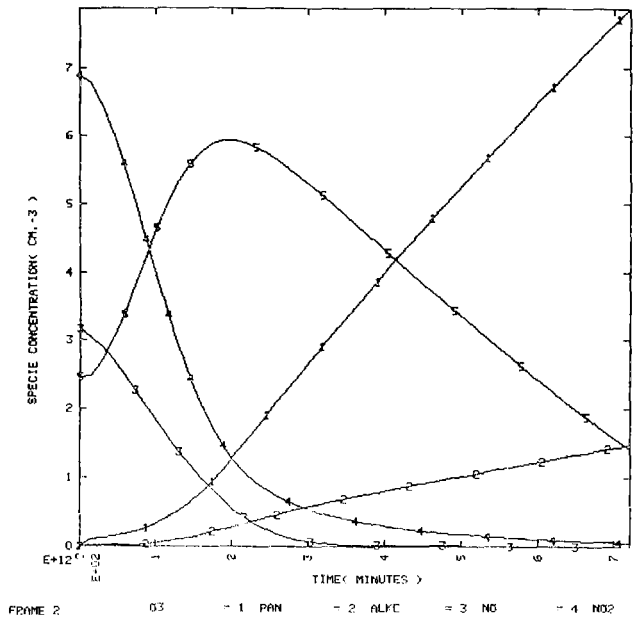

Figure 5.23. Simulation of smog chamber experiment IC871 from Carter et al. (1986) using the condensed mechanism of Lurmann et al. (1987).

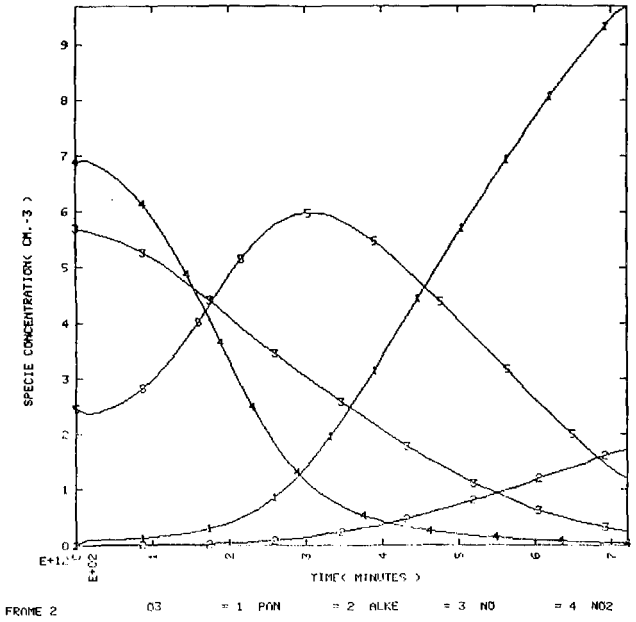

Figure 5.24. Simulation of smog chamber experiment IC871 from Carter et al. (1986) using the condensed mechanism of Lurmann et al. (1987), initialized with the hydrocarbon categories and reactivity weighting scheme of the more highly lumped mechanism developed here.

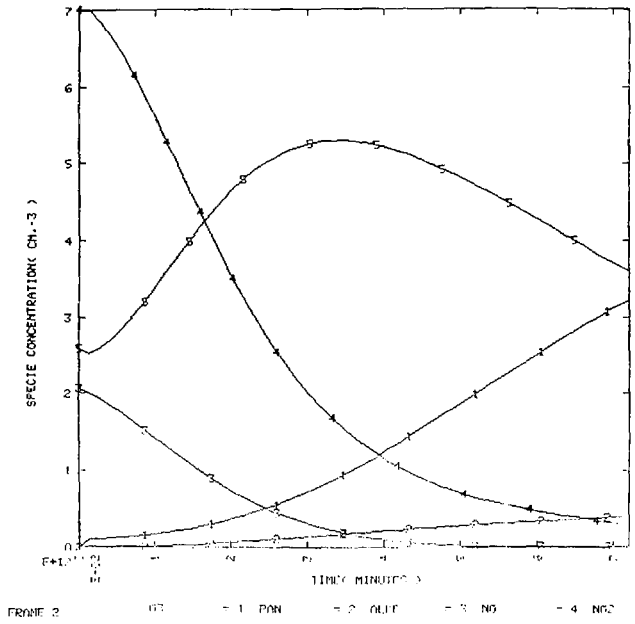

Figure 5.25. Simulation of smog chamber experiment IC873 from Carter et al. (1986) using the condensed mechanism of Lurmann et al. (1987).

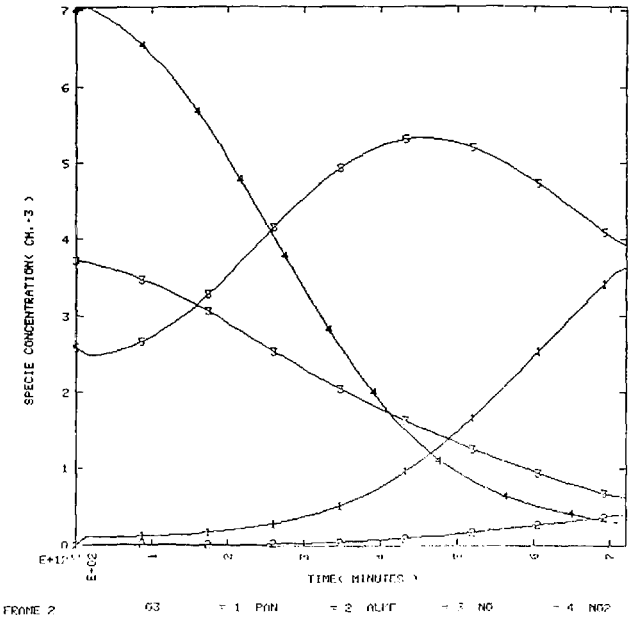

Figure 5.26. Simulation of smog chamber experiment IC873 from Carter et al. (1986) using the condensed mechanism of Lurmann et al. (1987), initialized with the hydrocarbon categories and reactivity weighting scheme of the more highly lumped mechanism developed here.

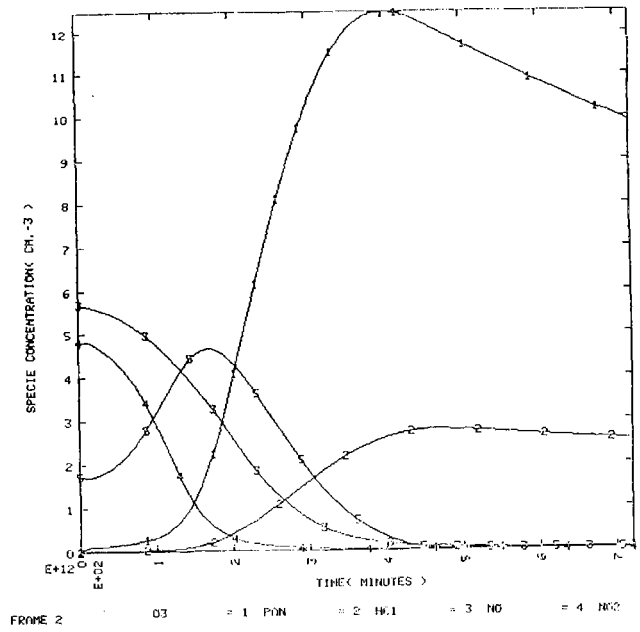

Figure 5.27. Simulation of a smog chamber experiment using the new mechanism with initial conditions as in Figure 5.21 except that NO and NO_2 have been reduced by 30 percent.

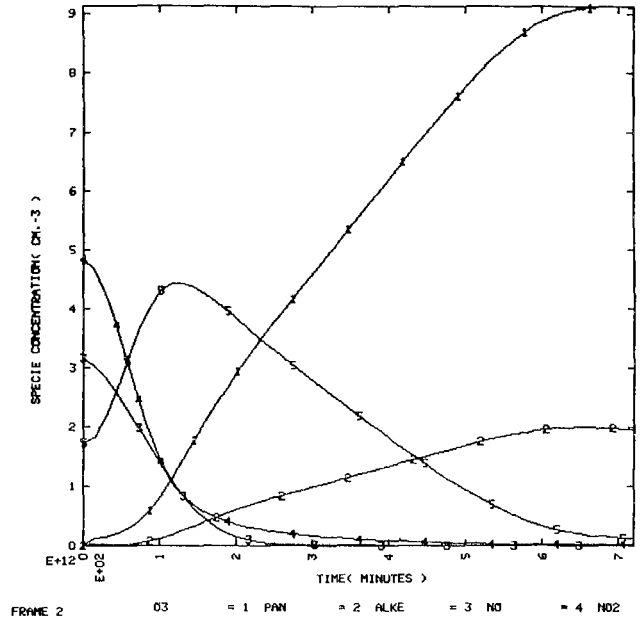

Figure 5.28. Simulation of a smog chamber experiment using the mechanism of Lurmann et al. (1987) with initial conditions as in Figure 5.23 except that NO and NO_2 have been reduced by 30 percent.

Chapter 6. Sensitivity Tests of New Model and Performance Evaluation

P. S. Connell
J. E. Penner
C. S. Atherton

A. Introduction

Two features of the new model other than the chemistry (treated in Chapter 5) are new and deserve description as well as an analysis of their effects on predicted concentration fields. These features are discussed here. They include the treatment of vertical mixing within the mixed-layer and the effect of including a layer above the mixed-layer. After a discussion of these features and their effects, we describe two different model simulations with two different meteorological fields. The first was produced before any ozone fields had been calculated and thus represents an "untuned" meteorology. Subsequently, attempts were made to improve model performance by altering the meteorological fields in ways that were consistent with meteorological observations. Previous experience has shown that one can enhance model performance by this "tuning" process. Unfortunately, this type of model manipulation can lead to overconfidence in model results and can mask uncertainties in the overall analysis. We therefore discuss the differences obtained with these two versions of the meteorology to show the uncertainty resulting from inadequate knowledge of the meteorology. In one sense, the best test of overall model performance should be based on the model's ability to reproduce ozone fields before any tuning is allowed.

After this work had been completed, it was discovered that the mobile emissions inventory NO_x used to develop the emissions in the BAAQMD had inadvertently been low by perhaps 25 to 40 tons/day. The use of a correct emissions inventory resulted in significant changes to the predicted O_3 field. The performance evaluation section reports results for a simulation with the correct emissions inventory and the sensitivity section tests the response of the corrected model to lowered NO_x emissions.

B. Treatment of vertical mixing

The LIRAQ model (MacCracken et al., 1978) assumed a vertical profile for pollutant concentrations that was based on a steady state solution of the vertical diffusion equation which accounted for surface sources and sinks (but not chemistry). This equation was solved analytically by assuming that species concentrations followed a profile that was logarithmic in altitude. In simulations with the LIRAQ model in St. Louis (Penner et al., 1983), it was discovered that such a formulation was far too sensitive to the mixed-layer depth. High inversion base heights in St. Louis are indicative of strong vertical mixing. This mixing should force surface concentrations to be very close to layer-average concentrations, but with the original formulation, the surface concentrations actually decreased relative to layer-average concentrations when mixing depths were high. Thus, the original LIRAQ formulation failed to account for the proper physical response, especially in cases where the mixed-layer depth increased in conjunction with strong vertical mixing. In past

simulations in the San Francisco Bay Area, this aspect of the LIRAQ model behavior was not noticed, in part because mixing depths are generally low, and in part because "tuning" of the meteorological fields was used to assure good verification. To correct the formulation in this work, we reformulated the assumed surface concentration calculation, in order to decrease the sensitivity of surface concentrations to layer height.

As before, we assume a vertical profile that is logarithmic in height. However, in the present case the logarithmic profile only applies to the lowest 50 meters above the surface. Thus,

$$c_i(x,y,z,t) = a_i(x,y,t) + b_i(x,y,t)\,\ln\left(\frac{z}{z_0}\right) \quad , \qquad \text{for } 0 \le z \le 50\ m \tag{6.1}$$

$$c_i(x,y,z,t) = \left(\frac{H\bar{c}(x,y,t) - \int_0^{50} c(x,y,z,t)dz}{H-50}\right) \qquad \text{for } 50\ m \le z \le H$$

where $\bar{c}(x,y,t)$ is the vertically averaged concentration calculated by the model.

Integrating the vertical diffusion equation from z=0 to z=z_0 (the height of a thin, well-mixed-layer near the surface) and assuming $dc/dt = 0$, we find:

$$K_z(x,y,z_0,t)\frac{\partial c_i}{\partial z}\,|_{z=z_0} + \frac{q_i}{\rho} - v_d c_i(x,y,z_0,t) = 0 \quad , \tag{6.2}$$

where q_i is the surface emission rate for species i at location (x,y) and v_d is its deposition velocity. This equation, together with the constraint that the vertically averaged concentration must equal that computed by the code, provides enough information to solve for the coefficients $a_i(x,y)$ and $b_i(x,y)$ in Equation (6.1). Thus,

$$a_i = \frac{\frac{q_i}{\rho}\left(\frac{z_0}{50} - 1 + \ln\frac{50}{z_0}\right) + \bar{c}_i\,\frac{K_{z_0}}{z_0}}{\frac{K_{z_0}}{z_0} + v_d\left(\frac{z_0}{50} - 1 + \ln\frac{50}{z_0}\right)} \quad , \tag{6.3a}$$

$$b_i = \frac{v_d\bar{c}_i - \frac{q_i}{\rho}}{\frac{K_{z_0}}{z_0} + v_d\left(\frac{z_0}{50} - 1 + \ln\frac{50}{z_0}\right)} \quad . \tag{6.3b}$$

Equation (6.1) is evaluated at an 8 m height to compare to surface observations.

The ratio of the surface concentration to the layer-average concentration as a function of the mixed-layer depth with this formulation is illustrated in Figure 6.1a. The new formulation is, appropriately, not very sensitive to H and yet still accounts for variations in mixing strength through its dependence on K_z (see Figure 6.1b). We, therefore, have used this formulation for the studies reported below.

We note here that this alteration will primarily affect the layer-average concentrations through its alteration of the deposition term. Thus, with the larger surface concentrations in the new formulation, deposition is more efficient than it was with the old formulation when mixed-layer depths are high. However, we have found that this alteration has very

little effect on the calculated vertically-averaged pollutant concentrations. To show that the new formulation did not significantly alter the layer-average ozone concentrations, we performed two simulations. In one, the surface concentration was assumed to be equal to the layer-average concentration. This assumption allows even less stratification than that allowed in the formulation above. In the second, we used the old LIRAQ formulation. Figure 6.2 shows the layer-average ozone concentration at 1600 hours for the well-mixed assumption, while Figure 6.3 shows the same field as generated with the original assumption. The two fields are nearly identical. Thus, the new formulation primarily acts to adjust the 8 meter values which are used to compare to observations. Previously, when mixed-layer depths were high, the surface concentrations of ozone used for verification purposes might be only half of the layer-average concentrations. With the new formulation, the surface values are much closer to the calculated layer-average values, as expected when mixing is strong.

C. Initial conditions and boundary conditions

Initial concentrations for NO, NO_2, CO and nonmethane hydrocarbons (NMHC) were developed from concentrations measured at measurement sites within the model domain. The measured NMHC must be split into the four classes followed in the chemical mechanism. For this study the splitting was based on measured concentrations of individual hydrocarbons in the Bay Area (Kopp, 1981). After splitting, the measured NMHC, as well as the NO, NO_2, and CO concentrations are interpolated to the entire grid. In previous studies (Penner et al., 1983), we found that a straight forward interpolation scheme created far too many pollutants when integrated over the entire grid. Therefore, in the present interpolation process, the estimated emission inventory for each grid point is used to constrain the values at grid points away from the observed station values. Thus the value at location i is first given an interpolation value, but then adjusted to reflect the ratio of the emissions at location i relative to those at the station observations that are used in the interpolation scheme. This procedure avoids the smoothing created when only observed concentrations are used for initialization. It cannot, however, account for high pollutant concentrations that may be present over the ocean because no observations from ocean locations are available. For this reason, sensitivity runs of the first day of a simulation must remain suspect.

The initial concentrations for the short-lived species were set to low values (near zero). Some species such as HNO_2 and H_2O_2 have been measured at up to ppb and 10's of ppb levels in polluted areas. Initial concentrations at these levels could significantly impact predicted O_3 concentrations (Harris, Carter, Winer, and Pitts, 1982). Unfortunately, there is not a great deal of information available to help determine their concentrations in the San Francisco Bay Area. The concentrations estimated for clean air for HNO_2 and H_2O_2 are low enough to have little effect on predicted ozone in an urban area. Their concentrations should be larger in the Bay Area but our estimates of their concentrations as predicted from gas phase chemistry are still too low to cause any appreciable change in predicted O_3. Similar arguments apply to the initial concentrations for all the short-lived species, and we have therefore set the initial concentrations to low values. This procedure has the added advantage of requiring no change when emission reduction scenarios are contemplated.

The initial concentration for PAN was set to 0.1 ppb. The exact value used here is more significant. We estimate that an increase in PAN concentrations to 5 ppb, as observed in Los Angeles, for example (Spicer, 1977), might increase peak O_3 during the first day by 10%; but, again, there are no measurements in the San Francisco Bay Area that can be used to set initial concentrations. Our estimate for its concentration as predicted from gas phase chemistry is less that 1 ppb.

Horizontal boundary conditions must usually also be set without the benefit of detailed data. Here our strategy is to choose conditions that are intermediate between rural and urban values, although in some cases it can be argued that larger pollutant concentrations may be warranted, if the previous day's air mass is recirculated back into the modeled region. Boundary conditions at the top of the modeled region are similarly chosen, although in specific cases there may be evidence of larger pollutant concentrations. The daytime boundary condition for this study are given in Table 6.1. Nighttime boundary conditions are similar except for the higher aldehydes, H_2CO, NO and O_3. These are reduced at night by factors of 2.5, 10, 10, and 20, respectively. Boundary conditions for species not listed in Table 6.1 are set to low values.

Table 6.1. Boundary Conditions

	Typical Clean or Rural Air (ppb)	Within Model Grid (ppb)	Daytime Boundary Value C_0 (ppb)
NO	.004–.02	.2–100	4. (.08 aloft and on west)
NO_2	.01–.1	.2–100	4. (.08 aloft and on west)
O_3	20–60	0–250	20 (100 aloft)
CO	100–200	1000–6000	1000
H_2CO	0.1–5.0	0.1–20	10 (1 aloft)
HC1	1–5	10–50	10 (3 on west)
HC2	5–20	50–400	50
HC3	1–5	10–100	10
HC4	0.1–5.0	10–70	2.5 (1 aloft)
PAN	.05–1.	.1–20	.1

D. Inclusion of upper layer

In this modeling study, a separate calculation of pollutant concentrations above the mixed-layer was fully accounted for. Originally, it was thought that the overnight storage of pollutants in this second layer could have a large impact on calculated concentrations on the second day of simulation. This is because these pollutants would be re-incorporated into the mixed-layer on the second day and contribute to the second day's smog formation. In fact, for the days we are simulating, September 30—October 1, 1980, and given the lack of upper layer wind data, very little overnight storage occurred. Wind speeds above the mixed-layer were strong enough to blow most of the pollutants off the grid by the end of the first day. Thus, as the inversion base height grew on the second day, essentially

clean air (or, more properly, air having pollutant concentrations specified at the region boundaries) was incorporated from above.

Figures 6.4a,b, 6.5a,b and 6.6a,b show the computed layer two NO_x, HC2, and O_3 concentrations at midnight on September 30 and at 0400 hours on October 1, 1980. Concentration peaks have been blown well off-shore. Given the upper layer wind directions for October 1, 1980, these pollutant highs will remain offshore and not contribute significantly to ozone formation at MBUAPCD stations, although, if the meteorological situation had been different, we would have appropriately accounted for overnight storage.

E. Sensitivity of predicted O_3 to changes in meteorology

As a measure of the sensitivity of predicted O_3 to meteorology, we discuss, in this section, two versions of meteorology for September 30, 1980. The first, labeled MET1, was developed before any knowledge of the generated ozone field had been obtained. The second, labeled MET4, attempted to improve model simulation characteristics for the MBUAPCD stations. It did so by generally introducing somewhat larger wind speeds in the afternoon (but still within limits that were consistent with observation).

Figures 6.7–6.18 show the averaged boundary layer winds for the hours of 0900, 1000, 1200, 1400, 1500, and 1700 for MET1 and MET4, respectively. As shown in the figures, MET1 has higher winds over the San Francisco Bay Area in the morning, but somewhat smaller winds in the afternoon. The boundary layer thickness used in these two meteorologies were similar for all hours except 1200 and 1400. For those two hours, the MET1 version had higher mixed-layer depths over the east bay hills, but lower depths over the ocean (see Figures 6.19–6.22).

We first consider model simulations on the full grid (200 km by 200 km). The two simulations presented (that for MET1 versus that for MET4) were obtained with two different versions of the chemistry. The first simulation–that for MET1–used the Penner and Walton (1982) mechanism. The second–that for MET4–used our updated chemistry in which H_2CO is treated explicitly. The first simulation also used the LIRAQ formulation for determining the surface concentration. As discussed above, this formulation does not properly treat the dependence of surface O_3 concentrations to variations in the mixed-layer depth, but this has relatively little effect on layer-average ozone concentrations; in our discussions here, we will limit the comparison to layer-average quantities. As discussed in Chapter 5, the latest version of chemistry would produce slightly less ozone than the Penner and Walton (1982) mechanism. Because, as will be shown, the simulation with MET4 produces more ozone at San Francisco Bay Area stations than the simulation with MET1, this comparison slightly underestimates the difference that would be predicted with the two versions of meteorology and the same chemistry.

Figures 6.23–6.25 show layer-average O_3 contours at 1500, 1600, and 1700 hours with the MET1 version of meteorology (and the Penner and Walton (1982) chemistry). Figures 6.26–6.28 show O_3 for the same times as predicted with the MET4 version of meteorology (and the new chemistry and vertical profile formulations). The highest concentration increases from 6×10^{12} cm^{-3} with MET 1 to somewhat more than 8×10^{12} cm^{-3} with MET4.

To understand why these differences occurred, we ran a smaller-grid version of the same two meteorology cases. In these simulations, the chemistry used was the latest version and the treatment of vertical mixing was the same in both simulations so that these runs are directly comparable. Figures 6.29–6.31 show layer-average O_3 contours at 1400, 1500, and 1600 hours for MET1. Figures 6.32–6.34 show layer-average O_3 at the same hours for MET4. We again note that ozone concentrations are significantly enhanced in the MET4 simulation.

Figures 6.35–6.38 show layer average NO_x for the MET1 meteorology for the hours of 0600, 0900, 1200, and 1500. Figures 6.39–6.40 show NO_x contours for 1200 and 1500 hours as predicted with the MET4 meteorology. (The meteorology up to 0900 hours was the same in the two cases.) Similarly, Figures 6.41–6.44 show HC2 contours for the hours of 0600, 0900, 1200, and 1500 as predicted with the MET1 meteorology, while Figures 6.45–6.46 show HC2 for 1200 and 1500 hours as predicted with MET4.

Consider the contour plots for 1200 hours for HC2 and NO_x in the two cases. For the higher winds of MET1, the contour maxima of HC2 and NO_x, which originate near San Francisco, Oakland, and San Jose, are dispersed further downwind (along the axis of the Bay) than they are for the same hours with MET4. In addition, the maximum concentrations for HC2 and NO_x are lower in MET4. Because, up to this point, the mixed-layer depths are similar in the two cases, the lower peaks are apparently due to increased photochemical activity in MET4. This is evident in the O_3 comparison plots for this hour (Figures 6.47 and 6.49).

Although the winds are increased in the afternoon in MET4, relative to those in MET1, the photochemistry that has been working up until noon has already had a substantial impact. The NO_x and HC2 fields at 1500 hours have maxima at approximately the same locations (compare Figure 6.38 with 6.40 and Figure 6.44 with 6.46), but the MET4 peak concentrations are lower. O_3 is similarly enhanced in MET4 (compare Figure 6.48 with 6.50). As a quantitative measure of the change, we note that the time and layer-average mean O_3 concentration at station locations for this simulation increases from 6.5 pphm with MET1 to 7.2 pphm with MET4. The observed surface mean concentration was 5.6 pphm.

F. Performance evaluation

This section presents a comparison of predicted surface concentrations for NO_2, NO, CO, and O_3 with observed concentrations. In this analysis, a statistical evaluation procedure is used although we also present station history plots for O_3 (see also Appendix B). The statistics presented are similar to those used in the past (Penner et al., 1983), but the implementation has been slightly changed. Previously we compared station values directly to the predicted concentration at the grid location of the station. In this work, we compare station values to a concentration that is an average concentration of grid locations near the station location. This averaging procedure was implemented to make the present statistics more comparable to previous analyses in which a certain amount of averaging took place through numerical dispersion. In addition, the averaging procedure masks small errors in wind field direction which otherwise could degrade the comparison.

Table 6.2 shows a set of statistics which are useful for judging the model's ability to predict mean concentrations. Table 6.3 shows statistics for judging the model's ability to predict concentration trends, and Table 6.4 shows a set of statistics for judging the model's ability to predict concentration maxima. Table B.1 in Appendix B provides a tabulation of the observed and predicted O_3 concentrations at all stations in our grid. The quantities shown have been calculated using the formulas given in Fox (1981). Figures 6.51 and 6.52 show a scatter plot of observed and computed O_3 concentrations for September 30, 1980 and October 1, 1980, respectively. The scatter plots and statistics are encouraging, but not as good as for previous simulations with LIRAQ in the San Francisco Bay Area or in St. Louis (compare Penner et al., 1983). The ozone concentration at Hollister is somewhat smaller than observed. We expect that the concentration at Hollister could be increased with somewhat faster transport along the San Jose/Hollister corridor, although time and resources did not permit such model tuning. In addition, it appears that wind speeds at Hayward, Los Gatos, and Redwood City should have been stronger. If these sites are removed from the statistical analysis, the RMS error for ozone decreases significantly, from 4.2 pphm to 3.0 pphm.

One aspect of the model performance which was quite satisfying was the reproduction of an ozone peak offshore between San Francisco and Monterey. This peak was observed in the study by Dabbert (1983), but was not necessarily anticipated in the model results because no previous studies with the LIRAQ model had predicted an offshore O_3 reservoir. Figure 6.53 shows an ozone contour plot for 1600 hours on October 1, 1980 that was drawn from the observations reported by Dabbert (1983) and from the station O_3 values. Figure 6.54 shows the model results for the same hour. Because the station values are so sparse, the observed field over land looks much more disperse than we would predict based on the full model. However, the O_3 concentrations found offshore are well represented by the model.

G. Sensitivity of Monterey Bay Unified Air Pollution Control District receptors to Bay Area emissions

We performed a sensitivity test to determine how the MBUAPCD might be affected by NO_x emissions from the BAAQMD. In the test, emissions and initial concentrations of NO_x were decreased by 30 percent for all counties under BAAQMD jurisdiction. Thus, NO_x emissions were lowered in the grid squares encompassing Morgan Hill and Gilroy as well as all areas north of UTM coordinate 4120. The area north of 4120 has traditionally been the area treated in the LIRAQ model and the area used by the BAAQMD to develop their emissions control strategy.

Figures 6.55–6.57 show the predicted layer-average O_3 concentrations at 1500, 1600 and 1700 hours, respectively, for September 30, 1980 while Figures 6.58–6.60 show the predicted concentrations for the same hours on October 1, 1980. Figures 6.61–6.66 show a corresponding set of concentrations for these two days as predicted with reduced NO_x emissions. The dotted line in each contour plot corresponds to a layer-average concentration of 3×10^{12} cm^{-3}, a value near the air quality standard of 0.12 ppm. As expected with previous model results, concentration maxima north of UTM coordinate 4120 are increased significantly. For example, the O_3 maxima near San Jose at 1600 hours increases

Table 6.1. Statistics for judging mean concentrations.[a]

Date	Species	Mean Observed Conc.	Mean Predicted Conc.	Residual or Bias	Average Absolute Error	RMS Error	Error Band (%)[b]	Mean res. / Mean obs. (%)
09/30/80	O_3	6.3	6.6	0.28	2.7	3.9	32.0	4.4
	NO_2	4.0	3.7	-0.32	2.2	5.0	24.0	-8.0
	NO	6.3	2.9	-3.4	4.9	12.0	9.0	-54.0
	CO	2.6	2.2	-0.41	1.1	2.5	34.0	-15.8
10/01/80	O_3	6.7	7.7	1.0	2.7	4.2[c]	3.8	14.9
	NO_2	4.0	2.5	-1.5	2.0	4.0	24.0	-37.5
	NO	6.6	2.1	-4.5	5.2	14.0	9.0	-68.2
	CO	2.8	2.5	-0.34	1.2	2.9	36.0	-12.1

[a]Concentration values for O_3, NO_2, and NO are reported at pphm. Values for CO are reported as ppm.

[b]Percent of predictions within 25 % of observations.

[c]The RMS error decreases to 3.0 pphm if Redwood City, Los Gatos, and Hayward are excluded from the analysis

Table 6.2. Statistics for judging concentration trends.

Date	Species	Correlation Coefficient	Average Spatial Correlation	Average Temporal Correlation	Slope	Intercept (pphm)	Mean Square Deviation $pphm^2$	Sample Size
09/30/80	O_3	0.73	0.30	0.81	0.82	1.4	14.0	271.0
	NO_2	0.23	0.24	0.10	0.75	0.70	21.0	169.0
	CO	0.48	0.43	0.22	0.36	1.2	2.4	148.0
10/01/80	O_3	0.74	0.48	0.71	0.82	1.8	15.0	265.0
	NO_2	0.33	0.28	0.39	0.61	0.72	12.0	165.0
	CO	0.52	0.37	0.70	0.42	1.3	3.1	142.0

Table 6.3. Statistics for judging prediction of concentration maxima.[a]

		Observed peak concentration			Predicted peak conc.			Residual
Date	Species	Value	Location	Time	Value	Time	Residual	Obs.conc. (%)
09/30/80	O_3[b]	19.0	dej	17:00	14.0	15:00	-5.0	-26.3
		14.0	hol	17:00	10.3	18:00	-3.6	-26.4
	NO_2[b]	14.0	dsj	11:00	12.0	13:00	-2.0	-14.3
		5.0	wat	10:00	2.0	09:00	-3.0	-60.0
10/01/80	O_3[b]	20.0	mhl	15:00	21.3	15:00	1.3	6.5
		15.0	wat	16:00	12.5	16:00	-2.5	-16.7
	NO_2[b]	17.0	dsj	10:00	12.5	10:00	-4.5	-26.5
		5.0	hol	18:00	0.2	18:00	-4.8	-96.0

[a]Concentration values are reported as pphm for NO_2, and O_3, and as ppm for CO.

[b]The first value reported is the maximum concentration reported for all BAAQMD stations. The second value is that for all MBUAPCD stations.

from 4×10^{12} cm^{-3} to 6×10^{12} cm^{-3}, and much of the area experiences enhanced concentrations. The behavior south of UTM coordinate 4120 responds differently, however. Here, O_3 concentrations are slightly decreased at downwind locations. The effect on the O_3 concentration over the ocean is easily discerned from the contour plots by comparing the countour lines corresponding to 3×10^{12} cm^{-3} in the two simulations. The effect of the NO_x emissions reduction over land, however, is so small that it cannot be discerned in the contour plots.

Figures 6.67–6.70 show layer-average O_3 concentrations for several Bay Area and Monterey station locations as well as for two grid locations over the ocean. The solid line in each graph corresponds to the base case simulation, while the long dashed line corresponds to the case with reduced NO_x emissions. These graphs show the layer-average ozone concentrations. The base case surface concentrations are shown in Figures 6.71–6.73. As shown in Figure 6.68, for the simulation of September 30, 1980 and October 1, 1980, O_3 at Hollister is slightly decreased when NO_x emissions are decreased. Very little effect can be seen at stations further south. There is also a discernable decrease in O_3 at the southernmost ocean grid point (UTM coordinate 560, 4090).

This reversed effect of NO_x on O_3 formation is, we believe, a result of the effect of NO_x on radical concentrations. At locations near the NO_x source region near San Jose, NO_x acts as a significant sink for radicals through the reaction of NO_2 with OH as well as through the formation of PAN. Thus when NO_x is reduced, the radical population is increased even more than NO is reduced, allowing more NO to NO_2 conversions than previously. Far enough downwind, much of this increased radical production potential is "used up" so that O_3 responds more directly to the NO_x reduction.

H. Discussion of limitations of study

The conclusions reached above, that MBUAPCD stations are essentially not impacted by Bay Area emissions, could be altered in several ways. First, a simulation with somewhat faster winds would have carried Bay Area pollutants further south, impacting the Hollister station and those further south somewhat more than was calculated here.

A second limitation concerns the resolution of the chemistry mechanism used for this study. In Chapter 5, it was argued that a less condensed mechanism would develop O_3 somewhat slower than the mechanism used here. If so, the ozone maxima might take longer to develop and would have extended further south in our simulation. Alternatively, we might have had difficulty reaching the observed ozone maxima, and altered the meteorology to enhance verification. The region impacted by a decrease in NO_x emissions would likely change as a result of these changes, and we could conceivably have calculated either an ozone increase or an ozone decrease at Monterey area stations as a result.

One final issue concerns our knowledge of NO_x removal mechanisms themselves. There is evidence that significant concentrations of nitrogen could be present in forms not here-to-for suspected. Most of the NO and NO_2 emitted into the atmosphere is thought to be converted to either HNO_3, PAN, or aerosol nitrate. However, Fahey et al. (1986) have observed that for air from urban sources, the sum of the known nitrogen species concentrations is often only half the total nitrogen present. If there is a chemical mechanism acting

which depletes NO and NO_2 much faster than we presently know of, we could be overestimating the effect of emissions changes in NO_x. These effects are presumably accounted for via the formation of PAN-analogues (called PAN in the condensed mechanism), but this needs confirmation (Atherton and Penner, 1988). Furthermore, it has also been speculated that aerosol reactions could significantly enhance the rate of conversion of NO_x to nitrate (Heikes and Thompson, 1983). Such conversion is accounted for in our model only through the reaction,

$$N_2O_5 + H_2O \rightarrow HNO_3,$$

which has been assigned a rate constant of 1.3×10^{-21} cm^{-3} s^{-1}. Alterations to this rate could occur if the modeled nighttime atmosphere had either increased or decreased aerosol concentrations. Continued work on the nitrogen cycle in the real and modeled atmosphere is needed to understand the impact of these possibilities.

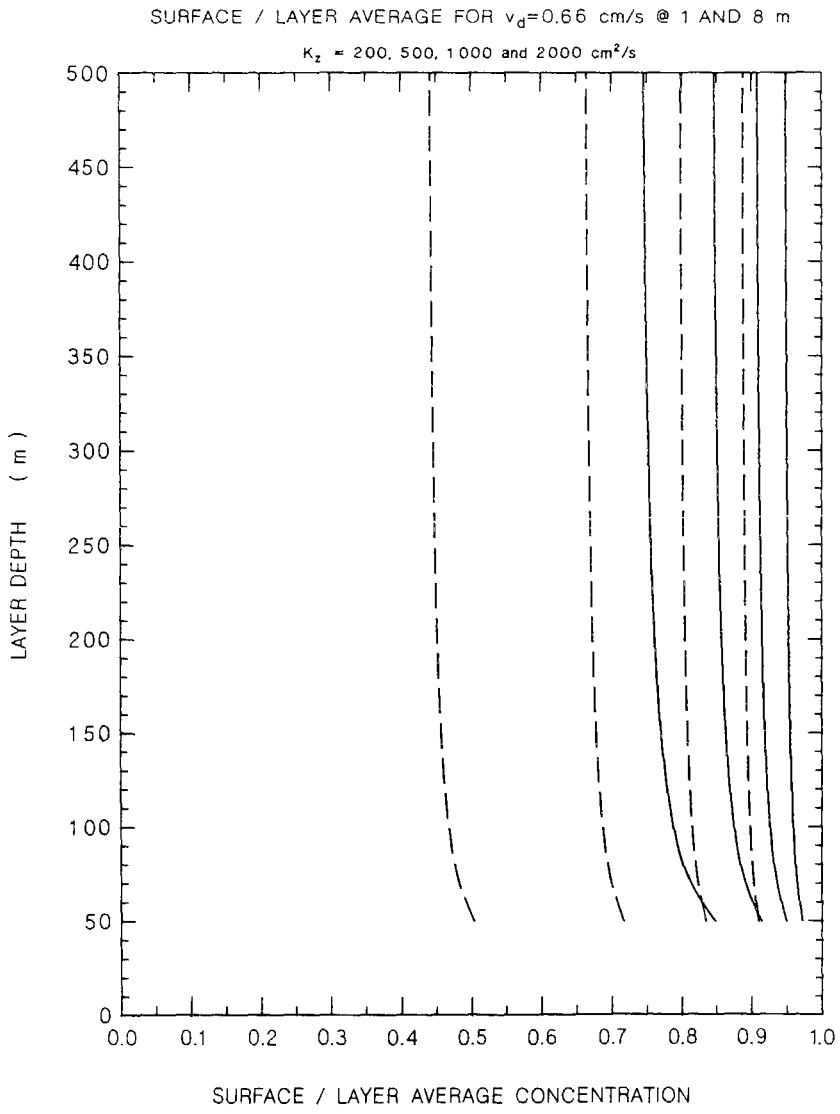

Figure 6.1a. Ratio of the surface O_3 concentration at 1 m (dashed line) and at 8 m (solid line) to the layer-average O_3 concentration as a function of the mixed-layer depth for the new formulation. The deposition velocity has been set to 0.66 cm s^{-1} while the four lines correspond to eddy mixing coefficients of 200, 500, 1000 and 2000 cm^2s^{-1}, respectively, increasing left to right.

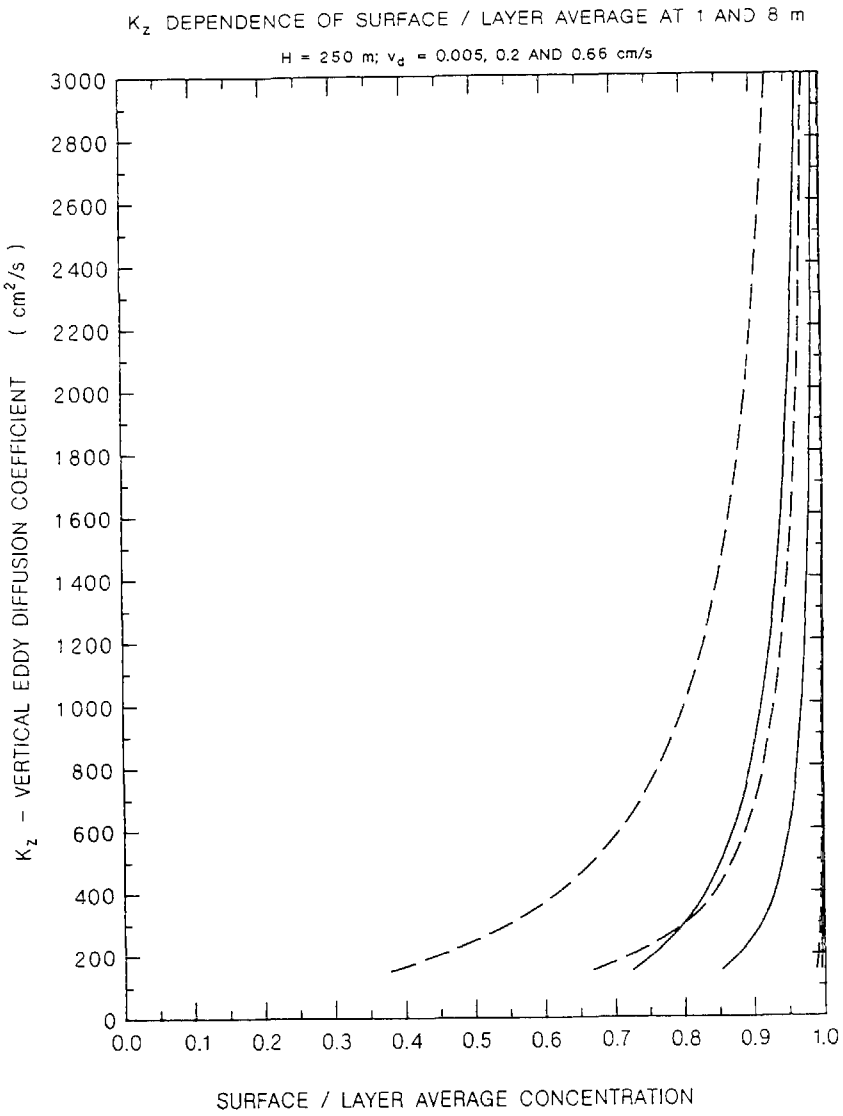

Figure 6.1b. Ratio of the surface O_3 concentration at 1 m (dashed line) and 8 m (solid line) to the layer-average O_3 concentration as a function of the surface eddy coefficient, K_z, for the new formulation. The assumed layer depth was 250 m. The three lines correspond to deposition velocities of 0.005, 0.2, and 0.66 cm s^{-1}, respectively, left to right.

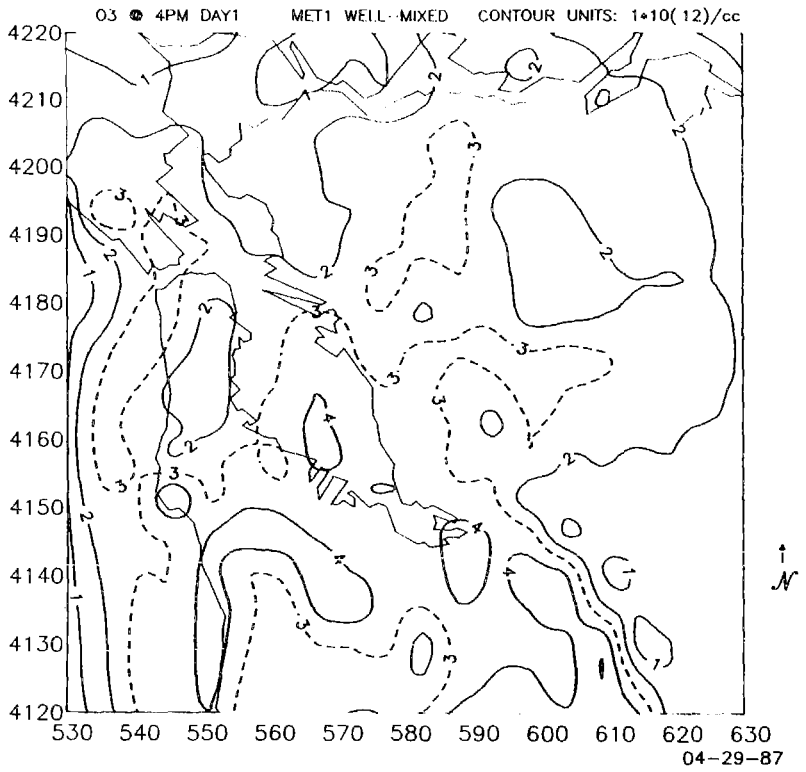

Figure 6.2. Layer-average O_3 concentration predicted when it is assumed that surface concentrations are identically equal to layer-average concentrations. The dashed contour line shows the approximate location of the 0.12 ppm contour.

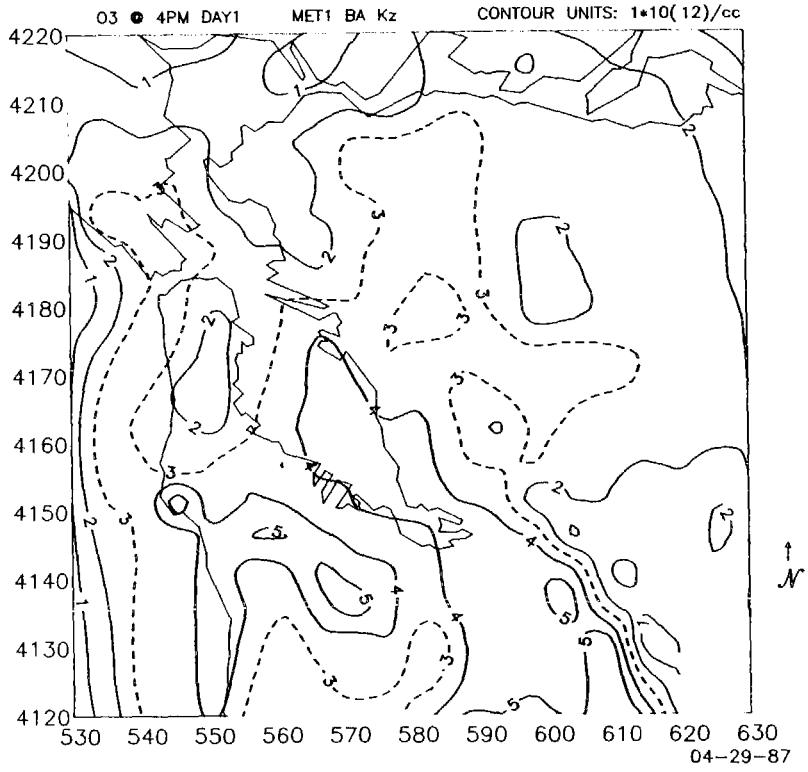

Figure 6.3. Layer-average O_3 concentration predicted using the old LIRAQ formulation of surface concentration. The dashed contour line shows the approximate location of the 0.12 ppm contour.

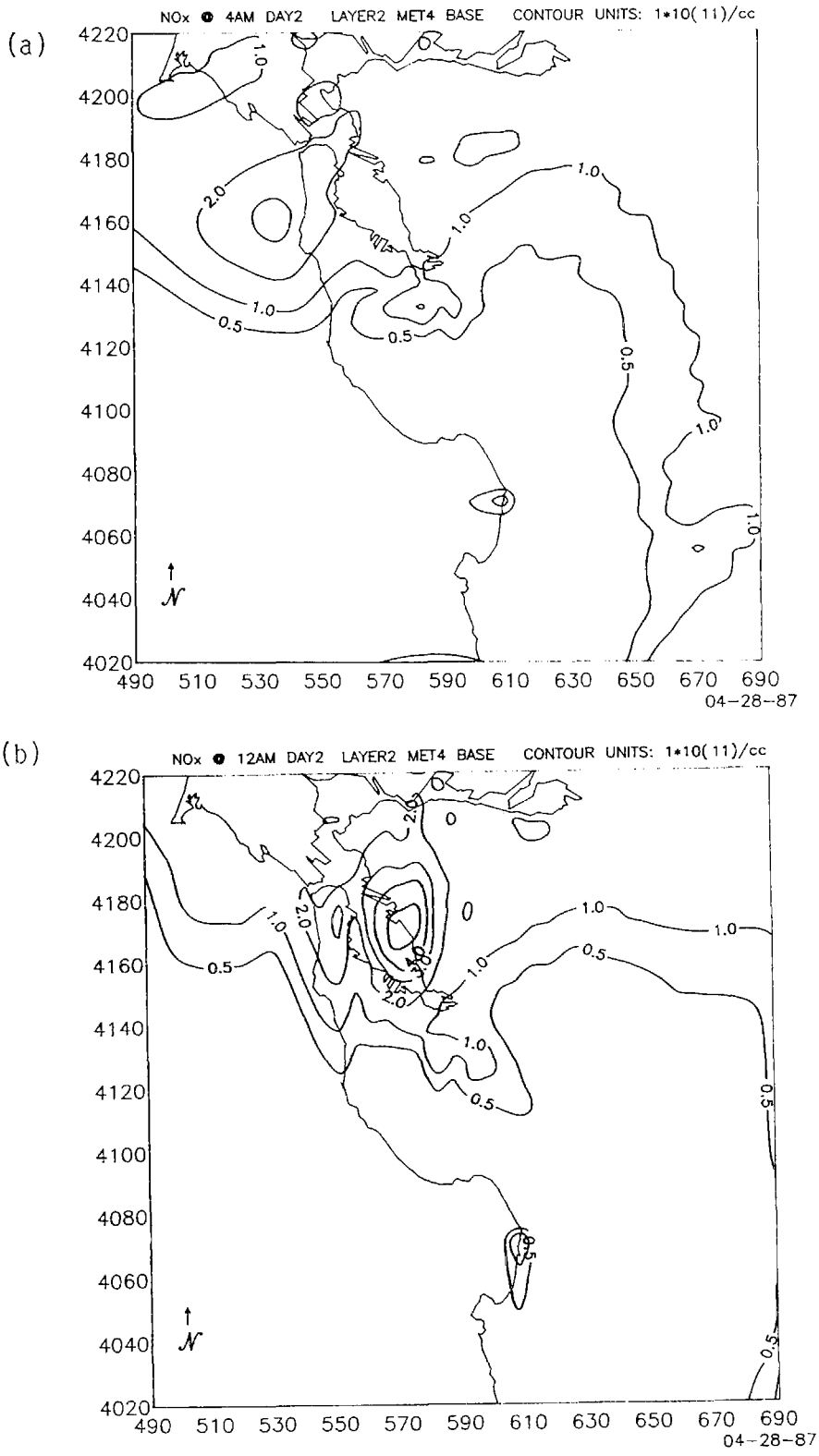

Figure 6.4. (a) Predicted NO_x concentration above the mixed-layer at midnight September 30, 1980. (b) Predicted NO_x concentration above the mixed-layer at 0400 hours on October 1, 1980.

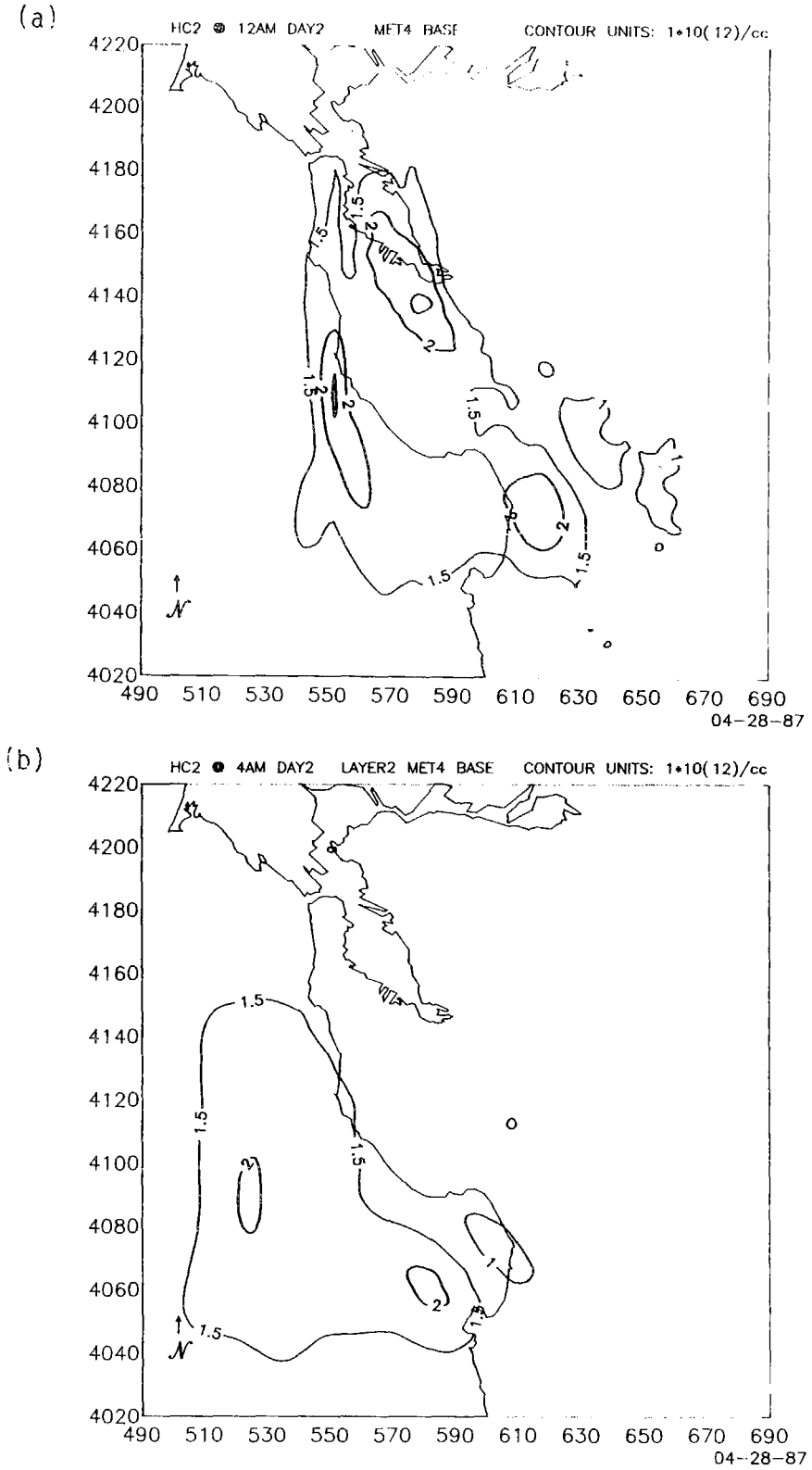

Figure 6.5. (a) Predicted HC2 concentration above the mixed-layer at midnight on September 30, 1980. (b) Predicted HC2 concentration above the mixed-layer at 0400 hours on October 1, 1980.

(a)

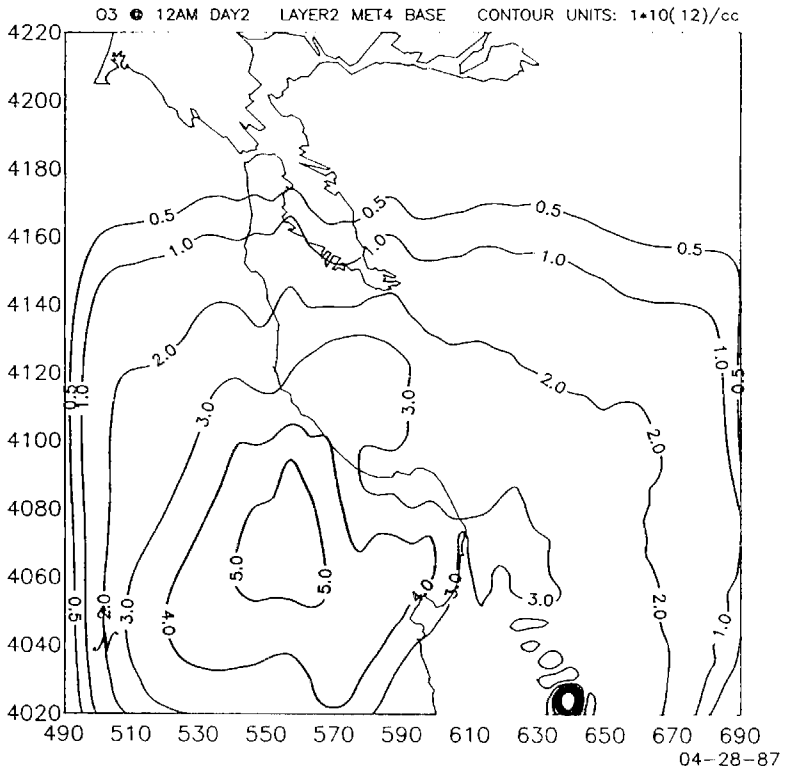

(b)

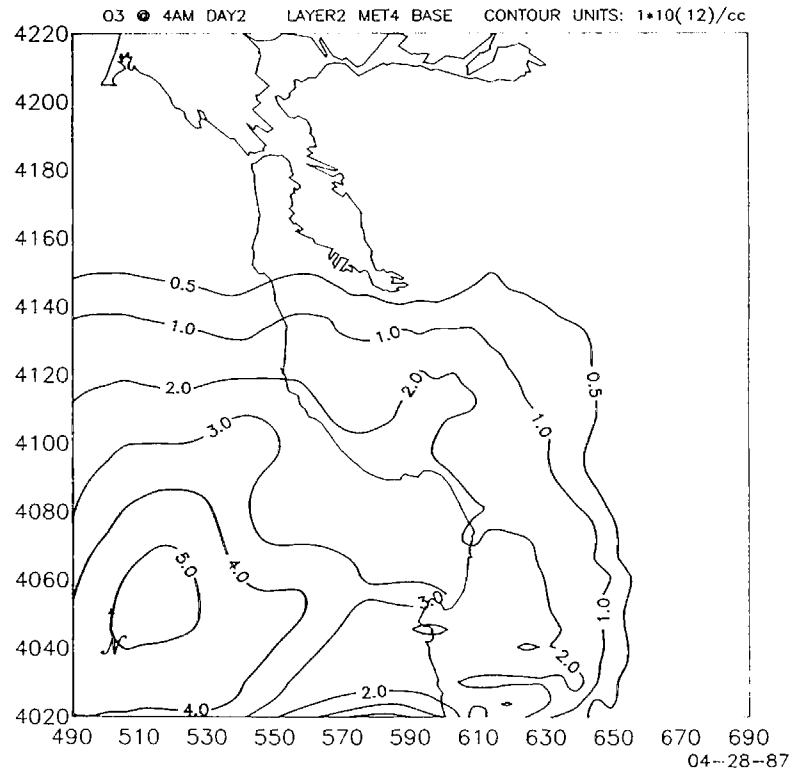

Figure 6.6. (a) Predicted O_3 concentration above the mixed-layer at midnight on September 30, 1980. (b) Predicted O_3 concentration above the mixed-layer at 0400 hours on October 1, 1980.

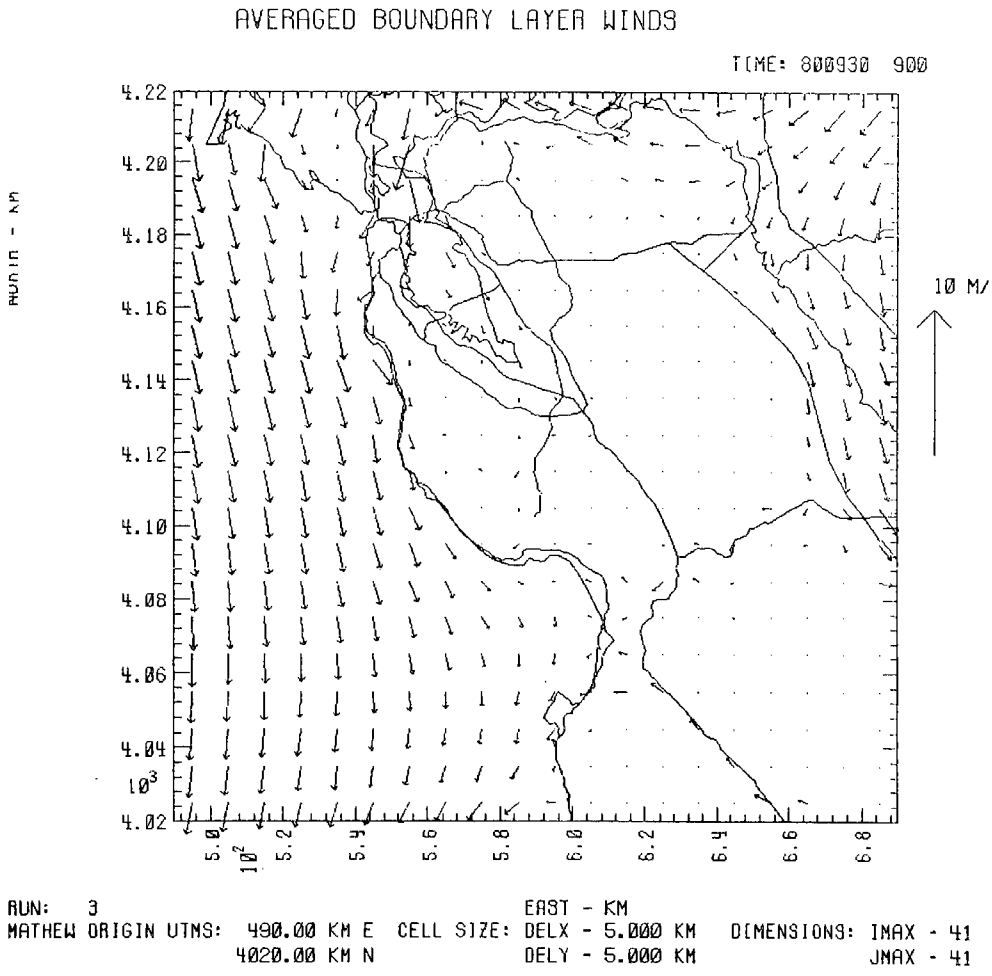

Figure 6.7. Averaged boundary layer winds for 0900 hours on September 30, 1980 for MET1.

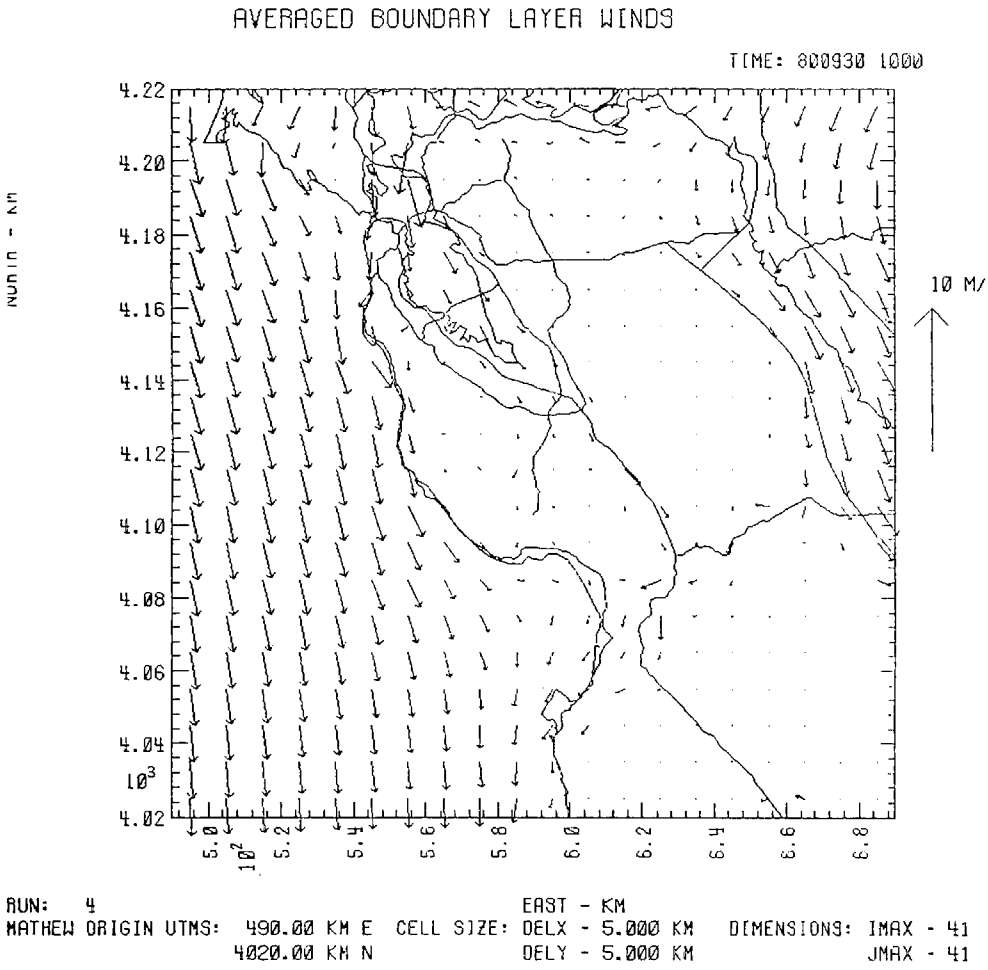

Figure 6.8. Averaged boundary layer winds for 1000 hours on September 30, 1980 for MET1.

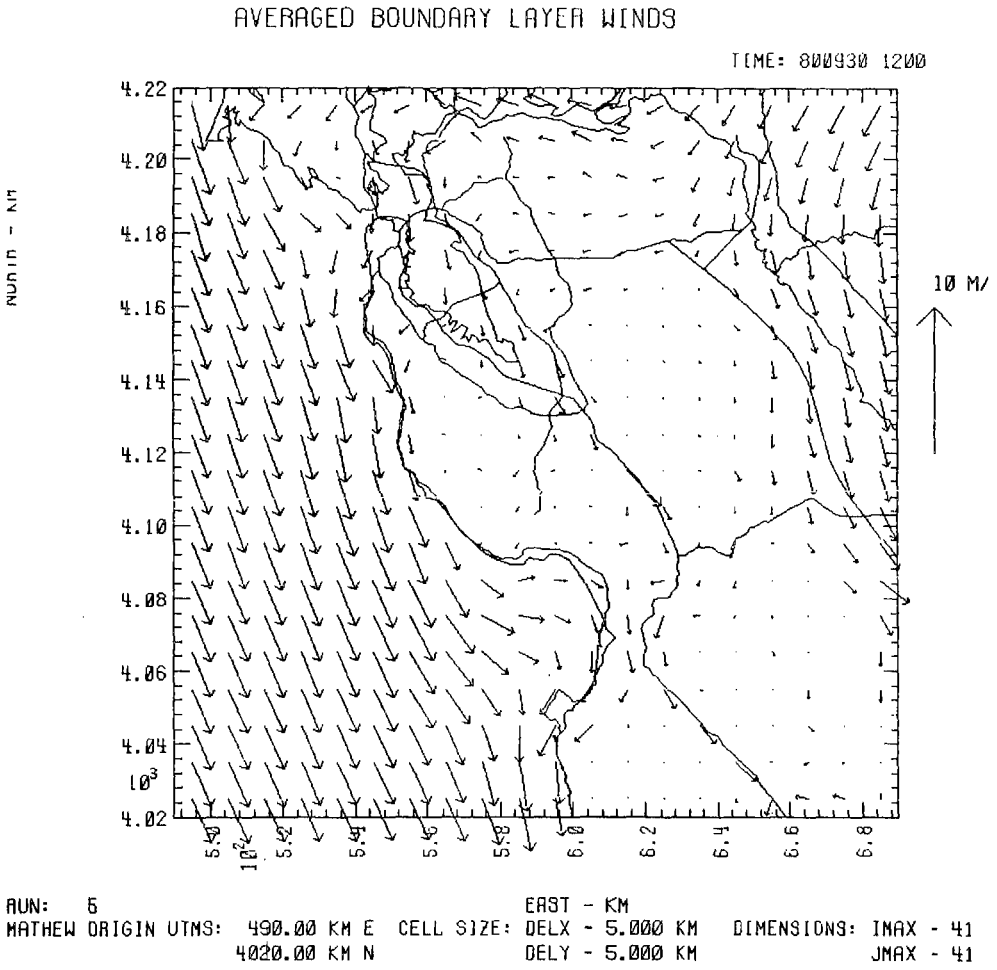

Figure 6.9. Averaged boundary layer winds for 1200 hours on September 30, 1980 for MET1.

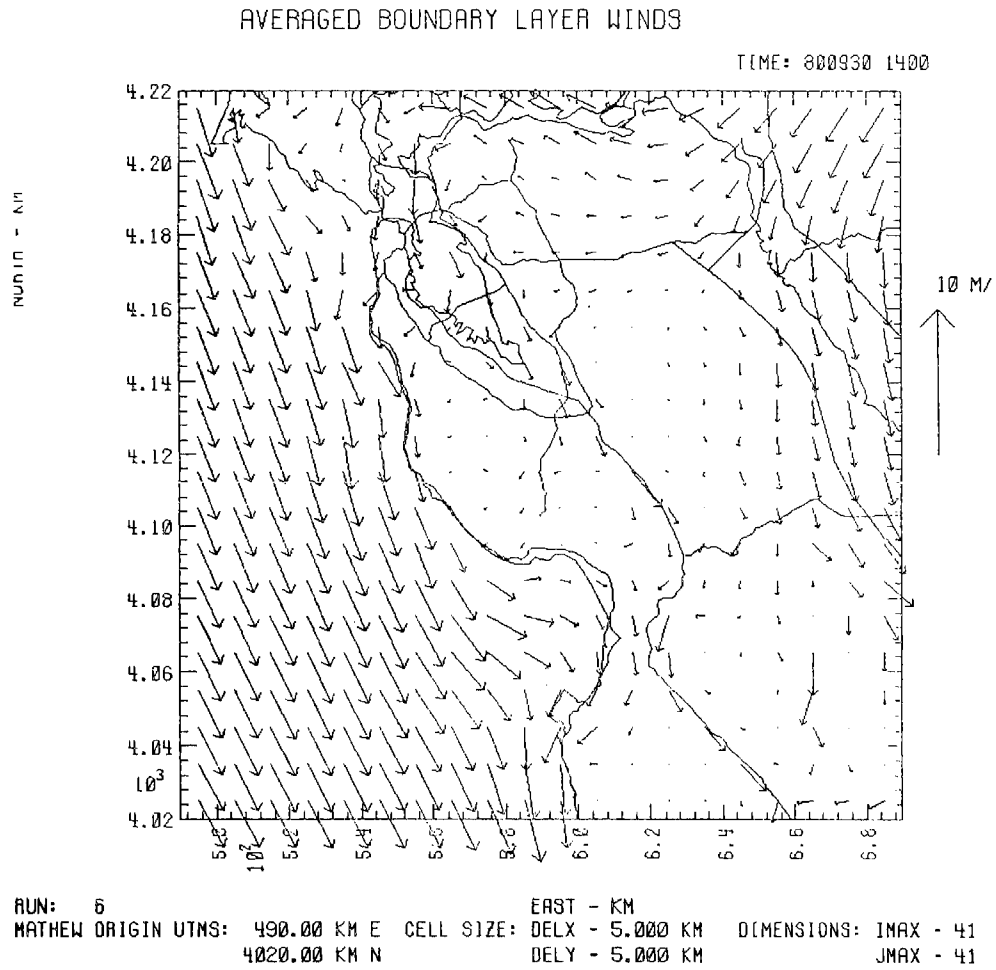

Figure 6.10. Averaged boundary layer winds for 1400 hours on September 30, 1980 for MET1.

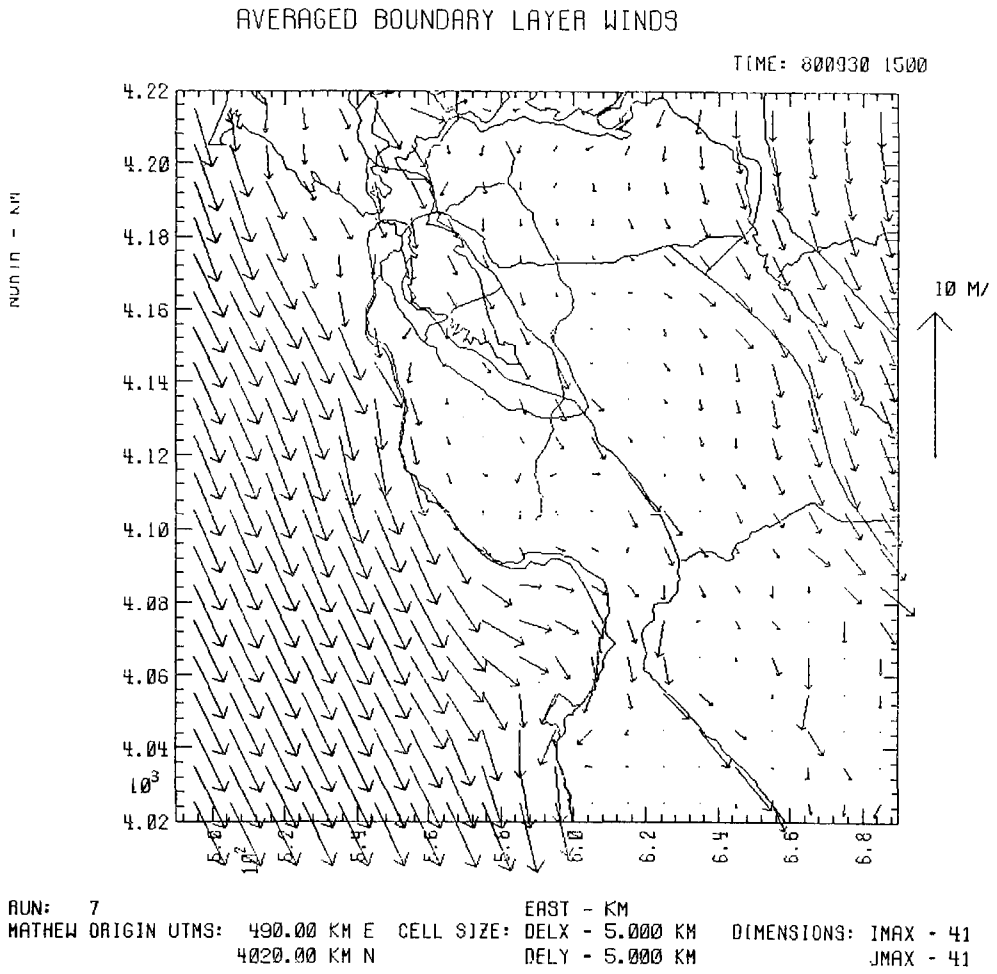

Figure 6.11. Averaged boundary layer winds for 1500 hours on September 30, 1980 for MET1.

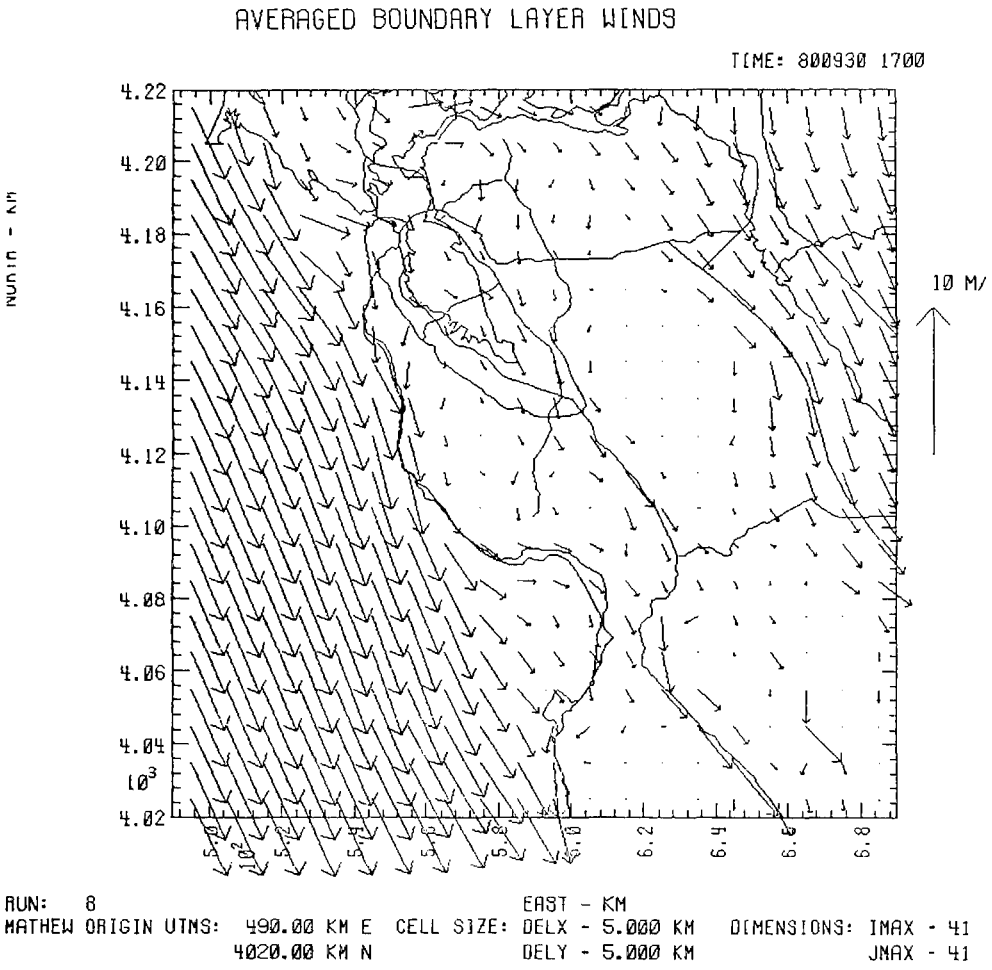

Figure 6.12. Averaged boundary layer winds for 1700 hours on September 30, 1980 for MET1.

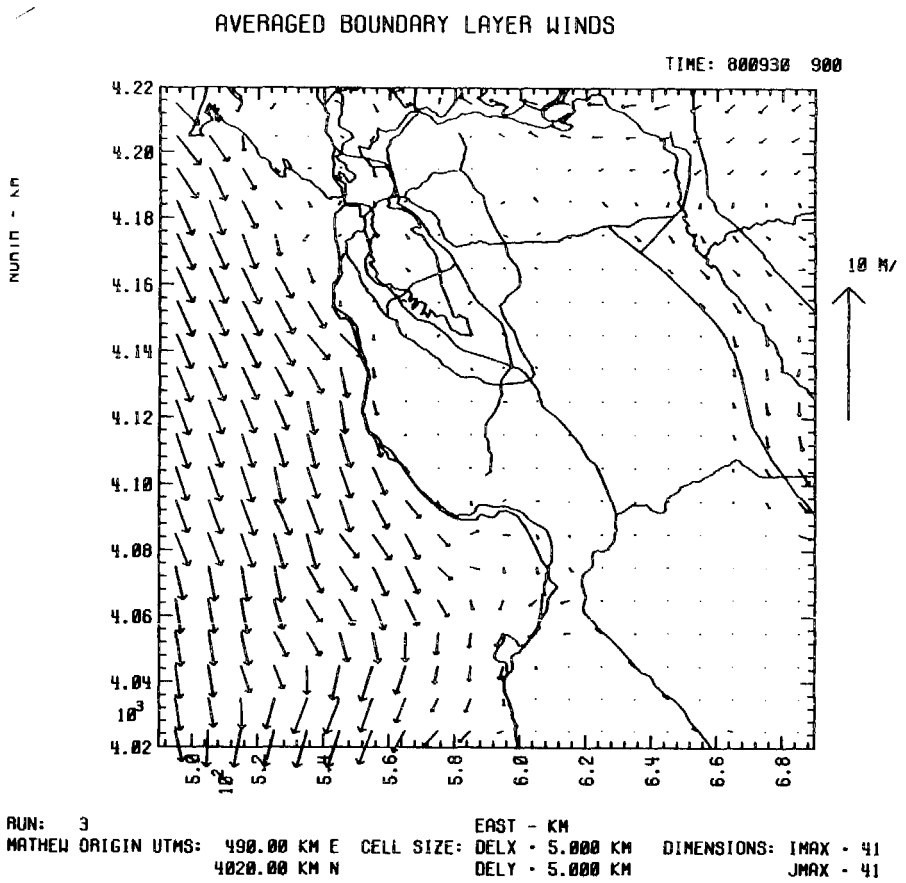

Figure 6.13. Averaged boundary layer winds for 0900 hours on September 30, 1980 for MET4.

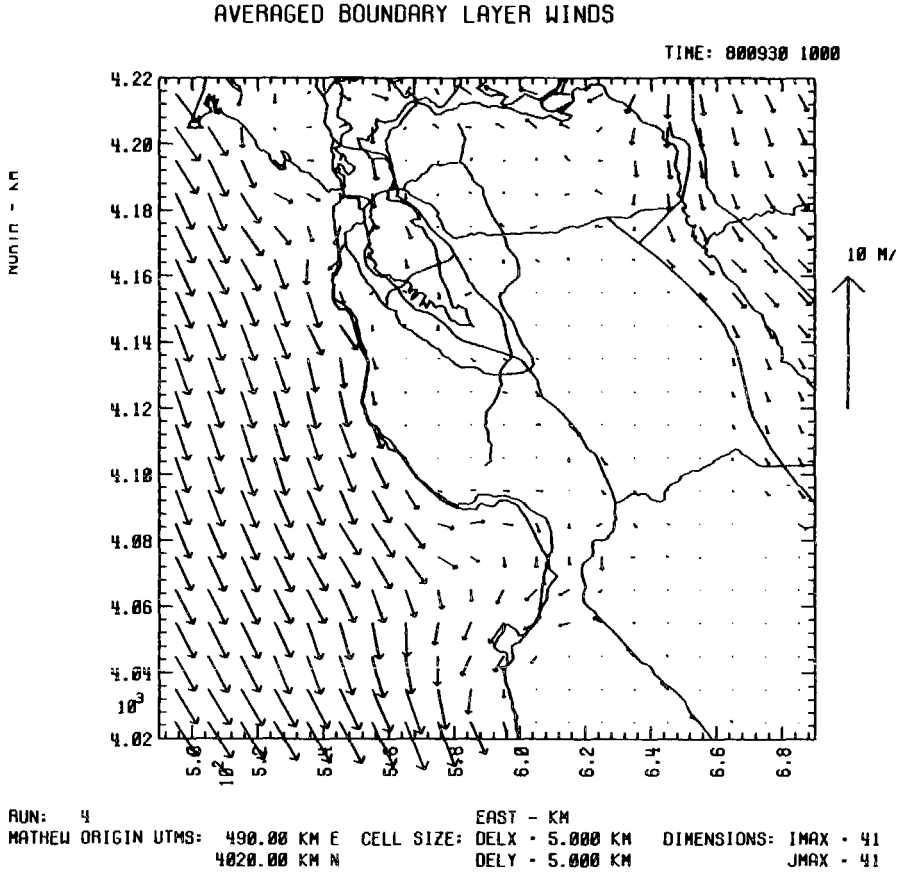

Figure 6.14. Averaged boundary layer winds for 1000 hours on September 30, 1980 for MET4.

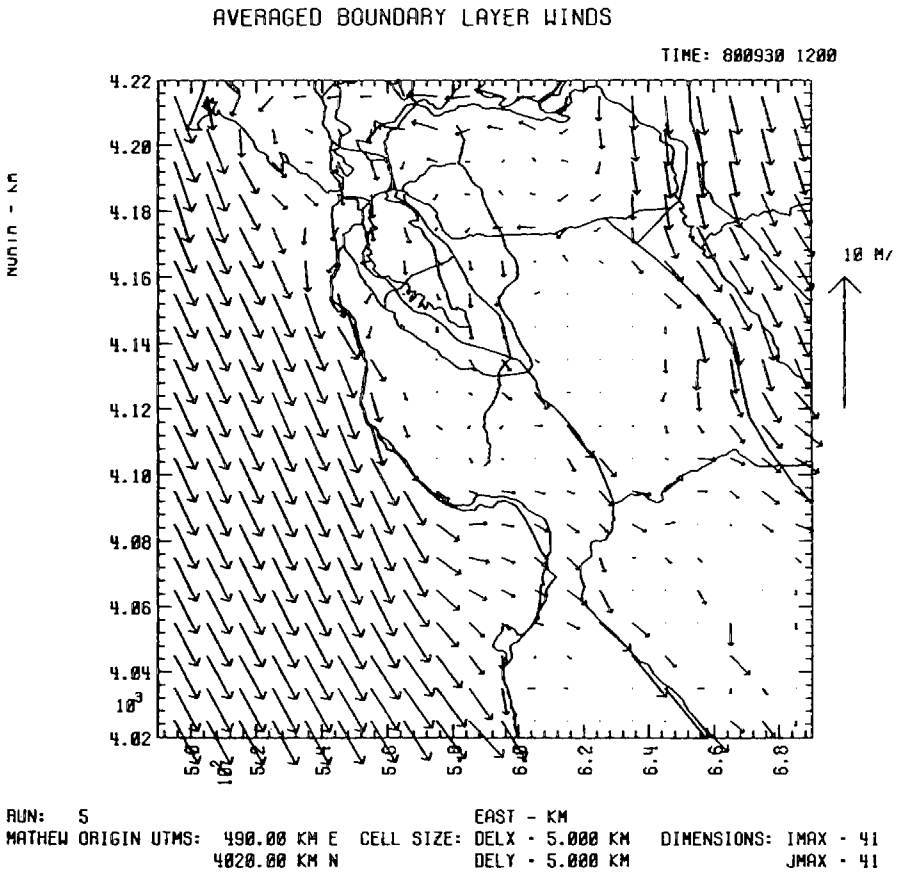

Figure 6.15. Averaged boundary layer winds for 1200 hours on September 30, 1980 for MET4.

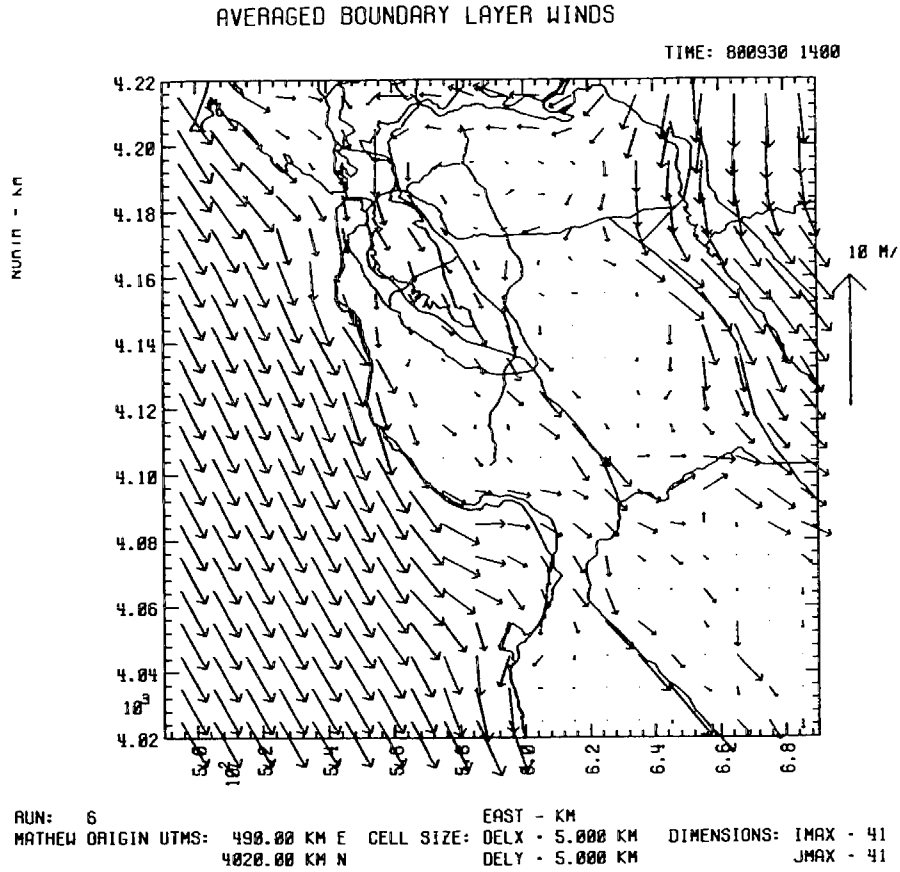

Figure 6.16. Averaged boundary layer winds for 1400 hours on September 30, 1980 for MET4.

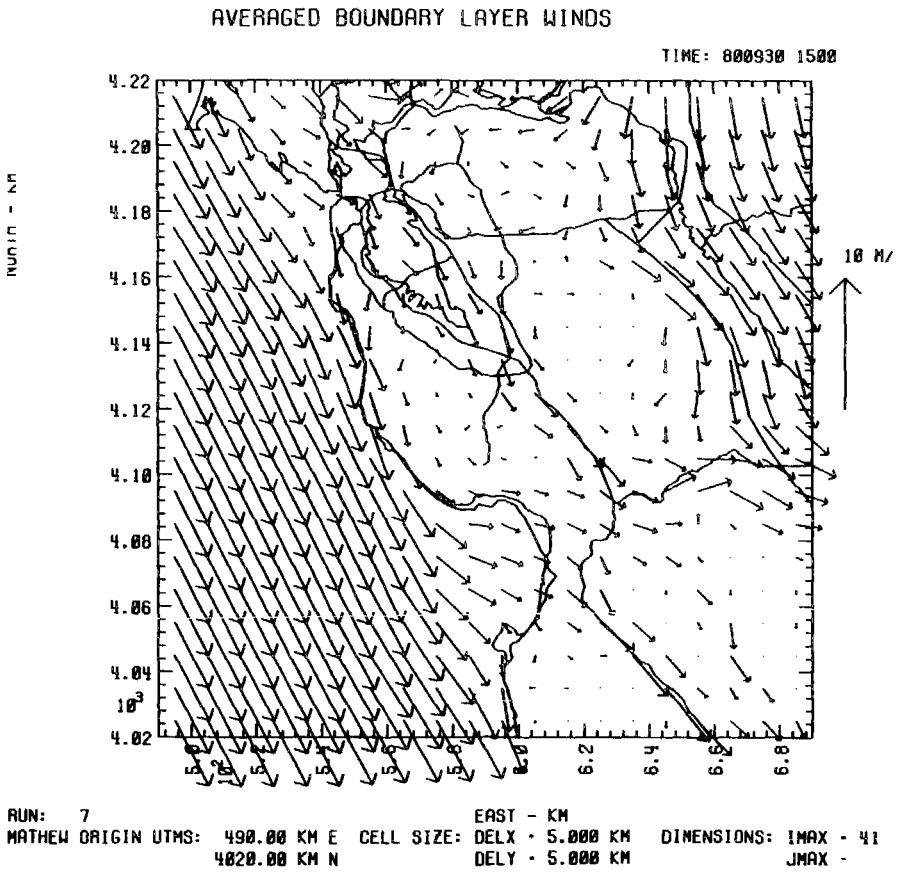

Figure 6.17. Averaged boundary layer winds for 1500 hours on September 30, 1980 for MET4.

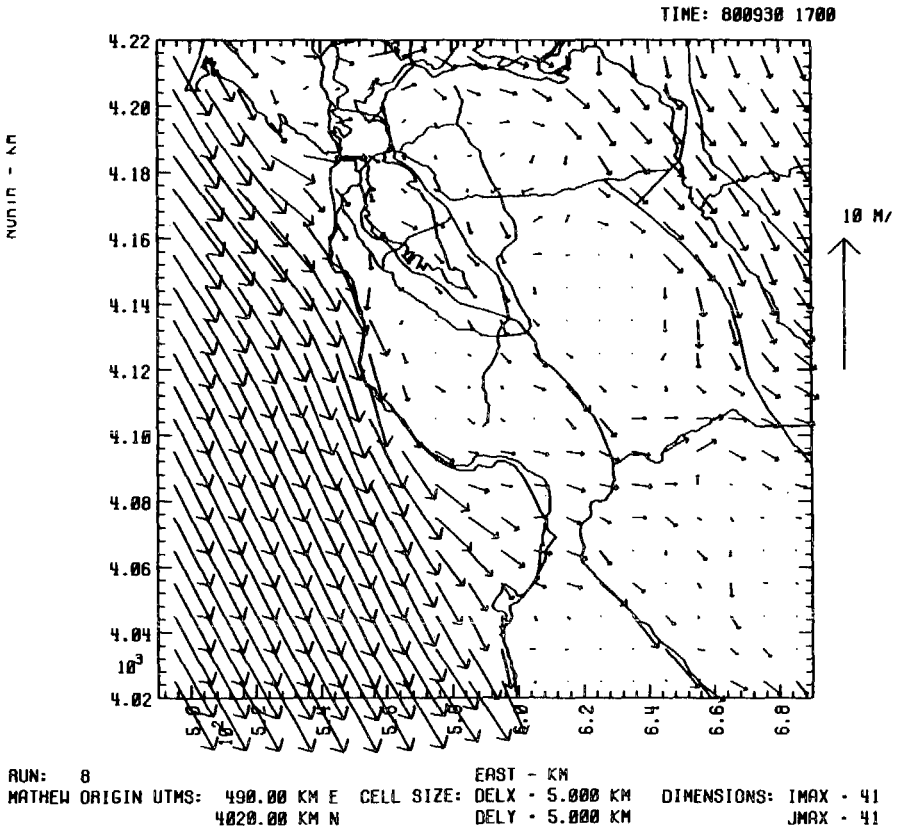

Figure 6.18. Averaged boundary layer winds for 1700 hours on September 30, 1980 for MET4.

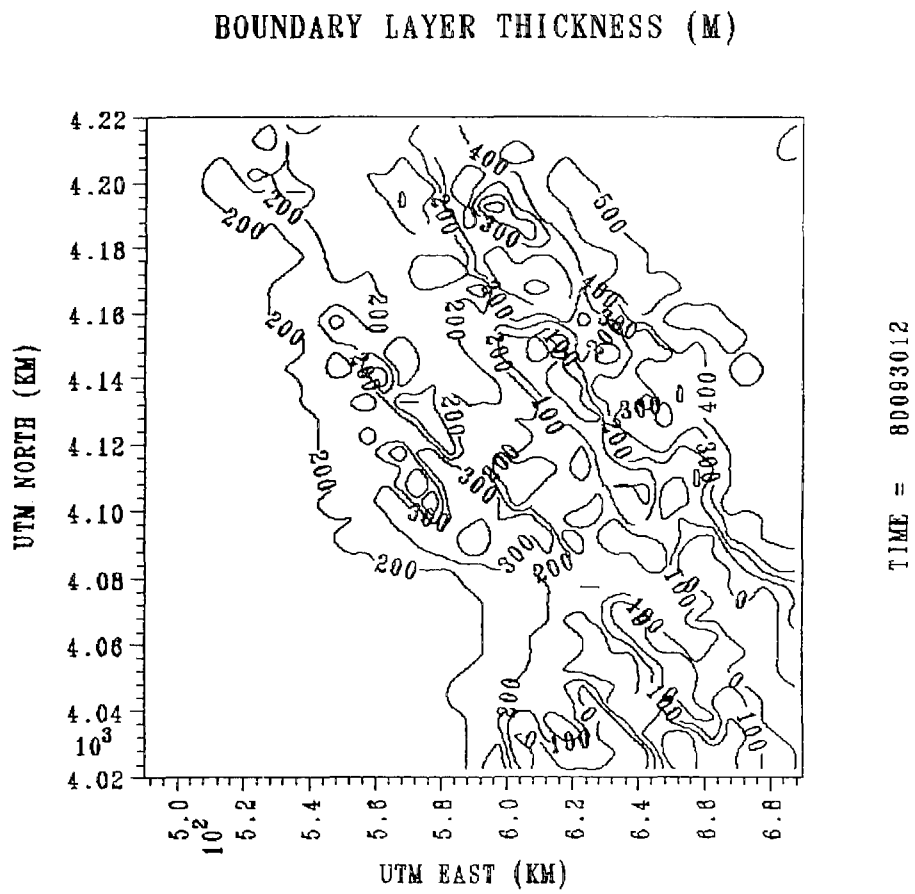

Figure 6.19. Boundary layer depth for 1200 hours used in MET1.

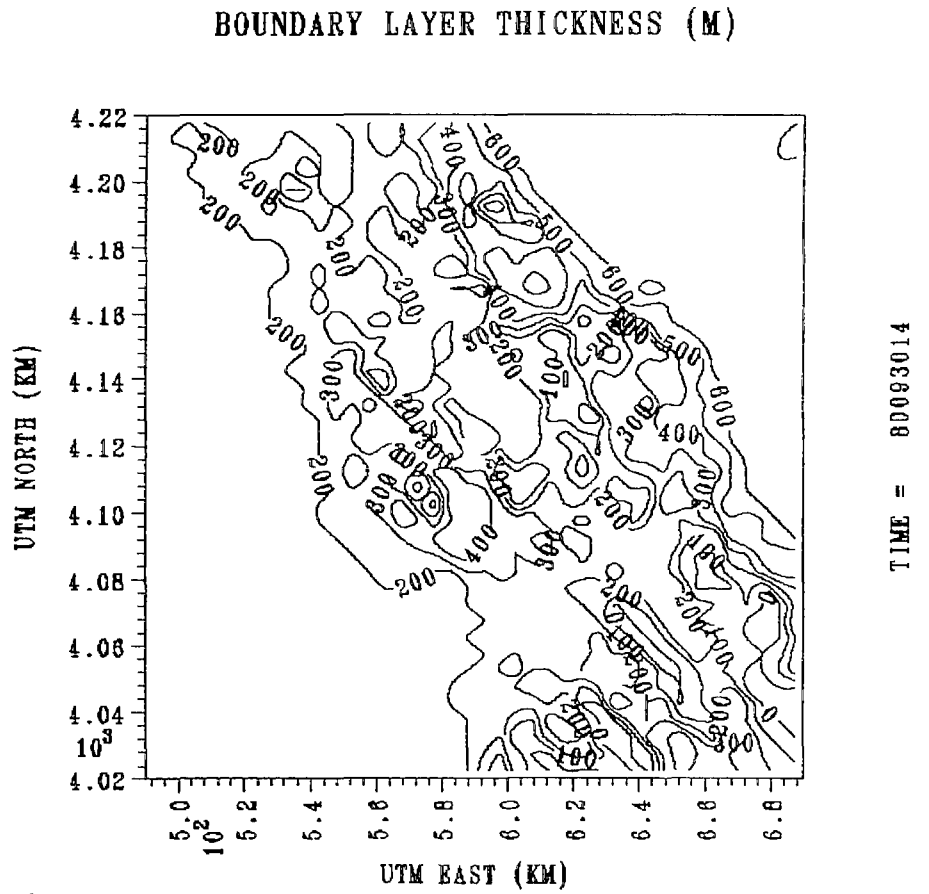

Figure 6.20. Boundary layer depth for 1400 hours used in MET1.

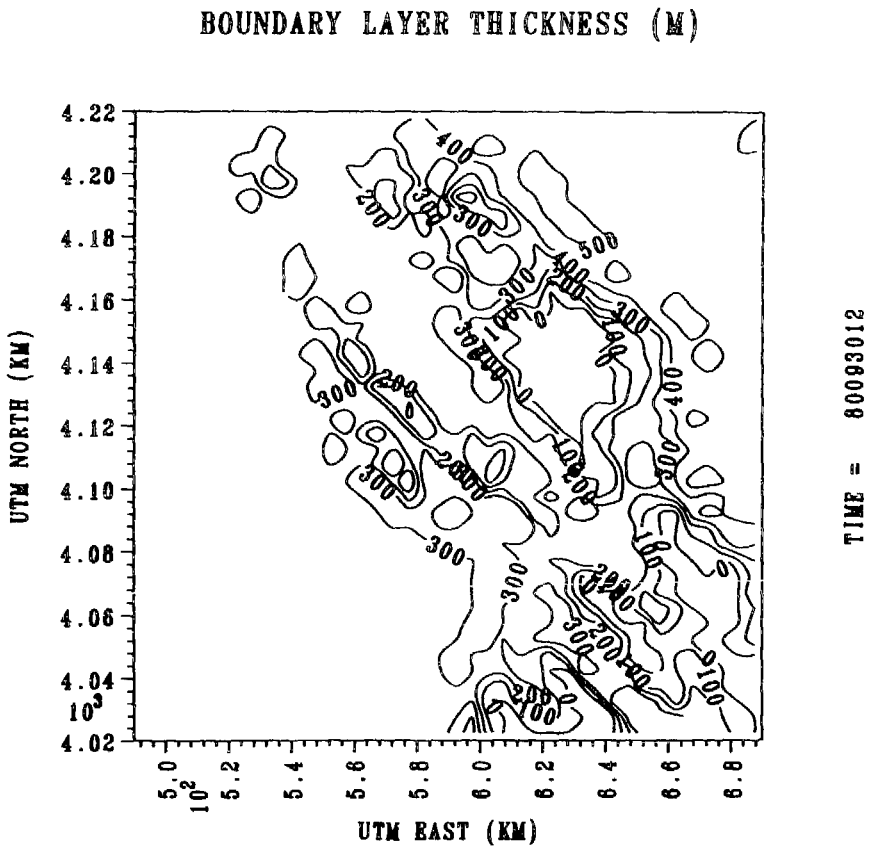

Figure 6.21. Boundary layer depth for 1200 hours used in MET4.

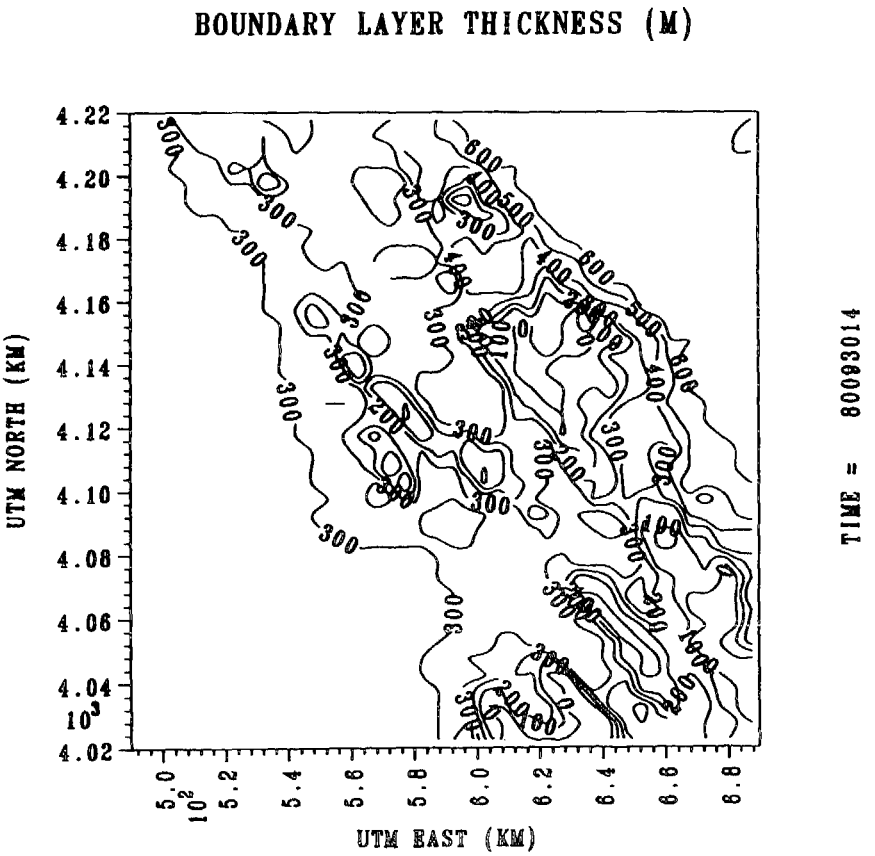

Figure 6.22. Boundary layer depth for 1400 hours used in MET4.

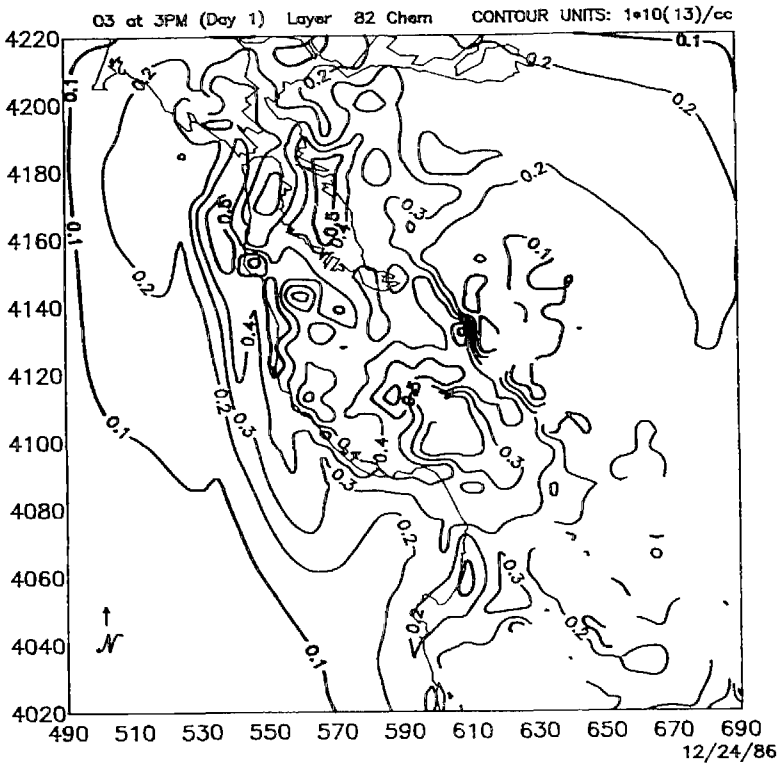

Figure 6.23. Layer-average O_3 concentrations at 1500 hours calculated using MET1.

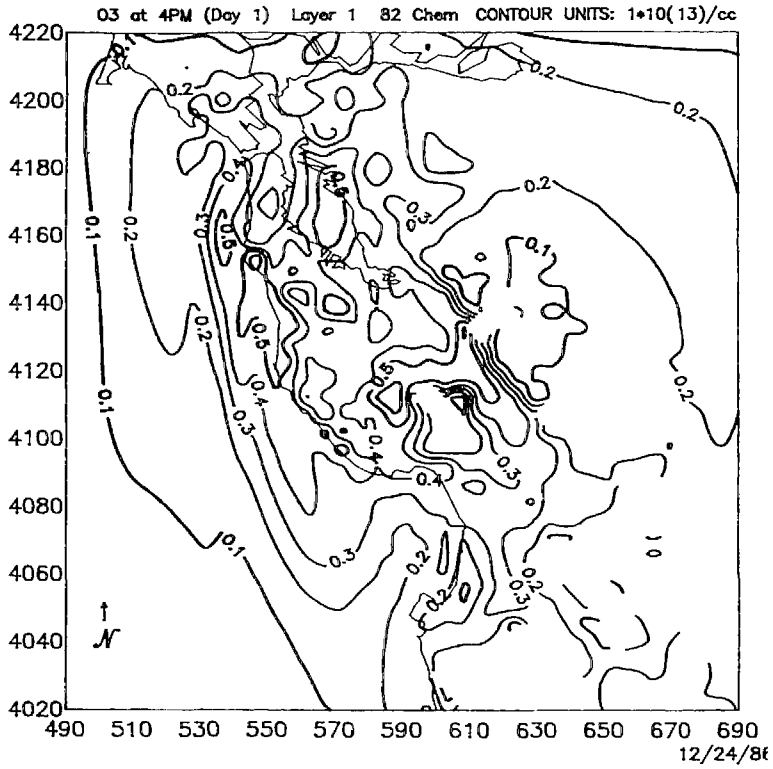

Figure 6.24. Layer-average O_3 concentrations at 1600 hours calculated using MET1.

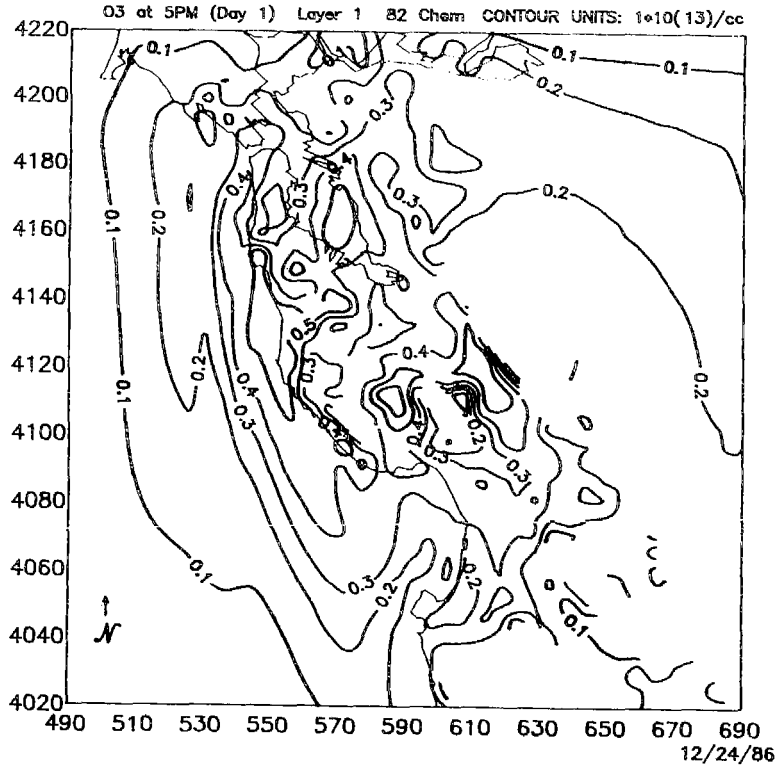

Figure 6.25. Layer-average O_3 concentrations at 1700 hours calculated using MET1.

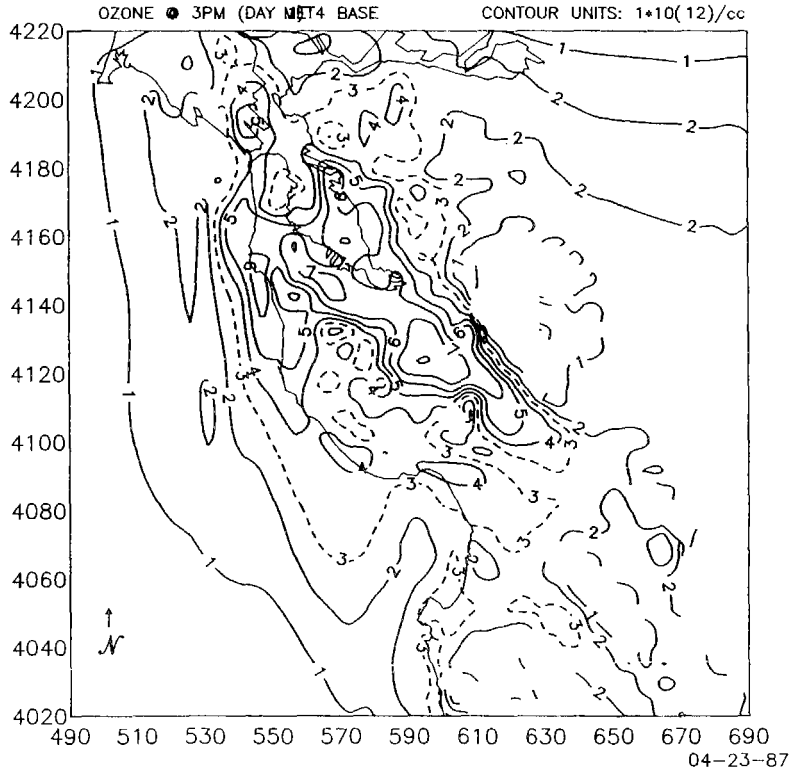

Figure 6.26. Layer-average O_3 concentrations at 1500 hours calculated using MET4. The dashed contour line shows the approximate location of the 0.12 ppm contour.

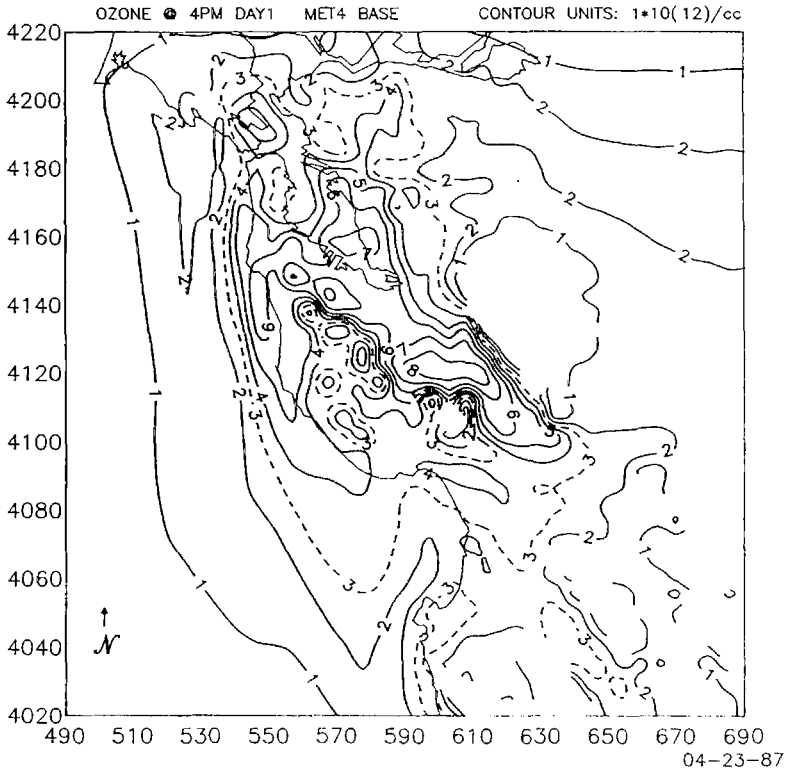

Figure 6.27. Layer-average O_3 concentrations at 1600 hours calculated using MET4. The dashed contour line shows the approximate location of the 0.12 ppm contour.

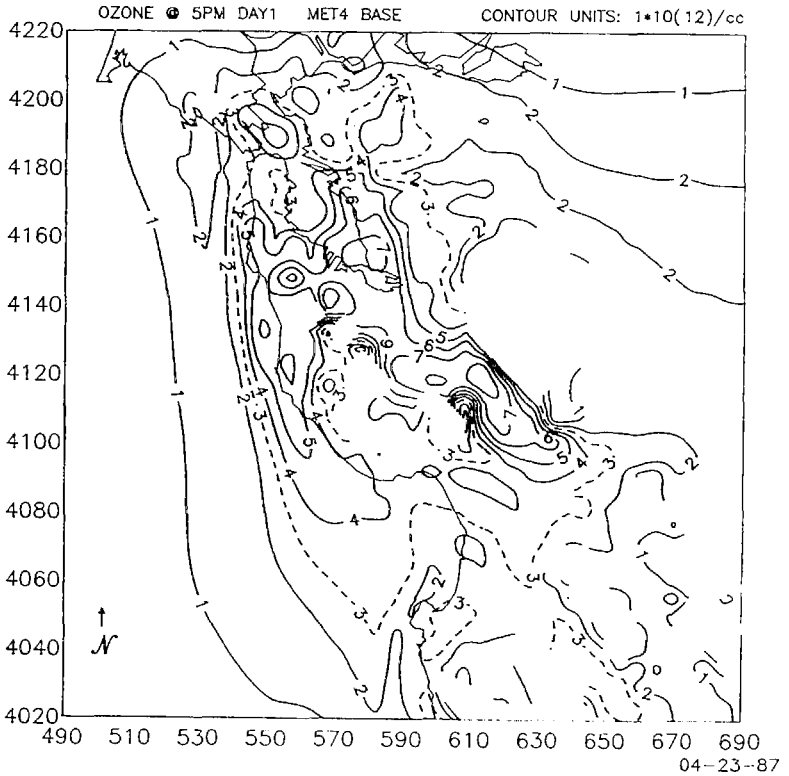

Figure 6.28. Layer-average O_3 concentrations at 1700 hours calculated using MET4. The dashed contour line shows the approximate location of the 0.12 ppm contour.

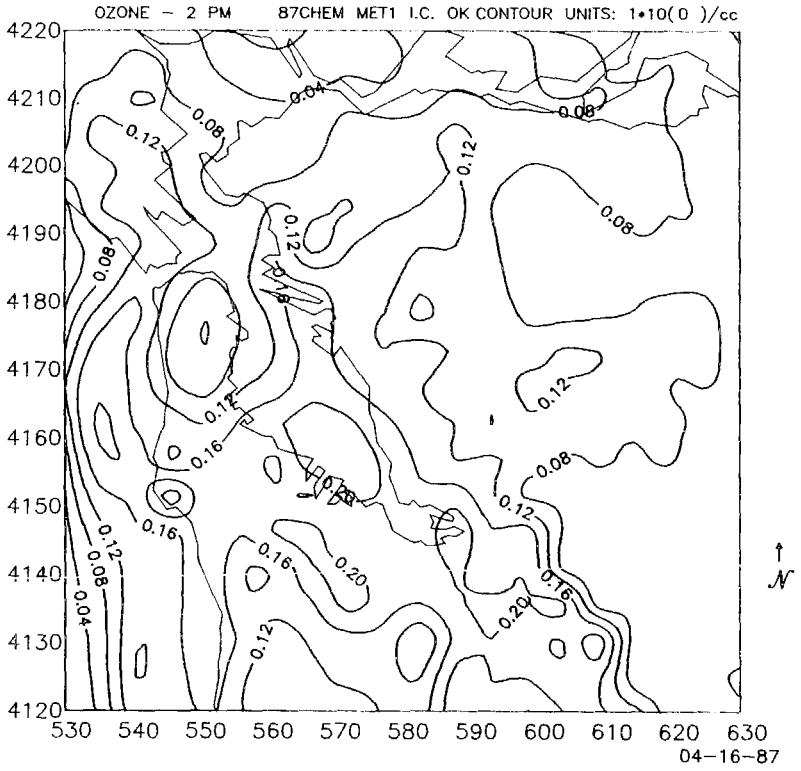

Figure 6.29. Layer-average O_3 concentrations on the 20 × 20 grid at 1400 hours calculated using MET1.

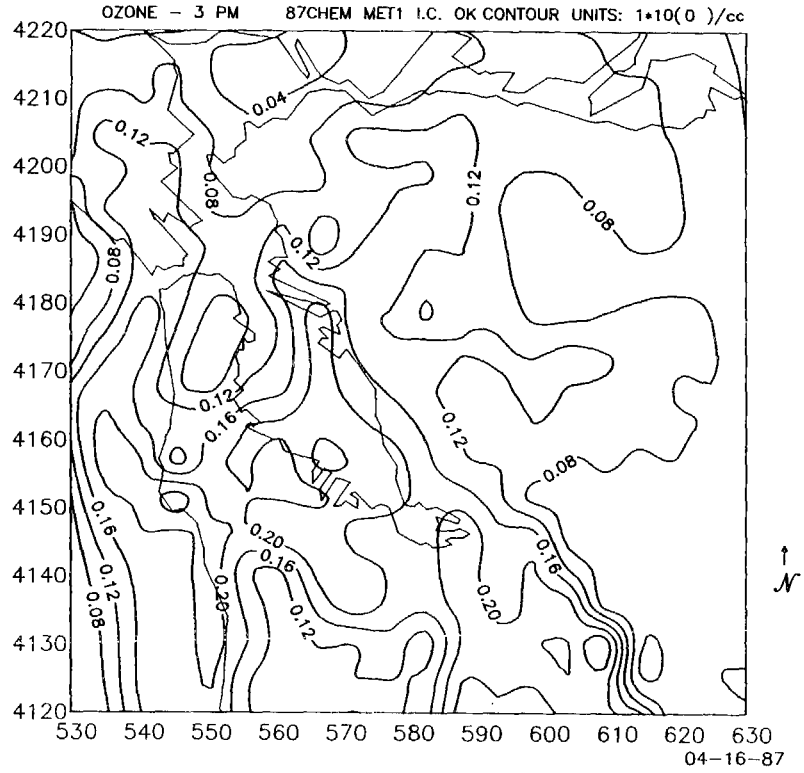

Figure 6.30. Layer-average O_3 concentrations on the 20 × 20 grid at 1500 hours calculated using MET1.

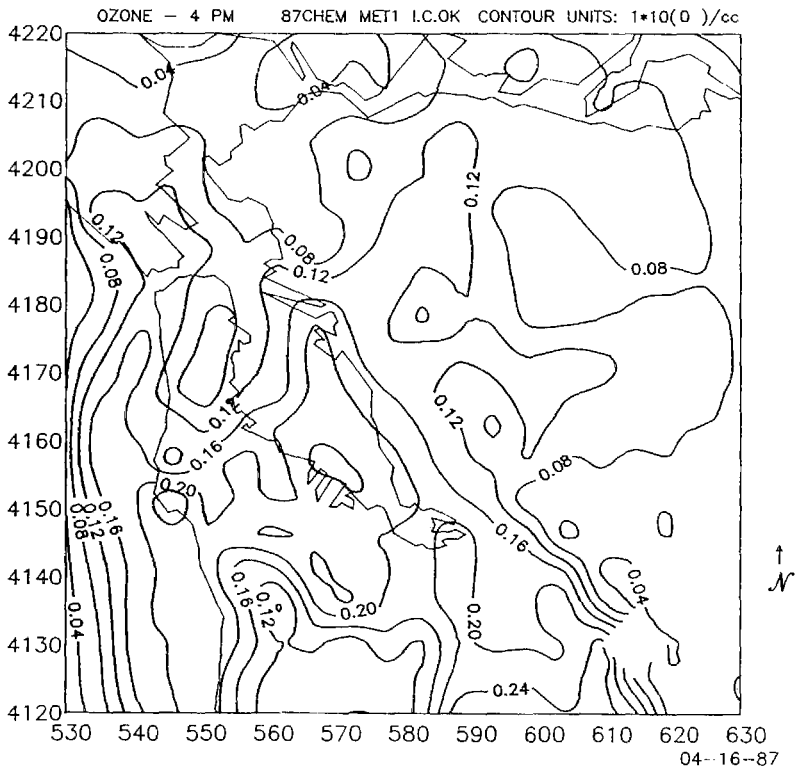

Figure 6.31. Layer-average O_3 concentrations on the 20 × 20 grid at 1600 hours calculated using MET1.

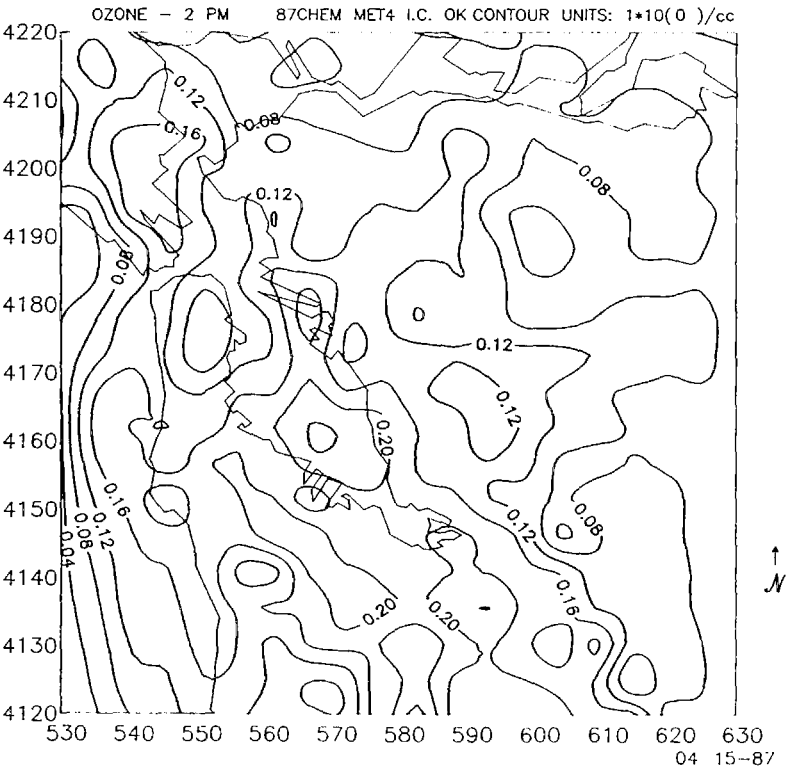

Figure 6.32. Layer-average O_3 concentrations on the 20 × 20 grid at 1400 hours calculated using MET4.

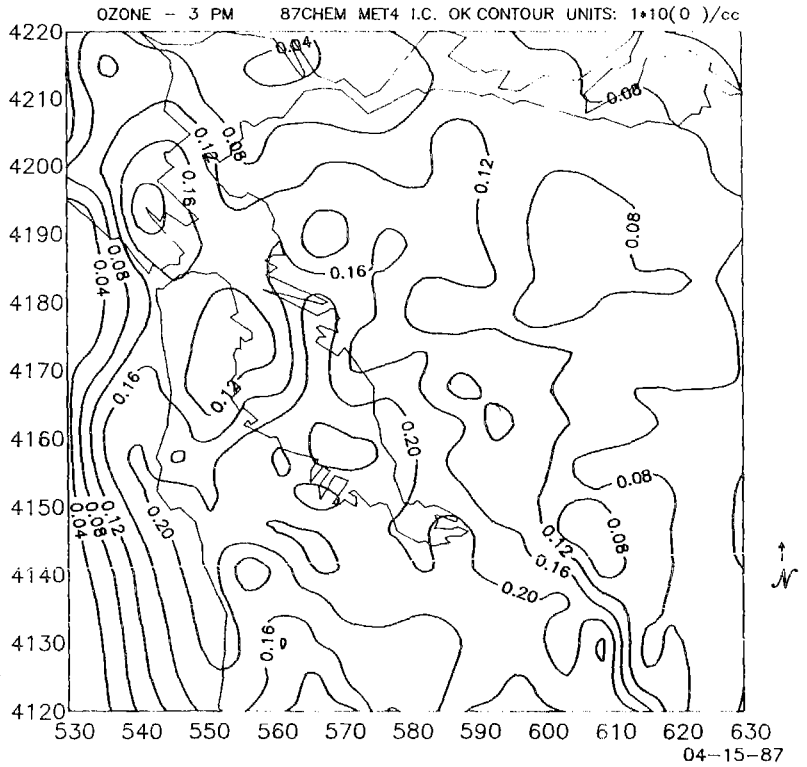

Figure 6.33. Layer-average O_3 concentrations on the 20 × 20 grid at 1500 hours calculated using MET4.

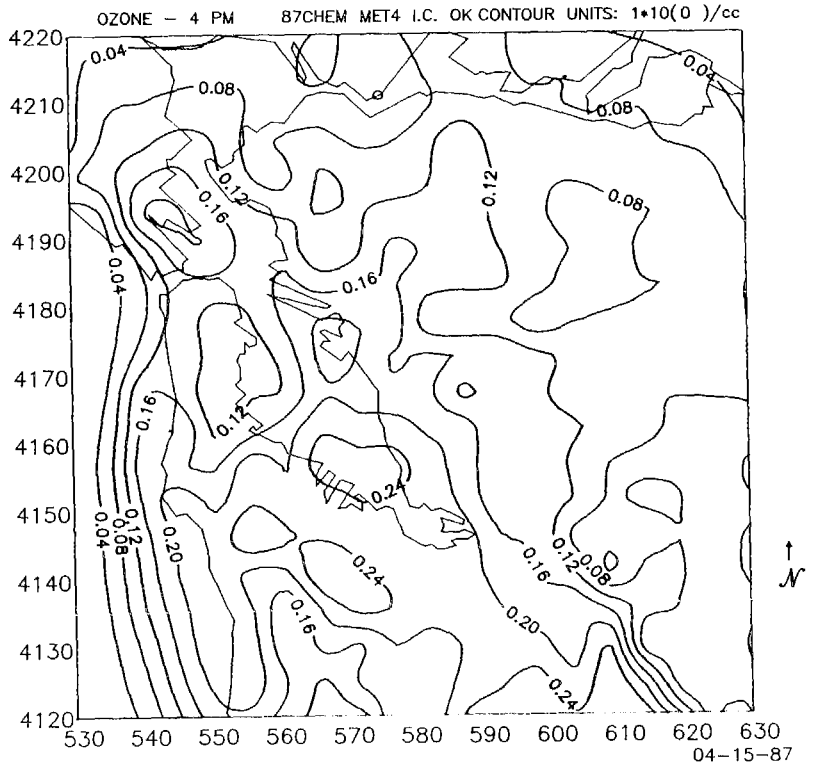

Figure 6.34. Layer-average O_3 concentrations on the 20 × 20 grid at 1600 hours calculated using MET4.

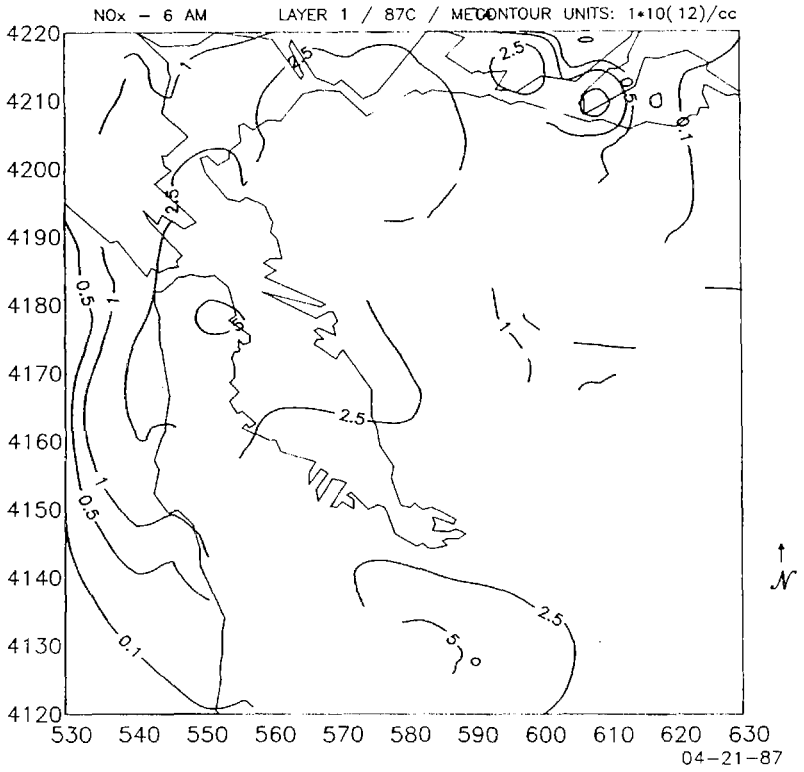

Figure 6.35. Layer-average NO_x concentrations at 0600 hours calculated using MET1.

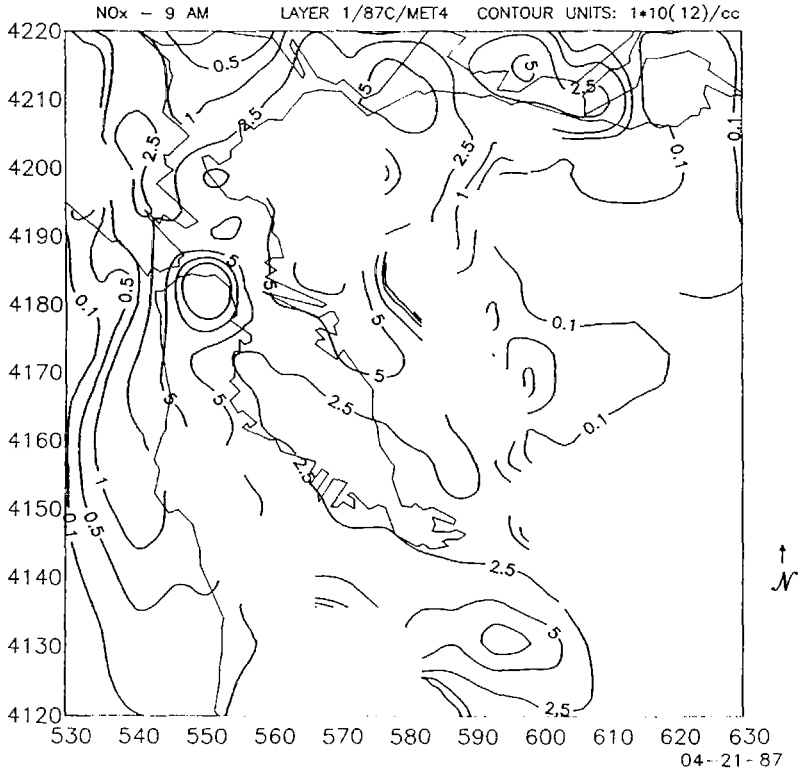

Figure 6.36. Layer-average NO_x concentrations at 0900 hours calculated using MET1.

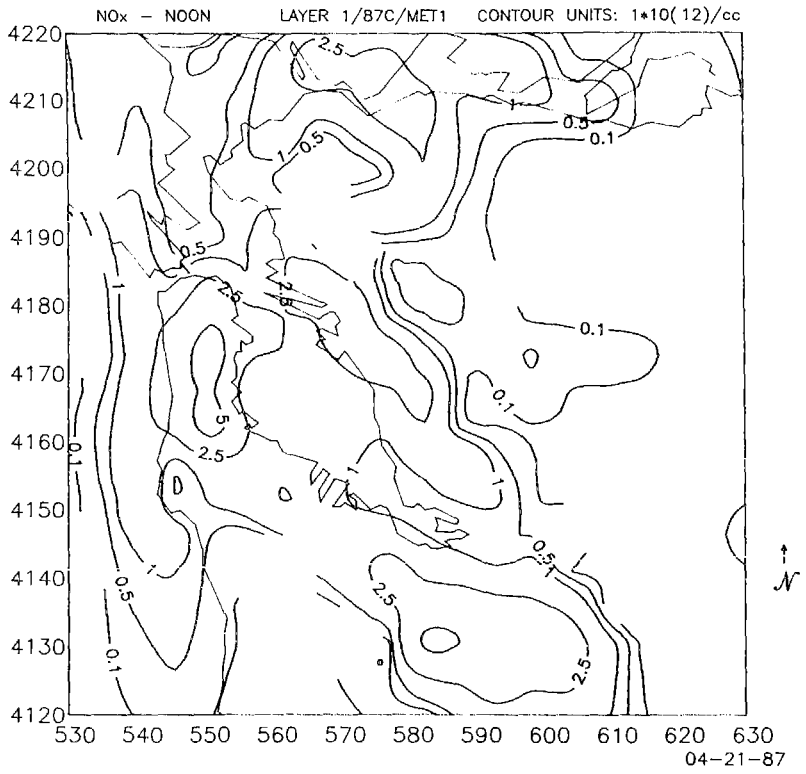

Figure 6.37. Layer-average NO_x concentrations at 1200 hours calculated using MET1.

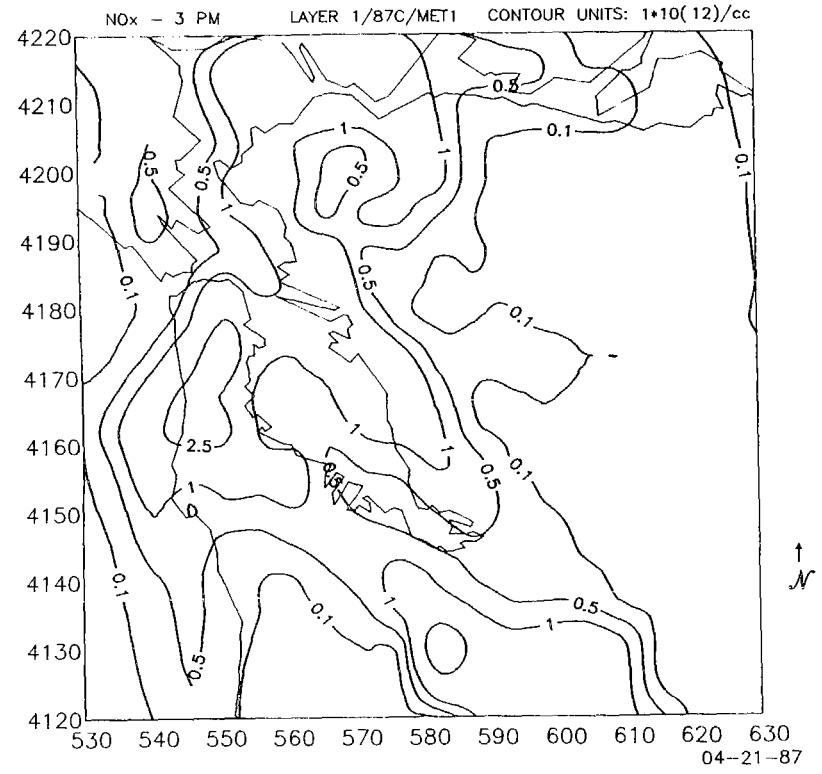

Figure 6.38. Layer-average NO_x concentrations at 1500 hours calculated using MET1.

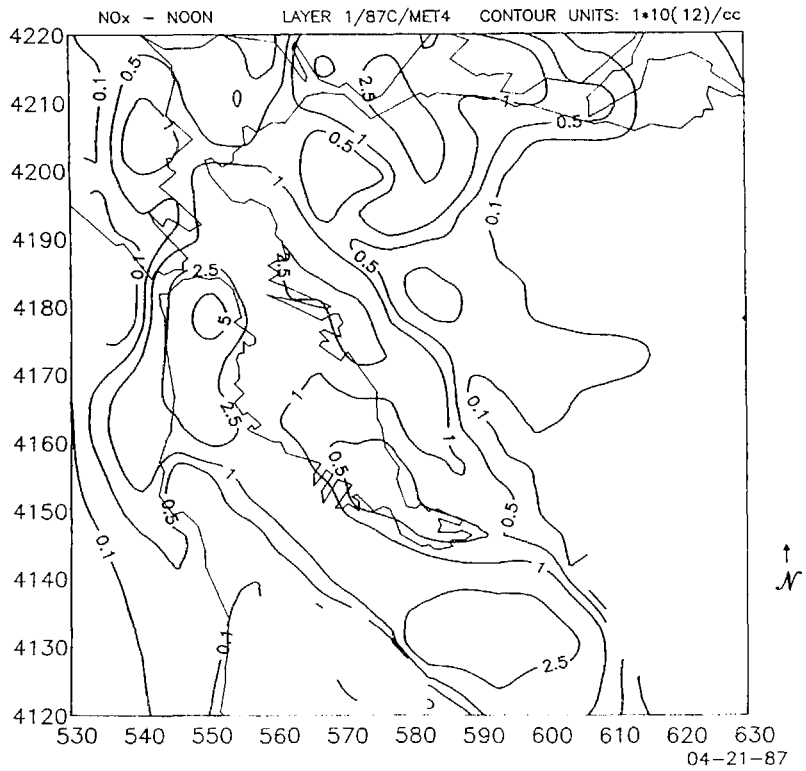

Figure 6.39. Layer-average NO_x concentrations at 1200 hours calculated using MET4.

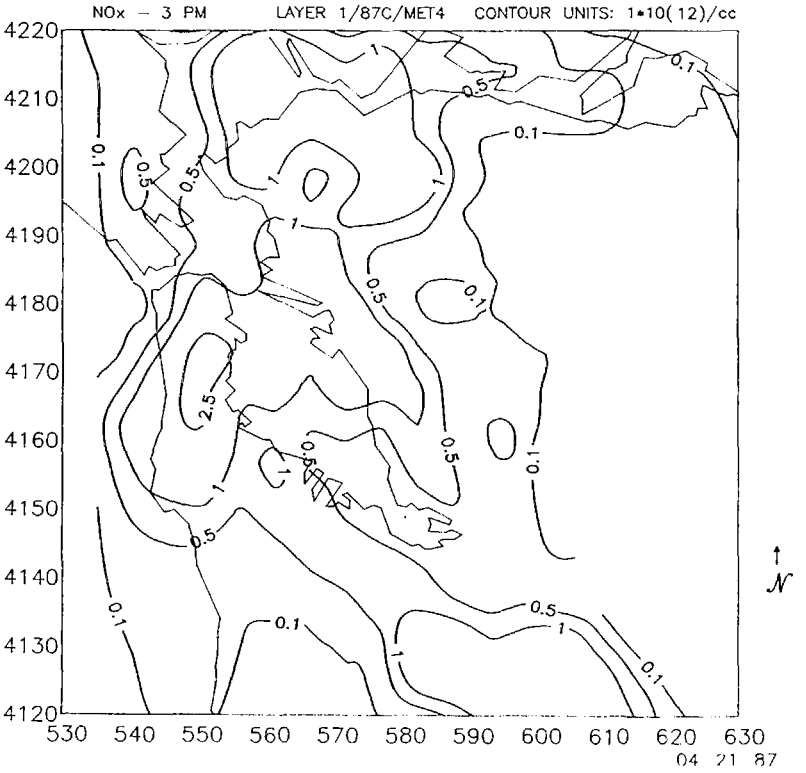

Figure 6.40. Layer-average NO_x concentrations at 1500 hours calculated using MET4.

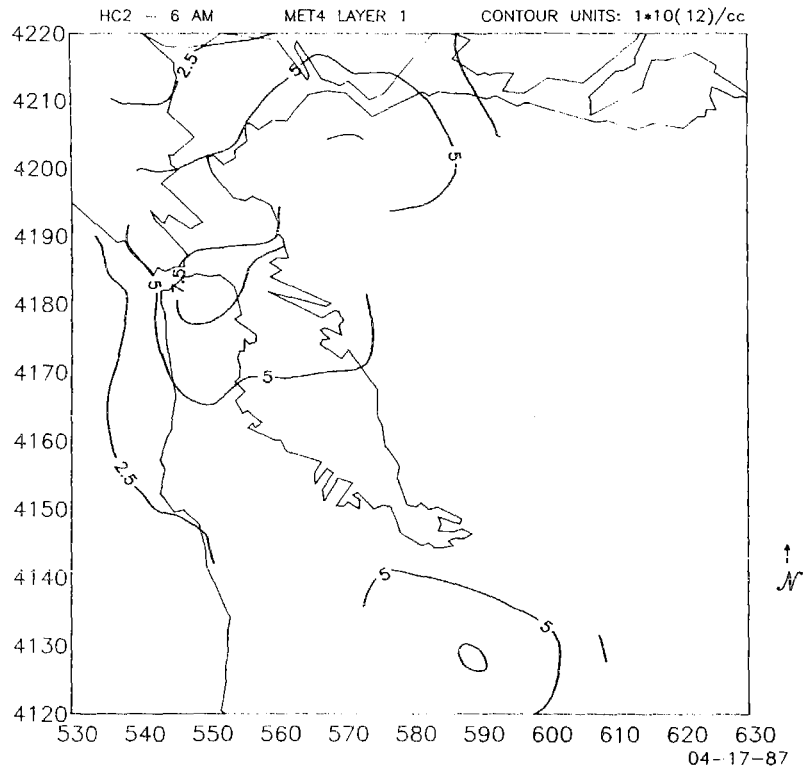

Figure 6.41. Layer-average HC2 concentrations at 0600 hours calculated using MET4.

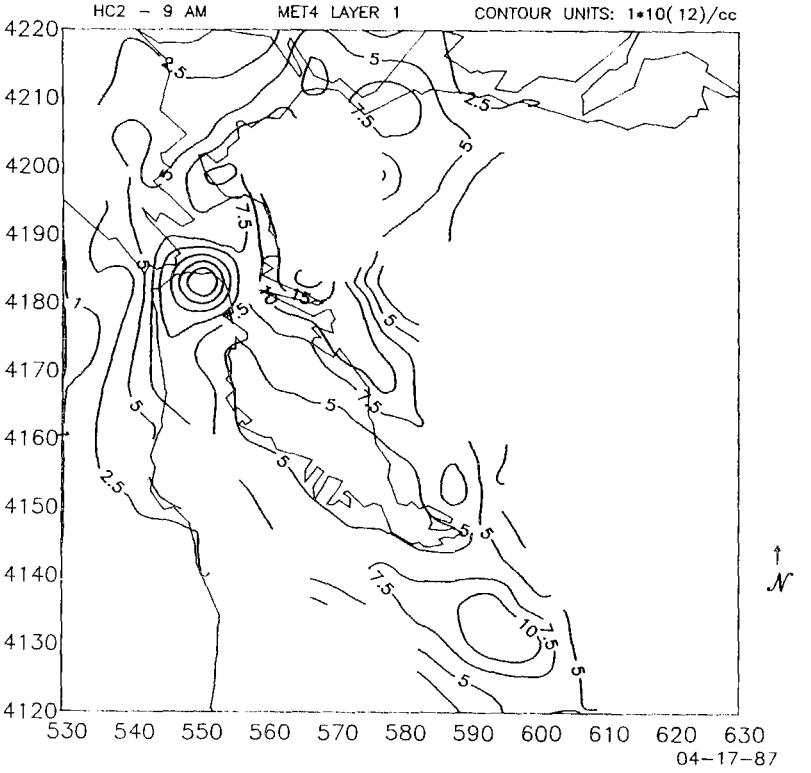

Figure 6.42. Layer-average HC2 concentrations at 0900 hours calculated using MET1.

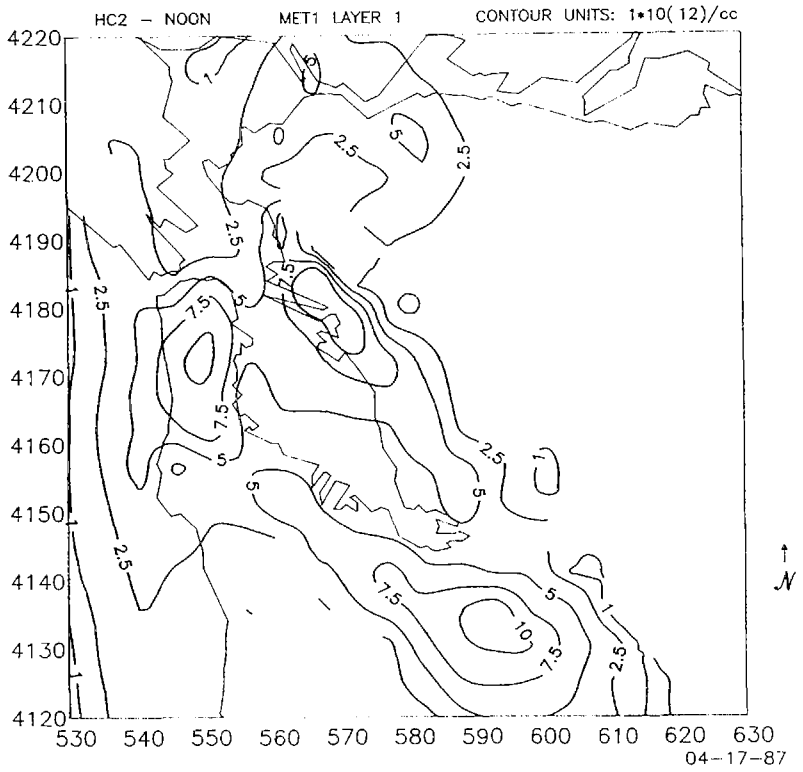

Figure 6.43. Layer-average HC2 concentrations at 1200 hours calculated using MET1.

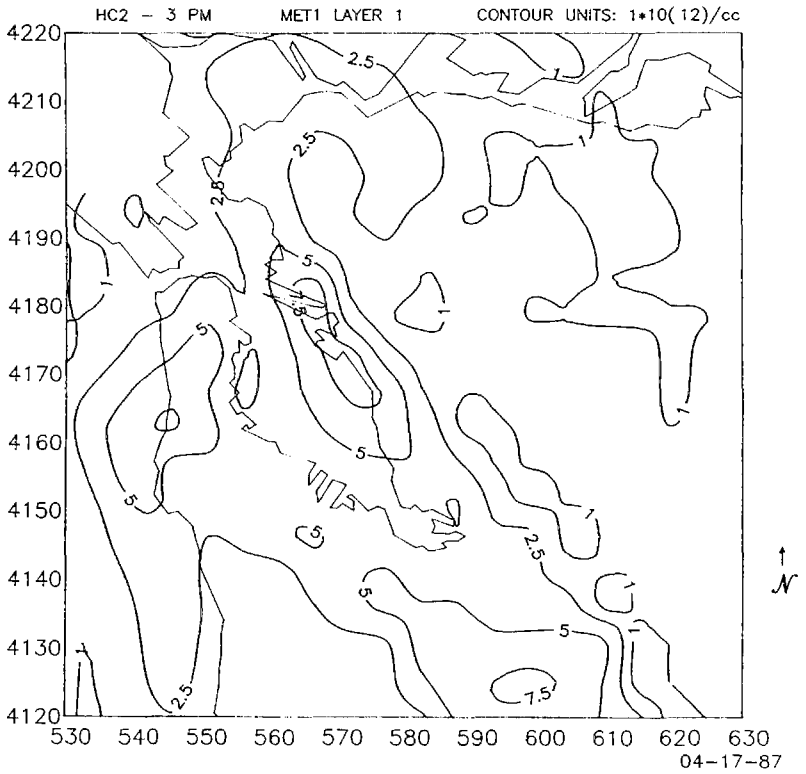

Figure 6.44. Layer-average HC2 concentrations at 1500 hours calculated using MET1.

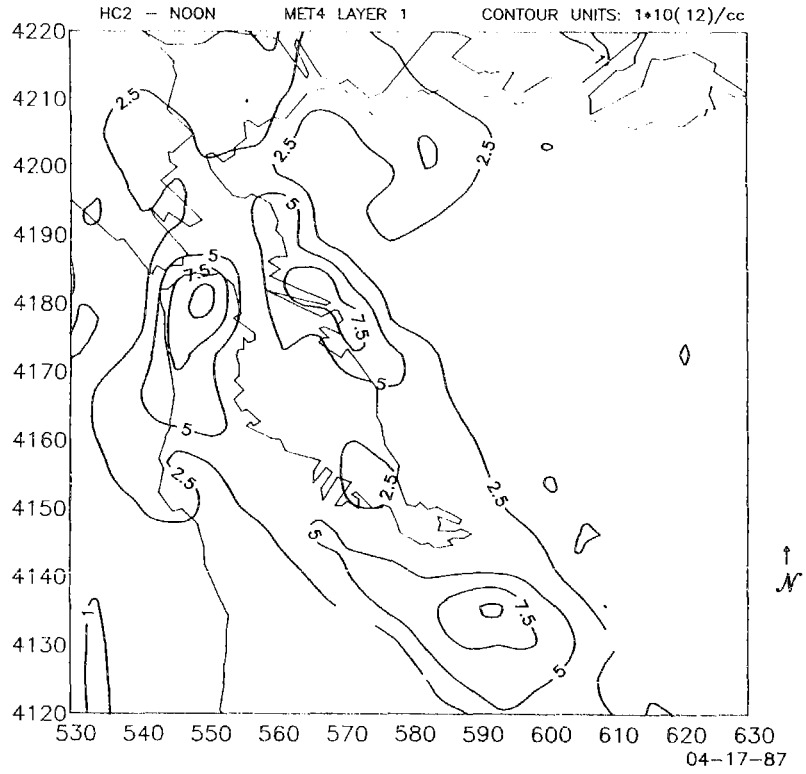

Figure 6.45. Layer-average HC2 concentrations at 1200 hours calculated using MET4.

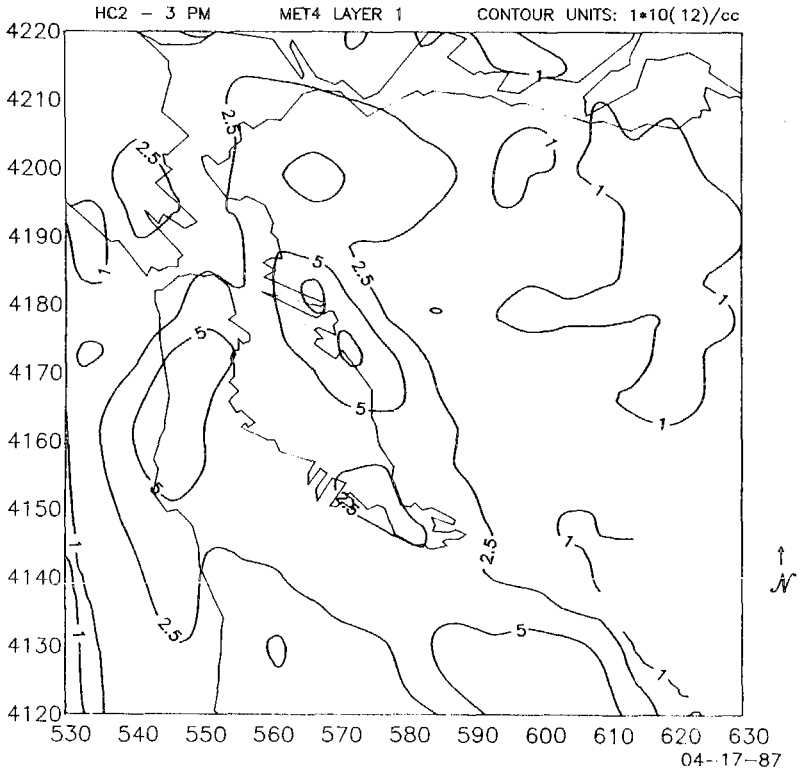

Figure 6.46. Layer-average HC2 concentrations at 1500 hours calculated using MET4.

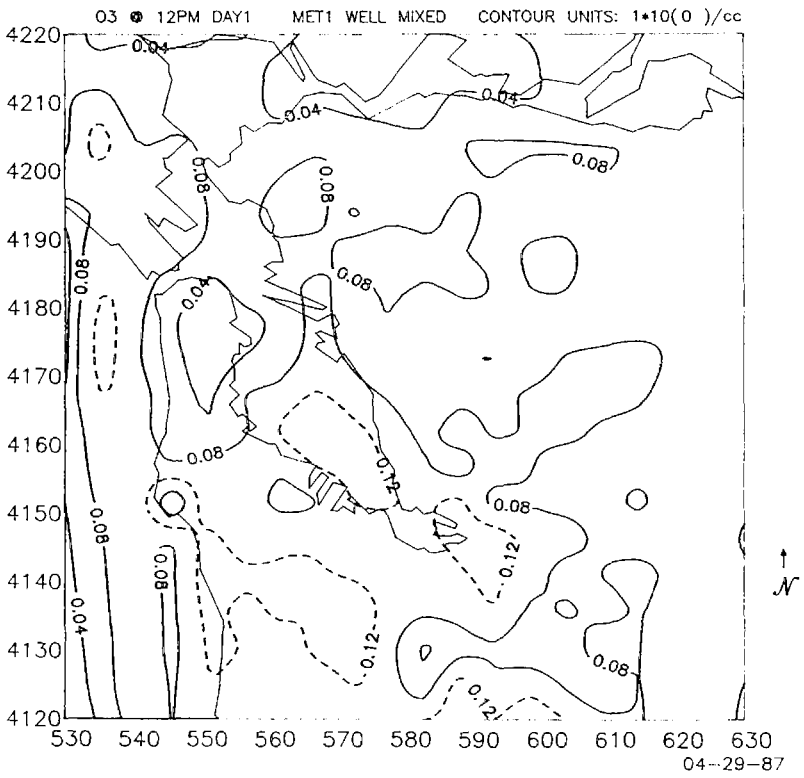

Figure 6.47. Layer-average O_3 concentration at 1200 hours calculated using MET1. The dashed contour line shows the approximate location of the 0.12 ppm contour.

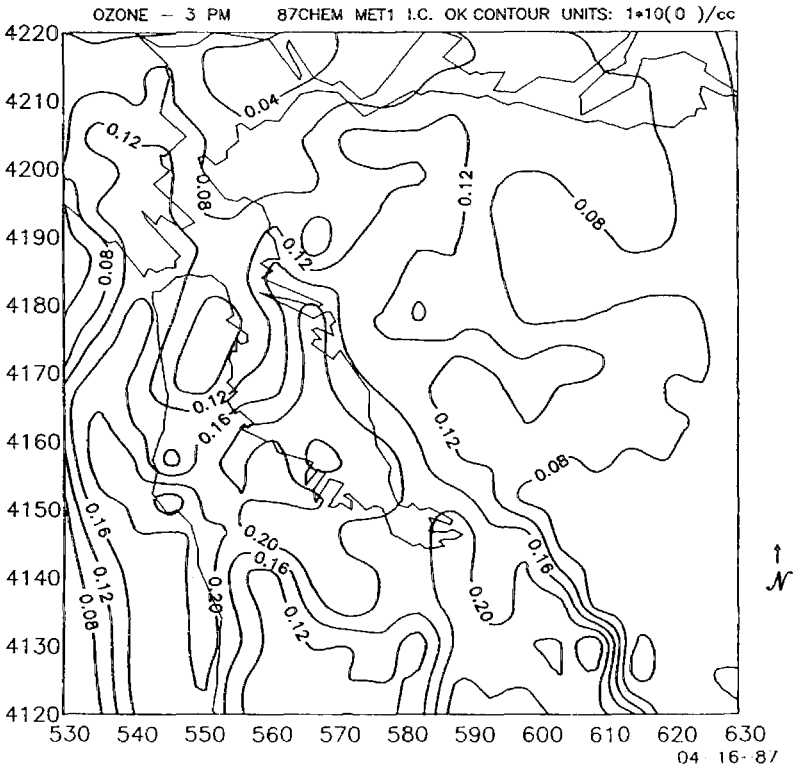

Figure 6.48. Layer-average O_3 concentration at 1500 hours calculated using MET1.

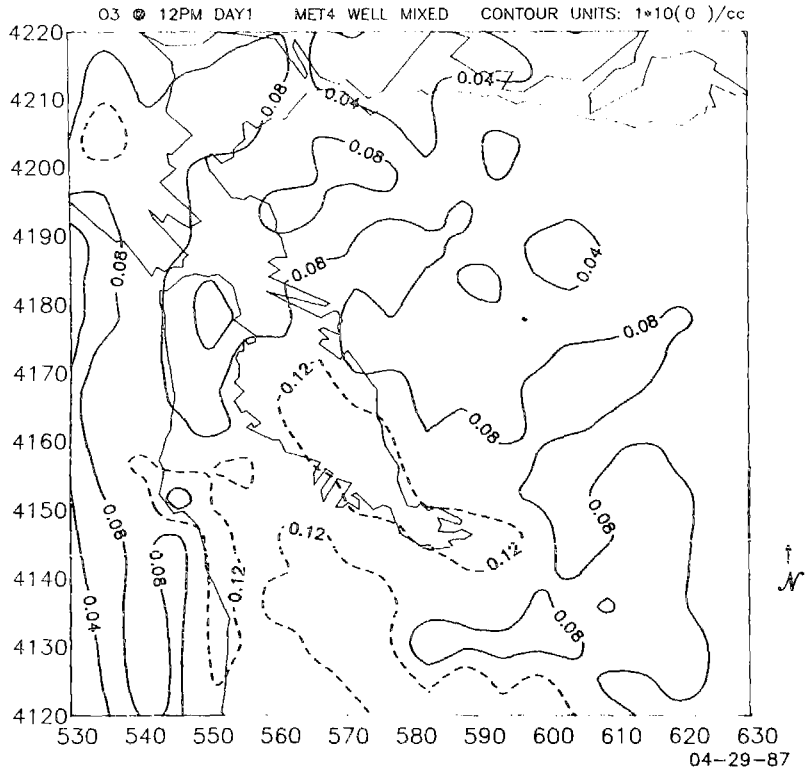

Figure 6.49. Layer-average O_3 concentration at 1200 hours calculated using MET4. The dashed contour line shows the approximate location of the 0.12 ppm contour.

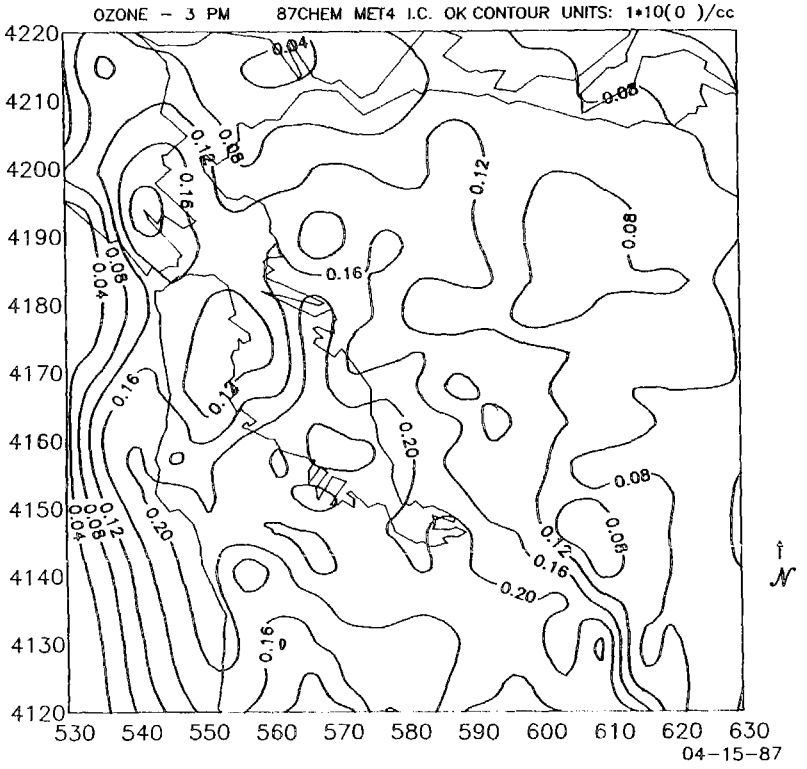

Figure 6.50. Layer-average O_3 concentration at 1500 hours calculated using MET4.

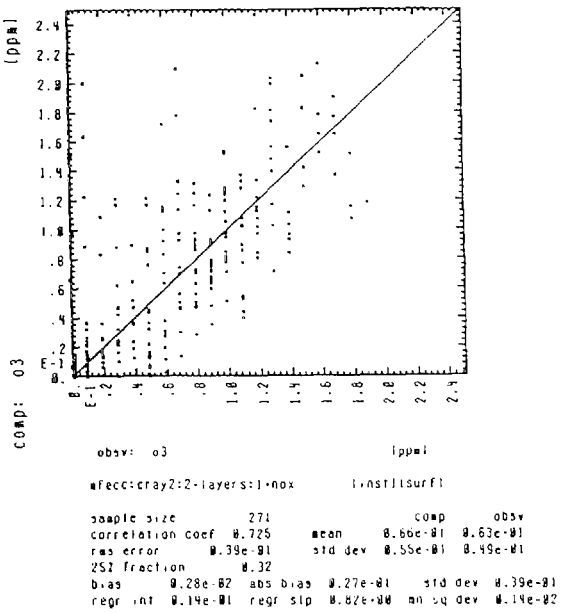

Figure 6.51. Scatter plot of observed and computed O_3 for September 30, 1980 with corrected inventory.

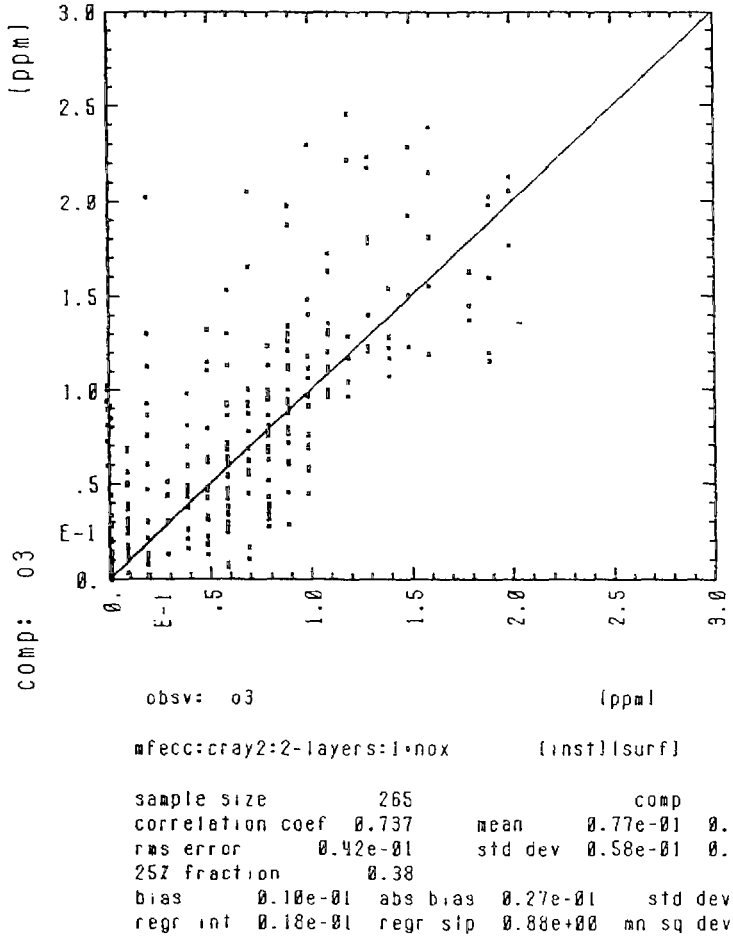

Figure 6.52. Scatter plot of observed and computed O_3 for October 1, 1980 with corrected inventory.

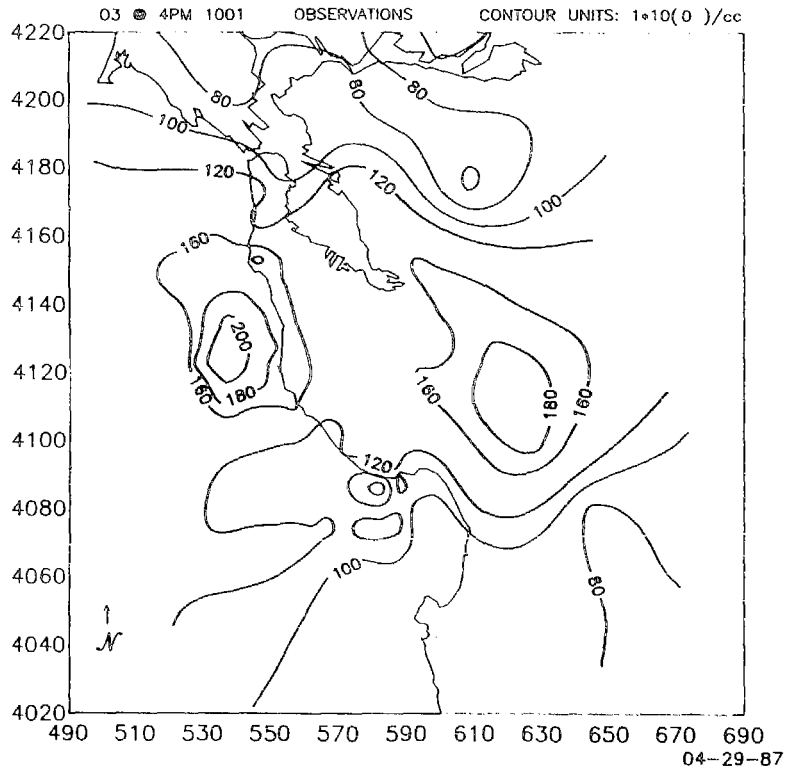

Figure 6.53. Observed surface O_3 concentrations at 1600 hours on October 1, 1980.

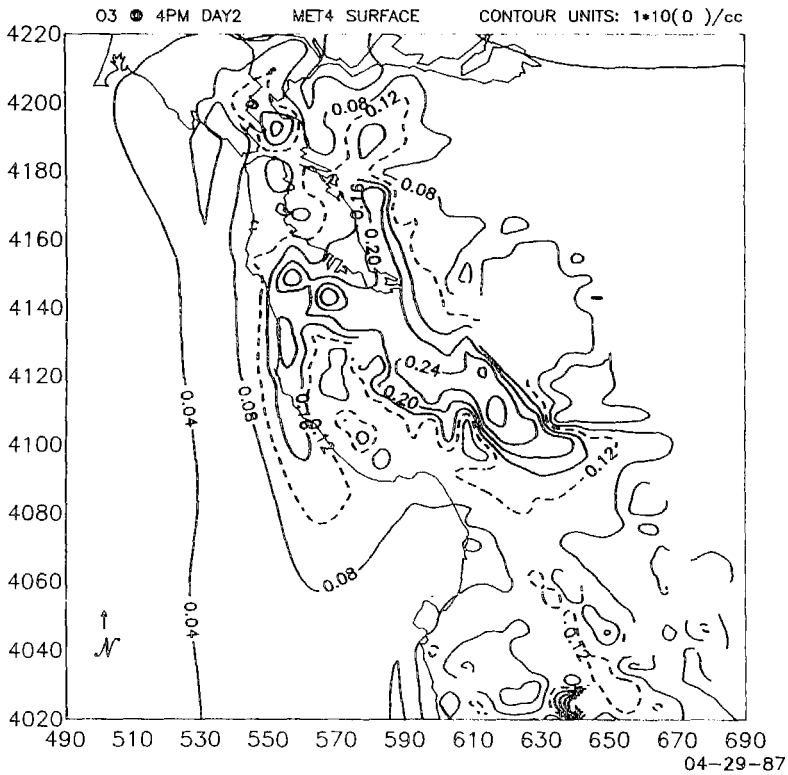

Figure 6.54. Computed surface O_3 concentrations at 1600 hours on October 1, 1980. The dashed contour line shows the approximate location of the 0.12 ppm contour.

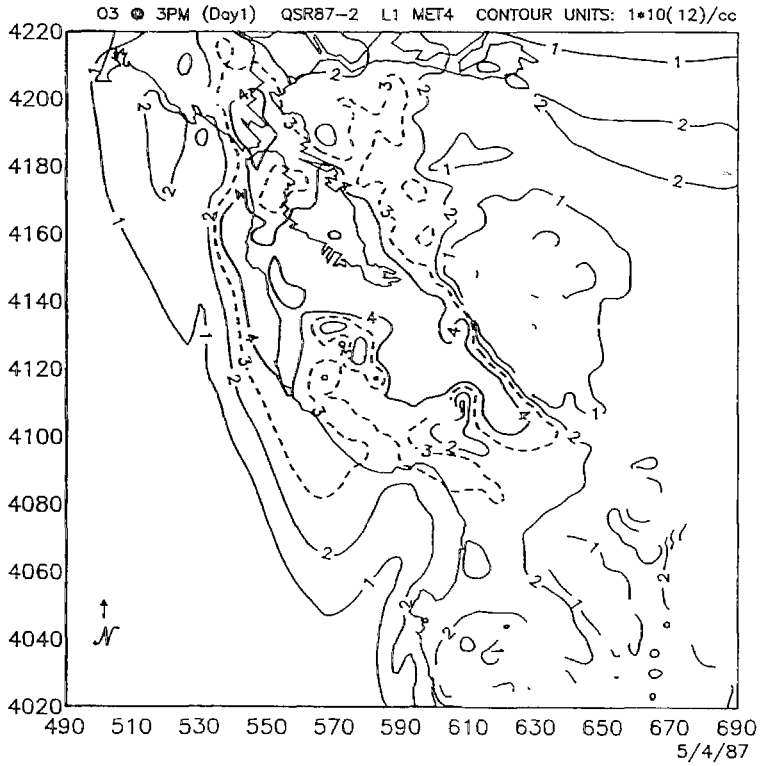

Figure 6.55. Layer-average O_3 concentration at 1500 hours for the base case on September 30, 1980. The dashed contour line shows the approximate location of the 0.12 ppm contour.

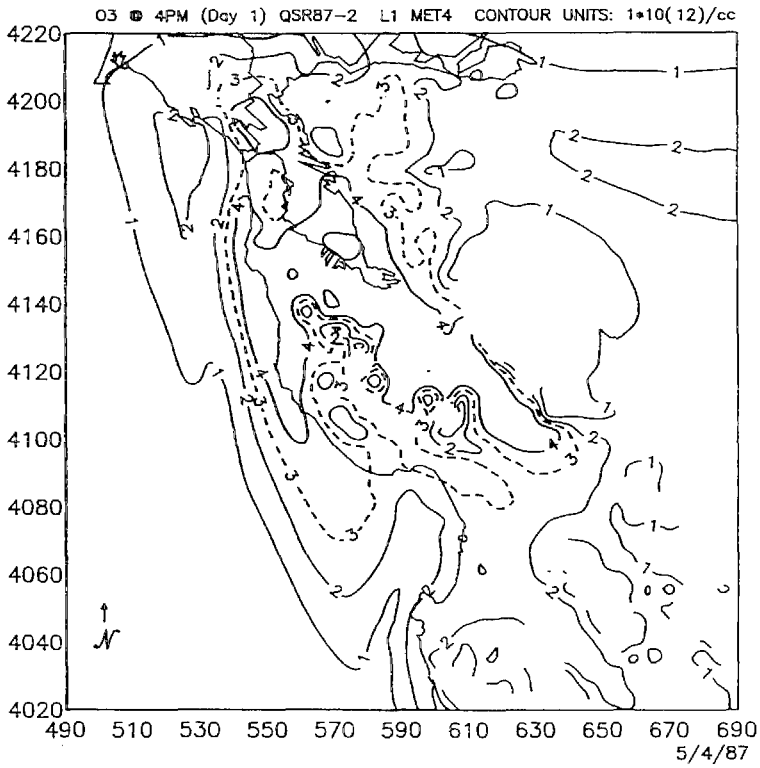

Figure 6.56. Layer-average O_3 concentration at 1600 hours for the base case on September 30, 1980. The dashed contour line shows the approximate location of the 0.12 ppm contour.

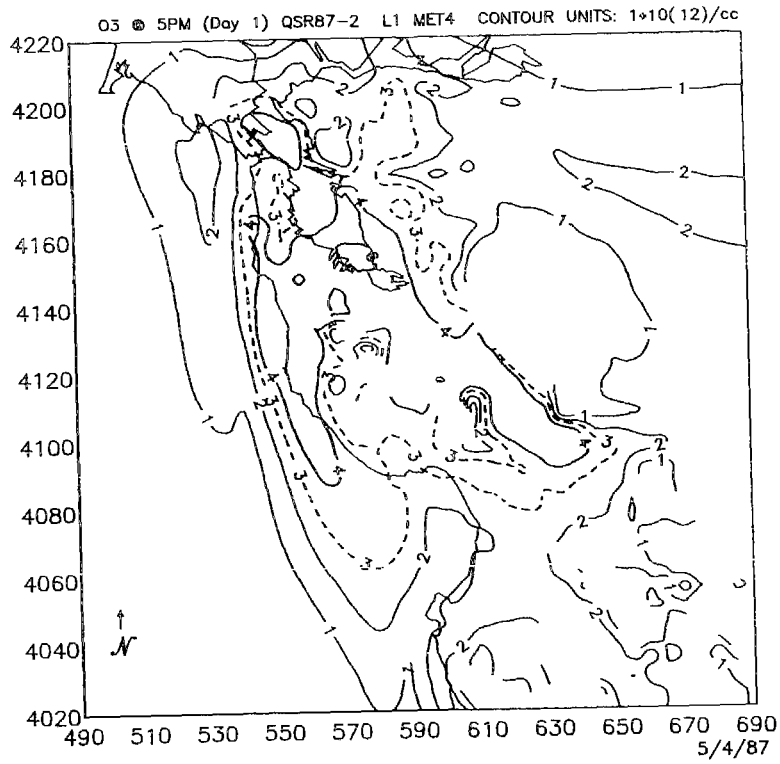

Figure 6.57. Layer-average O_3 concentration at 1700 hours for the base case on September 30, 1980. The dashed contour line shows the approximate location of the 0.12 ppm contour.

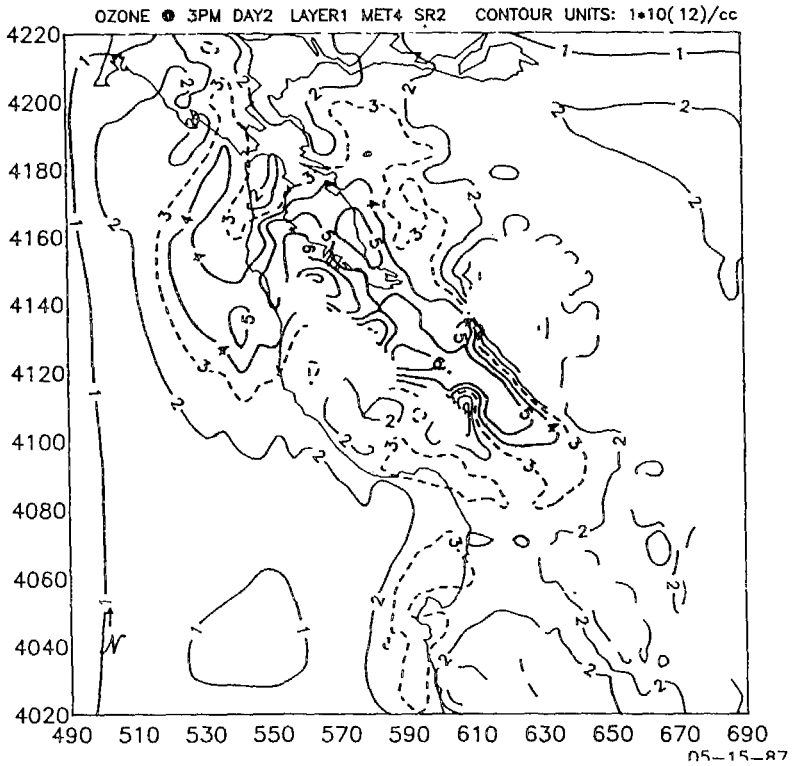

Figure 6.58. Layer-average O_3 concentration at 1500 hours for the base case on October 1, 1980. The dashed contour line shows the approximate location of the 0.12 ppm contour.

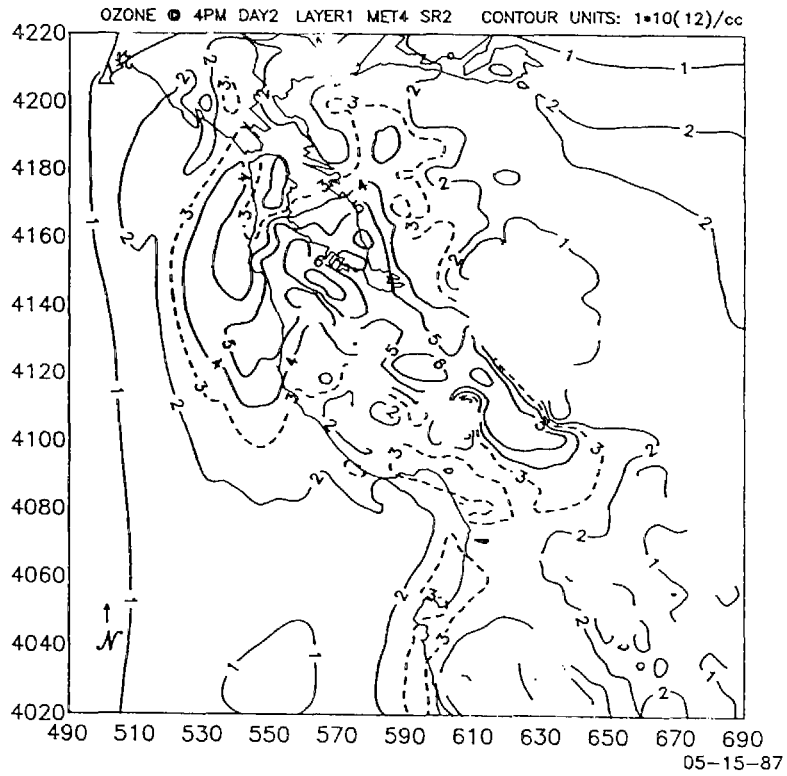

Figure 6.59. Layer-average O_3 concentration at 1600 hours for the base case on October 1, 1980. The dashed contour line shows the approximate location of the 0.12 ppm contour.

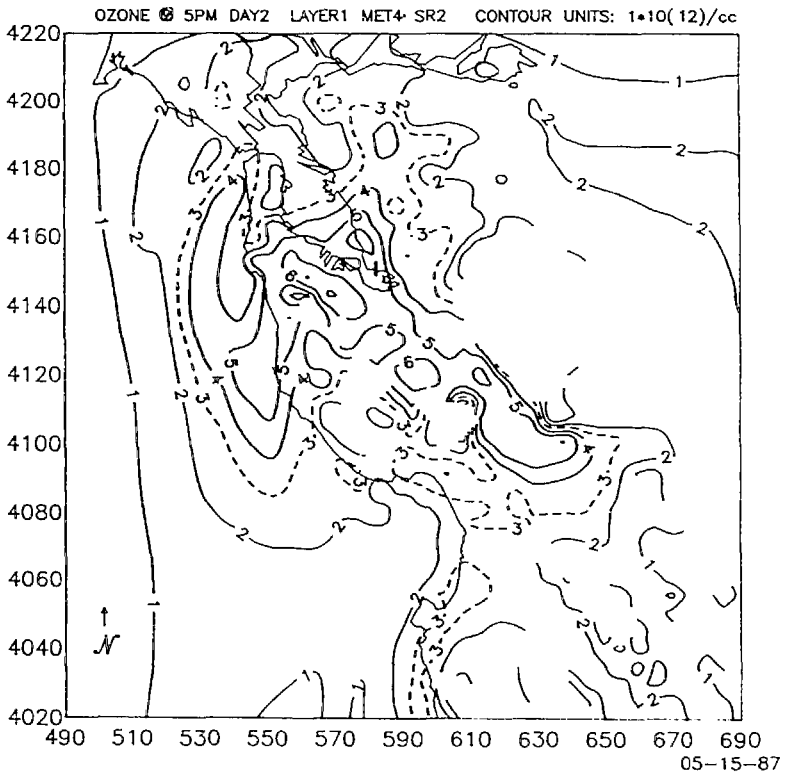

Figure 6.60. Layer-average O_3 concentration at 1700 hours for the base case on October 1, 1980. The dashed contour line shows the approximate location of the 0.12 ppm contour.

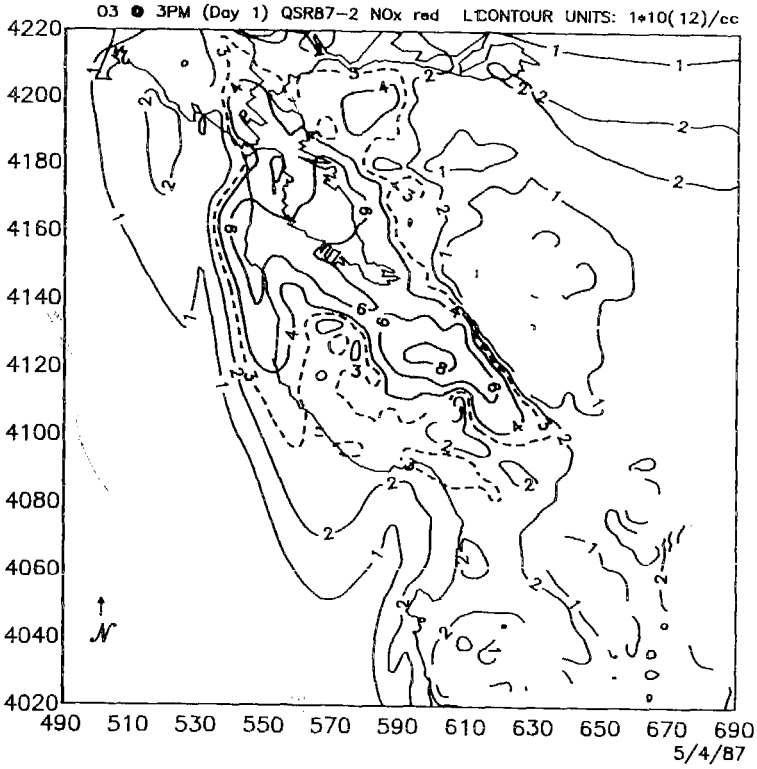

Figure 6.61. Layer-average O_3 concentration at 1500 hours for the case with reduced NO_x on September 30, 1980. The dashed contour line shows the approximate location of the 0.12 ppm contour.

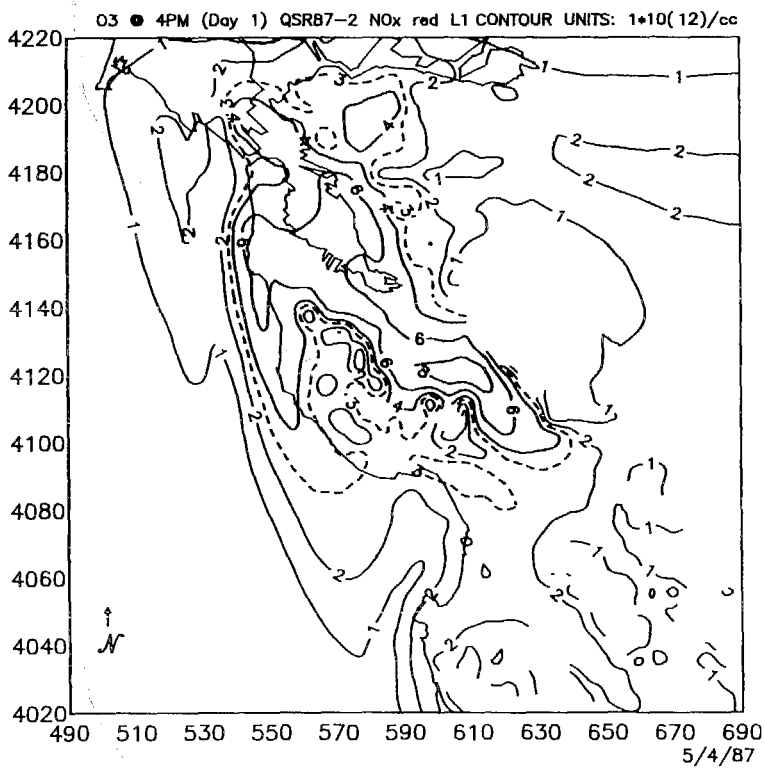

Figure 6.62. Layer-average O_3 concentration at 1600 hours for the case with reduced NO_x on September 30, 1980. The dashed contour line shows the approximate location of the 0.12 ppm contour.

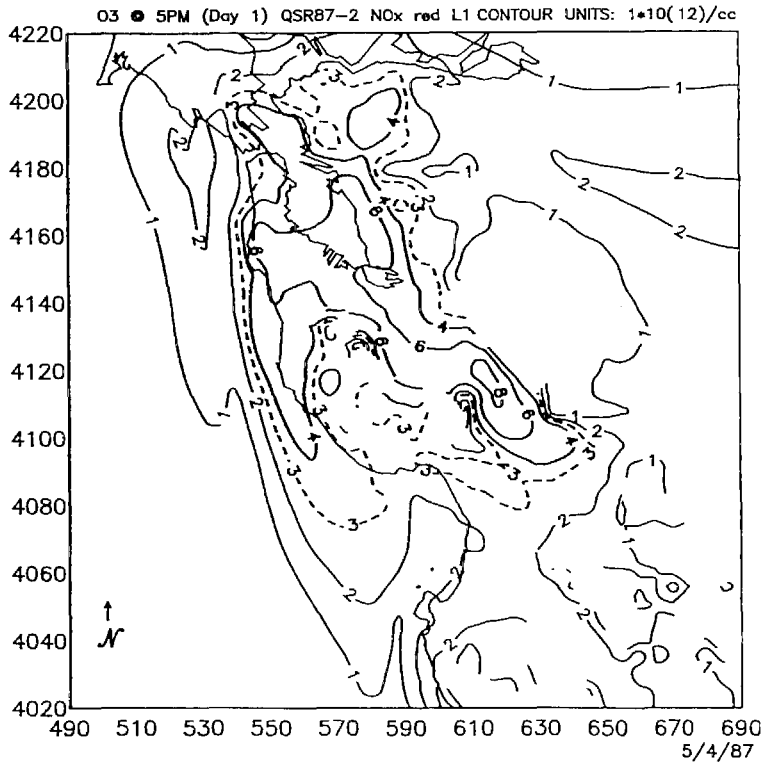

Figure 6.63. Layer-average O_3 concentration at 1700 hours for the case with reduced NO_x on September 30, 1980. The dashed contour line shows the approximate location of the 0.12 ppm contour.

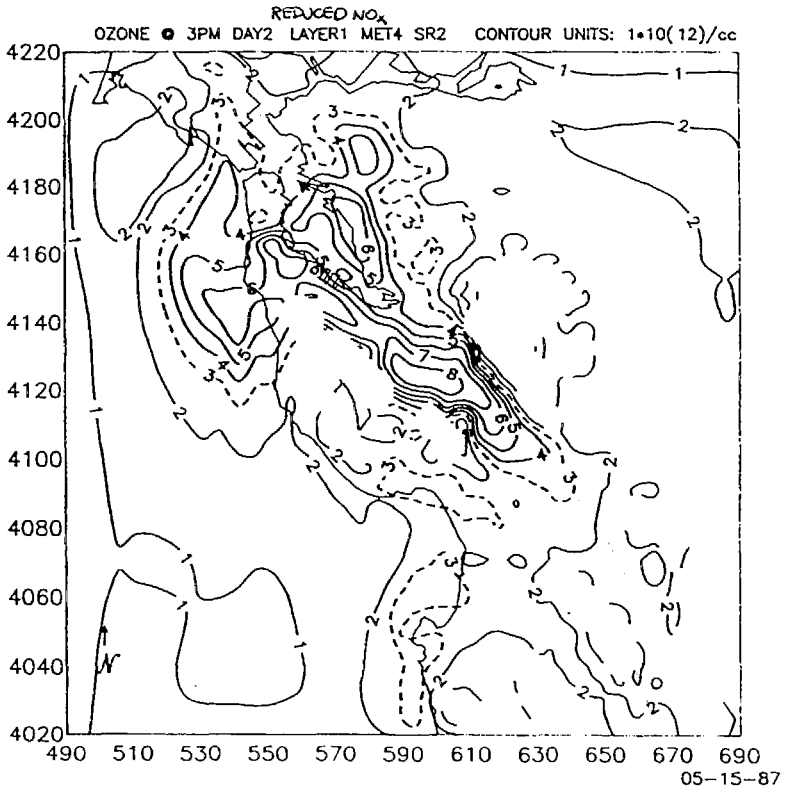

Figure 6.64. Layer-average O_3 concentration at 1500 hours for the case with reduced NO_x on October 1, 1980. The dashed contour line shows the approximate location of the 0.12 ppm contour.

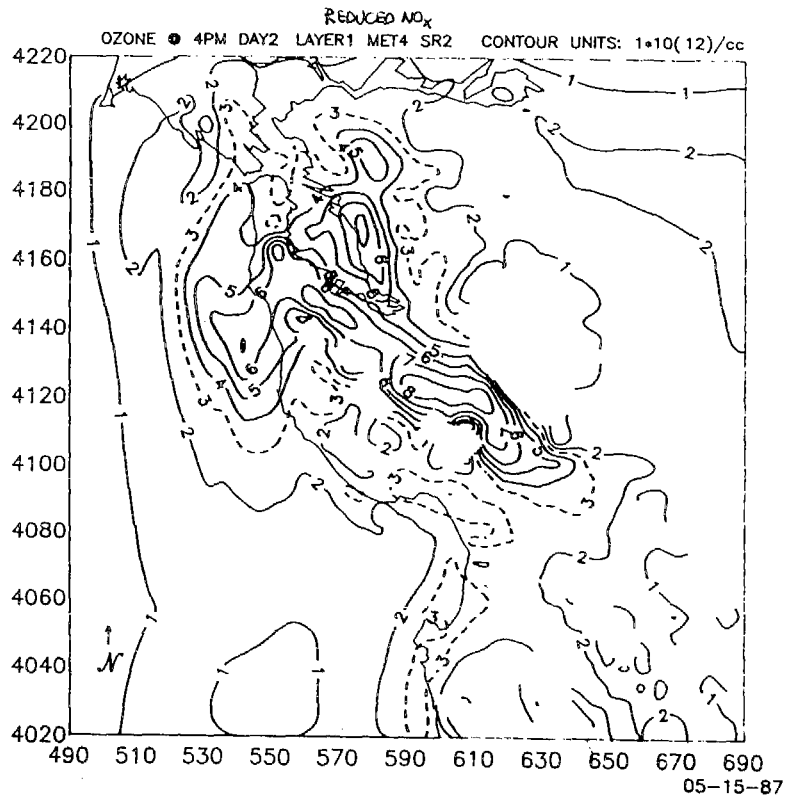

Figure 6.65. Layer-average O_3 concentration at 1600 hours for the case with reduced NO_x on October 1, 1980. The dashed contour line shows the approximate location of the 0.12 ppm contour.

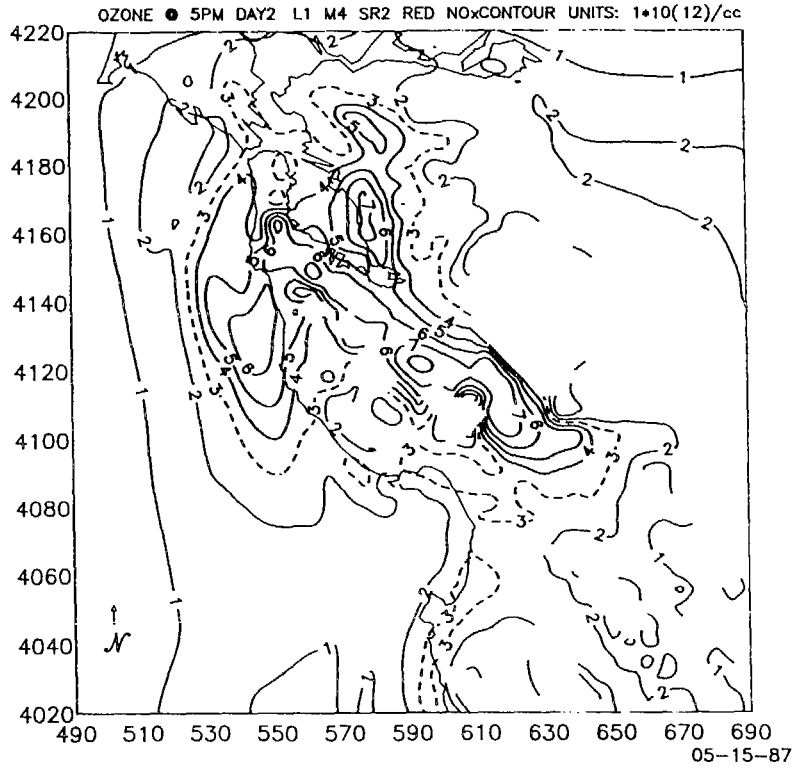

Figure 6.66. Layer-average O_3 concentration at 1700 hours for the case with reduced NO_x on October 1, 1980. The dashed contour line shows the approximate location of the 0.12 ppm contour.

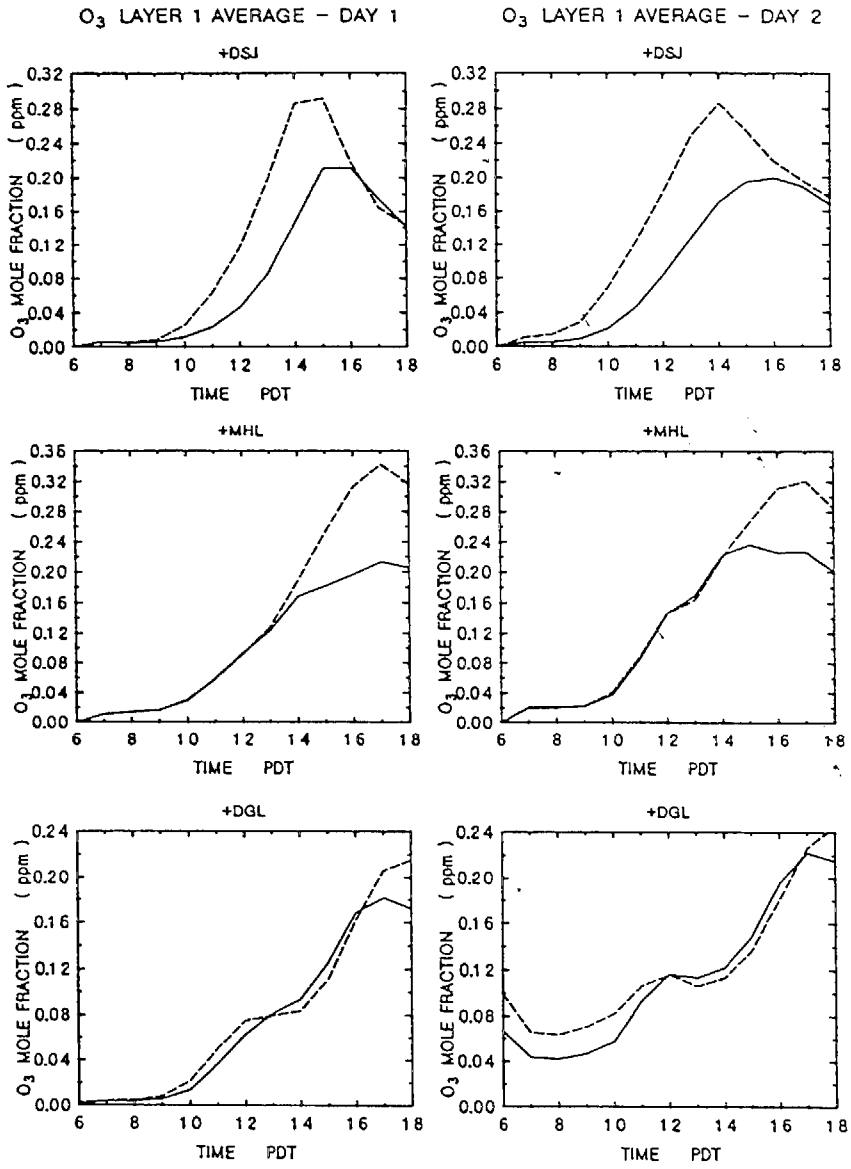

Figure 6.67. Time history for layer-average O_3 at San Jose, Morgan Hill and Gilroy. The solid line is the base case and the long dashed line is the reduced NO_x case.

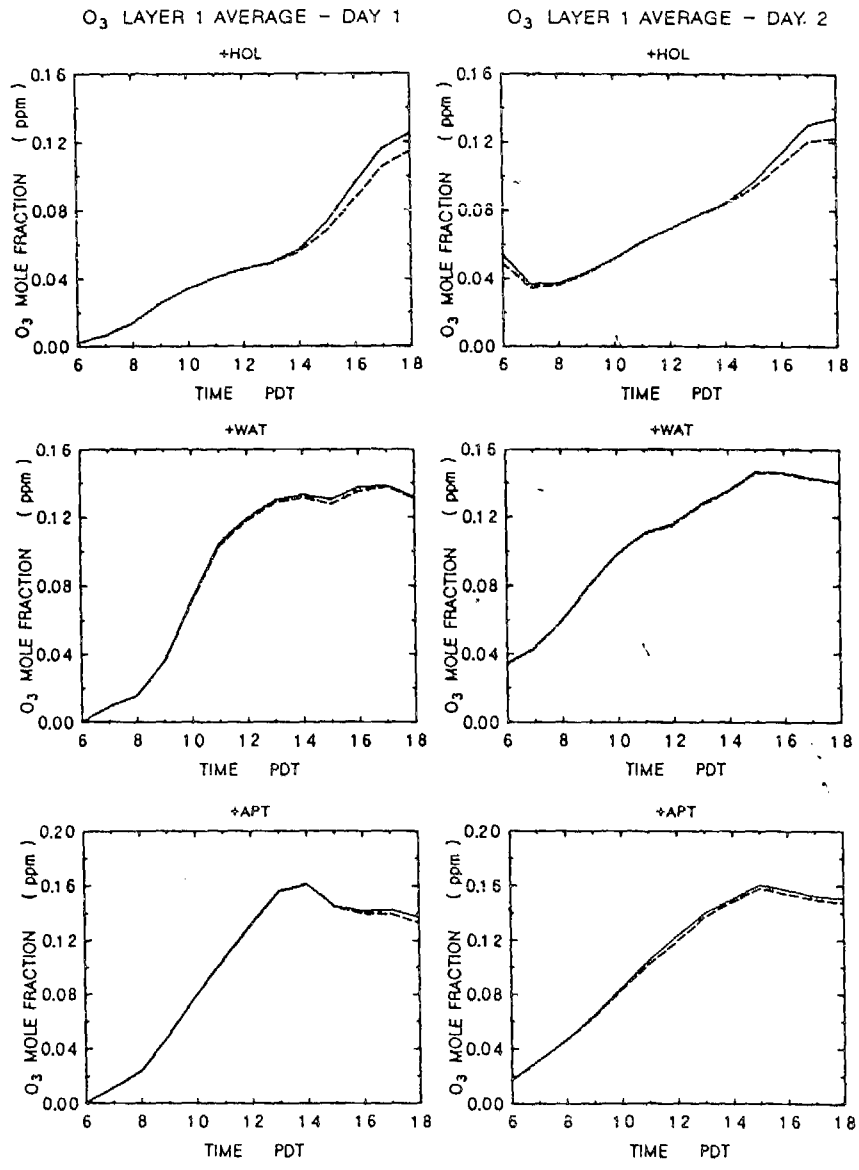

Figure 6.68. Time history for layer-average O_3 at Hollister, Watsonville and Aptos (see caption for Figure 6.67).

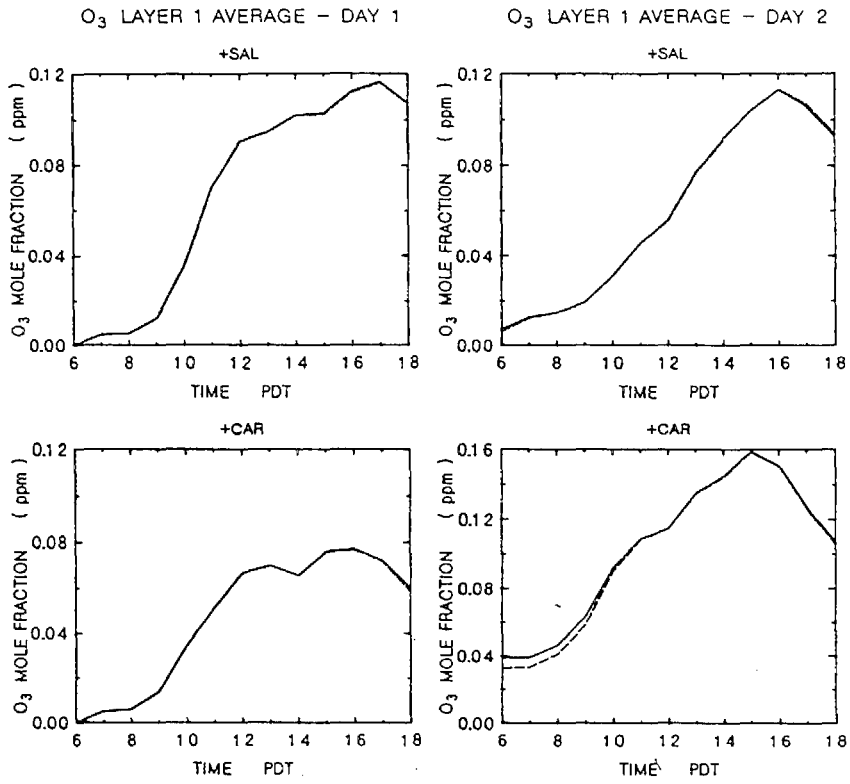

Figure 6.69. Time history for layer-average O_3 at Salinas and Carmel (see caption for Figure 6.67).

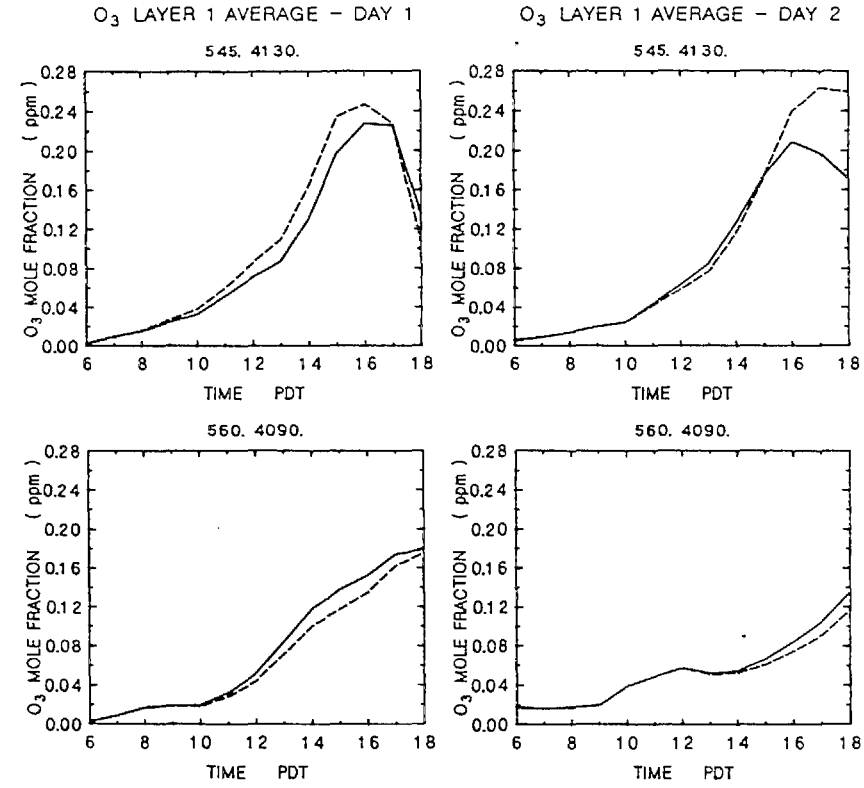

Figure 6.70. Time history for layer-average O_3 at two grid points over the ocean with UTM coordinates (545,4130 and 560,4090), respectively. See caption for Figure 6.67.

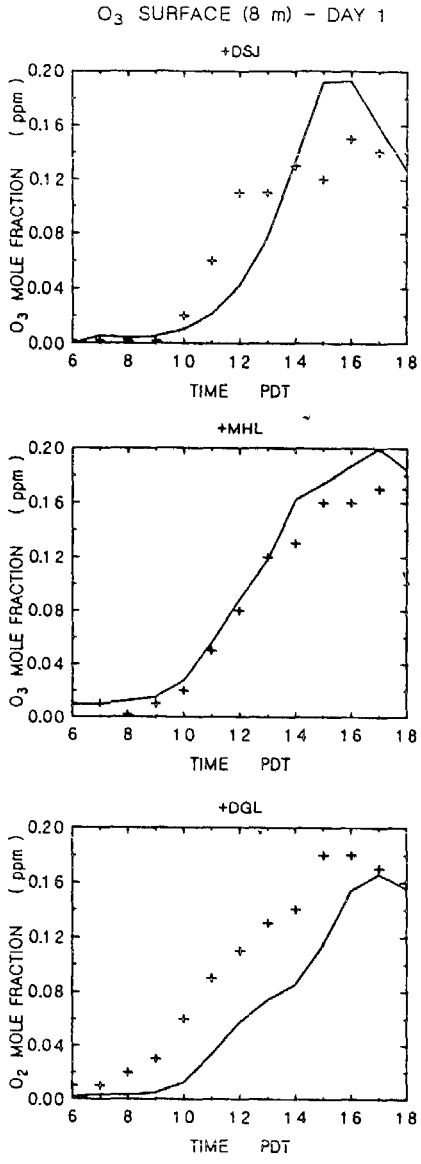

Figure 6.71. Time history for surface ozone at San Jose, Morgan Hill and Gilroy for the base case with corrected inventory.

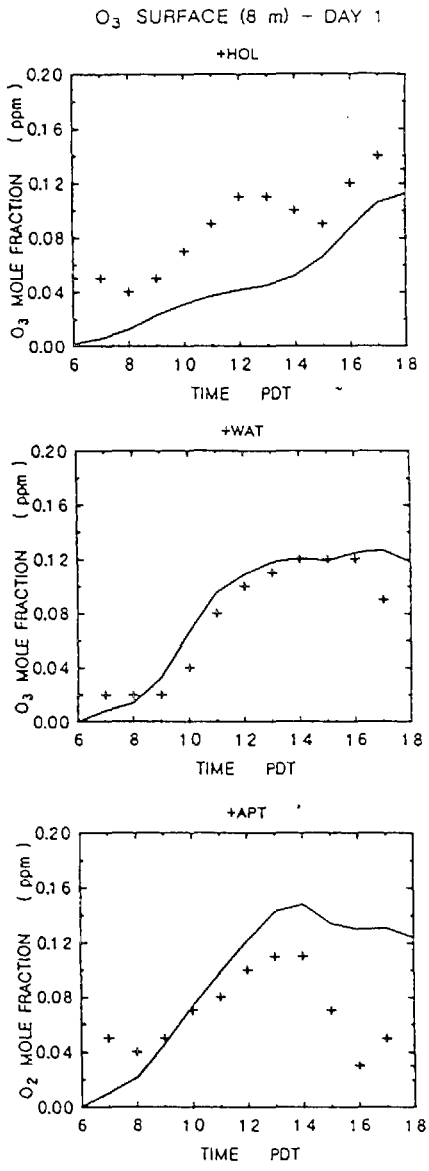

Figure 6.72. Time history for surface ozone at Hollister, Watsonville and Aptos for the base case with corrected inventory.

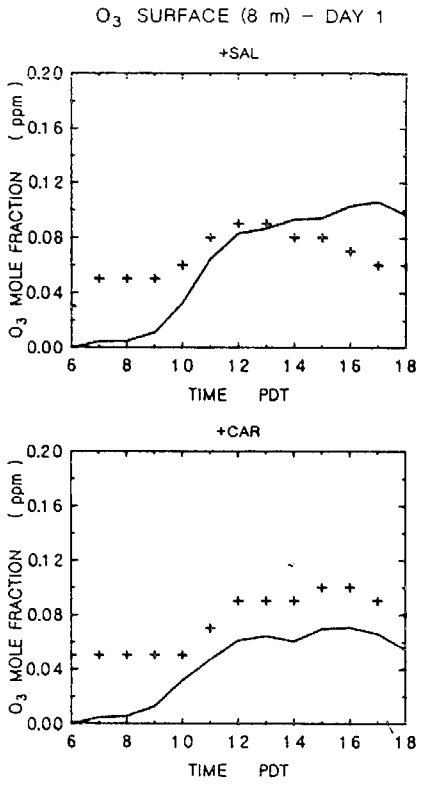

Figure 6.73. Time history for surface ozone at Salinas and Carmel for the base case with corrected inventory.

Chapter 7. Conclusions and Recommendations

A. Appraisal of "state of the model" and future modeling directions

A model that includes the basic framework for full three dimensional simulations of the long range transport and photochemical production of urban smog has been developed. The model has been built in a "modular" fashion so that changes to the chemical mechanism as well as changes to the number of layers treated in the model can be easily adapted. An "operator splitting" technique has been employed in which the calculation of advection and diffusion in the x- and y- directions and advection and diffusion in the vertical as well as all chemical interactions are separately stepped forward in time. While this technique is not as accurate as a method that fully couples the calculation of chemistry and transport, it was found to be approximately a factor of two faster than the Gear technique and allows easy adaptation of a variety of different numerical formulations for either the chemistry step or other aspects of the model.

Using this feature of the model, we tested several different numerical treatments of advection in this study. The methods tested included a simple upstream differencing technique, a fourth-order accurate finite element technique, and a second (or higher) order accurate technique based on upstream differencing with a corrective "anti-diffusion" step. This last method was found superior to either of the other two in our application, in that it maintains positive concentrations without resort to filtering negative concentrations, and it can be made as accurate as needed for any given simulation by repeated "anti-diffusion" steps.

We applied the model to study the long-range transport of pollutants, and in particular the effect of Bay Area emissions of NO_x on the Monterey Bay Unified Air Pollution Control District. For the time period studied, i.e. September 30–October 1, 1980—we found only a small impact of these emissions on Monterey. Surprisingly, at downwind locations, the impact of NO_x on ozone reverses in sign. Thus, near the source area, control of NO_x actually increases ozone–a result used to justify a strategy that only actively controls hydrocarbon emissions in the Bay Area. However, there is a small region downwind of the source location wherein active control of NO_x emissions would help to decrease ozone. However, because the magnitude of the O_3 decrease is quite small (only about 1 pphm), and since the area of effects is also small (a band of perhaps 10–15 km in width), the predicted result and its frequency of occurrence is probably quite uncertain. If, as was observed on October 1, 1980, somewhat slower transport along the San Jose-Hollister corridor occurs, little to no impact is predicted.

The chemical mechanism used in this study was necessarily limited by the available resolution of the emissions inventory. The mechanism we employed produces about the same ozone concentration as the mechanism tested by Leone and Seinfeld (1985) which quite accurately reproduced the results of their explicit mechanism at low hydrocarbon to NO_x ratios. On the other hand, our mechanism is more reactive than that developed by Lurmann et al. (1987) which has been verified by testing against the explicit mechanism developed by Carter et al. (1986). We believe that a more highly resolved chemical mechanism could alter slightly the conclusions drawn in this study, especially if it were

less reactive and if the area in which NO_x increases tend to lower O_3 concentrations became more extensive due to this lowered reactivity. The apparant differences between the Leone and Seinfeld (1985) mechanism and the Carter et al. (1986) mechanism will require further research to resolve. At the very least, the conclusions reached here should be tested by incorporating other mechanisms into the model.

B. Data needs

As pointed out in Chapter 6, model validation is often accompanied by "tuning" the meteorology. This tuning is possible because meteorological data are sparse and inadequate for a full characterization. Fortunately, even with such tuning, it is not possible to radically alter concentration fields. Thus, in the present case, the high concentrations in the Bay Area that were calculated primarily as a result of an emissions inventory error, could not be entirely obviated by meteorological manipulation.

In the present simulation, the lack of knowledge of any vertical structure in the wind field (as well as computer resources for a region this large) has caused us to limit our study to only two layers in the vertical, although more model resolution is theoretically possible. The extent to which increased vertical resolution would alter results is not known. Vertical wind shear would allow faster transport aloft with reduced transport at ground level. If turbulent mixing is fast, such wind shear may be relatively unimportant, but with the present data this cannot be adequately addressed. The vertical mixing processes are unknown and difficult to estimate because both surface temperatures and temperature gradients are not available on a routine basis at a sufficient number of places. Vertical wind shear is similarly unknown except for a twice daily radiosonde measurement at Oakland. Still it is satisfying that a relatively good simulation was possible based on fairly standard assumptions for wind shear and mixing.

The Hollister area remains a difficult area to simulate. The convergence of winds from the west and north-west had to be manipulated to obtain relatively good simulation results, but the fact that the relative influence of winds from San Jose versus winds from off the Monterey Bay could not be deduced from the meteorological data (Ungar and Nielson, 1983; Dabbert, 1983) meant that we had to rely on the ozone simulation to try to improve results in that area. In order to resolve this issue, more and better meteorological data would be required. Such data might include path-averaged optical wind sensor measurements and path averaged NO_2 measurements across the Santa Clara valley (Porch et al., 1981) and more intensive single-point meteorological stations around the Hollister and Monterey area.

References

Ahrens, D. and A. Miller, (1969) Variations of the temperature inversion over the San Francisco Bay Area. San Jose State College Department of Meteorology, San Jose, CA. 55 pp.

AMBAG (1980) AMBAG regional forecasts for April 1, 1987, Association of Monterey Bay Area Governments.

Atherton, C. S. and J. E. Penner (1988) The transformation of nitrogen oxides in the polluted troposphere, accepted for publication in *Tellus.*

Atkinson, R., W. P. Carter, K. R. Darnall, A. M. Winer and J. N. Pitts, Jr. (1980) A smog chamber and modeling study of the gas-phase NO_x-air photooxidation of toluene and the cresols. *Int. J. Chem. Kin. 12,* 779–836.

Baulch, D. L., R. A. Cox, R. F. Hampson, J. A. Kerr, J. Troe, R. T. Watson (1984) Evaluated kinetic and photochemical data for atmospheric chemistry: Supplement 11, *J. Phys. Chem. Ref. Data, 13,* 1259–1380.

Bornstein, R. D. (1968) Observations of the urban heat island effect in New York City. *J. of Applied Meteor., 7,* 575–582.

Bucon, H. W., J. F. Macho, and H. J. Taback (1978) Volatile organic compound (VOC) species data manual, Environmental Protection Agency report #EPA-450/3-78-119.

Caltrans (1984) 1982, 1983 and 1984 traffic volumes on California highway. California Department of Transportation.

Caltrans (1984) 1985 and 2005 demand traffic projections for state routes in Santa Cruz County. California Department of Transportation.

Caltrans (1984) Route concept report on routes 1 and 17 in Santa Cruz County. California Department of Transportation.

CARB (1983) Predicted California vehicle emissions for Monterey, Santa Cruz and San Benito Counties. California Air Resources Board.

Carter, W. P. L., R. Atkinson, A. M. Winer and J. N. Pitts, Jr. (1982) Experimental investigation of chamber-dependent radical sources. *Int. J. Chem. Kinet., 14,* 1071–1103.

Carter, W. P. L., R. Atkinson, W. D. Long, L. N. Parker and M. C. Dodd (1986) Effects of methanol fuel substitution on multi-day air pollution episodes. Final Report for California Air Resources Board Contract No. A3-125-32.

Cox, R. A., R. G. Derwent and P. M. Holt (1976) Relative rate constants for the reactions of OH radicals with H_2, CH_4, CO, NO, and HONO at atmospheric pressure and 296 K. *J. Chem. Soc. Faraday I, 72,* 2031–2043.

Dabbert, W. F. (1983) Ozone transport in the north central coast air basin. Final report to the California Air Resources Board, contract number A9–143–31, SRI International, Menlo Park, California.

DeMore, W. B., L. J. Stief, F. Kaufman, D. M. Golden, R. F. Hampson, M. J. Kurylo, J. J. Margitan, M. J. Molina and R. T. Watson (1981) Chemical kinetic and photochemical data for use in stratospheric modeling. JPL Publication 81–3.

DeMore, W. B., J. J. Marqitan, M. J. Molina, R. T. Watson, D. M. Golden, R. F. Hampson, M. J. Kurylo, C. J. Howard, and A. R. Ravishankara (1985) Chemical kinetics and photochemical data for use in stratospheric modeling. Evaluation number 7, JPL publication 85–27.

Dickerson, M. H. (1978) MASCON—A mass consistent atmospheric flux model for regions with complex topography. *J. Appl. Meteor., 17,* 241–253.

Duckworth, F. A. and J. S. Sandberg (1954) The effect on cities upon horizontal and vertical temperature gradients. *Bull. Amer. Meteor. Soc., 35,* 198–207.

Duewer, W. H., R. J. Gelinas, and R. F. Reinisch (1975) Appendix 9-3: Photochemical rates, hydrocarbon reactivities, validation with data and sensitivity studies, in *Development of an Air Pollution Model for the San Francisco Bay Area,* M. C. MacCracken and G. D. Sauter, Eds., Lawrence Livermore National Laboratory report UCRL-51920.

Duewer, W. H., M. C. MacCracken, and J. J. Walton (1978) The Livermore Regional Air Quality Model: II. Verification and sample application in the San Francisco Bay Area. *J. App. Met., 17,* 273–311.

Duewer, W. H., J. J. Walton, K. E. Grant, and H. Walker (1980) Livermore regional air quality model (LIRAQ) transfer to EPA. EPA-IAG-D5-0738. Lawrence Livermore Lab., University of Calif., Livermore, CA.

Environmental Protection Agency (1981) Addendum to the user's manual for the kinetics model and ozone isopleth plotting package (OZIPP). MDAD, Research Triangle Park, NC 27711, 10 pp.

Fahey, D. W., G. Hubler, D. D. Parrish, E. J. Williams, R. B. Norton, B. A. Ridley, H. B. Singh, S. C. Liu, and F. C. Fehsenfeld. Reactive nitrogen species in the troposphere: measurements of NO, NO_2, HNO_3, particulate nitrate, peroxyacetyl nitrate (PAN), O_3, and total reactive odd nitrogen (NOy) at Niwot Ridge, Colorado. *J. Geophys. Res., 91,* 9781–9793.

Fox, D. G. (1981) Judging air quality model performance. *Bull. Am. Meteor. Soc., 62,* 599–603.

Gelinas, R. J. and P. D. Skewes-Cox (1977) Tropospheric photochemical mechanisms, *J. Phys. Chem., 81,* 2468–2479.

Godowitch, J. M., J. K. S. Ching, and J. F. Clark (1979) Dissipation of the nocturnal inversion layer at an urban and rural site in St. Louis, MO. Fourth Sym. on Turbulence, Diffusion, and Air Pollution, January 15–18, 1979, Reno, NV, 416–420.

Harris, G. W., W. P. L. Carter, A. M. Winer, J. N. Pitts, Jr., U. Platt, and D. Perner (1982) Observations of nitrous acid in the Los Angeles atmosphere and implications for predictions of ozone-precuser relationships, *Environ. Sci. Tech., 16,* 414–419.

Heikes, B. G., and A. M. Thompson. Effects of heteogeneous processes on NO_3, HONO, and HNO_3 chemistry in the troposphere. *J. Geophys. Res., 88,* 10883–10895.

Hindmarsh, A. C. (1974) GEARB: Solution of ordinary differential equations having banded Jacobian. Lawrence Livermore Laboratory Rept. UCID-30059, Rev. 1.

Horowitz, A. and J. G. Calvert (1982) Wavelength dependence of the primary processes in acetaldehyde photolysis, *J. Phys. Chem., 86,* 3105–3114.

Hudson, R. D. and E. I. Reed, Eds. (1979) The stratosphere: present and future. NASA Reference Pulication 1049 432 pp.

Hunsaker, D. (1981) Selection of biogenic hydrocarbon emissions factors for land cover classes found in the San Francisco Bay Area, Air Quality Technical Memorandum 31, Association of Bay Area Governments, Bay Area Air Quality Management District, Metropolitan Transportation Commission.

Leone, J. A. and J. H. (1985) Comparative analysis of chemical reaction mechanisms for photochemical smog. *Atmos. Env., 19,* 437–464.

Lurmann, F. W., W. P. L. Carter and L. A. Coyner (1987) A surrogate species chemical reaction mechanism for urban-scale air quality simulation models. Volume I–Adaptation of the mechanism. Final Report for EPA Contract No. 68–02–4104.

Luther, F. M., D. J. Wuebbles, W. H. Duewer, and J. S. Chang (1978) Effect of multiple scattering on species concentrations and model sensitivity, *J. Geophys. Res., 83,* 3563–3570.

Luther, F. M. (1982) Personal communication, February 1982.

MacCracken, M. C., D. J. Wuebbles, J. J. Walton, W. H. Duewer, and K. E. Grant (1978) The Livermore regional air quality model: I. Concept and development. *App. Meteor., 17,* 254–272.

McCaldin, R. O. and R. S. Sholtes (1970) Mixing height determinations by means of an instrumented aircraft. Final Report NAPCA. Research Contract No. CPA22-69-76.

McRae, G. J., W. R. Goodin and J. J. Seinfeld (1982) Mathematical Modeling of Photochemical Air Pollution. California Institute of Technology, Environmental Quality Laboratory Report No. 18.

Meyrahn, H., G. K. Moortgat and P. Warneck (1982) The photolysis of acetaldehyde under atmospheric conditions, XV Informal Conference on Photochemistry Abstracts, 89–92.

Monterey County (1984) Monterey bay area 1984 transportation system management element, Association of Monterey bay area government. Monterey County Transportation Commission, and Santa Cruz County Transportation Commission.

Monterey County (1984) Monterey county 1982 VMT survey. Monterey County Transportation Study.

Monterey County (1984) Monterey county transportation study—2000. Monterey County Transportation Study Commission.

NCAR (1986) Preliminary evaluation studies with the regional acid deposition model (RADM). NCAR/TN-265 + STR, National Center for Atmospheric Research.

Neiburger, M. (1960) The relation of air mass structure to the field of motion over the eastern North Pacific Ocean in summer, *Tellus, 12,* 31–40.

Penner, J. E. and J. J. Walton (1982) Air Quality Model Update. Lawrence Livermore Laboratory Report UCID-19300. Lawrence Livermore National Laboratory, University of California, Livermore, California.

Penner, J. E., J. J. Walton and T. Umeda (1983) Air quality model validation: Application to the San Francisco Bay Area and St. Louis. Proceedings of the 76th Annual Meeting of the Air Pollution Control Association, paper no. 83–47.5, Atlanta, Georgia.

Penner, J. E. (1984) Modeling the effect of biogenic hydrocarbon emissions in the San Francisco Bay Area. Proceedings of the APCA Specialty Meeting on the Environmental Impact of Natural Emissions, March 7–9, 1984, Research Triangle Park, North Carolina.

Pitts, J. N., Jr., K. Darnall, W. P. L. Carter, A. M. Winer, and R. Atkinson (1979) Mechanism of photochemical reactions in air. Final report EPA-600/3-79-110.

Plum, C. N., E. Sanhveza, R. Atkinson, W. P. L. Carter and J. N. Pitts (1983) OH radical rate constants and photolysis rates of alpha-dicarbonyls. *Envir. Sci. Technol., 17,* 479–484.

Porch, W. M., T. R. Gallaway, T. J. Green, and H. W. Ellsaesser (1981) Long path optical extinction and meteorology in the San Francisco Bay Area. *Atmos. Environ., 15,* 2555–2560.

Rodriguez, D. J., G. D. Greenly, P. M. Gresho, R. Lange, B. S. Lawver, L. A. Lawson, and H. Walker (1982) User's guide to the MATHEW/ADPIC models. Lawrence Livermore National Laboratory Report UASG–82–16, Lawrence Livermore National Laboratory, University of California, Livermore, California.

Russell, P. B. and E. E. Uthe (1975) Regional patterns of mixing depth and stability: sodar network measurements for input to air quality models. *Bull. Amer. Meteor. Soc., 59,* 1275–1287.

Russell, P. B. (1979) Sodar network support for LIRAQ utilization in conjunction with Project MABLE. Final Report Project 8052, SRI International, Menlo Park, CA, 39 pp.

Russell, A. G., G. R. Cass and J. H. Seinfeld (1986) On some aspects of nighttime atmospheric chemistry, *Environ. Sci. Technol., 20,* 1167–1172, and sources noted herein.

Sandberg, J. S., W. J. Walker, and R. H. Thullier (1970) Fluorescent tracer studies of pollutant transport in the San Francisco Bay Area. *APCA Journal, 20,* pp 593–598.

Santa Cruz County (1984) 1980 vehicle miles of travel. Santa Cruz County Transportation Study Commission.

Schacher, G. E., E. Garner, T. Usher, and C. W. Fairall (1978) 1978 Marine Boundary Layer Study (MABLES-WC). Naval Postgraduate School, Monterey, CA.

Schere, K. L. and K. L. Demerjian (1978). A photochemical box model for urban air quality simulation. American Chemical Society Proceedings, 4th Joint Conf. on Sensing of Environmental Pollution, 427–433.

Sehmel, G. A. (1980) Particle and gas dry deposition: a review. *Atmos. Environ., 14,* 983–100.

Sherman, C. A. (1978) A mass-consistent model for wind fields over complex terrain. *J. Appl. Meteoro., 17,* 312–319.

Sholtes, R. S. (1972) The growth and decay of turbulent mixing in the planetary boundary layer. EPA-R4-72-001, Contract No. EHSD 71–40. Meteorology Lab., Research Triangle Park, NC, 95 pp.

Singleton, D. L. and R. J. Cvetanovic (1976) Temperature dependence of the reaction of oxygen atoms with olefins. *J. Atm. Chem. Soc., 98,* 6812–68XX.

Slade, D. H. (1968) Meteorology and Atomic Energy 1968. U.S. Atomic Energy Commision Office of Information Services, NTIS #TID-24190, p 39.

Smolarkiewicz, P. K. (1983) A simple positive definite advection scheme with small implicit diffusion. *Monthly Weather Review 111,* 479–486.

Spicer, C. N. (1977) Photochemical atmospheric pollutants derived from nitrogen oxides, *Atmos. Env., 11,* 1089–1095.

Stockwell, W. R. (1986) A homogeneous gas phase mechanism for use in a regional acid deposition model. *Atmos. Environ., 20,* 1615–1632.

Unger, C. D. and D. Nielsen (1983) Supplemental analysis—Monterey transport study. Draft report, California Air Resources Board.

U.S. Bureau of Census (1980) 1980 census of population and housing for Monterey and Santa Cruz standard metropolitan statistical areas, U.S. Department of Commerce.

Williams, W. A. and R. E. DeMandel (1966) Land-sea boundary effects on small-scale circulation. Progress Report No. 2, NSF Grant GP-4248, Department of Meteorology, San Jose State University, San Jose, CA, 97 pp.

World Meteorological Organization (WMO) global ozone research and monitoring project report (1981). The stratosphere 1981: theory and measurements. edited by R. D. Hudson, E. I. Reed, and R. D. Bojkov.

Wuebbles, D. J. (1981) A summary of the LLNL one-dimensional model of the troposphere and stratosphere: 1981. Lawrence Livermore National Laboratory Report UCID-19185.

Appendix A

Table A.1. 1980 and 1987 mobile source inventroy by 5 km UTM grid square for Monterey, Santa Cruz and San Benito Counties. UTM coordinates indicate lower left-hand corner of a 5 km square.

COUNTY CODE	UTM		HYDROCARBONS (HC) 1980	HYDROCARBONS (HC) 1987	NITROGEN DIOXIDE (NOx) 1980	NITROGEN DIOXIDE (NOx) 1987
1	3960	645	14219	8281	16507	12676
1	3960	700	35548	20702	41269	31689
1	3965	645	7110	4145	8254	6338
1	3965	675	9480	5512	11005	8444
1	3965	695	28439	16560	33015	25351
1	3965	700	85316	49686	99045	76054
1	3965	710	9480	5512	11005	8444
1	3970	635	14219	8281	16507	12676
1	3970	640	7110	4145	8254	6338
1	3970	685	9480	5512	11005	8444
1	3970	690	37919	22072	44020	33795
1	3970	695	56877	33124	66030	50703
1	3970	700	9480	5512	11005	8444
1	3975	635	14219	8281	16507	12676
1	3975	670	9480	5512	11005	8444
1	3975	675	9480	5512	11005	8444
1	3975	680	9480	5512	11005	8444
1	3975	685	9480	5512	11005	8444
1	3975	690	78206	45545	90791	69716
1	3975	730	9480	5512	11005	8444
1	3980	635	14219	8281	16507	12676
1	3980	660	9480	5512	11005	8444
1	3980	665	9480	5512	11005	8444
1	3980	670	9480	5512	11005	8444
1	3980	685	35548	20702	41269	31689
1	3980	690	35548	20702	41269	31689
1	3980	725	9480	5512	11005	8444
1	3980	730	9480	5512	11005	8444
1	3985	625	14219	8281	16507	12676
1	3985	630	14219	8281	16507	12676
1	3985	660	9480	5512	11005	8444
1	3985	670	9480	5512	11005	8444
1	3985	680	7110	4145	8254	6338
1	3985	685	89128	52428	104547	80267
1	3990	625	14219	8281	16507	12676
1	3990	650	9480	5512	11005	8444
1	3990	655	9480	5512	11005	8444
1	3990	660	9480	5512	11005	8444
1	3990	675	23699	13793	27512	21120
1	3990	680	94796	55198	110050	84498
1	3990	685	9480	5512	11005	8444
1	3990	710	9480	5512	11005	8444

Table A.1 cont'd.

COUNTY CODE	UTM		HYDROCARBONS (HC) 1980	HYDROCARBONS (HC) 1987	NITROGEN DIOXIDE (NOx) 1980	NITROGEN DIOXIDE (NOx) 1987
1	3995	620	21329	12421	24761	19014
1	3995	665	9480	5512	11005	8444
1	3995	670	9480	5512	11005	8444
1	3995	675	94796	55198	110050	84498
1	3995	680	18959	11023	22010	16889
1	3995	705	9480	5512	11005	8444
1	4000	615	21329	12421	24761	19014
1	4000	620	7110	4145	8254	6338
1	4000	660	9480	5512	11005	8444
1	4000	665	9480	5512	11005	8444
1	4000	670	21329	12421	24761	19014
1	4000	675	108851	63279	126094	97038
1	4000	680	192496	111684	222460	171612
1	4000	685	144372	83763	166845	128709
1	4000	690	127047	73711	146824	113264
1	4005	610	21329	12421	24761	19014
1	4005	615	7110	4145	8254	6338
1	4005	660	7110	4145	8254	6338
1	4005	665	116125	67619	134811	103512
1	4005	670	16590	51057	19259	78160
1	4005	675	9480	5512	11005	8444
1	4005	690	19250	11168	22246	17161
1	4005	695	65449	37973	75636	58348
1	4005	700	65449	37973	75636	58348
1	4005	705	67374	39089	77861	60064
1	4005	710	13475	7817	15571	12013
1	4010	605	21329	12421	24761	19014
1	4010	610	7110	4145	8254	6338
1	4010	640	9480	5512	11005	8444
1	4010	660	101905	59338	118303	90836
1	4010	665	9480	5512	11005	8444
1	4010	670	9480	5512	11005	8444
1	4010	675	9480	5512	11005	8444
1	4010	685	67374	39089	77861	60064
1	4010	690	15400	8935	17797	13729
1	4015	595	7110	4145	8254	6338
1	4015	600	28439	15650	33015	25351
1	4015	605	7110	4145	8254	6338
1	4015	635	9480	5512	11005	8444
1	4015	645	9480	5512	11005	8444
1	4015	650	9480	5512	11005	8444
1	4015	655	54507	31725	63279	48578
1	4015	660	123234	71760	143065	109849
1	4015	665	9480	5512	11005	8444
1	4015	675	9480	5512	11005	8444
1	4015	680	9625	5584	11123	8581
1	4015	685	26949	15636	31444	24026
1	4020	595	28439	15650	33015	25351
1	4020	630	9480	5512	11005	8444
1	4020	645	9480	5512	11005	8444

Table A.1 cont'd.

COUNTY CODE	UTM		HYDROCARBONS (HC) 1980	HYDROCARBONS (HC) 1987	NITROGEN DIOXIDE (NOx) 1980	NITROGEN DIOXIDE (NOx) 1987
1	4020	650	18959	11023	22015	16889
1	4020	655	137454	80041	159572	122525
1	4020	660	9480	5512	11005	8444
1	4020	670	9480	5512	11005	8444
3	4020	680	1634	999	2179	1816
3	4020	685	1144	699	1525	1271
3	4020	700	2506	1471	3351	2751
3	4020	705	6683	3923	8935	7337
1	4025	595	28439	15650	33015	25351
1	4025	650	116125	67619	134811	103512
1	4025	655	18959	11023	22010	16889
1	4025	660	9480	5512	11005	8444
3	4025	675	4975	2960	6646	5484
3	4025	680	1634	999	1525	1816
3	4025	685	4177	2452	5584	4585
3	4025	690	4177	2452	5584	4585
3	4025	695	4177	2452	5584	4585
3	4025	700	1671	981	2234	1834
3	4025	705	2506	1471	3351	2751
3	4025	710	6683	3923	8935	7337
1	4030	595	28439	15650	33015	25351
1	4030	610	9480	5512	11005	8444
1	4030	615	9480	5512	11005	8444
1	4030	640	18959	11023	22010	16889
1	4030	645	94796	55198	110050	84498
1	4030	650	160526	93228	185750	255702
1	4030	655	286819	166409	331465	50703
3	4030	675	9117	5430	12176	10052
1	4035	595	56877	33124	66030	50703
1	4035	610	9480	5512	11005	8444
1	4035	635	9480	5512	11005	8444
1	4035	640	113754	66248	132060	101405
1	4035	645	42658	24843	49522	38026
1	4035	655	282969	164173	327016	252270
1	4035	660	7700	4467	8898	6865
3	4035	665	645	400	872	726
3	4035	670	6956	4150	9289	7672
3	4035	675	4177	2452	5584	4585
3	4035	695	9189	5394	12285	10088
1	4040	595	315194	183361	365915	280845
1	4040	600	113754	66139	132060	101333
1	4040	605	18959	11023	22010	16889
1	4040	610	9480	5512	11005	8444
1	4040	630	9480	5512	11005	8444
1	4040	635	9480	5512	11005	8444
1	4040	640	123334	71760	143065	109849
1	4040	645	59248	34495	68781	52809
3	4040	660	1798	1099	2397	1998
3	4040	665	10950	6692	14601	12167
3	4040	670	8717	5266	11632	9652

Table A.1 cont'd.

COUNTY CODE	UTM		HYDROCARBONS (HC) 1980	HYDROCARBONS (HC) 1987	NITROGEN DIOXIDE (NOx) 1980	NITROGEN DIOXIDE (NOx) 1987
3	4040	675	835	490	1117	917
3	4040	695	10024	5884	13402	11005
1	4045	590	549812	319761	638288	489775
1	4045	595	945582	550003	1097745	842479
1	4045	600	338893	197072	393428	301910
1	4045	605	149302	86950	173328	133095
1	4045	610	149302	86950	173328	133095
1	4045	615	28439	15650	33015	25351
1	4045	625	9480	5512	11005	8444
1	4045	630	161152	93833	187084	143646
1	4045	635	33178	19304	38517	29565
3	4045	650	1671	981	2234	1834
3	4045	655	2506	1471	3351	2751
3	4045	660	9988	6083	13321	11087
3	4045	665	4104	1688	5475	4549
3	4045	690	5848	3432	7818	6420
1	4050	590	218029	126766	253114	194221
1	4050	595	1343722	781325	1559954	1197035
1	4050	600	1028795	604075	1224022	924851
1	4050	605	199070	115743	231104	177332
1	4050	615	75836	44147	88040	67592
1	4050	620	18959	11023	22010	16889
1	4050	625	9480	5512	11005	8444
1	4050	630	139823	81411	162323	124632
1	4050	635	35548	20702	41269	31689
3	4050	655	4086	2497	5448	4540
3	4050	660	7028	4295	9371	7809
3	4050	685	6683	3923	8935	7337
3	4050	690	9189	5394	12285	10088
3	4050	695	14201	8335	18986	15590
3	4050	700	7518	4413	10052	8254
1	4055	600	49768	28983	57776	44365
1	4055	605	416578	248629	515223	379620
1	4055	615	556922	323815	646542	496113
1	4055	620	1794369	1044692	2092440	1599369
1	4055	625	42658	24843	49522	38026
3	4055	655	12276	7482	16371	13629
3	4055	660	835	490	1117	917
3	4055	665	7518	4413	10052	8254
3	4055	670	7518	4413	10052	8254
3	4055	675	11695	6865	15636	12839
3	4055	680	5012	2942	6701	5503
3	4055	685	2506	1471	3351	2751
3	4055	690	835	490	1117	917
1	4060	605	309934	186322	371782	284503
1	4060	615	359222	209657	418188	321033
1	4060	620	926623	538843	1075735	825499
3	4060	645	5848	3432	7810	6420
3	4060	650	14565	8698	19449	16072
3	4060	655	10442	6220	13947	11514

Table A.1 cont'd.

COUNTY CODE	UTM		HYDROCARBONS (HC) 1980	HYDROCARBONS (HC) 1987	NITROGEN DIOXIDE (NOx) 1980	NITROGEN DIOXIDE (NOx) 1987
3	4060	660	9189	5394	12285	10088
3	4060	690	8354	4903	11168	9171
1	4065	605	85316	49686	99045	76054
1	4065	610	267276	161479	331895	246176
1	4065	615	226509	132495	264119	202811
3	4065	645	5848	3432	7810	6420
3	4065	650	19305	11595	25769	21338
3	4065	655	6683	3923	8935	7337
3	4065	660	9189	5394	12285	10088
1	4070	605	120864	70388	140313	107743
1	4070	610	49768	28983	57776	44365
1	4070	615	239728	140776	287627	214487
1	4070	620	120864	70388	140313	107743
3	4070	625	1671	981	2234	1834
3	4070	640	9044	5466	12068	10015
3	4070	645	29928	17723	39989	32842
3	4070	650	3341	1961	4467	3668
3	4070	655	10024	5884	13402	11005
3	4070	660	13366	7845	17869	14673
1	4075	605	142193	82810	165074	126757
1	4075	610	94795	55116	110050	84444
1	4075	620	267276	161478	331895	246176
1	4075	625	42658	24843	49522	38026
3	4075	630	72467	42095	96666	78896
3	4075	635	108806	63161	145117	118394
3	4075	640	61454	35903	81938	67010
3	4075	645	5394	3296	7191	5993
3	4075	650	25896	15200	34622	28330
3	4075	655	9189	5394	12285	10088
1	4080	605	63987	37264	74284	57041
1	4080	610	113754	66139	132060	101333
1	4080	615	919513	534621	1067481	819129
1	4080	620	158802	92444	184333	141521
3	4080	625	388433	266872	518359	424109
3	4080	630	176261	103748	235653	194221
3	4080	635	74347	43639	99399	81620
3	4080	640	54507	31598	72676	59247
3	4080	650	4177	2452	5584	4585
1&2	4085	600	340600	203074	402018	317555
1&2	4085	605	750042	447241	885609	699686
1&2	4085	610	914474	549532	1086385	865488
1&2	4085	615	448498	270938	534867	428449
2	4085	620	324519	196927	388297	317497
2&3	4085	625	82773	48376	108714	88557
3	4085	630	5557	3396	7409	6174
2&3	4085	635	229970	137508	291034	236770
3	4085	640	50748	29419	67664	55161
2&3	4085	650	59846	35752	72240	58294
2&3	4085	655	26041	15763	31363	25293
2	4090	570	91254	55388	108960	87849

Table A.1 cont'd.

COUNTY CODE	UTM		HYDROCARBONS (HC) 1980	HYDROCARBONS (HC) 1987	NITROGEN DIOXIDE (NOx) 1980	NITROGEN DIOXIDE (NOx) 1987
2	4090	575	259161	157302	309446	249491
2	4090	580	507781	308093	606635	488849
2	4090	585	1611628	977680	1935868	1551563
2	4090	590	1493823	906293	1795219	1438181
2	4090	595	807530	489911	964895	777429
2	4090	600	286138	173619	341826	275469
2	4090	605	146224	88693	174772	140776
2	4090	610	610040	370164	729814	587421
3	4090	640	14411	8354	19213	15663
2	4095	565	120455	73112	143827	115961
2	4095	570	172792	104874	206334	166345
2	4095	575	36556	22173	43693	35194
2	4095	580	97483	59129	116515	93851
2	4095	585	589655	354843	704428	567682
2	4095	590	481322	291949	575491	463389
2	4095	595	18278	11087	21847	17597
2	4095	600	18278	11087	21487	17597
2	4095	605	42649	25869	50975	41060
2	4095	610	24371	14782	29129	23463
2	4100	560	32851	19940	39226	31626
2	4100	565	236108	143292	281970	227300
2	4100	570	6093	3696	7282	5866
2	4100	575	79205	48042	94668	76254
2	4100	580	557548	338321	667053	536882
2	4100	585	430882	261486	514683	414811
2	4100	590	109641	66511	131024	105555
2	4100	600	60927	36956	72822	58657
2	4105	560	94904	57604	113318	91363
2	4105	570	6093	3696	7282	5866
2	4105	575	582764	353620	697217	561162
2	4105	580	117641	71387	140758	113282
2	4105	585	405195	245932	483837	390077
2	4105	590	54834	33260	65539	52791
2	4105	595	36556	22173	43693	35194
2	4110	570	30510	18478	36411	29328
2	4110	575	196191	119048	234718	188918
2	4110	580	24371	14839	29129	23463
2	4110	585	12185	7391	14564	11731
2	4115	570	12185	7391	14568	11731
2	4115	575	155886	94595	186521	150101

Table A.2

BAY AREA AIR QUALITY MANAGEMENT DISTRICT
District Emissions By Source Categories

SEPTEMBER 1980 WEEK DAY AVERAGE.

	TONS/DAY		
	TOG	ROG	NOX
Petroleum Refining	46.7	37.9	33.5
Fuels -Bulk Loading	4.9	4.9	--
Fuels -Filling Stations	10	10	--
Structures Coating	43.2	43.2	--
Other Coating & Printing	121	118	--
Solvent Degreasing	14.2	9.1	--
Dry Cleaners	15.6	15.5	--
Rubber, Plastic Products Mfg.	7.4	7.4	--
Other Solvent Usage	17.3	16.1	--
Chemical Mfg.	4.2	1.9	1.7
Metallurgical & Mineral Ind.	1.4	0.4	--
Gas Distribution	164	17	--
Other Industrial/Commercial	18.5	13.2	4.4
Domestic Fuel Usage	5.1	4.2	10.6
Commercial Fuel Usage	0.5	0.3	4.8
Industrial Fuel Usage	3.5	2.5	49.6
Electrical Generating Plants	0.9	0.7	66.9
Waste Burning & Incineration	1.4	0.8	1.2
Domestic Reciprocating Engines	4.7	4.6	0.5
Other Reciprocating Engines	29.7	25	21.6
Farm & Construction Equipments	5.8	5.5	31.7
Ships	12.1	11.1	7.8
Locomotives	1.8	1.7	5.3
Sub-total(District Jurisdiction)	534	351	240
Aircraft	18.3	16.8	12
Cars & Light Duty Trucks	286	254	202
Medium Duty Gas Vehicles	11.4	10.6	17
Heavy Duty Gas vehicles	24.8	23.1	22.5
Diesel Buses & Trucks	7	6.7	53.7
Motorcycles	5.3	4.8	0.3
Sub-total (Mobile Sources)	353	316	307
Accidental Fires	2.8	2.5	0.3
Vegetation	320	320	--
Bio Degradation	794	6.3	--
Consumer Solvent Usage	70.6	70.6	--
Pesticides Usage	5.6	5.6	--
Sub-total (Other Sources)	1190	405	0.3
TOTAL EMISSIONS	2080	1070	547

Table A.2 cont'd.

BAY AREA AIR QUALITY MANAGEMENT DISTRICT
District Emissions By Source Categories

SEPTEMBER 1987 WEEK DAY AVERAGE.

	TONS/DAY		
	TOG	ROG	NOX
Petroleum Refining	44.8	36.4	45.1
Fuels -Bulk Loading	2.8	2.8	--
Fuels -Filling Stations	6.1	6.1	--
Structures Coating	34	34	--
Other Coating & Printing	73.2	70	--
Solvent Degreasing	13.2	8.2	--
Dry Cleaners	6.2	6.2	--
Rubber, Plastic Products Mfg.	3.8	3.8	--
Other Solvent Usage	10.2	9.7	--
Chemical Mfg.	4.5	2.1	1.4
Metallurgical & Mineral Ind.	2	0.6	0.1
Gas Distribution	113	11.7	--
Other Industrial/Commercial	14.7	8.8	3.9
Domestic Fuel Usage	1	0.7	7.6
Commercial Fuel Usage	0.4	0.3	5.1
Industrial Fuel Usage	2.6	1.6	33.7
Electrical Generating Plants	0.3	0.2	33.3
Waste Burning & Incineration	1.3	0.7	1.1
Domestic Reciprocating Engines	3.5	3.4	0.4
Other Reciprocating Engines	25.3	22.3	16.8
Farm & Construction Equipments	6.7	6.4	32.8
Ships	11.2	10.2	7.3
Locomotives	1.6	1.6	4.9
Sub-total(District Jurisdiction)	382	248	194
Aircraft	18.9	17.3	16.3
Cars & Light Duty Trucks	168	146	136
Medium Duty Gas Vehicles	5.7	5.3	7.8
Heavy Duty Gas vehicles	15.7	14.7	15.1
Diesel Buses & Trucks	5.7	5.4	25
Motorcycles	2.9	2.7	0.3
Sub-total (Mobile Sources)	217	192	201
Accidental Fires	8.1	7.3	1.2
Vegetation	320	320	--
Bio Degradation	136	1.1	--
Consumer Solvent Usage	63.4	63.4	--
Pesticides Usage	4.3	4.3	--
Sub-total (Other Sources)	531	396	1.2
TOTAL EMISSIONS	1130	835	395

Table A.3

MONTEREY BAY UNIFIED AIR POLLUTION CONTROL DISTRICT
District Emissions By Source Categories

SEPTEMBER 1980 WEEK DAY AVERAGE.

	TONS/DAY		
	TOG	ROG	NOX
Petroleum Refining	--	--	--
Fuels -Bulk Loading	0.5	0.5	--
Fuels -Filling Stations	3.8	3.8	--
Structures Coating	4.4	4.4	--
Other Coating & Printing	3.9	3.9	--
Solvent Degreasing	1	0.9	--
Dry Cleaners	1.8	1.8	--
Rubber, Plastic Products Mfg.	--	--	--
Other Solvent Usage	2.9	2.4	--
Chemical Mfg.	--	--	--
Metallurgical & Mineral Ind.	--	--	0.7
Gas Distribution	--	--	--
Other Industrial/Commercial	2.5	2.5	--
Domestic Fuel Usage	0.1	0.1	0.9
Commercial Fuel Usage	--	--	0.3
Industrial Fuel Usage	0.4	0.3	18.7
Electrical Generating Plants	0.4	0.4	42.1
Waste Burning & Incineration	2.3	2.3	--
Domestic Reciprocating Engines	0.2	0.2	--
Other Reciprocating Engines	0.6	0.4	0.7
Farm & Construction Equipments	3.5	3.3	9.1
Ships	0.5	0.4	0.1
Locomotives	0.6	0.6	2.2
Sub-total(District Jurisdiction)	29.3	28.1	74.9
Aircraft	0.4	0.3	0.3
Cars & Light Duty Trucks	32	26.4	30.7
Medium Duty Gas Vehicles	1.2	1.1	2.3
Heavy Duty Gas vehicles	2.5	2.3	3
Diesel Buses & Trucks	0.7	0.7	7.1
Motorcycles	0.1	0.1	--
Sub-total (Mobile Sources)	36.9	30.9	43.3
Accidental Fires	6.2	5.6	0.9
Vegetation	271	271	--
Bio Degradation	--	--	--
Consumer Solvent Usage	2.1	2.1	--
Pesticides Usage	43.1	43.1	--
Sub-total (Other Sources)	322	322	0.9
TOTAL EMISSIONS	389	381	119

Table A.3 cont'd.

MONTEREY BAY UNIFIED AIR POLLUTION CONTROL DISTRICT
District Emissions By Source Categories

SEPTEMBER 1987 WEEK DAY AVERAGE.

	TONS/DAY		
	TOG	ROG	NOX
Petroleum Refining	--	--	--
Fuels -Bulk Loading	0.6	0.6	--
Fuels -Filling Stations	4	4	--
Structures Coating	3	3	--
Other Coating & Printing	4.6	4.6	--
Solvent Degreasing	1	0.8	--
Dry Cleaners	2	2	--
Rubber, Plastic Products Mfg.	--	--	--
Other Solvent Usage	2.3	2	--
Chemical Mfg.	--	--	--
Metallurgical & Mineral Ind.	--	--	0.7
Gas Distribution	--	--	--
Other Industrial/Commercial	2.9	2.9	--
Domestic Fuel Usage	0.3	0.2	2.1
Commercial Fuel Usage	0.1	--	1
Industrial Fuel Usage	0.4	0.3	19.2
Electrical Generating Plants	0.5	0.5	53
Waste Burning & Incineration	2.7	2.5	--
Domestic Reciprocating Engines	0.5	0.5	0.1
Other Reciprocating Engines	1	0.8	0.9
Farm & Construction Equipments	1.8	1.7	8
Ships	1.1	1.1	0.2
Locomotives	0.8	0.8	2.7
Sub-total(District Jurisdiction)	29.5	28.2	87.9
Aircraft	0.5	0.5	0.4
Cars & Light Duty Trucks	18.4	15.2	25
Medium Duty Gas Vehicles	0.6	0.6	1.4
Heavy Duty Gas vehicles	1.7	1.6	2.8
Diesel Buses & Trucks	0.6	0.6	4.6
Motorcycles	0.5	0.5	0.1
Sub-total (Mobile Sources)	22.4	18.8	34.2
Accidental Fires	2.4	2.2	0.4
Vegetation	271	271	--
Bio Degradation	--	--	--
Consumer Solvent Usage	4.8	4.8	--
Pesticides Usage	24.6	24.6	--
Sub-total (Other Sources)	303	303	0.4
TOTAL EMISSIONS	355	350	123

Table A.4

BAY AREA AIR QUALITY MANAGEMENT DISTRICT
County Emissions By Source Categories

ALAMEDA COUNTY September 1980 WEEK DAY AVERAGE.

	TONS/DAY		
	TOG	ROG	NOX
Petroleum Refining	--	--	--
Fuels -Bulk Loading	0.2	0.2	--
Fuels -Filling Stations	2.1	2.1	--
Structures Coating	9.7	9.7	--
Other Coating & Printing	52.2	50.6	--
Solvent Degreasing	3.4	2.7	--
Dry Cleaners	3.1	3	--
Rubber, Plastic Products Mfg.	2.2	2.2	--
Other Solvent Usage	3.4	3.2	--
Chemical Mfg.	1.6	0.7	--
Metallurgical & Mineral Ind.	0.1	--	--
Gas Distribution	23.6	2.5	--
Other Industrial/Commercial	2.7	2.2	0.2
Domestic Fuel Usage	0.5	0.4	2.1
Commercial Fuel Usage	0.2	0.2	1
Industrial Fuel Usage	2.1	1.7	14.8
Electrical Generating Plants	--	--	0.2
Waste Burning & Incineration	0.2	0.1	0.1
Domestic Reciprocating Engines	1	1	0.1
Other Reciprocating Engines	5.9	5.4	3
Farm & Construction Equipments	0.7	0.7	4.8
Ships	2.5	2.2	2.1
Locomotives	0.5	0.5	1.4
Sub-total(District Jurisdiction)	118	91.3	29.9
Aircraft	4.7	4.3	1.7
Cars & Light Duty Trucks	59.5	52.9	44.4
Medium Duty Gas Vehicles	2.6	2.4	3.8
Heavy Duty Gas vehicles	5.5	5.2	5
Diesel Buses & Trucks	1.6	1.5	12
Motorcycles	1.2	1.1	0.1
Sub-total (Mobile Sources)	75	67.3	67
Accidental Fires	0.5	0.4	--
Vegetation	22.8	22.8	--
Bio Degradation	179	1.4	--
Consumer Solvent Usage	15.4	15.4	--
Pesticides Usage	1	1	--
Sub-total (Other Sources)	218	40.9	--
TOTAL EMISSIONS	411	199	96.9

Table A.4 cont'd.

BAY AREA AIR QUALITY MANAGEMENT DISTRICT
County Emissions By Source Categories

CONTRA COSTA COUNTY Septembl980 WEEK DAY AVERAGE.

	TONS/DAY		
	TOG	ROG	NOX
Petroleum Refining	41.9	34	28.6
Fuels -Bulk Loading	2.1	2.1	--
Fuels -Filling Stations	1.1	1.1	--
Structures Coating	5.6	5.6	--
Other Coating & Printing	10.9	10.6	--
Solvent Degreasing	1	0.7	--
Dry Cleaners	1.5	1.5	--
Rubber, Plastic Products Mfg.	0.7	0.7	--
Other Solvent Usage	4	3.8	--
Chemical Mfg.	1.6	0.8	1.6
Metallurgical & Mineral Ind.	--	--	--
Gas Distribution	68.3	7.1	--
Other Industrial/Commercial	4.2	1.3	3.9
Domestic Fuel Usage	0.4	0.3	1.3
Commercial Fuel Usage	0.1	--	0.8
Industrial Fuel Usage	0.6	0.4	12.7
Electrical Generating Plants	0.7	0.6	53.2
Waste Burning & Incineration	0.3	0.1	0.5
Domestic Reciprocating Engines	0.7	0.7	0.1
Other Reciprocating Engines	6.7	3.8	10.7
Farm & Construction Equipments	0.9	0.8	4.5
Ships	2.2	2	1.2
Locomotives	0.3	0.3	1
Sub-total(District Jurisdiction)	156	78.3	120
Aircraft	0.1	0.1	0.1
Cars & Light Duty Trucks	37.9	33.6	27.3
Medium Duty Gas Vehicles	1.4	1.3	2.1
Heavy Duty Gas vehicles	3.1	2.9	2.8
Diesel Buses & Trucks	0.9	0.8	6.8
Motorcycles	0.7	0.7	--
Sub-total (Mobile Sources)	44.3	39.5	39.1
Accidental Fires	0.3	0.3	--
Vegetation	22.3	22.3	--
Bio Degradation	99.9	0.8	--
Consumer Solvent Usage	9.3	9.3	--
Pesticides Usage	0.7	0.7	--
Sub-total (Other Sources)	132	33.4	--
TOTAL EMISSIONS	332	151	159

Table A.4 cont'd.

BAY AREA AIR QUALITY MANAGEMENT DISTRICT
County Emissions By Source Categories

MARIN COUNTY September 1980 WEEK DAY AVERAGE.

	TONS/DAY		
	TOG	ROG	NOX
Petroleum Refining	--	--	--
Fuels -Bulk Loading	--	--	--
Fuels -Filling Stations	0.5	0.5	--
Structures Coating	2	2	--
Other Coating & Printing	2.2	2.1	--
Solvent Degreasing	0.3	0.3	--
Dry Cleaners	0.7	0.7	--
Rubber, Plastic Products Mfg.	--	--	--
Other Solvent Usage	0.7	0.6	--
Chemical Mfg.	--	--	--
Metallurgical & Mineral Ind.	--	--	--
Gas Distribution	3.7	0.4	--
Other Industrial/Commercial	0.4	0.3	--
Domestic Fuel Usage	0.3	0.3	0.6
Commercial Fuel Usage	--	--	0.1
Industrial Fuel Usage	--	--	0.5
Electrical Generating Plants	--	--	--
Waste Burning & Incineration	--	--	--
Domestic Reciprocating Engines	0.3	0.2	--
Other Reciprocating Engines	1.1	1	0.5
Farm & Construction Equipments	0.1	0.1	0.8
Ships	0.7	0.6	0.2
Locomotives	--	--	0.1
Sub-total(District Jurisdiction)	13.1	9.1	2.7
Aircraft	0.1	0.1	--
Cars & Light Duty Trucks	13.9	12.4	9.1
Medium Duty Gas Vehicles	0.4	0.4	0.6
Heavy Duty Gas vehicles	0.9	0.9	0.9
Diesel Buses & Trucks	0.3	0.3	2.1
Motorcycles	0.3	0.2	--
Sub-total (Mobile Sources)	15.9	14.2	12.7
Accidental Fires	0.1	0.1	--
Vegetation	46.4	46.4	--
Bio Degradation	36.4	0.3	--
Consumer Solvent Usage	3	3	--
Pesticides Usage	0.2	0.2	--
Sub-total (Other Sources)	86.1	50	--
TOTAL EMISSIONS	115	73.3	15.4

Table A.4 cont'd.

BAY AREA AIR QUALITY MANAGEMENT DISTRICT
County Emissions By Source Categories

NAPA COUNTY September 1980 WEEK DAY AVERAGE.

	TONS/DAY		
	TOG	ROG	NOX
Petroleum Refining	--	--	--
Fuels -Bulk Loading	0.1	0.1	--
Fuels -Filling Stations	0.2	0.2	--
Structures Coating	0.9	0.9	--
Other Coating & Printing	1.2	1.1	--
Solvent Degreasing	0.1	0.1	--
Dry Cleaners	0.5	0.5	--
Rubber, Plastic Products Mfg.	0.1	0.1	--
Other Solvent Usage	0.4	0.4	--
Chemical Mfg.	--	--	--
Metallurgical & Mineral Ind.	--	--	--
Gas Distribution	1.5	0.2	--
Other Industrial/Commercial	0.7	0.7	--
Domestic Fuel Usage	0.2	0.2	0.2
Commercial Fuel Usage	--	--	0.1
Industrial Fuel Usage	--	--	0.1
Electrical Generating Plants	--	--	--
Waste Burning & Incineration	--	--	--
Domestic Reciprocating Engines	0.1	0.1	--
Other Reciprocating Engines	0.5	0.5	0.2
Farm & Construction Equipments	0.8	0.7	3
Ships	0.3	0.3	0.1
Locomotives	--	--	--
Sub-total(District Jurisdiction)	7.6	6	3.7
Aircraft	0.1	0.1	--
Cars & Light Duty Trucks	6	5.3	3.8
Medium Duty Gas Vehicles	0.3	0.3	0.5
Heavy Duty Gas vehicles	0.7	0.6	0.6
Diesel Buses & Trucks	0.2	0.2	1.5
Motorcycles	0.1	0.1	--
Sub-total (Mobile Sources)	7.4	6.6	6.5
Accidental Fires	0.7	0.6	0.1
Vegetation	60.1	60.1	--
Bio Degradation	15.9	0.1	--
Consumer Solvent Usage	1.4	1.4	--
Pesticides Usage	0.2	0.2	--
Sub-total (Other Sources)	78.3	62.5	0.1
TOTAL EMISSIONS	93.3	75.1	10.2

Table A.4 cont'd.

BAY AREA AIR QUALITY MANAGEMENT DISTRICT
County Emissions By Source Categories

SAN FRANCISCO COUNTY Septem1980 WEEK DAY AVERAGE.

	TONS/DAY		
	TOG	ROG	NOX
Petroleum Refining	0.7	0.7	--
Fuels -Bulk Loading	0.1	0.1	--
Fuels -Filling Stations	0.9	0.9	--
Structures Coating	5.6	5.6	--
Other Coating & Printing	8.1	7.7	--
Solvent Degreasing	0.9	0.7	--
Dry Cleaners	2.9	2.9	--
Rubber, Plastic Products Mfg.	0.1	0.1	--
Other Solvent Usage	1.7	1.7	--
Chemical Mfg.	--	--	--
Metallurgical & Mineral Ind.	--	--	--
Gas Distribution	22.3	2.3	--
Other Industrial/Commercial	1.4	1	0.3
Domestic Fuel Usage	0.5	0.4	1.4
Commercial Fuel Usage	--	--	0.6
Industrial Fuel Usage	0.1	0.1	2.4
Electrical Generating Plants	0.1	0.1	13.6
Waste Burning & Incineration	0.1	--	0.1
Domestic Reciprocating Engines	0.4	0.4	--
Other Reciprocating Engines	3.4	3.1	1.5
Farm & Construction Equipments	0.8	0.8	5.6
Ships	1.4	1.3	2.6
Locomotives	0.2	0.2	0.7
Sub-total(District Jurisdiction)	51.7	30	28.8
Aircraft	--	--	--
Cars & Light Duty Trucks	28.4	25.2	19.2
Medium Duty Gas Vehicles	1.1	1	1.6
Heavy Duty Gas vehicles	2.3	2.1	2.1
Diesel Buses & Trucks	0.7	0.6	5
Motorcycles	0.4	0.3	--
Sub-total (Mobile Sources)	32.7	29.2	27.8
Accidental Fires	0.1	0.1	--
Vegetation	2	2	--
Bio Degradation	--	--	--
Consumer Solvent Usage	9.3	9.3	--
Pesticides Usage	0.2	0.2	--
Sub-total (Other Sources)	11.6	11.6	--
TOTAL EMISSIONS	96	70.8	56.6

Table A.4 cont'd.

BAY AREA AIR QUALITY MANAGEMENT DISTRICT
County Emissions By Source Categories

SAN MATEO COUNTY September 1980 WEEK DAY AVERAGE.

	TONS/DAY		
	TOG	ROG	NOX
Petroleum Refining	--	--	--
Fuels -Bulk Loading	0.7	0.7	--
Fuels -Filling Stations	1.3	1.3	--
Structures Coating	5.2	5.2	--
Other Coating & Printing	9.8	9.3	--
Solvent Degreasing	2.5	1.9	--
Dry Cleaners	2	2	--
Rubber, Plastic Products Mfg.	2.4	2.4	--
Other Solvent Usage	1.4	1.3	--
Chemical Mfg.	0.6	0.3	--
Metallurgical & Mineral Ind.	--	--	--
Gas Distribution	10.3	1.1	--
Other Industrial/Commercial	0.4	0.3	--
Domestic Fuel Usage	0.5	0.4	1.3
Commercial Fuel Usage	--	--	0.2
Industrial Fuel Usage	0.1	0.1	1.6
Electrical Generating Plants	--	--	--
Waste Burning & Incineration	0.1	--	0.1
Domestic Reciprocating Engines	0.6	0.6	0.1
Other Reciprocating Engines	3.1	2.9	1.6
Farm & Construction Equipments	0.5	0.5	2.6
Ships	1.2	1.1	0.4
Locomotives	0.1	0.1	0.3
Sub-total(District Jurisdiction)	42.8	31.3	8.2
Aircraft	7.3	6.7	6.2
Cars & Light Duty Trucks	38.4	34.1	26.9
Medium Duty Gas Vehicles	1.3	1.2	2
Heavy Duty Gas vehicles	2.9	2.7	2.6
Diesel Buses & Trucks	0.8	0.8	6.3
Motorcycles	0.6	0.5	--
Sub-total (Mobile Sources)	51.3	46	44
Accidental Fires	0.4	0.3	--
Vegetation	41.9	41.9	--
Bio Degradation	192	1.5	--
Consumer Solvent Usage	8	8	--
Pesticides Usage	0.8	0.8	--
Sub-total (Other Sources)	243	52.5	--
TOTAL EMISSIONS	337	130	52.2

Table A.4 cont'd.

BAY AREA AIR QUALITY MANAGEMENT DISTRICT
County Emissions By Source Categories

SANTA CLARA COUNTY Septembe1980 WEEK DAY AVERAGE.

	TONS/DAY		
	TOG	ROG	NOX
Petroleum Refining	--	--	--
Fuels -Bulk Loading	1.1	1.1	--
Fuels -Filling Stations	3	3	--
Structures Coating	10.7	10.7	--
Other Coating & Printing	29.9	29.3	--
Solvent Degreasing	5.4	2.3	--
Dry Cleaners	4.3	4.2	--
Rubber, Plastic Products Mfg.	1.6	1.6	--
Other Solvent Usage	4.4	4	--
Chemical Mfg.	0.2	0.1	--
Metallurgical & Mineral Ind.	1.2	0.3	--
Gas Distribution	25.1	2.6	--
Other Industrial/Commercial	7.3	6.9	--
Domestic Fuel Usage	0.6	0.5	2.3
Commercial Fuel Usage	0.1	--	0.8
Industrial Fuel Usage	0.1	0.1	10.7
Electrical Generating Plants	--	--	--
Waste Burning & Incineration	0.3	0.2	0.3
Domestic Reciprocating Engines	1.1	1.1	0.1
Other Reciprocating Engines	7	6.4	3.2
Farm & Construction Equipments	1.3	1.2	6.9
Ships	2.5	2.3	0.6
Locomotives	0.5	0.4	1.4
Sub-total(District Jurisdiction)	108	78.3	26.3
Aircraft	1.6	1.5	1.1
Cars & Light Duty Trucks	77.1	68.4	53.5
Medium Duty Gas Vehicles	3	2.8	4.5
Heavy Duty Gas vehicles	6.5	6.1	5.9
Diesel Buses & Trucks	1.9	1.8	14.1
Motorcycles	1.5	1.3	0.1
Sub-total (Mobile Sources)	91.6	81.9	79.3
Accidental Fires	0.5	0.4	--
Vegetation	73.4	73.4	--
Bio Degradation	206	1.6	--
Consumer Solvent Usage	18	18	--
Pesticides Usage	1.9	1.9	--
Sub-total (Other Sources)	299	95.4	--
TOTAL EMISSIONS	499	256	106

Table A.4 cont'd.

BAY AREA AIR QUALITY MANAGEMENT DISTRICT
County Emissions By Source Categories

SOLANO COUNTY September 1980 WEEK DAY AVERAGE.

	TONS/DAY		
	TOG	ROG	NOX
Petroleum Refining	4.1	3.2	4.9
Fuels -Bulk Loading	0.3	0.3	--
Fuels -Filling Stations	0.5	0.5	--
Structures Coating	1.4	1.4	--
Other Coating & Printing	3.8	3.7	--
Solvent Degreasing	0.2	0.2	--
Dry Cleaners	0.3	0.3	--
Rubber, Plastic Products Mfg.	0.1	0.1	--
Other Solvent Usage	0.7	0.7	--
Chemical Mfg.	0.1	0.1	--
Metallurgical & Mineral Ind.	--	--	--
Gas Distribution	5.8	0.6	--
Other Industrial/Commercial	1	0.2	--
Domestic Fuel Usage	0.3	0.2	0.4
Commercial Fuel Usage	--	--	1.2
Industrial Fuel Usage	0.4	0.1	6.7
Electrical Generating Plants	--	--	--
Waste Burning & Incineration	0.1	0.1	--
Domestic Reciprocating Engines	0.2	0.2	--
Other Reciprocating Engines	0.8	0.8	0.5
Farm & Construction Equipments	0.4	0.4	1.7
Ships	0.6	0.6	0.2
Locomotives	0.1	0.1	0.3
Sub-total(District Jurisdiction)	21.5	13.8	15.9
Aircraft	4.2	3.9	2.9
Cars & Light Duty Trucks	9.5	8.3	7.1
Medium Duty Gas Vehicles	0.4	0.4	0.6
Heavy Duty Gas vehicles	0.9	0.8	0.8
Diesel Buses & Trucks	0.2	0.2	1.9
Motorcycles	0.2	0.2	--
Sub-total (Mobile Sources)	15.4	13.8	13.2
Accidental Fires	--	--	--
Vegetation	15.1	15.1	--
Bio Degradation	26.3	0.2	--
Consumer Solvent Usage	2.6	2.6	--
Pesticides Usage	0.5	0.5	--
Sub-total (Other Sources)	44.5	18.4	--
TOTAL EMISSIONS	81.4	46	29

Table A.4 cont'd.

BAY AREA AIR QUALITY MANAGEMENT DISTRICT
County Emissions By Source Categories

SONOMA COUNTY September 1980 WEEK DAY AVERAGE.

	TONS/DAY		
	TOG	ROG	NOX
Petroleum Refining	--	--	--
Fuels -Bulk Loading	0.2	0.2	--
Fuels -Filling Stations	0.5	0.5	--
Structures Coating	2.2	2.2	--
Other Coating & Printing	3.4	3.3	--
Solvent Degreasing	0.4	0.3	--
Dry Cleaners	0.5	0.5	--
Rubber, Plastic Products Mfg.	0.1	0.1	--
Other Solvent Usage	0.6	0.6	--
Chemical Mfg.	--	--	--
Metallurgical & Mineral Ind.	--	--	--
Gas Distribution	3	0.3	--
Other Industrial/Commercial	0.4	0.4	--
Domestic Fuel Usage	1.8	1.6	1
Commercial Fuel Usage	--	--	--
Industrial Fuel Usage	--	--	0.1
Electrical Generating Plants	--	--	--
Waste Burning & Incineration	0.2	0.2	--
Domestic Reciprocating Engines	0.4	0.4	--
Other Reciprocating Engines	1.3	1.2	0.6
Farm & Construction Equipments	0.4	0.3	1.9
Ships	0.7	0.7	0.2
Locomotives	--	--	0.1
Sub-total(District Jurisdiction)	16.1	12.6	4
Aircraft	0.1	0.1	--
Cars & Light Duty Trucks	15.7	13.9	10.7
Medium Duty Gas Vehicles	0.9	0.8	1.3
Heavy Duty Gas vehicles	1.9	1.8	1.8
Diesel Buses & Trucks	0.5	0.5	4.2
Motorcycles	0.3	0.3	--
Sub-total (Mobile Sources)	19.4	17.4	18
Accidental Fires	0.3	0.3	--
Vegetation	35.9	35.9	--
Bio Degradation	39.2	0.3	--
Consumer Solvent Usage	3.7	3.7	--
Pesticides Usage	0.2	0.2	--
Sub-total (Other Sources)	79.4	40.5	--
TOTAL EMISSIONS	115	70.5	22.1

Table A.4 cont'd.

BAY AREA AIR QUALITY MANAGEMENT DISTRICT
County Emissions By Source Categories

ALAMEDA COUNTY September 1987 WEEK DAY AVERAGE.

TONS/DAY

	TOG	ROG	NOX
Petroleum Refining	--	--	--
Fuels -Bulk Loading	0.1	0.1	--
Fuels -Filling Stations	1.3	1.3	--
Structures Coating	7.6	7.6	--
Other Coating & Printing	36	34.5	--
Solvent Degreasing	3.3	2.4	--
Dry Cleaners	1.2	1.2	--
Rubber, Plastic Products Mfg.	1.1	1.1	--
Other Solvent Usage	2	1.9	--
Chemical Mfg.	1.6	0.7	--
Metallurgical & Mineral Ind.	0.4	0.1	0.1
Gas Distribution	16.1	1.7	--
Other Industrial/Commercial	2.2	1.8	0.2
Domestic Fuel Usage	0.2	0.1	1.6
Commercial Fuel Usage	0.2	0.2	1.3
Industrial Fuel Usage	0.6	0.3	8.3
Electrical Generating Plants	--	--	0.2
Waste Burning & Incineration	0.2	0.1	0.2
Domestic Reciprocating Engines	0.7	0.7	0.1
Other Reciprocating Engines	5.6	5	3.4
Farm & Construction Equipments	0.9	0.9	5.1
Ships	2.6	2.4	1.5
Locomotives	0.4	0.4	1.3
Sub-total(District Jurisdiction)	84.3	64.6	23.3
Aircraft	2.2	2.1	2.3
Cars & Light Duty Trucks	35	30.6	28.4
Medium Duty Gas Vehicles	1.3	1.2	1.7
Heavy Duty Gas vehicles	3.5	3.2	3.3
Diesel Buses & Trucks	1.2	1.2	5.5
Motorcycles	0.6	0.6	0.1
Sub-total (Mobile Sources)	43.8	38.8	41.3
Accidental Fires	4.6	4.1	0.7
Vegetation	22.8	22.8	--
Bio Degradation	29.7	0.2	--
Consumer Solvent Usage	13.8	13.8	--
Pesticides Usage	0.7	0.7	--
Sub-total (Other Sources)	71.5	41.6	0.7
TOTAL EMISSIONS	200	145	65.3

Table A.4 cont'd.

BAY AREA AIR QUALITY MANAGEMENT DISTRICT
County Emissions By Source Categories

CONTRA COSTA COUNTY September 1987 WEEK DAY AVERAGE.

	TONS/DAY		
	TOG	ROG	NOX
Petroleum Refining	40.2	32.7	38.7
Fuels -Bulk Loading	1.2	1.2	--
Fuels -Filling Stations	0.7	0.7	--
Structures Coating	4.4	4.4	--
Other Coating & Printing	6.8	6.5	--
Solvent Degreasing	1	0.7	--
Dry Cleaners	0.7	0.7	--
Rubber, Plastic Products Mfg.	0.4	0.4	--
Other Solvent Usage	2.7	2.7	--
Chemical Mfg.	1.7	0.9	1.4
Metallurgical & Mineral Ind.	0.1	--	--
Gas Distribution	45.6	4.8	--
Other Industrial/Commercial	5	1.2	3.4
Domestic Fuel Usage	0.1	0.1	1.1
Commercial Fuel Usage	--	--	0.6
Industrial Fuel Usage	0.8	0.3	12.7
Electrical Generating Plants	0.2	0.1	24.1
Waste Burning & Incineration	0.2	0.1	0.4
Domestic Reciprocating Engines	0.5	0.5	0.1
Other Reciprocating Engines	3.5	2.8	3.8
Farm & Construction Equipments	1	1	4.6
Ships	2.3	2.1	1.1
Locomotives	0.3	0.3	0.9
Sub-total(District Jurisdiction)	119	63.9	92.9
Aircraft	0.2	0.2	0.1
Cars & Light Duty Trucks	22.7	19.8	18.4
Medium Duty Gas Vehicles	0.8	0.7	1
Heavy Duty Gas vehicles	2.1	2	2
Diesel Buses & Trucks	0.8	0.7	3.3
Motorcycles	0.4	0.4	--
Sub-total (Mobile Sources)	26.9	23.7	24.9
Accidental Fires	0.2	0.2	--
Vegetation	22.3	22.3	--
Bio Degradation	17.8	0.1	--
Consumer Solvent Usage	8.3	8.3	--
Pesticides Usage	0.4	0.4	--
Sub-total (Other Sources)	49.1	31.4	--
TOTAL EMISSIONS	195	119	118

Table A.4 cont'd.

BAY AREA AIR QUALITY MANAGEMENT DISTRICT
County Emissions By Source Categories

MARIN COUNTY September 1987 WEEK DAY AVERAGE.

	TONS/DAY		
	TOG	ROG	NOX
Petroleum Refining	--	--	--
Fuels -Bulk Loading	--	--	--
Fuels -Filling Stations	0.3	0.3	--
Structures Coating	1.6	1.6	--
Other Coating & Printing	1.5	1.4	--
Solvent Degreasing	0.3	0.3	--
Dry Cleaners	0.3	0.3	--
Rubber, Plastic Products Mfg.	--	--	--
Other Solvent Usage	0.3	0.2	--
Chemical Mfg.	--	--	--
Metallurgical & Mineral Ind.	--	--	--
Gas Distribution	2.7	0.3	--
Other Industrial/Commercial	0.2	0.2	--
Domestic Fuel Usage	0.1	--	0.4
Commercial Fuel Usage	--	--	0.1
Industrial Fuel Usage	--	--	0.3
Electrical Generating Plants	--	--	--
Waste Burning & Incineration	--	--	--
Domestic Reciprocating Engines	0.2	0.2	--
Other Reciprocating Engines	1	0.9	0.4
Farm & Construction Equipments	0.2	0.1	0.8
Ships	0.6	0.6	0.2
Locomotives	--	--	--
Sub-total(District Jurisdiction)	9.2	6.4	2.3
Aircraft	0.1	0.1	--
Cars & Light Duty Trucks	7.8	6.8	6.4
Medium Duty Gas Vehicles	0.2	0.2	0.3
Heavy Duty Gas vehicles	0.6	0.6	0.6
Diesel Buses & Trucks	0.2	0.2	1
Motorcycles	0.1	0.1	--
Sub-total (Mobile Sources)	9.1	8	8.3
Accidental Fires	0.1	0.1	--
Vegetation	46.4	46.4	--
Bio Degradation	5.9	--	--
Consumer Solvent Usage	2.7	2.7	--
Pesticides Usage	0.1	0.1	--
Sub-total (Other Sources)	55.2	49.3	--
TOTAL EMISSIONS	73.5	63.7	10.7

Table A.4 cont'd.

BAY AREA AIR QUALITY MANAGEMENT DISTRICT
County Emissions By Source Categories

NAPA COUNTY September 1987 WEEK DAY AVERAGE.

TONS/DAY

	TOG	ROG	NOX
Petroleum Refining	--	--	--
Fuels -Bulk Loading	0.1	0.1	--
Fuels -Filling Stations	0.1	0.1	--
Structures Coating	0.7	0.7	--
Other Coating & Printing	0.8	0.8	--
Solvent Degreasing	0.1	0.1	--
Dry Cleaners	0.2	0.2	--
Rubber, Plastic Products Mfg.	0.1	0.1	--
Other Solvent Usage	0.2	0.2	--
Chemical Mfg.	--	--	--
Metallurgical & Mineral Ind.	--	--	--
Gas Distribution	1.1	0.1	--
Other Industrial/Commercial	0.6	0.6	--
Domestic Fuel Usage	--	--	0.1
Commercial Fuel Usage	--	--	0.1
Industrial Fuel Usage	--	--	0.2
Electrical Generating Plants	--	--	--
Waste Burning & Incineration	--	--	--
Domestic Reciprocating Engines	0.1	0.1	--
Other Reciprocating Engines	0.5	0.4	0.3
Farm & Construction Equipments	0.6	0.6	2.8
Ships	0.4	0.3	0.1
Locomotives	--	--	--
Sub-total(District Jurisdiction)	5.6	4.3	3.6
Aircraft	0.2	0.2	0.1
Cars & Light Duty Trucks	3.4	3	2.7
Medium Duty Gas Vehicles	0.2	0.2	0.2
Heavy Duty Gas vehicles	0.5	0.4	0.4
Diesel Buses & Trucks	0.2	0.2	0.7
Motorcycles	0.1	0.1	--
Sub-total (Mobile Sources)	4.4	3.9	4.2
Accidental Fires	2.4	2.1	0.4
Vegetation	60.1	60.1	--
Bio Degradation	2.7	--	--
Consumer Solvent Usage	1.2	1.2	--
Pesticides Usage	0.2	0.2	--
Sub-total (Other Sources)	66.6	63.7	0.4
TOTAL EMISSIONS	76.6	72	8.1

Table A.4 cont'd.

BAY AREA AIR QUALITY MANAGEMENT DISTRICT
County Emissions By Source Categories

SAN FRANCISCO COUNTY September 1987 WEEK DAY AVERAGE.

	TONS/DAY		
	TOG	ROG	NOX
Petroleum Refining	0.6	0.6	--
Fuels -Bulk Loading	--	--	--
Fuels -Filling Stations	0.5	0.5	--
Structures Coating	4.4	4.4	--
Other Coating & Printing	5.6	5.3	--
Solvent Degreasing	0.9	0.7	--
Dry Cleaners	1.1	1.1	--
Rubber, Plastic Products Mfg.	0.1	0.1	--
Other Solvent Usage	0.7	0.7	--
Chemical Mfg.	--	--	--
Metallurgical & Mineral Ind.	--	--	--
Gas Distribution	16.9	1.8	--
Other Industrial/Commercial	1	0.8	0.2
Domestic Fuel Usage	0.1	0.1	1.1
Commercial Fuel Usage	--	--	0.8
Industrial Fuel Usage	--	--	0.7
Electrical Generating Plants	0.1	--	9
Waste Burning & Incineration	0.1	--	0.1
Domestic Reciprocating Engines	0.3	0.3	--
Other Reciprocating Engines	3.1	2.8	1.6
Farm & Construction Equipments	1.2	1.1	6.1
Ships	0.8	0.8	3
Locomotives	0.2	0.2	0.6
Sub-total(District Jurisdiction)	37.9	21.4	23.4
Aircraft	--	--	--
Cars & Light Duty Trucks	16.5	14.4	13.4
Medium Duty Gas Vehicles	0.5	0.5	0.7
Heavy Duty Gas vehicles	1.5	1.4	1.4
Diesel Buses & Trucks	0.5	0.5	2.4
Motorcycles	0.3	0.2	--
Sub-total (Mobile Sources)	19.3	17	18
Accidental Fires	0.2	0.1	--
Vegetation	2	2	--
Bio Degradation	--	--	--
Consumer Solvent Usage	8.3	8.3	--
Pesticides Usage	0.1	0.1	--
Sub-total (Other Sources)	10.6	10.5	--
TOTAL EMISSIONS	67.8	49	41.4

Table A.4 cont'd.

BAY AREA AIR QUALITY MANAGEMENT DISTRICT
County Emissions By Source Categories

SAN MATEO COUNTY September 1987 WEEK DAY AVERAGE.

	TONS/DAY		
	TOG	ROG	NOX
Petroleum Refining	--	--	--
Fuels -Bulk Loading	0.4	0.4	--
Fuels -Filling Stations	0.8	0.8	--
Structures Coating	4.1	4.1	--
Other Coating & Printing	5.7	5.4	--
Solvent Degreasing	2.1	1.5	--
Dry Cleaners	0.8	0.8	--
Rubber, Plastic Products Mfg.	0.9	0.9	--
Other Solvent Usage	0.7	0.7	--
Chemical Mfg.	0.6	0.3	--
Metallurgical & Mineral Ind.	--	--	--
Gas Distribution	7.2	0.7	--
Other Industrial/Commercial	0.3	0.2	--
Domestic Fuel Usage	0.1	0.1	0.9
Commercial Fuel Usage	--	--	0.2
Industrial Fuel Usage	0.1	0.1	0.9
Electrical Generating Plants	--	--	--
Waste Burning & Incineration	0.1	--	0.1
Domestic Reciprocating Engines	0.4	0.4	0.1
Other Reciprocating Engines	2.9	2.6	1.7
Farm & Construction Equipments	0.5	0.5	2.7
Ships	1.1	1	0.4
Locomotives	0.1	0.1	0.3
Sub-total(District Jurisdiction)	29	20.6	7.3
Aircraft	6.3	5.8	8.7
Cars & Light Duty Trucks	22.2	19.4	18.2
Medium Duty Gas Vehicles	0.6	0.6	0.9
Heavy Duty Gas vehicles	1.8	1.6	1.7
Diesel Buses & Trucks	0.6	0.6	2.8
Motorcycles	0.3	0.3	--
Sub-total (Mobile Sources)	31.8	28.3	32.3
Accidental Fires	0.1	0.1	--
Vegetation	41.9	41.9	--
Bio Degradation	30.3	0.2	--
Consumer Solvent Usage	7.2	7.2	--
Pesticides Usage	0.6	0.6	--
Sub-total (Other Sources)	80.1	50	--
TOTAL EMISSIONS	141	98.9	39.6

Table A.4 cont'd.

BAY AREA AIR QUALITY MANAGEMENT DISTRICT
County Emissions By Source Categories

SANTA CLARA COUNTY September 1987 WEEK DAY AVERAGE.

TONS/DAY

	TOG	ROG	NOX
Petroleum Refining	--	--	--
Fuels -Bulk Loading	0.6	0.6	--
Fuels -Filling Stations	1.7	1.7	--
Structures Coating	8.4	8.4	--
Other Coating & Printing	12.8	12.3	--
Solvent Degreasing	4.9	2.2	--
Dry Cleaners	1.7	1.6	--
Rubber, Plastic Products Mfg.	1.1	1.1	--
Other Solvent Usage	2.9	2.7	--
Chemical Mfg.	0.4	0.2	--
Metallurgical & Mineral Ind.	1.5	0.4	--
Gas Distribution	17.3	1.8	--
Other Industrial/Commercial	3.7	3.5	--
Domestic Fuel Usage	0.2	0.2	1.8
Commercial Fuel Usage	0.1	--	1
Industrial Fuel Usage	1	0.9	7.9
Electrical Generating Plants	--	--	--
Waste Burning & Incineration	0.3	0.1	0.3
Domestic Reciprocating Engines	0.9	0.8	0.1
Other Reciprocating Engines	6.8	5.9	4.6
Farm & Construction Equipments	1.5	1.4	7.2
Ships	2.3	2.1	0.6
Locomotives	0.4	0.4	1.3
Sub-total(District Jurisdiction)	70.3	48.3	24.7
Aircraft	2	1.8	1.8
Cars & Light Duty Trucks	45.3	39.5	36.9
Medium Duty Gas Vehicles	1.4	1.3	2
Heavy Duty Gas vehicles	4	3.7	3.8
Diesel Buses & Trucks	1.4	1.4	6.3
Motorcycles	0.8	0.7	0.1
Sub-total (Mobile Sources)	54.8	48.4	50.8
Accidental Fires	0.4	0.4	0.1
Vegetation	73.4	73.4	--
Bio Degradation	37.9	0.3	--
Consumer Solvent Usage	16.2	16.2	--
Pesticides Usage	1.6	1.6	--
Sub-total (Other Sources)	129	91.8	0.1
TOTAL EMISSIONS	255	189	75.6

Table A.4 cont'd.

BAY AREA AIR QUALITY MANAGEMENT DISTRICT
County Emissions By Source Categories

SOLANO COUNTY September 1987 WEEK DAY AVERAGE.

	TONS/DAY		
	TOG	ROG	NOX
Petroleum Refining	4	3.2	6.4
Fuels -Bulk Loading	0.2	0.2	--
Fuels -Filling Stations	0.3	0.3	--
Structures Coating	1.1	1.1	--
Other Coating & Printing	2.3	2.2	--
Solvent Degreasing	0.2	0.2	--
Dry Cleaners	0.1	0.1	--
Rubber, Plastic Products Mfg.	0.1	0.1	--
Other Solvent Usage	0.4	0.4	--
Chemical Mfg.	0.1	0.1	--
Metallurgical & Mineral Ind.	--	--	--
Gas Distribution	4.4	0.5	--
Other Industrial/Commercial	1.4	0.2	--
Domestic Fuel Usage	--	--	0.2
Commercial Fuel Usage	--	--	1
Industrial Fuel Usage	0.1	--	2.5
Electrical Generating Plants	--	--	--
Waste Burning & Incineration	0.1	0.1	--
Domestic Reciprocating Engines	0.1	0.1	--
Other Reciprocating Engines	0.8	0.7	0.4
Farm & Construction Equipments	0.4	0.4	1.6
Ships	0.5	0.5	0.2
Locomotives	0.1	0.1	0.3
Sub-total(District Jurisdiction)	16.8	10.4	12.6
Aircraft	7.8	7.1	3.2
Cars & Light Duty Trucks	5.6	4.9	4.5
Medium Duty Gas Vehicles	0.2	0.2	0.3
Heavy Duty Gas vehicles	0.6	0.6	0.6
Diesel Buses & Trucks	0.2	0.2	1
Motorcycles	0.1	0.1	--
Sub-total (Mobile Sources)	14.6	13.1	9.7
Accidental Fires	0.1	0.1	--
Vegetation	15.1	15.1	--
Bio Degradation	4.8	--	--
Consumer Solvent Usage	2.3	2.3	--
Pesticides Usage	0.3	0.3	--
Sub-total (Other Sources)	22.7	17.9	--
TOTAL EMISSIONS	54.1	41.5	22.3

Table A.4 cont'd.

BAY AREA AIR QUALITY MANAGEMENT DISTRICT
County Emissions By Source Categories

SONOMA COUNTY September 1987 WEEK DAY AVERAGE.

TONS/DAY

	TOG	ROG	NOX
Petroleum Refining	--	--	--
Fuels -Bulk Loading	0.2	0.2	--
Fuels -Filling Stations	0.3	0.3	--
Structures Coating	1.7	1.7	--
Other Coating & Printing	1.7	1.6	--
Solvent Degreasing	0.4	0.3	--
Dry Cleaners	0.2	0.2	--
Rubber, Plastic Products Mfg.	0.1	0.1	--
Other Solvent Usage	0.3	0.3	--
Chemical Mfg.	--	--	--
Metallurgical & Mineral Ind.	--	--	--
Gas Distribution	1.8	0.2	--
Other Industrial/Commercial	0.3	0.3	--
Domestic Fuel Usage	0.1	--	0.3
Commercial Fuel Usage	--	--	--
Industrial Fuel Usage	--	--	0.1
Electrical Generating Plants	--	--	--
Waste Burning & Incineration	0.1	0.1	--
Domestic Reciprocating Engines	0.3	0.3	--
Other Reciprocating Engines	1.2	1.1	0.7
Farm & Construction Equipments	0.4	0.4	2
Ships	0.7	0.6	0.2
Locomotives	--	--	0.1
Sub-total(District Jurisdiction)	9.7	7.6	3.5
Aircraft	0.2	0.2	0.1
Cars & Light Duty Trucks	9.3	8.2	7.5
Medium Duty Gas Vehicles	0.5	0.4	0.6
Heavy Duty Gas vehicles	1.3	1.2	1.2
Diesel Buses & Trucks	0.4	0.4	2
Motorcycles	0.2	0.2	--
Sub-total (Mobile Sources)	11.8	10.5	11.3
Accidental Fires	--	--	--
Vegetation	35.9	35.9	--
Bio Degradation	6.8	0.1	--
Consumer Solvent Usage	3.4	3.4	--
Pesticides Usage	0.2	0.2	--
Sub-total (Other Sources)	46.3	39.6	--
TOTAL EMISSIONS	67.8	57.7	14.8

Table A.5

MONTEREY BAY UNIFIED AIR POLLUTION CONTROL DISTRICT
County Emissions By Source Categories

Monterey COUNTY September 1980 WEEK DAY AVERAGE.

	TONS/DAY		
	TOG	ROG	NOX
Petroleum Refining	--	--	--
Fuels -Bulk Loading	0.2	0.2	--
Fuels -Filling Stations	2.5	2.5	--
Structures Coating	2.6	2.6	--
Other Coating & Printing	1.3	1.3	--
Solvent Degreasing	0.6	0.6	--
Dry Cleaners	1	1	--
Rubber, Plastic Products Mfg.	--	--	--
Other Solvent Usage	1.7	1.4	--
Chemical Mfg.	--	--	--
Metallurgical & Mineral Ind.	--	--	--
Gas Distribution	--	--	--
Other Industrial/Commercial	2.4	2.4	--
Domestic Fuel Usage	--	--	0.6
Commercial Fuel Usage	--	--	0.2
Industrial Fuel Usage	0.4	0.3	17.9
Electrical Generating Plants	0.4	0.4	42.1
Waste Burning & Incineration	1.6	1.6	--
Domestic Reciprocating Engines	0.1	0.1	--
Other Reciprocating Engines	0.3	0.2	0.3
Farm & Construction Equipments	2.6	2.4	6.4
Ships	0.4	0.4	0.1
Locomotives	0.6	0.6	2.1
Sub-total(District Jurisdiction)	18.8	18	69.7
Aircraft	0.3	0.3	0.3
Cars & Light Duty Trucks	17.9	14.8	16.8
Medium Duty Gas Vehicles	0.7	0.6	1.3
Heavy Duty Gas vehicles	1.4	1.3	1.7
Diesel Buses & Trucks	0.4	0.4	3.9
Motorcycles	0.1	0.1	--
Sub-total (Mobile Sources)	20.8	17.4	23.9
Accidental Fires	4.3	3.9	0.6
Vegetation	160	160	--
Bio Degradation	--	--	--
Consumer Solvent Usage	1.3	1.3	--
Pesticides Usage	40.2	40.2	--
Sub-total (Other Sources)	206	205	0.6
TOTAL EMISSIONS	245	241	94.2

Table A.5 cont'd.

MONTEREY BAY UNIFIED AIR POLLUTION CONTROL DISTRICT
County Emissions By Source Categories

San Benito COUNTY September1980 WEEK DAY AVERAGE.

	TONS/DAY		
	TOG	ROG	NOX
Petroleum Refining	--	--	--
Fuels -Bulk Loading	0.1	0.1	--
Fuels -Filling Stations	0.2	0.2	--
Structures Coating	0.2	0.2	--
Other Coating & Printing	0.2	0.2	--
Solvent Degreasing	--	--	--
Dry Cleaners	0.1	0.1	--
Rubber, Plastic Products Mfg.	--	--	--
Other Solvent Usage	0.5	0.4	--
Chemical Mfg.	--	--	--
Metallurgical & Mineral Ind.	--	--	--
Gas Distribution	--	--	--
Other Industrial/Commercial	--	--	--
Domestic Fuel Usage	--	--	--
Commercial Fuel Usage	--	--	--
Industrial Fuel Usage	--	--	0.3
Electrical Generating Plants	--	--	--
Waste Burning & Incineration	0.6	0.6	--
Domestic Reciprocating Engines	--	--	--
Other Reciprocating Engines	--	--	0.1
Farm & Construction Equipments	0.4	0.4	1
Ships	--	--	--
Locomotives	--	--	0.1
Sub-total(District Jurisdiction)	2.3	2.2	1.5
Aircraft	--	--	--
Cars & Light Duty Trucks	1.6	1.3	1.7
Medium Duty Gas Vehicles	0.1	0.1	0.1
Heavy Duty Gas vehicles	0.1	0.1	0.2
Diesel Buses & Trucks	--	--	0.4
Motorcycles	--	--	--
Sub-total (Mobile Sources)	1.8	1.5	2.4
Accidental Fires	1.8	1.6	0.3
Vegetation	52	52	--
Bio Degradation	--	--	--
Consumer Solvent Usage	0.1	0.1	--
Pesticides Usage	0.6	0.6	--
Sub-total (Other Sources)	54.5	54.4	0.3
TOTAL EMISSIONS	58.7	58.1	4.1

Table A.5 cont'd.

MONTEREY BAY UNIFIED AIR POLLUTION CONTROL DISTRICT
County Emissions By Source Categories

Santa Cruz COUNTY September1980 WEEK DAY AVERAGE.

	TONS/DAY		
	TOG	ROG	NOX
Petroleum Refining	--	--	--
Fuels -Bulk Loading	0.2	0.2	--
Fuels -Filling Stations	1.2	1.2	--
Structures Coating	1.6	1.6	--
Other Coating & Printing	2.5	2.5	--
Solvent Degreasing	0.3	0.3	--
Dry Cleaners	0.7	0.6	--
Rubber, Plastic Products Mfg.	--	--	--
Other Solvent Usage	0.7	0.6	--
Chemical Mfg.	--	--	--
Metallurgical & Mineral Ind.	--	--	0.7
Gas Distribution	--	--	--
Other Industrial/Commercial	--	--	--
Domestic Fuel Usage	--	--	0.3
Commercial Fuel Usage	--	--	0.1
Industrial Fuel Usage	--	--	0.5
Electrical Generating Plants	--	--	--
Waste Burning & Incineration	0.1	0.1	--
Domestic Reciprocating Engines	0.1	0.1	--
Other Reciprocating Engines	0.3	0.2	0.3
Farm & Construction Equipments	0.4	0.4	1.7
Ships	--	--	--
Locomotives	--	--	--
Sub-total(District Jurisdiction)	8.2	7.9	3.7
Aircraft	--	--	--
Cars & Light Duty Trucks	12.5	10.3	12.1
Medium Duty Gas Vehicles	0.5	0.4	0.9
Heavy Duty Gas vehicles	1	0.9	1.2
Diesel Buses & Trucks	0.3	0.3	2.8
Motorcycles	0.1	--	--
Sub-total (Mobile Sources)	14.3	12	17
Accidental Fires	0.1	0.1	--
Vegetation	59	59	--
Bio Degradation	--	--	--
Consumer Solvent Usage	0.8	0.8	--
Pesticides Usage	2.3	2.3	--
Sub-total (Other Sources)	62.1	62.1	--
TOTAL EMISSIONS	84.7	82	20.7

Table A.5 cont'd.

MONTEREY BAY UNIFIED AIR POLLUTION CONTROL DISTRICT
County Emissions By Source Categories

Monterey COUNTY September 1987 WEEK DAY AVERAGE.

	TONS/DAY		
	TOG	ROG	NOX
Petroleum Refining	--	--	--
Fuels -Bulk Loading	0.3	0.3	--
Fuels -Filling Stations	2.5	2.5	--
Structures Coating	1.7	1.7	--
Other Coating & Printing	1.5	1.5	--
Solvent Degreasing	0.6	0.5	--
Dry Cleaners	1.1	1.1	--
Rubber, Plastic Products Mfg.	--	--	--
Other Solvent Usage	1.4	1.2	--
Chemical Mfg.	--	--	--
Metallurgical & Mineral Ind.	--	--	--
Gas Distribution	--	--	--
Other Industrial/Commercial	2.8	2.8	--
Domestic Fuel Usage	0.2	0.1	1.3
Commercial Fuel Usage	0.1	--	0.7
Industrial Fuel Usage	0.4	0.3	18.4
Electrical Generating Plants	0.5	0.5	53
Waste Burning & Incineration	1.9	1.8	--
Domestic Reciprocating Engines	0.2	0.2	--
Other Reciprocating Engines	0.4	0.4	0.4
Farm & Construction Equipments	1.3	1.2	5.6
Ships	1.1	1	0.2
Locomotives	0.7	0.7	2.5
Sub-total(District Jurisdiction)	18.6	17.7	82.1
Aircraft	0.4	0.4	0.4
Cars & Light Duty Trucks	10.1	8.4	13.4
Medium Duty Gas Vehicles	0.3	0.3	0.8
Heavy Duty Gas vehicles	0.9	0.9	1.5
Diesel Buses & Trucks	0.3	0.3	2.5
Motorcycles	0.3	0.2	0.1
Sub-total (Mobile Sources)	12.4	10.5	18.5
Accidental Fires	1.9	1.7	0.3
Vegetation	160	160	--
Bio Degradation	--	--	--
Consumer Solvent Usage	2.8	2.8	--
Pesticides Usage	21.3	21.3	--
Sub-total (Other Sources)	186	186	0.3
TOTAL EMISSIONS	217	214	101

Table A.5 cont'd.

MONTEREY BAY UNIFIED AIR POLLUTION CONTROL DISTRICT
County Emissions By Source Categories

San Benito COUNTY September1987 WEEK DAY AVERAGE.

	TONS/DAY		
	TOG	ROG	NOX
Petroleum Refining	--	--	--
Fuels -Bulk Loading	0.1	0.1	--
Fuels -Filling Stations	0.2	0.2	--
Structures Coating	0.2	0.2	--
Other Coating & Printing	0.2	0.2	--
Solvent Degreasing	--	--	--
Dry Cleaners	0.1	0.1	--
Rubber, Plastic Products Mfg.	--	--	--
Other Solvent Usage	0.4	0.3	--
Chemical Mfg.	--	--	--
Metallurgical & Mineral Ind.	--	--	--
Gas Distribution	--	--	--
Other Industrial/Commercial	--	--	--
Domestic Fuel Usage	--	--	0.1
Commercial Fuel Usage	--	--	--
Industrial Fuel Usage	--	--	0.3
Electrical Generating Plants	--	--	--
Waste Burning & Incineration	0.7	0.7	--
Domestic Reciprocating Engines	--	--	--
Other Reciprocating Engines	0.1	--	0.1
Farm & Construction Equipments	0.2	0.2	1
Ships	--	--	--
Locomotives	--	--	0.1
Sub-total(District Jurisdiction)	2.3	2.1	1.7
Aircraft	--	--	--
Cars & Light Duty Trucks	0.9	0.7	1.5
Medium Duty Gas Vehicles	--	--	0.1
Heavy Duty Gas vehicles	0.1	0.1	0.2
Diesel Buses & Trucks	--	--	0.3
Motorcycles	--	--	--
Sub-total (Mobile Sources)	1.1	0.9	2
Accidental Fires	0.5	0.5	0.1
Vegetation	52	52	--
Bio Degradation	--	--	--
Consumer Solvent Usage	0.2	0.2	--
Pesticides Usage	0.9	0.9	--
Sub-total (Other Sources)	53.6	53.6	0.1
TOTAL EMISSIONS	57	56.7	3.7

Table A.5 cont'd.

MONTEREY BAY UNIFIED AIR POLLUTION CONTROL DISTRICT
County Emissions By Source Categories

Santa Cruz COUNTY September1987 WEEK DAY AVERAGE.

	TONS/DAY		
	TOG	ROG	NOX
Petroleum Refining	--	--	--
Fuels -Bulk Loading	0.2	0.2	--
Fuels -Filling Stations	1.3	1.3	--
Structures Coating	1.1	1.1	--
Other Coating & Printing	2.9	2.9	--
Solvent Degreasing	0.3	0.3	--
Dry Cleaners	0.7	0.7	--
Rubber, Plastic Products Mfg.	--	--	--
Other Solvent Usage	0.6	0.5	--
Chemical Mfg.	--	--	--
Metallurgical & Mineral Ind.	--	--	0.7
Gas Distribution	--	--	--
Other Industrial/Commercial	0.1	0.1	--
Domestic Fuel Usage	0.1	0.1	0.8
Commercial Fuel Usage	--	--	0.3
Industrial Fuel Usage	--	--	0.6
Electrical Generating Plants	--	--	--
Waste Burning & Incineration	0.1	0.1	--
Domestic Reciprocating Engines	0.2	0.2	--
Other Reciprocating Engines	0.5	0.4	0.4
Farm & Construction Equipments	0.2	0.2	1.4
Ships	0.1	--	--
Locomotives	--	--	--
Sub-total(District Jurisdiction)	8.6	8.3	4.2
Aircraft	0.1	0.1	--
Cars & Light Duty Trucks	7.4	6.1	10.1
Medium Duty Gas Vehicles	0.3	0.2	0.6
Heavy Duty Gas vehicles	0.7	0.6	1.1
Diesel Buses & Trucks	0.3	0.2	1.9
Motorcycles	0.2	0.2	--
Sub-total (Mobile Sources)	8.9	7.4	13.7
Accidental Fires	0.1	--	--
Vegetation	59	59	--
Bio Degradation	--	--	--
Consumer Solvent Usage	1.8	1.8	--
Pesticides Usage	2.4	2.4	--
Sub-total (Other Sources)	63.3	63.3	--
TOTAL EMISSIONS	80.7	79	17.9

Appendix B

Table B.1

OBSERVED OZONE MIXING RATIOS (**BOLD**) AND MODEL CALCULATED SURFACE VALUES
SEPTEMBER 30, 1980

STATION		AM 6	7	8	9	10	11	12	PM 13	14	15	16	17	18	19	20	21	22	23	24
+dpt	**8**	**.2**	**.2**	**1**	**7**	**8**	**9**	**-**	**10**	**10**	**10**	**9**	**7**	**.2**	**.2**	**.2**	**.2**	**.2**	**.2**	**.2**
+dpt		.0	.5	.4	.6	1	3	5	7	8	8	8	8	7	6	3	1	.5	.4	.3
+drm	**17**	**.2**	**.2**	**1**	**1**	**3**	**6**	**9**	**10**	**11**	**10**	**5**	**3**	**.2**	**.2**	**.2**	**.2**	**.2**	**.2**	**.2**
+drm		.0	1	1	1	2	4	7	9	10	8	8	9	9	10	10	10	7	5	3
+dco	**15**	**.2**	**.2**	**1**	**4**	**6**	**7**	**10**	**10**	**10**	**8**	**7**	**1**	**.2**	**1**	**.2**	**.2**	**.2**	**.2**	**.2**
+dco		.1	1	1	2	2	4	6	8	10	12	13	13	12	10	9	7	5	4	3
+dsr	**4**	**.2**	**.2**	**.2**	**1**	**4**	**6**	**10**	**10**	**11**	**10**	**8**	**1**	**.2**	**.2**	**.2**	**.2**	**.2**	**.2**	**.2**
+dsr		.1	.7	.7	1	2	5	8	13	15	14	12	9	9	8	7	6	4	3	2
+dna	**5**	**.2**	**1**	**3**	**5**	**7**	**8**	**9**	**9**	**10**	**11**	**9**	**5**	**2**	**.2**	**.2**	**.2**	**1**	**.2**	**.2**
									<not in model grid>											
+drc	**13**	**1**	**1**	**1**	**2**	**4**	**4**	**8**	**10**	**13**	**13**	**7**	**1**	**1**	**1**	**1**	**1**	**3**	**2**	**2**
+drc		.0	1	1	1	3	5	9	12	15	18	20	21	20	17	15	13	11	10	8
+dlg	**58**	**.2**	**.2**	**1**	**3**	**6**	**7**	**12**	**13**	**15**	**16**	**13**	**7**	**2**	**4**	**4**	**4**	**5**	**5**	**5**
+dlg		.4	2	2	3	5	6	9	13	17	20	21	20	18	14	10	8	7	5	4
+dsj	**11**	**.2**	**.2**	**-**	**2**	**6**	**11**	**11**	**13**	**12**	**15**	**14**	**10**	**3**	**.2**	**.2**	**.2**	**.2**	**.2**	**.2**
+dsj		.0	.6	.5	.7	1	3	5	9	14	18	18	16	13	10	7	4	2	1	.5
+dej	**91**	**1**	**.2**	**1**	**3**	**6**	**11**	**11**	**13**	**15**	**17**	**19**	**12**	**6**	**2**	**2**	**6**	**6**	**4**	**6**
+dej		.2	.7	.7	1	2	3	6	9	12	14	14	12	10	8	6	5	3	2	2
+dgl	**90**	**1**	**2**	**3**	**6**	**9**	**11**	**13**	**14**	**18**	**18**	**17**	**16**	**13**	**8**	**7**	**8**	**8**	**7**	**6**
+dgl		.3	.5	.6	1	2	4	6	7	8	12	15	16	15	13	10	8	7	7	7
+dfa	**59**	**.2**	**.2**	**1**	**5**	**6**	**7**	**7**	**8**	**8**	**8**	**8**	**5**	**.2**	**.2**	**.2**	**1**	**.2**	**.2**	**.2**
									<not in model grid>											

Table B.1 cont'd.

+dva	**6**	**.2**	**.2**	**.2**	**1**	**3**	**5**	**8**	**8**	**8**	**8**	**7**	**3**	**2**	**1**	**.2**	**.2**	**.2**	**.2**	**.2**
+dva		.0	.6	.5	.6	1	2	4	5	5	5	5	5	5	3	2	.7	.4	.5	.7
+dsa	**2**	**.2**	**.2**	**.2**	**1**	**3**	**4**	**6**	**7**	**10**	**8**	**4**	**2**	**.2**	**1**	**1**	**.2**	**.2**	**.2**	**.2**
									<not in model grid>											
+dso	**49**	**1**	**1**	**2**	**6**	**7**	**8**	**9**	**10**	**10**	**11**	**10**	**6**	**7**	**5**	**4**	**3**	**3**	**3**	**3**
									<not in model grid>											
+dsl	**57**	**.2**	**.2**	**1**	**3**	**5**	**8**	**11**	**15**	**13**	**6**	**1**	**.2**	**.2**	**.2**	**.2**	**.2**	**.2**	**.2**	**3**
+dsl		.0	1	1	2	2	4	7	10	13	16	17	16	15	12	10	9	8	7	6
+oak	**103**	**.2**	**.2**	**1**	**1**	**1**	**3**	**5**	**7**	**10**	**8**	**2**	**.2**	**.2**	**.2**	**.2**	**.2**	**.2**	**.2**	**.2**
+oak		.0	1	1	2	2	4	6	9	11	13	12	11	10	8	6	5	4	3	3
+dli	**9**	**.2**	**.2**	**.2**	**1**	**2**	**3**	**3**	**3**	**3**	**3**	**3**	**2**	**1**	**1**	**.2**	**.2**	**.2**	**.2**	**.2**
+dli		.1	.6	.9	2	3	5	6	8	7	6	6	5	6	5	5	4	3	3	2
+dfr	**10**	**.2**	**.2**	**1**	**1**	**3**	**5**	**9**	**11**	**14**	**18**	**14**	**6**	**1**	**.2**	**.2**	**.2**	**.2**	**.2**	**1**
+dfr		.2	1	1	1	3	5	8	9	10	10	11	11	11	10	9	8	7	6	5
+dhw	**88**	**6**	**5**	**3**	**3**	**4**	**5**	**7**	**10**	**12**	**14**	**12**	**8**	**9**	**7**	**6**	**6**	**7**	**7**	**8**
+dhw		.8	1	2	2	3	2	2	5	7	8	9	10	10	6	4	8	6	4	3
+dfc	**93**	**.2**	**.2**	**1**	**2**	**3**	**4**	**7**	**9**	**9**	**5**	**3**	**2**	**.2**	**.2**	**.2**	**.2**	**.2**	**.2**	**.2**
+dfc		.0	.9	.9	1	2	2	4	5	7	11	12	12	8	4	3	2	2	1	.9
+hol	**99**	**5**	**4**	**5**	**7**	**9**	**11**	**11**	**10**	**9**	**12**	**14**	**13**	**13**	**12**	**11**	**10**	**9**	**8**	**8**
+hol		.2	.6	1	2	3	4	4	4	5	6	8	10	10	9	8	6	5	5	5
+car	**101**	**5**	**5**	**5**	**5**	**7**	**9**	**9**	**9**	**10**	**10**	**9**	**8**	**6**	**6**	**7**	**6**	**6**	**7**	**7**
+car		.0	.6	.8	2	3	4	6	7	7	8	8	8	6	5	5	5	6	6	7
+apt	**102**	**5**	**4**	**5**	**7**	**8**	**10**	**11**	**11**	**7**	**3**	**5**	**3**	**2**	**3**	**6**	**7**	**7**	**.2**	**7**
+apt		.3	1	2	5	7	9	11	13	13	12	12	12	12	11	10	9	8	8	7
+sal	**97**	**5**	**5**	**5**	**6**	**8**	**9**	**9**	**8**	**8**	**7**	**6**	**6**	**3**	**2**	**1**	**1**	**1**	**2**	**5**
+sal		.1	.6	.7	1	3	6	7	8	9	9	10	10	9	8	6	5	4	4	3

Table B.1 cont'd.

+wat	**95**	**2**	**2**	**2**	**4**	**8**	**10**	**11**	**12**	**12**	**12**	**9**	**6**	**5**	**4**	**3**	**2**	**2**	**3**	**5**
+wat		.1	1	2	4	6	9	10	11	11	12	12	12	12	11	10	9	8	6	6
+mhl	**94**	**1**	**.2**	**1**	**2**	**5**	**8**	**12**	**13**	**16**	**16**	**17**	**17**	**18**	**11**	**7**	**4**	**4**	**5**	**5**
+mhl		.9	1	1	2	3	5	7	11	15	16	18	19	18	13	9	7	7	8	8